Catalytic conversion of biomass to fuels and commodity chemicals

Giuseppe Bagnato

Submitted for the degree of Doctor of Philosophy

Heriot-Watt University
School of Engineering and Physical Science

February 2020

ABSTRACT

The production of biofuels from pyrolysis of biomass is one of the alternatives to fossil fuels, but the high oxygen content, acidity and instability of the pyrolysis bio-oils still represent a challenge limiting its widespread diffusion.

The aim of this research project focuses on develop further an existing technology to stabilise the pyrolytic oil by hydrogenation reaction and in evaluating the economic feasibility for industrial development.

Based on literature review, new catalysts have been synthesised and tested for the bio-oil hydrogenation. By impregnation technique, the zirconia has been doped with Pd and not noble metals (Cu and Fe), characterised and their performances studied, in term of conversion and selectivity for key bio-compounds. Vanillin was completely converted after 80 min at 100°C and 50 bar, in presence of $PdFe/ZrO_2$. Furthermore, promising results were obtained testing the $PdFe/ZrO_2$ catalyst on a real water bio-oil fraction, where the catalyst was able to maintain ~90% of carbon in the liquid phase, reduce the polymerisation degree and the acidity of the bio-oil under mild conditions.

With the idea to minimise the hydrogen consumption and lowering the energy demand for the hydrogenation, the reaction was carried out at low operating conditions using a membrane reactor. A Ru–polyethersulfone (PES) catalytic membrane was synthesised and tested for furfural hydrogenation achieving a TOF equal to 48,000 h^{-1}, at 70 ºC and 7 bar, but metal leaching with consequent deactivation was noticed

To address the deactivation of the Ru-PES membrane, Ra u- Polyether ether ketone (PEEK –WC) membrane was developed using a green solvent and tested with a simulated water bio-oil fraction at different temperature (65-85°C), pressure (11-18 bar) and H_2 flow rate (5 -25 mL/min.). The PEEK-WC membrane resulted in an enhanced stability and good hydrogenation activity.

Finally, to enhance the understanding of the real feasibility at industrial level of the proposed biorefinery pathway (Pyrolysis/HDO), an economic feasibility study was designed and carried out for two different scenarios: (i) using micro algae as feedstock for producing drop-in bio-fuels, which resulted in a minimum fuel selling price of 1.418 $/L, ~ 50 % higher than fossil fuels; and (ii) pinewood bio-oil (current feedstock) orientate to for producing chemicals (for 75% of bio oil processed) and fuels achieving an economic potential of 38,234 MM$/y for 10Mt/y feedstock treated, suggestion a valid alternative for green chemicals production, with relative price decrement.

ACADEMIC REGISTRY

Research Thesis Submission

Please note this form should be bound into the submitted thesis.

Name*:*	Giuseppe Bagnato		
School:	Engineering and Physical Science		
Version: *(i.e. First, Resubmission, Final)*	Final	Degree Sought:	Doctor of Philosophy

Declaration

In accordance with the appropriate regulations I hereby submit my thesis and I declare that:

The thesis embodies the results of my own work and has been composed by myself
Where appropriate, I have made acknowledgement of the work of others
Where the thesis contains published outputs under Regulation 6 (9.1.2) these are accompanied by a critical review which accurately describes my contribution to the research and, for multi-author outputs, a signed declaration indicating the contribution of each author (complete Inclusion of Published Works Form – see below)
The thesis is the correct version for submission and is the same version as any electronic versions submitted*.
My thesis for the award referred to, deposited in the Heriot-Watt University Library, should be made available for loan or photocopying and be available via the Institutional Repository, subject to such conditions as the Librarian may require
I understand that as a student of the University I am required to abide by the Regulations of the University and to conform to its discipline.
Inclusion of published outputs under Regulation 6 (9.1.2) shall not constitute plagiarism.
I confirm that the thesis has been verified against plagiarism via an approved plagiarism detection application e.g. Turnitin.

ACADEMIC REGISTRY

* *Please note that it is the responsibility of the candidate to ensure that the correct version of the thesis is submitted.*

Signature of Candidate*:*		Date:	07/07/2020

Submission

Submitted By *(name in capitals):*	Giuseppe Bagnato
Signature of Individual Submitting:	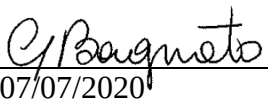
Date Submitted:	07/07/2020

For Completion in the Student Service Centre (SSC)

Received in the SSC by *(name in capitals):*			
1.1 Method of Submission *(Handed in to SSC; posted through internal/external mail):*			
E-thesis Submitted (mandatory for final theses)			
Signature:		Date:	

ACADEMIC REGISTRY

Inclusion of Published Works

Declaration

This thesis contains one or more multi-author published works. In accordance with Regulation 6 (9.1.2) I hereby declare that the contributions of each author to these publications is as follows:

Citation details	G. Bagnato, M. Signoretto, C. Pizzolitto, F. Menegazzo, X. Xi, G. ten Brink, B. Kooi, H. J. Heeres, A. Sanna, Bimetallic catalysts for mono-alcohols production by biobased aldehyde hydrogenation, ACS Sustainable Chemistry & Engineering (under review.
Giuseppe Bagnato	Manuscript preparation; characterisation and reaction tests.
Michela Signoretto	Research plan discussion and revision of the manuscript.
Cristina Pizzolitto	Revision of the manuscript, synthesise and characterisation of catalysts.
Federica Menegazzo	Revision of the manuscript, synthesise and characterisation of catalysts.
X. Xi	XRD analysis and revision of the manuscript.
G. ten Brink	XRD analysis and revision of the manuscript.
B. Kooi	XRD analysis and revision of the manuscript.
Hero Jan Heeres	Research plan discussion and revision of the manuscript.
Aimaro Sanna	Revision of the manuscript; manager of the research project.
Signature:	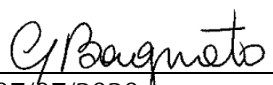
Date:	07/07/2020

ACADEMIC REGISTRY

Citation details	G. Bagnato, A. Sanna, Process and techno-economic analysis for fuel and chemical production by hydrodeoxygenation of bio-oil, Catalysts 2019, 9(12), 1021.
Giuseppe Bagnato	Manuscript preparation; Computational settings.
Aimaro Sanna	Revision of the manuscript; manager of the research project.
Signature:	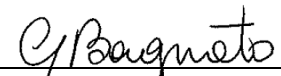
Date:	07/07/2020

Citation details	G. Bagnato, F. Boulet, A. Sanna, Effect of Li-LSX zeolite, NiCe/Al_2O_3 and NiCe/ZrO_2 on the production of drop-in bio-fuels by pyrolysis and hydrotreating of Nannochloropsis and Isochrysis microalgae Energy, Energy, 179 (2019), 199-213.
Giuseppe Bagnato	Manuscript preparation; Computational settings.
Flaurant Boulet	Revision of the manuscript, Computational settings.
Aimaro Sanna	Revision of the manuscript; manager of the research project.
Signature:	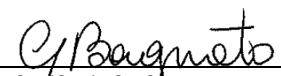
Date:	07/07/2020

ACADEMIC REGISTRY

Citation details	G. Bagnato, A. Figoli, C. Ursino, F. Galiano and A, Sanna, A novel Ru–polyethersulfone (PES) catalytic membrane for highly efficient and selective hydrogenation of furfural to furfuryl alcohol, J. Mater. Chem. A, 6 (2018), 4955-4965
Giuseppe Bagnato	Manuscript preparation; synthesis of membrane, characterisation and reaction tests.
Alberto Figoli	Research plan discussion and revision of the manuscript.
Claudia Ursino	Revision of the manuscript; synthesis of membrane and characterisation tests.
Francesco Galiano	Revision of the manuscript; synthesis of membrane and characterisation tests.
Aimaro Sanna	Revision of the manuscript; manager of the research project
Signature:	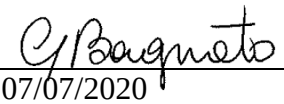
Date:	07/07/2020

ACADEMIC REGISTRY

Citation details	G. Bagnato, A. Iulianelli, A. Sanna, A. Basile. Glycerol production and transformation: a critical review with particular emphasis on glycerol reforming reaction for producing hydrogen in conventional and membrane reactors, Membranes (2017), 7-17.
Giuseppe Bagnato	Manuscript preparation;
A. Iulianelli	Revision of the manuscript;
Aimaro Sanna	Revision of the manuscript;
A. Basile.	Revision of the manuscript
Signature:	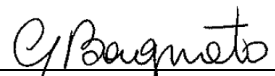
Date:	07/07/2020

Ancora imparo-

(I am still learning)

Michelangelo Buonarroti,

at age 87 when he was working on St. Peter's Basilica.

ACKNOWLEDGEMENTS

At the end of this long journey, finally, the day has arrived: writing these sentences of thanks is the final touch of my thesis. It was a period of profound learning, not only scientifically, but also personally. Writing this thesis has had a strong impact on my personality. I want to say a few words of thanks to all the people who supported and helped me during these years.

First of all, I would like to thank the people I met in this experience, for having given me fantastic moments. You have supported me and you have always been ready to help me. In particular, I turn to my friend and supervisor, Dr Aimaro Sanna, thanking him for the incredible availability and for all the opportunities I have been given in conducting my research project. Also, a special thanks to Professor Valeria Arrighi, for her support and her valuable advice.

Special thanks to my friends Angelo, Adolfo and Simona, who with patience and critical spirit, directed me towards a scientific world. I am grateful to them for the esteem and friendship shown me.

I'm grateful for my friends and colleagues, Montserrat, Edwin and Li Anne, supporting each other during the efforts that have characterised our journey in moments of joy and satisfaction to reach the goal cannot be omitted from this list of thanks. Thanks also to Caterina, Simon, William and Raul and all those people with whom I shared unforgettable moments, establishing a sincere friendship.

I do not mention the rest of my friends, because I assure another thesis would be needed. I do not know if I find the right words to thank my parents and part of my family, but I would like that my goal achieved, as far as possible, was a reward for them and for the sacrifices they made.

TABLE OF CONTENTS

LISTS OF TABLES AND FIGURES

GLOSSARY

AAS	Atomic absorption spectroscopy
BET	Nitrogen physisorption analyses
CAPEX	Capital cost, MM$
CMR	Catalytic membrane reactor
CNMR	Catalytic not perm-selective membrane reactor
COD	Crystallography Open Database
D	Diameter, ft
DCFROR	Discounted cash flow rate of return
d_{pore}	Pore diameter, m
Ea	Activation energy, J/mol
EP	Economic Potential
ePTFE	Expanded polytetrafluoroethylene
Fc	Correction factor
FCI	Fixed capital investment, MM$
F_d	Design factor
F_m	Material factor
GGE	Gallon gasoline-equivalent
GHG	Greenhouse gases
H	High, ft
IBO	Insoluble bio-oil
ICP –EOS	Inductively coupled plasma optical emission spectrometry
IPV	Investment value
LG	Levoglucosan
LHHW	Langmuir-Hinshelwood-Hougen-Watson
M&S	Marshall and Shift index
MFSP	Minimum fuel product selling price, $/L
M$	Billion dollar
MM$	Million dollar
MR	Molar ratio
MW	Molecular weight, lb/lbmol
NH_3-TPD	Temperature programmed desorption of ammonia
NMR	Not perm-selective membrane reactor

NP	Nanoparticle
OPEX	Annual operating cost, MM$/yr
P	Flow of matter, SCFM
PBMR	Packed bed membrane reactor
PBR	Packed bed reactor
PEEK-WC	Polyether ether ketone
PES	Polysulfone
PFD	Process flow diagram
Q	Heat supplied, 10^6 Btu/hr
R	Universal gas constant, J/mol K
ROI	Return of investment
R_1	Vapour recycle fraction
R_2	Liquid recycle fraction
RPV	Return value
SARE	Sale, administration, research and engineering cost, MM$/yr
SMB	Simulated moved bed
SEM	Scanning Electron Mycroscopy
T	Temperature, K
T_{bp}	Temperature boiling point
TCI	Total capital investment
TEM	Transmission electron microscope
TGA	Thermo Gravimetric Analysis
TOF	Turnover frequency
TPC	Total product cost
TPO	Temperature programmed oxidation
TPR	Temperature programmed reduction
V	Vapour molar flowrate, lbmol/hr
WBO	Water-soluble bio-oil
XRD	X-ray diffractometric
FCI	Fixed-capital investment
HDO	Hydrodeoxygenation
HHV	Higher heating value
Keq	Equilibrium constant

K_j	Equilibrium constant for j reaction
LHSV	Liquid hourly space velocity
ΔH_v	Heat of vaporization, Btu/lbmole,
ρ_m	Vapour molar density, lbmol/ft^3
∇p	Pressure gradient
ε	Membrane void fraction
τ	Tortuosity,
η	Viscosity

LIST OF PUBLICATIONS BY THE CANDIDATE

Journal publications

G. Bagnato, M. Signoretto, C. Pizzolitto, F. Menegazzo, X. Xi, G. ten Brink, B. Kooi, H. J. Heeres, A. Sanna, Bimetallic catalysts for mono-alcohols production by biobased aldehyde hydrogenation, ACS Sustainable Chemistry & Engineering, XX (2019), YY (correction undergoing).

G. Bagnato, A. Sanna, Process and techno-economic analysis for fuel and chemical production by hydrodeoxygenation of bio-oil, Catalysts 2019, 9(12), 1021.

G. Bagnato, F. Boulet, A. Sanna, Effect of Li-LSX zeolite, NiCe/Al_2O_3 and NiCe/ZrO_2 on the production of drop-in bio-fuels by pyrolysis and hydrotreating of Nannochloropsis and Isochrysis microalgae Energy, Energy, 179 (2019), 199-213.

G. Bagnato, A. Figoli, C. Ursino, F. Galiano and A, Sanna, A novel Ru–polyethersulfone (PES) catalytic membrane for highly efficient and selective hydrogenation of furfural to furfuryl alcohol, J. Mater. Chem. A, 6 (2018), 4955-4965.

Chapters book

G. Bagnato, A. Sanna, Membrane Considerations and Plant Design for Pre-Combustion CO_2 Capture, Ch. 15, in Current Trends and Future Developments on (Bio-) Membranes (2018),Elsevier, Editor(s): Angelo Basile, E.P. Favvas, ISBN 9780128136454.

Poster presentations

G. Bagnato, N. A. Abd Rahman, A. Sanna, Techno-Economic Assessment of an Algae-Based Biorefinery, 26th European biomass conference and exhibition (EUBCE), 14-17 May 2018, Copenhagen (Denmark).

G. Bagnato, A. Sanna, A Thermodynamic and economic evaluation of lignocellulosic bio-oil upgrading by hydrodeoxygenation, International Conference on Coal Science & Technology (ICCS&T), Sep. 25- 29, 2017, Beijing (China).

G. Bagnato, A. Iulianelli, V. Palma, K. Ghasemzadeh, A. Sanna, A. Basile, Ethanol steam reforming reaction over a novel Pt-Co based catalyst in a dense Pd-Ag membrane

reactor, Symposium on heterogeneous catalysis for fine chemicals (FineCat 2017), 5th April 2017, Palermo (Italy).

G. Bagnato, A. Iulianelli, A.Vita, K. Ghasemzadeh, F. Dalena, A. Basile, Pure hydrogen production from biogas steam reforming in a membrane reactor, Symposium on heterogeneous catalysis for fine chemicals (FineCat 2017), 5th April 2017, Palermo (Italy).

G. Bagnato, A. Iulianelli, A. Vita, A. Sanna, A. Basile, Comparison of packed bed reactor and membrane reactor for bioethanol steam reforming whit Ni-Ce based catalyst, Symposium on heterogeneous catalysis for fine chemicals (FineCat 2017), 5th April 2017, Palermo (Italy).

G. Bagnato, A. Iulianelli, S. Liguori, J. Wilcox, Y.H. Ma, I.P. Mardilovich, K. Ghasemzadeh, F. Dalena, A. Sanna, A. Basile, Supported Pd-Au membrane reactor for hydrogen production, Symposium on heterogeneous catalysis for fine chemicals (FineCat 2017), 5th April 2017, Palermo (Italy).

G. Bagnato, A. Iulianelli, Y. Huang, V. Palma, K. Ghasemzadeh, F. Dalena, A. Sanna, A. Basile, From biomass to high grade hydrogen generation for low-temperature PEM fuel cells, Symposium on heterogeneous catalysis for fine chemicals (FineCat 2017), 5th April 2017, Palermo (Italy).

G. Bagnato, A. Sanna, Hydrogenation of bio-oil: a thermodynamic study, Symposium on heterogeneous catalysis for fine chemicals (FineCat 2017), 5th April 2017, Palermo (Italy).

Chapter 1- Introduction

Bio-oils obtained from biomass are dark brown organic liquids, highly viscous with the presence of many organic compounds and large oxygen content that impede its processing into crude oil processing settings [1, 2].

The catalytic hydrodeoxygenation (HDO) of biomass-derived fast pyrolysis oil represents a fascinating route for production of liquid transportation fuels and commodity chemicals. The path for the conversion of sustainable biomasses such as lignocellulose and microalgae into petroleum-compatible product through pyrolysis/HDO can be divided into a series of steps including feed purification, chemical modification and products separation. Removal of oxygen can be achieved through catalytic HDO under high-pressure H_2, followed by catalytic hydrocracking (HC) to produce light products, with a possible ultimate input into a petroleum refinery infrastructure.

Gas-phase HDO of bio-oil has been studied under several process condition (temperature between 350 and 400°C and pressure from 130 to 250 bar) leading to high coke formation and carbon losses in gas phase. Alternatively, HDO in liquid phase under mild operating conditions (T= 125-250 °C, P= 40-100 bar), has shown promising results in terms of minimising coke formation and in terms of products selectivity. Despite this, large amount of H_2 are still required to overcome the mass transfer limitation due mainly to the limited solubility of H_2 in water. Therefore, this PhD project aim was focused on developing alternative technologies for efficient and economically feasible hydrogenation/hydrodeoxygenation of pyrolysis bio-oil and its representative model compounds. The present thesis (research project) followed a straight line starting from:

1. A comprehensive literature review of the state of the art of biorefinering, for having the largest point of view about the HDO reaction, studying the main strengths and weaknesses. Moreover, the literature review influenced the choice done during the experimental campaign;
2. Then, starting an experimental campaign towards the synthesis of a shortlist of catalysts and relative support, with subsequent characterization and reaction tests. At the meantime, understanding the mechanism involved onto the catalytic surface. In particular, the mono e bi metallic catalysts have been synthesised on zirconia base and tested for the hydrogenation reaction for model compounds and real mixture of bio-oil water fraction;

3. Subsequently, the new technologies has been evaluated to minimise the mass transfer limitation of HDO reaction, such as catalytic membrane reactors able to improve the contact area among the phases, able to reduce the conventional HDO operating condition, but maintaining high conversion. Synthesising different membranes, in term of materials and different technique for doping them with the active phase, then testing for the HDO reaction. Different polymers have been used for producing the porous membrane and consecutively Ru doped, with the target to have a stable catalytic membrane compatible with the bio-oil;
4. At the end, to facilitate the transition to a low carbon footprint industry the evaluation of techno-economical assessment HDO process has been considerate, founding the mainly project parameters to realise a higher economic potential, for different feedstock and products. This last point.

This thesis is structured in ten chapters, following the introduction (*Chapter 1*), *Chapter 2* discusses the main research involved on the development of bio-refinery focused on the upgrading of the pyrolysis oil from biomass by hydrogenation reaction, the evaluation of the most promising catalysts under development for HDO/hydrogenation of biomass derived substrates and the novel processes proposed for advancing bio-oil hydrogenation, such as membrane reactors (MRs) and finishes with a discussion on the TEA of hydrogenation process from different biomass feedstock [3, 4]. According to IUPAC definition, a MR is an equipment combining the typical characteristics of the separation with the properties of the chemical reaction in a single unit. Using MRs eliminates the need of a separation unit since the MRs work as extractors, selectively removing one or more reaction products. The presence of a membrane in an equilibrium reaction, increases the conversion respect to a traditional reactor under the same operating conditions, by removing a limiting reactant or product. In particular, the membranes have the target to decrease the mass transfer limitation, behaving as activated contactor among the phases (gas/solid/liquid).

Chapter 3 presents the methodology applied for realising the research project, describing the analytic techniques used, the reactor configuration and the techno-economical approach.

The experimental campaign regarding the hydrogenation reaction of model compounds and water bio-oil fraction has been studied in presence of different mono (Pd, Fe and Cu) and bimetallic (PdCu and PdFe) zirconia base catalysts on *Chapter 4 and 5* The reaction

has been studied at low operating condition (100ºC and 50 bar), recoding the best conversion values for the bimetallic catalysts.

While, the result of the hydrogenation reaction to MRs are reported into *Chapter 6 and 7*, where different polymeric membranes have been synthesised and doped with Ru catalyst and tested for hydrogenation reaction of organic compounds using a flat membrane reactor build in-house. The Ru-PES membrane shown TOF equal to 48,000 h^{-1}, the high vale achieved compared with the traditional reactor, for hydrogenation of furfural. Moreover, Ru-PEEK-WC membrane has been synthetised and tested at different temperature (65-85°C), pressure (11-18 bar) and H_2 flow rate (5 -25 mL/min.) to minimise losses of metal denoted in presence of Ru-PES membrane, achieving a stable conversion of furfural of ~ 75 %, at 85 ºC and 11 bar, and a 57.53% furfuryl selectivity for 80 hours.

The high-level techno-economic assessment of the biorefinery approach proposed in chapters 4-7 was then studies with the target to accelerate the transition for zero carbon emission economy, *Chapters 8 and 9* expose different approaches for techno-economical assessment (TEA). *Chapter 7* explores the possibility to for producing bio-fuels, from 2000 t/day of microalgae as future sustainable biomass resource, by catalytic pyrolysis in presence of different catalysts to produce bio-oil, which was subsequently hydrogenated. obtaining a minimum fuel selling price of 1.418 $/L.

While, in *Chapter 8*, the TEA for the HDO of lignocellulose biomass (pinewood bio-oil) for producing biofuels and chemical was studies, reaching an economic potential of 38,234 MM$/y for a capacity of bio-oil processed of 10 Mton/y.

At the end, the main results have been summarised on *Conclusions and future work* present based on the outcome of the present investigation.

Chapter 2- Literature review

2.1 Introduction

The large amount of fossil fuels used for the energy production and the industrial sector has led to the increase in greenhouse gases (GHG) in the atmosphere, which are gradually raising the global temperature, thus causing a series of problems to our planet. Currently, the scientific community in sync with national and international policies (e.g. COP21) are seeking into alternative source of clean energy for reducing GHG emissions. Renewable energy, also called alternative energy, represents energy derived from renewable sources such as solar energy, wind power, hydroelectric power, geothermal energy, tidal power and biofuels[5].

Due to the discontinuity and diversity of renewable energy technologies, the use of an energy carrier such as hydrogen would improve their deployment. Hydrogen, as energy carrier, can be used in normal internal combustion engines and in fuel-cells with efficiencies in energy of about 60%. The fuel cell can be used in many fields, from domestic to industrial uses, and it is also designed for the automotive industry, but high storage pressure (350-700 bar) limits its commercialisation.

Despite the fact that a "hydrogen economy" has been proposed since decades, the absence of dedicated infrastructures has limited its development so far and would require very large investment and a time-scale not compatible for reducing GHG level in the atmosphere.

Another alternative renewable technology in the portfolio is the use of biomass as a precursor of bio-fuel. Biomass has a unique advantage among the renewables, since it is the only source able to replace fossil fuels in all energy utilisation areas such as heat, electricity and transportation fuels. Already at the beginning of XX century a mixture of syngas (CO and hydrogen), obtained from the gasification of wood was used in Germany and United Kingdom. The solid fuel-based transport had many disadvantages (e.g. energy density), and with the oil advent, it was abandoned [6]. Nowadays, there is strong interest, in both the academic community and in industry, towards the production of liquid bio-fuels with characteristics similar to those of petroleum derivatives. One of the main reasons for this interest is the fact that these bio-fuels would enable the use of current refining and distribution infrastructures.

2.2 Biomass and biofuel

The term biomass (greek *bio* meaning life and *maza* meaning mass) refers to any organic material of plant and animal origin from which, it is possible to derive energy directly or through transforming it into gas, liquid or solid. This involves a variety of types of biomass, edible plant products with high sugar concentration, lignocellulosic materials, and civil and industrial waste products. The technologies used for the transformation of biomass into bio-fuels can be classified into bio- and thermochemical- processes.

Different types of biomasses can be classified in different ways. A classification can be made according to the areas of origin. The biomass for energy/fuels use can be obtained from: (i) the agricultural sector, (ii) the forestry sector, (iii) the livestock sector, (iv) the industrial waste, (v) energy crops.

Biomass is represented, for the most part, by residues of agricultural crops and forest, from manure, residues from agro-industry and the primary and secondary processing of wood, but can also be produced specifically through dedicated energy crops. By its nature, biomass is a renewable resource distributed throughout the territory; part of this resource is in some way already "available" as consisting of residues of various types. For much of the residual biomass, to date, several issues remain related to the optimisation of the production cycle, logistics (collection, transport, storage) and advanced energy conversion processes. Also, a careful environmental impact assessment and life cycle assessment for each specific biomass resource is required. Energy crops are represented by to crops for the production of biofuels (oil for production of vegetable oil or pure starchy for bioethanol production), or for the production of biogas of lignocellulosic biomass for combustion (annual or perennial crops and short rotation forestry), which in some cases retain the same principles of traditional agronomic and silvicultural crops, while others differ in the varieties, cultural practices and harvesting methods.

Bio-fuels can also be classified as 1^{st}, 2^{nd}, 3^{rd} and 4^{th} generation. With the first-generation being bio-fuels from conventional processes such as bio-ethanol from fermentation, and bio-diesel. In this category are typically edible plants in competition with food crops. The second-generation biofuels are based on non-food crops and other lignocellulosic biomass. The third-generation biofuels are produced from microorganisms using advances in biochemistry (i.e. algae). Genetically modified microorganisms capable of capturing large CO_2 amounts and produce bio-fuel are considered as biofuels of 4^{th} generation [7].

The term “Green Biorefinery” was been defined in the year 1997 as: “Green biorefineries represent complex (to fully integrated) systems of sustainable, environmentally and resource-friendly technologies for the comprehensive (holistic) material and energetic utilization as well as exploitation of biological raw materials in form of green and residue biomass from a targeted sustainable regional land utilization” [8]. The aim of a biorefinery is to produce compounds with high added value from a variety of biomasses. The different types of biorefineries depend on the raw materials and technologies used, as shown in Figure 2-1. Two main routes exist: the thermo-chemical and the biological pathways.

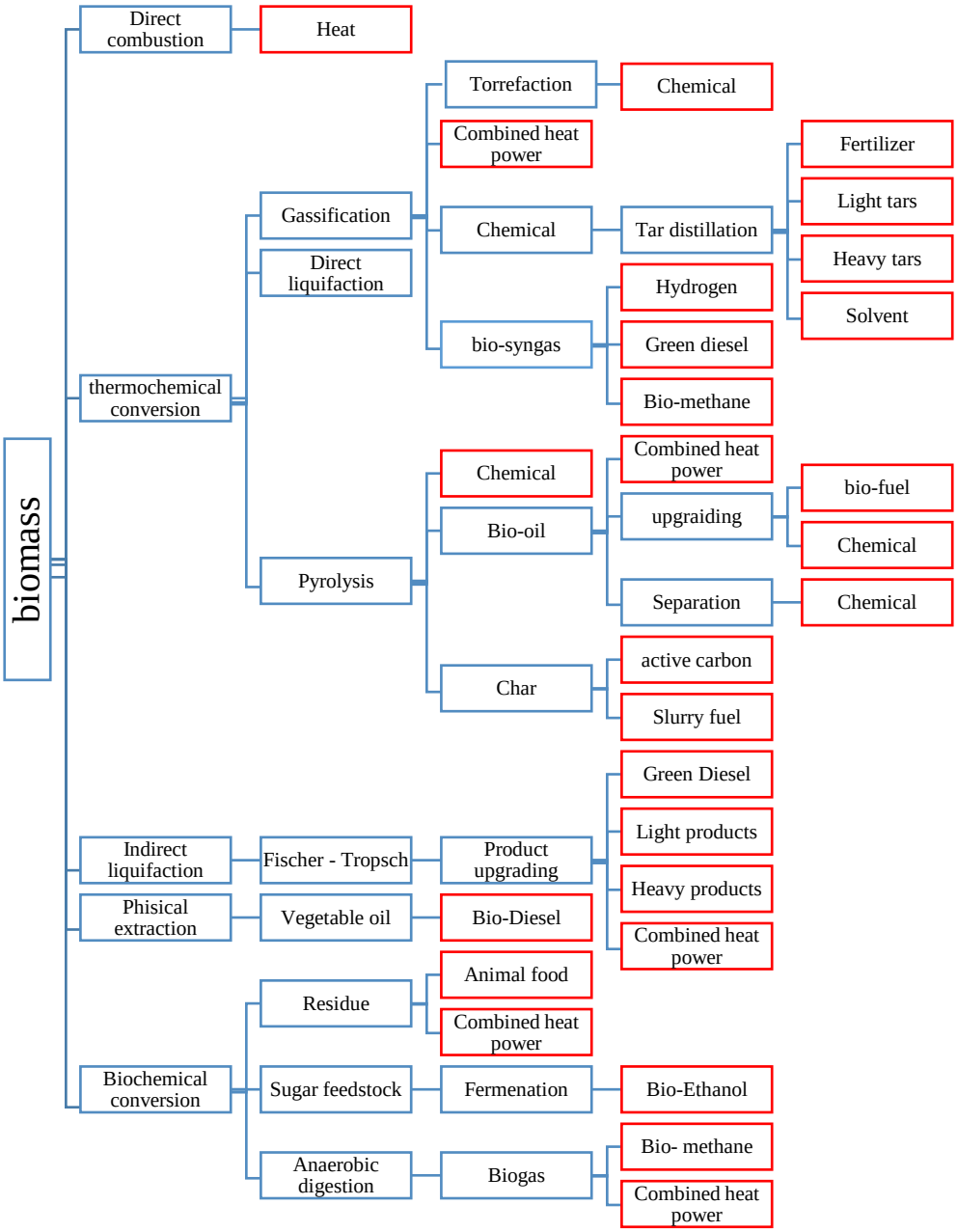

Figure 2-1. Biorifinery[9]

2.3 Bio-oil production

The bio-oil is the main product of wood pyrolysis. Historical documents report that this process was already used in ancient Egypt to prepare sealants for boats and ointments. In the 18th century, wood distillation provided compounds such us soluble tar, pitch, creosote oil, chemical, and non-condensable gases. Interest in biomass pyrolysis was revived in the 1980s, when the process has been perfected to have a high yield of liquid compound[10]. The pyrolysis process carried out with a temperature between 300º e 600º C and varying the residence time, the product distribution changes. To maximise the process in term of liquid yield, the fast pyrolysis is used, advantageously producing a liquid yield 3 times larger than the conventional and slow pyrolysis, at the same temperature, as shown in Table 2-1[11].

Table 2-1. Products distribution of the pyrolysis process[11]

	Residence time [s]	Temperature [K]	Char	Liquid	Gas
Conventional pyrolysis	1800	470	85-95	7-12	2-5
	1200	500	58-65	17-23	8-14
	900	550	44-49	26-30	16-22
	600	600	36-42	27-31	23-29
	600	650	32-38	28-33	27-34
	600	850	27-33	20-26	26-41
	450	950	25-31	12-17	48-54
Slow pyrolysis	200	600	32-38	28-32	25-29
	180	650	30-35	29-34	27-32
	120	700	29-32	30-35	32-36
	90	750	26-32	27-34	33-37
	60	850	24-30	26-32	35-43
	30	950	22-28	23-29	40-46
Fast pyrolysis	5	650	29-34	46-53	11-15
	5	700	22-27	53-59	12-16
	4	750	17-23	58-64	13-18
	3	800	14-19	65-72	14-20
	2	850	11-17	68-76	15-21
	1	950	9-13	64-71	17-24

In Figure 2-2 is shown the flow diagram of the BTG Bioliquids BV pyrolysis plant [12]. The first part of the plant consists in a drying unit where biomass from different origin (for example wood, rice husk, bagasse, sludge, tobacco, energy crops, palm-oil residues, straw, olive stone residues, chicken manure) is dried to decrease the water content. The dry biomass, in presence of hot carrier (sand), is then converted in a fluidised bed reactor into pyrolysis oil, gas and char. After that, the products and the sand are separated from the vapour/gas phase by a series of cyclones. Then, the char and sand fraction is moved to a fluid bed combustor, where the char is used to heat the sand recycled in the fluidised bed. The vapour/gas phase is instead quenched by re-circulated oil to divide the bio-oil and the incondensable gases are captured as high-pressure steam and utilised in a steam turbine system.

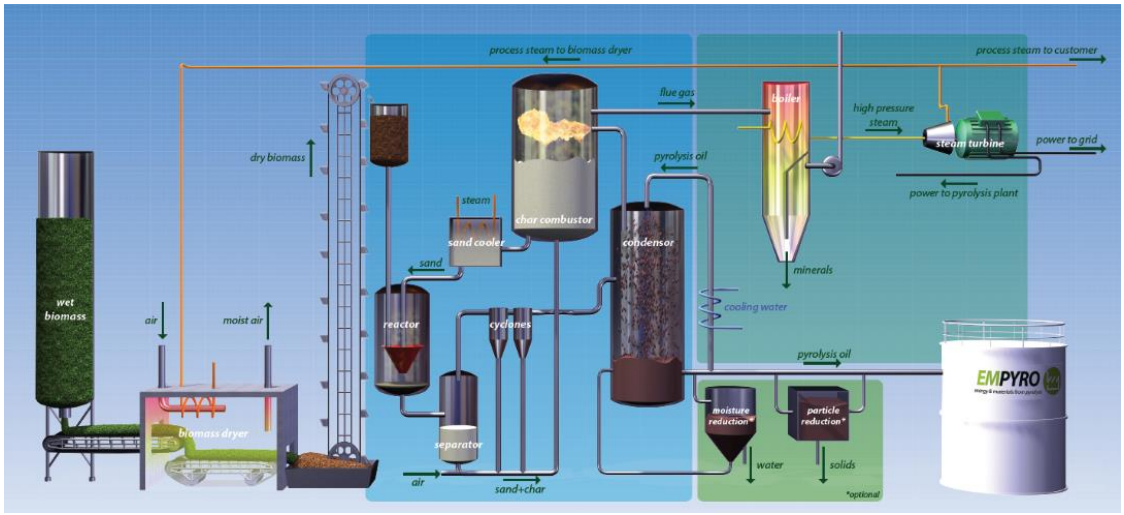

Figure 2-2. Pyrolysis plant [12]

Furthermore, recent researchers are focusing their attention to microalgae as feedstock for fast pyrolytic reaction[13]. Microalgae are classified as third-generation biofuel due to their fast growth cycle and high lipid content (~ 50%), easily converted in fuels. Moreover, microalgae do not require arable land and also are adaptable at different water sources, including wastewater.

The pyrolysis of microalgae is carried out in presence of zeolites, aluminosilicates, transitional metal-loaded zeolites, MOFs, silica gel, CuY [14-16].The pyrolysis process for microalgae are two major processes: (i) in-situ, where microalgae and catalyst are mixed together (ii) and ex-situ, the pyrolysis vapours from microalgae are swept over a catalyst at a specific temperature[17, 18].

The fast pyrolysis of biomass produces hundreds of different compounds (see Table 2-2), where their composition depends of the cellulose, hemicellulose, lignin and the extractive amount present in the feedstock. The influence of biomass composition on bio-oils composition can be appreciated from the variability of the bio-oils elemental composition reported in Table 2-3, where the C content can vary from 39% (pine sawdust) to about 60% (beech wood) under the same pyrolysis conditions. Furthermore, the operating condition of the fast pyrolysis influences the bio-oil composition [19, 20].

Table 2-2. Feedstock composition updated from [26]

Feedstock for bio-oil	C	H	O	N	S	Ref.
Beechwood	51.1	7.3	41.6			[21]
Typical wood	55–58	5.5–7	35–40	0–0.2		[22]
Pine wood	40.1	7.6	52.1	0.1		[23]
Rice husk	39.92	8.15	51.29	0.61	0.03	[24]
Beech wood	58.6	6.2	35.2			[25]
Pine sawdust	38.8	7.7	53.4	0.09	0.02	[26]
Eucalyptus	44.8	7.2	48.1	0.2		[27]
Hybrid poplar	46.7	7.6	45.7	0.2	0.03	[27]
Whole tree poplar	49.06	6.3	43.6	1		[28]
White spruce	49.6	6.4	43.1	0.2		[29]
Poplar	49.5	6.05	44.4	0.07		[29]
Sawdust	60.4	6.9	31.8	0.9		[30]
Microalgae	54.8	7.6	28.7	8.5	0.4	[31]
Scenedesmus	44.6	6.1	40.8	4.8	3.6	[32]
Nannochloropsis gaditana	40.3	5.97	14.5	6.3	0.37	[33]
Chlorella protothecoides	62.1	8.7	11.2	9.7	n/a	[34]
Chlorella sp.	73.2	9.6	7.2	7.25	n/a	[35]
Spirulina	67.5	9.8	11.3	10.7	n/a	[36]
Nannochloropsis sp.	80.2	6.2	5.8	6.2	n/a	[35]
Cyanobacteria	67.6	8.9	14.5	7.7	n/a	[37]

Table 2-3. Bio-oil composition

Fraction/Chemical groups	Compound types	Wt% (wet basis) [38]	Wt% (wet basis) [39]	Wt% [39]
	Water solubles 75-85 %			
Acids alcohols	Small acids, small alcohols	5-10	6.5	8.5
Ether-solubles	Catechols, syringols, guaiacols, aldehydes, ketones, furans and pyrans	5-15	15.4	20.3
Ether-insolubles	Sugars	30-40	34.4	45.3
Water	Water	20-30	23.9	-
	Water insoluble 15-25 %			
Hexane-solubles	Extractives (High MW compounds with functional groups such as acids, alcohols)	2-6	4.35	5.7
DCM solubles	Stilbenes, Low MW lignin degraded compounds	5-10	13.4	17.7
DCM insolubles	High MW lignin degraded compounds	2-10	1.95	2.6

2.4 Catalytic hydrogenation of bio-oil

In refineries, the hydrogenation reactions are common operations to limit the presence of oxygen, nitrogen, sulphur, olefins and aromatics. The reaction is catalysed by molybdenum together with Ni or Co supported by γAl_2O_3. The operating conditions depend on the type of feed: LHSV 0.2 to 8.0, H_2 circulation from 50 to 675 Nm^3 / m^3, H_2 pressure between 14-138 bar and temperatures between 290 and 470 ºC[40].

Actually, there are not industrial processes for HDO of bio-oil, but several catalysts are been tested from noble metals to Ni and Co, typical for hydrogenation process, in presence of acid supports such as Al_2O_3 and SiO_2, or C, with temperature range 150-500 ºC, pressure range between 2 -200 bar, with oil yield up to 75% [29]. This section has been dived into three parts: the first one related to recent catalysts developed for bio-oil HDO and the relative kinetics rates. The catalyst reported were commercial and

experimental, both tested on batch and continuous reactors. While, the second part is focused on typical HDO reactors and innovative membrane reactors, defined and classifying them and reporting the main works present in literature on biooils HDO. Finally, the last section is related to the recent works about the TEA of hydrogenation of pyrolytic oil from different biomasses.

2.4.1 Catalysts

|H|ydro-processing is catalysed in presence of metals from group VIII, such as nickel, palladium, and platinum [41]. Furthermore, group VIB metals (tungsten and molybdenum) have also been used for oxygen removal, since they are resistant to attack by oxygen, acids, and alkalis [42, 43]. According to Masel [44], hydrogen is reactive in the surfaces of Co, Ni, Ru, Rh, Pd, Os, Ir, Pt as well as on Sc, Ti, V, Y, Zr, Nb, Mo, La, Hf, Ta, W, Cr, Mn, Fe, Tc and Re. A slower uptake of hydrogen was observed with Cu, whereas Ag and Au were inert [44]. Some authors increased the catalyst activity adding a second metal as Mo due to its efficient adsorption of hydrogen at low temperature [45, 46]. The most used supports were alumina-silica, carbon, titania (rutile), and zirconia (monoclinic form). Activated carbon is a well-known high-surface area (typically ~1000 m^2/g) support material, which has been shown to be stable in hot water processing environments; rutile titania and monoclinic zirconia have lesser surface area (typically 30-80 m^2/g) but have also demonstrated their utility as catalytic metal support and have been used in the hot water processing environment [47-49]. A possible pathway for upgrading bio oils is represented by hydrogenation reactions in liquid phase, with the conversion of aldehydes, ketones, sugars, phenols, etc. in more stable alcohols. In order to improve the conversion of the bio-oils compounds and enhance the selectivity on desired products, several catalysts have been studied (see Table 2-4). Interesting is the work of Wie et al.[50], where Pt over different ceria-zirconia supports were evaluated for the hydrogenation of cinnamaldehyde at 10 bar and 60 ºC, obtaining a conversion in the range 60-95%.

Table 2-4. Hydrogenation reaction (continue)

Catalyst	Reactant	Pressure (bar)	Temperature (ºC)	Time (h)	Conversion (%)	Note	Ref.
30% Ni/CNT	acetic acid	40	150	4	5.8	2 wt% cat	[51]
30% Cu/CNT	acetic acid	40	150	4	3.5	2 wt% cat	[51]
Ru/C	acetic acid	40	150	4	4.7	2 wt% cat	[51]
20% Mo/CNT	acetic acid	40	150	4	<2	2 wt% cat	[51]
10/ 10wt.% NiMo/CNT	acetic acid	40	150	4	14.8	2 wt% cat	[51]
3 wt.% Ru/TiO_2	acetic acid	62	120	33*	37.5	*time on stream	[52]
3 wt.% Ru/TiO_2	acetol	62	70	14*	93.6	*time on stream	[52]
3 wt.% Ru/TiO_2	Bio oil	62	120	21	27/38/79*	*acetic acid/ acetol/ formic acid	[52]
3 wt.% Ru/C	Bio oil	52	120	6	33/99/97*		[52]
Ru/Zr-MOFs	furfural	5	20	5	20-95*	TOF: 2-11 Selectivity to Furfuryl alcohol: 20-95	[53]
AuNCs/CNTs membrane	4-nitro-phenol				53/100	5/10 μmol Au /17 cm^2	[54]
Au/SiO_2	25 compounds	80	6	5-24	40-99	1 mmol of alkyne, 0.01 mmol of Au, and 1 mmol of piperazine	[55]

continue

Catalyst	Reactant	Pressure (bar)	Temperature (ºC)	Time (h)	Conversion (%)	Note	Ref.
Rh–MoOx/SiO_2	cyclohexanecarboxamide	80	140	4	18	Rh 4 wt%, Mo/Rh = 1 Rh–MoO_x/SiO_2 100 mg, metal oxide 100 mg	[56]
Rh–MoOx/SiO_2+ H-ZSM-5	cyclohexanecarboxamide	80	140	4	34		[56]
Rh–MoOx/SiO_2+ SiO_2–Al_2O_3	cyclohexanecarboxamide	80	140	4	27		[56]
Rh–MoOx/SiO_2+ MgO	cyclohexanecarboxamide	80	140	4	20		[56]
Rh–MoOx/SiO_2+ γ-Al_2O_3	cyclohexanecarboxamide	80	140	4	61		[56]
Rh–MoOx/SiO_2+ TiO_2	cyclohexanecarboxamide	80	140	4	24		[56]
Rh–MoOx/SiO_2+ ZrO_2	cyclohexanecarboxamide	80	140	4	26		[56]
Rh–MoOx/SiO_2+ CeO_2	cyclohexanecarboxamide	80	140	4	89		[56]

Catalyst	Reactant	Pressure (bar)	Temperature (ºC)	Time (h)	Conversion (%)	Note	Ref.

$ReOx{-}Pd/CeO_2$	16 compounds	80	140	4	1-60	substrate 0.5 g, 1,4 dioxane 4 g, Wcat = 150 mg (2 wt. % Re, 0.3 wt. % Pd)	[57]
$Re–Pd/SiO_2$	Stearic acid	80	140	1	15	Re/Pd=1/8	[58]
$Re–Pd/SiO_2$	Stearic acid	80	140	4	13		[58]
Ni/rutile	crotonaldehyde	10	70		60		[59]
Pt/MWNT	furfural	20	150	5	75-100	50g furfural (4%)+water 0.2g catalyst Max Furfuryl alcohol selectivity: 79% Solvent: 2-propanol	[60]
Pd-Cu/MgO Pd-Cu/C	furfural	6-8	80-130	0.5	100	98.7% selectivity of Furfuryl alcohol 5 wt.%-5 wt.% Cu Different solvents (water, 80 min)	[61]
5 wt% Ru/C, 5% Pt/C	Bio oil (WSBO)	52-100	75-275	4-100	99/41	*All reactants /acetic acid 0.8-1.6g catalyst loaded in tubular reactor	[62, 63]

Liou et al. [64] used CeO as support with different metals (Ni, Co and Cu) for the hydrogenation in liquid phase of maleic anhydride at 50 bar and 210 °C, converting all the reactant after 60, 180 and 420 minutes, for Ni, Co and Cu respectively. Eliott al. [65] elaborated a reactivity scale of hydrogenation of different organic compounds in presence of CoMo and NiMo sulphided catalysts (see Figure 2-3) based on literature work[66]. Olefins, aldehydes and ketones are hydrogenated at low temperatures as low as 150– 200 °C, while the alcohols at 250–300 C. Carboxylic and phenolic ethers react at around 300 C.

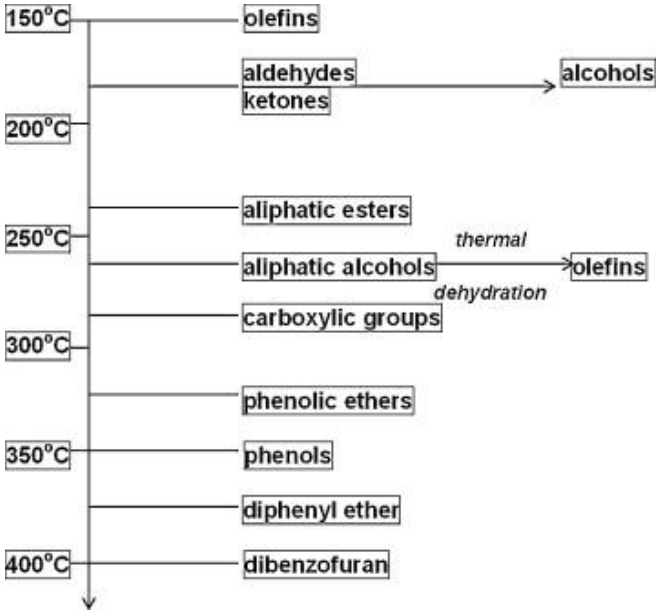

Figure 2-3. Reactivity scale of organic compounds under hydrotreatment conditions[65]

Recently, copper catalysts have attracted much attention for the conversion of glycerol to propylene glycol because of their intrinsic ability to selectively cleave the C-O bonds in glycerol rather than the C-C bonds. To increase the activity of Cu metal, Cu-based catalysts such as Cu-Cr, Cu-Al, Cu-Mg have been developed to promote the hydrogenolysis reaction. Bienholz et al. prepared a highly dispersed silica-supported copper catalyst (Cu/SiO_2) using an ion-exchange method and achieved 100% glycerol conversion with 87% propylene glycol selectivity at optimum conditions of 5 mL/h of 40 wt. % aqueous glycerol solution, 255 °C, and 300 mL/min of H_2 at 15 bar[67]. Liu's group studied the glycerol hydrogenolysis over Ru-Cu catalysts supported on different support materials including SiO_2, Al_2O_3, NaY zeolite, TiO_2, ZrO_2, and HY zeolite. The best activity was observed for $Ru-Cu/ZrO_2$ with 100% glycerol conversion and 78.5% propylene glycol selectivity. The high activity of this catalyst was attributed to the synergistic effect of Ru in the catalyst related to hydrogen spill-over, while the high

selectivity was attributed mainly at the low acidity of the support and the Cu amount[68].The HDO of the Water soluble fraction of Bio-Oil (WBO) at different temperatures (220, 270 and 310 °C) at 190 bar, using 5 wt% Ru/C catalyst was studied by de Miguel Mercader et al.[69], where the recovery of carbon in oil phase increased from 16.3 wt% to 38.5 wt%, when the temperature was increased from 220 to 310 ºC. In another study, several lignin model compounds (phenol, m-cresol, anisole, guaiacol, and diphenyl ether) were tested for HDO reactions in presence of MoO_3 at atmospheric pressure and temperature between 150- 250 ºC [70]. The authors noted that, according to the bond dissociation energy, the highest catalytic reactivity was obtained with diphenyl ether, but important carburization phenomena have been noted onto the catalyst surface. Bergem et al.[52] investigated the HDO of a model WBO using Ru/TiO_2 and Ru/C catalysts in a packet bed reactor (PBR) at temperature between 100 -140 °C, ~ 62 bar. A completed conversion was noted already a 100 °C for compound as acetone, acetaldehyde, propionaldehyde, 2-propen-1-ol, 1-hydroxy-2-butanone, 3-hydroxy-2-butanone, 2-hexanone, and 2-furanone. While, other compounds as furfural and hydroxyacetaldehyde required elevate temperature for converting completely. Furthermore, the authors observed a decrement of catalyst activity, about 25% after 90 hours, due at acid leaching. Sanna et al [62] studied the HDO of a real WBO in presence of Ru/C and Pt/C catalysts, in a two stage continuous reactors. The first stage the reaction was carried out in presence of Ru/C catalyst at 125 °C, while the second stage at a temperature between 200- 250 °C with Pt/C, at 50 and 100 bar, and different weight hourly space velocities from 0.75 to 6 h^{-1}. During the first stage, the unstable bio-oil functionalities were converted into stable alcohols, where the main product were ethylene glycol, propylene glycol and sorbitol, losing 7% of carbon as gas and solid phase. Furthermore, the catalyst showed a constant activity for about 80 h. While, the second stage converted 45 % carbon in gasoline blend stocks and C2 to C6 diols.

2.4.2 Kinetic mechanism

The reactions involved during the hydrotreating of bio-oil have been widely studied [71-73], as shown below:

Hydrodeoxygination (HDO): $R - OH + H_2 \rightarrow R - H + H_2O$

Hydrodesulphuration (HDS): $R - SH + H_2 \rightarrow R - H + H_2S$

Hydrodenitrogenation (HDN): $Pyridine + H_2 \rightarrow Pentane + NH_3$

Hydrodealkylation: $R - C_6H_5 + H_2 \rightarrow C_6H_6 + R - H$

Hydrocracking: $R_1 - CH_2CH_2 - R_2 + H_2 \rightarrow R_1 - CH_3 + R_2 - CH_3$

Isomerization of alkanes: $n - alkane \rightarrow i - alkane$

Decarboxylation: $R - CO - OH \rightarrow R - H + CO_2$

Decarbonilation: $R - CHO \rightarrow R - H + CO$

Water gas shift reaction: $CO_2 + H_2 \leftrightarrow CO + H_2O$

Coke formation: $polyaromatic \rightarrow coke$

In the following section, the reaction mechanisms of some of the most representative bio-oil compounds will be discussed.

Phenol

The phenol hydrogenation has been widely studied [74-78]. The reaction pathways are shown in Figure 2-4, where hydrogen reacts with the phenol attacking the hydroxyl group to produce benzene with subsequent production of cyclohexene and cyclohexane. Another reaction pathway of the aromatic ring is the formation of cyclohexanol with consecutive hydrogenation in cyclohexene and cyclohexane. A further reaction pathway is represented by the formation of cyclohexanone with subsequent cyclohexanol hydrogenation in cyclohexene and cyclohexane. Finally, methyl pentene can be produced by isomerization reaction.

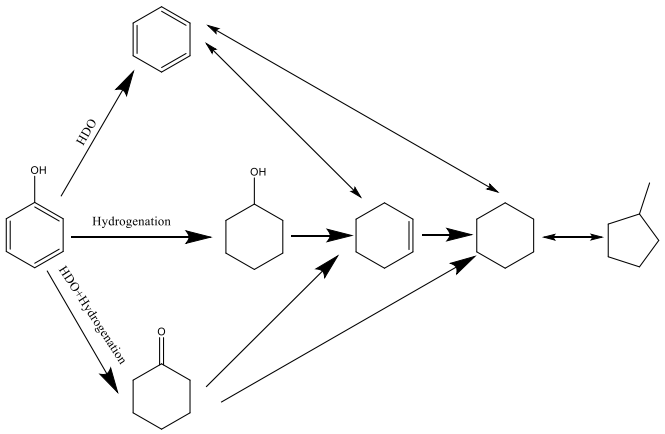

Figure 2-4. Phenol hydrogenation pathways.

Guaiacol

Another representative compound in bio-oil is guaiacol that reacts forming phenol [11-15] via two paths: 1) direct reaction of demethoxylation; and 2) indirect reaction through demethylation to catechol with subsequent hydrogenation of the latter compound. The

undesired reaction is the polymerisation of the molecule in the first reaction step (Figure 2-5), which leads to coke.

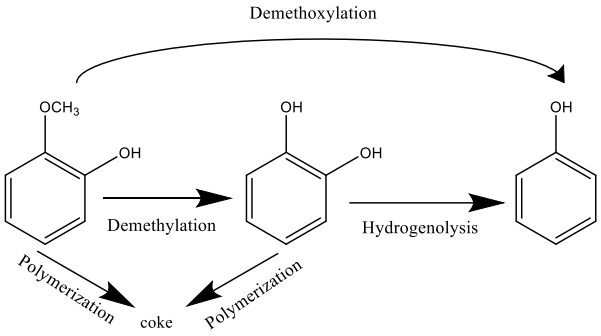

Figure 2-5. Guaiacol reaction path [11-15]

Bindwal et al.[79] proposed a kinetic rate for the hydrogenation of guaiacol in 1,2 cycloexanediol in presence of 5% Ru/ C catalyst according to the Langmuir-Hinshelwood-Hougen-Watson (LHHW) model. The authors, according to the experimental data obtained, identified the limitation step for the reaction taking place on the catalyst surface, assuming the dissociative adsorption of H_2. The reaction rate was described by the following equation:

$$r = \frac{k_{3,a} K_B C_B \sqrt{K_{H_2} C_{H_2}}}{(1+\sqrt{K_{H_2} C_{H_2}}+K_B C_B)^2} \qquad 2\text{-}1$$

Where C_B C_{H2} are the molar concentration of guaiacol and hydrogen, respectively, $k_{3,a}$ the kinetic costant, K_B and K_{H2} are the adsorption constant of guaiacol and hydrogen. The kinetics data obtained are presented in Table 2-5.

Table 2-5. Guaiacol kinetic data

	Unit	Guaiacol
k^{o}_{3}	kmol/ kg min	$9.1 \cdot 10^4$
E_a	kJ/mol	27.7
$K^{o}_{H_2}$	m^3/kmol	$3.7 \cdot 10^2$
ΔH_{H_2}	kJ/mol	45.7
K^{o}_{B}	m^3/kmol	$1.2 \cdot 10^4$
ΔH_B	kJ/mol	26.4

Levoglucosan

The hydrolysis of levoglucosan has been studied in a solution of water and in the presence of Ru/C [80]. The path involves the production of glucose (hydrolysis reaction) with subsequent hydrogenation into sorbitol. Finally, ethylene glycol, propylene glycol and 1,4-Butanediol are produced by the hydrogenation of sorbitol.

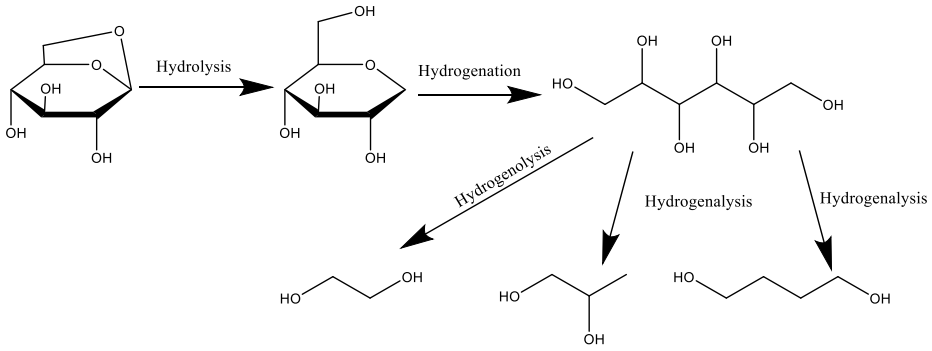

Figure 2-6. Levoglucosan reaction path

Bindwal et al. [80] proposed a kinetic rate for the hydrogenation in presence of Ru/C, where the H_2 and levoglucosan (LG) chemisorbed and dissociated on the surface catalyst are as follow:

$$H_2 + X \leftrightarrow 2HX \quad 2\text{-}2$$

$$LG + X \leftrightarrow LGX \quad 2\text{-}3$$

$$2HX + LGX \leftrightarrow products \quad 2\text{-}4$$

Represented by the following equation:

$$r = \frac{k_3 K_{H_2} K_{LG} C_{H_2} C_{LG}}{\left(1 + \sqrt{K_{H_2} C_{H_2}} + K_{LG} C_{LG}\right)^3} \quad 2\text{-}5$$

$$k_3 = 5.86 \cdot 10^{11} \exp\left(-\frac{94.5}{TR}\right) [=] kmol/kg_{cat} min \quad 2\text{-}6$$

$$K_{H_2} = 5.86 \cdot 10^{-9} \exp\left(\frac{61.6}{TR}\right) [=] m^3/kmol \quad 2\text{-}7$$

$$K_{LG} = 6.73 \cdot 10^{-5} \exp\left(\frac{39.2}{TR}\right) [=] m^3/kmol \quad 2\text{-}8$$

Other compounds

Bindwal et al. [79] studied the kinetics rate of other compounds using 5% Ru/C catalyst to convert hydroxycetone, hydroxyacetaldehyde and 2-furanone in 1,2 propanediol, ethylene glycol and γ-butyrolactone, according to the reactions in Figure 2-7.

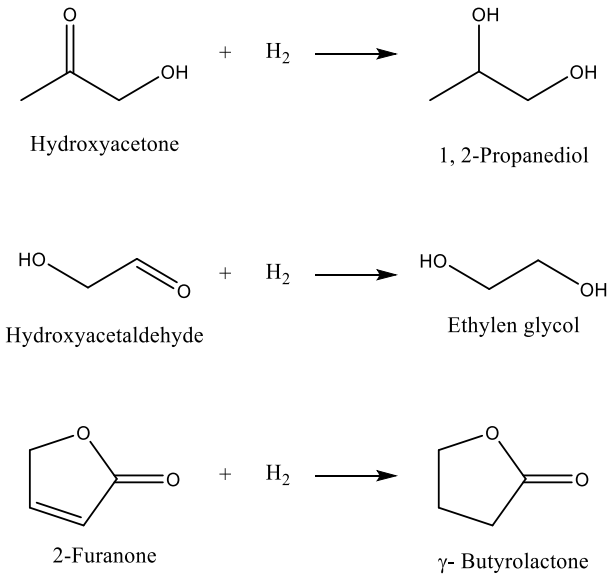

Figure 2-7. Hydrogenation of hydroxyacetone, hydroxyacetaldehyde and 2 furanone

The authors proposed different kinetics rate varying the limitation step and the possibility to have an atomic or molecular H_2 adsorption. The kinetics rates (reported in Table 2-6) hypothesized were validated experimentally confirming that the reactions are surface-reaction limited in presence of dissociative adsorption of H_2. The equation for the kinetics rate are:

$$r = \frac{k_3\sqrt{K_{H_2}C_{H_2}}K_BC_B}{\left(1+\sqrt{K_{H_2}C_{H_2}}+K_BC_B\right)^2} \quad 2\text{-}9$$

$$r = \frac{k_3K_{H_2}K_BC_{H_2}C_B}{\left(1+\sqrt{K_{H_2}C_{H_2}}+K_BC_B\right)^3} \quad 2\text{-}10$$

Table 2-6. Kinetic parameters [32]

	Unit	Hydroxycetone	Hydroxyacetaldehyde	2 Furanone
k^{o}_{3}	kmol/ kg min	$1.3\cdot10^{12}$	$2.9\cdot10^{14}$	$6.2\cdot10^{2}$
E_a	kJ/mol	71	89.5	22.1
$K^{o}_{H_2}$	m^3/kmol	$5.5\cdot10^{4}$	$3.2\cdot10^{7}$	5.7
ΔH_{H_2}	kJ/mol	30.7	45.7	2.1
K^{o}_{B}	m^3/kmol	30.3	$1.2\cdot10^{4}$	47.6
ΔH_B	kJ/mol	4.8	26.4	13.1

Zhang et al. [81, 82] described the reaction kinetics by dividing the products as: Light oil ranged from 36 °C to 250 °C, heavy oil from 250 ºC to 450 ºC, vapours, water and coke.

They assumed a series of parallel reactions with a first-order kinetics in presence of CoMo / γAl_2O_3 catalyst. The kinetic data are shown in Table 2-7.

$$Bio - oil \underset{k_1}{\rightarrow} light\ fraction\ oil \quad 2\text{-}11$$

$$Bio - oil \underset{k_2}{\rightarrow} heavy\ fraction\ oil \underset{k_4}{\rightarrow} light\ fraction\ oil \quad 2\text{-}12$$

$$Bio - oil \underset{k_2}{\rightarrow} heavy\ fraction\ oil \underset{k_5}{\rightarrow} gas + water + char \quad 2\text{-}13$$

$$Bio - oil \underset{k_3}{\rightarrow} gas + water + char \quad 2\text{-}14$$

Table 2-7. Kinetic data [34,35]

	1	2	3	4	5
K_{i0} [min^{-1}]	$2.15 \cdot 10^3$	$2.20 \cdot 10^4$	$9.57 \cdot 10^2$	$2.51 \cdot 10^5$	4.28
Ea [kJ/mol]	64.81	75.44	66.28	97.12	27.88
$k_i = k_{i0} \exp(-E_a/RT)$					

Also Yu-Hwa et al. [83] divided the bio-oil in six groups (heavy non volatiles, light non-volatile, phenols, aromatics, alkanes, Coke + H_2O + Outlet Gases) and using 3 different catalysts ($Pt/Al_2O_3/SiO_2$, CoMo/γ-Al_2O_3 and Ni-W/ γ-Al_2O_3) the hydrogenation of bio-oil was studied. Moreover, the authors proposed a reaction pathway by series-parallels of first-order reactions.

$$heavy\ nonvolatiles \underset{k_1}{\rightarrow} light\ nonvolatiles \underset{k_3}{\rightarrow} phenols \quad 2\text{-}15$$

$$heavy\ nonvolatiles \underset{k_2}{\rightarrow} \text{aromatics} + \text{alkanes} \quad 2\text{-}16$$

$$phenols \underset{k_4}{\rightarrow} aromatics + alkanes \underset{k_5}{\rightarrow} Coke + H_2O + outlet\ gases \quad 2\text{-}17$$

k_i is a kinetic constant and depend of the temperature and pressure by:

$$k_i = k_{i0} P^{n_i} \exp\left(-\frac{Ea}{RT}\right) \quad 2\text{-}18$$

Where k_{i0} and n_i are the parameters of the reaction and the catalysts used (Table 2-8).

Table 2-8. Kinetic parameters [37]

	Unit	$Pt/Al_2O_3/SiO_2$	$CoMo/\gamma\text{-}Al_2O_3$	$Ni\text{-}W/\ \gamma\text{-}Al_2O_3$
n_1		1.35	0.83	0.16
n_2		0.40	0.71	0.17
n_3	-	1.58	0.93	0.31
n_4		1.08	0.73	0.25
n_5		-0.64	1.34	0.30
k_{10}		$1.85 \cdot 10^{-2}$	1.88	2060
K_{20}		2000	507	139860
k_{30}	$min^{-1}kPa^{-ni}$	$4.93 \cdot 10^{-3}$	1.67	1837
k_{40}		$5.27 \cdot 10^{-2}$	4.12	198.7
k_{50}		1330425	$2.36 \cdot 10^{-3}$	1078
Ea_1		74.0	74.5	82.2
Ea_2		91.8	96.4	105.8
Ea_3	kJ/ mol	80.6	81.8	90.4
Ea_4		62.3	69.0	68.4
Ea_5		69.6	55.8	74.9

2.4.3 Industrial reactors for hydrogenation

The hydrogenation reaction is largely use in refinery to convert the heavy oil fraction into light hydrocarbons, the existing process have been based on the following reactors: fixed beds (FBRs), moving beds (MBRs) and expanded or ebullated beds (EBRs), reported in Figure 2-8. The main different among the reactors involve on the transport phenomena and some technical details.

The FBRs are the mainly reactor systems used commercially and used for hydrogenating light hydrocarbon mixture such as naphtha and middle distillate. The FBRs are designed for operating in adiabatic condition. The reactor is divided into three catalytic zones separated to an inert material (ceramic balls), the liquid and gas stream through the first catalytic bed. The output fed exchange heat by the inert bed and subsequently quenched adding fresh gas reactant and then fed inlet of the second catalytic bed. The output of the second reactor is cooled again by the inert bed and by quenching.

MBR and EBR reactors have been used to hydrogenate feeds such as vacuum residue.

In a MBR the fresh catalyst is fed from the top and trough the reactor, while the reactant stream is fed from the bottom. Afterthought, the products leaves the MBR and the deactivated catalyst is send to the regenerator reactor where the coke deposition is burned and the activated catalyst returns to MBR.

The EBRs are used for heavy feeds with a large amount of metals and asphaltenes, where the liquid and gas streams are fed from bottom expanding and mixing the catalyst bed, reducing pressure drop effect. In output of the catalytic bed the hydrogen is recycled not reacted is recycles, while the liquid products are recovered by a flash unit.

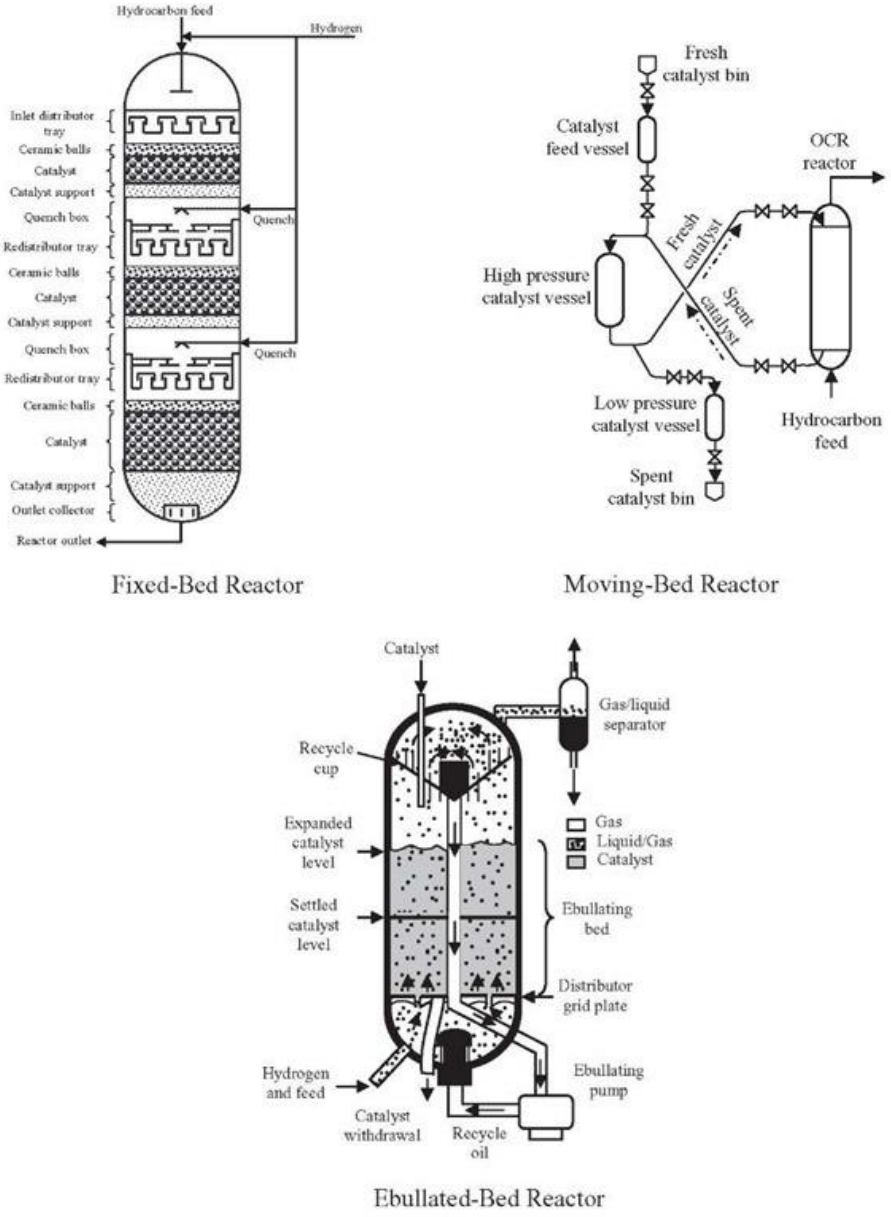

Figure 2-8. Industrial reactor for hydrogenation reaction[84]

2.5 Membrane technology

A membrane reactor (MR) is an operation unit to produce new species by chemical reaction and separation process in a single equipment. The use of MRs can reduce the process footprint, since the plant will be more compact and can result in lower investment costs, improving the economics of the process. The MRs can be used for different specific functions such as extractor, removing selectively one or more reaction products. The presence of the membrane, in an equilibrium reaction, increases the conversion respect to a traditional reactor under the same operating conditions[85, 86].

The MRs can better control the reactants contact (by enhanced H_2 delivery to the active catalysts sites), reducing the undesirable reactions and increasing the desirable products. The MRs can be used to dissipate the heat in exothermic reaction using an endothermic reaction at the other side of the membrane, such as, for example, in the hydrogenation / dehydrogenation [87-89].

The membrane can be classified according to its nature, geometry and the type of transport mechanism. The membrane can also be classified based on their porosity as follow: (i) macroporous membranes, with a pore size greater than 50 nm; (ii) mesoporous membranes, with a pore size between 2 nm and 50 nm; (iii) microporous membranes, with smaller pore size of 2 nm; (iv) dense membranes.

From the point of view of the transport mechanism, this classification correlate the membrane and gas characteristics. For example, in the dense membrane, the transport mechanism is by solution-diffusion, while in porous membranes different types of permeation mechanisms, often competitive with each other, control the gas separation[90]:

Poiseuille mechanism. The Poiseuille mechannism takes place when the average pore diameter of the membrane is much larger than the mean free path of the molecules; by doing so, the conflict of the various molecules are more frequent than those between molecules and porous walls:

$$J_i = -\frac{\varepsilon \cdot d_{pore}^2}{32 \cdot R \cdot T \cdot \eta \cdot \tau} p \nabla p \qquad 2\text{-}19$$

Where ε = membrane void fraction, d_{pore} = pore diameter, R = universal constant, T = temperature, P = pressure, τ = tortuosity ∇p = pressure gradient and η= viscosity.

Knudsen diffusion mechanism. When the pores diameters are comparable or less than the mean free path, the quantum momentum is transferred by the collisions between the

molecules and the wall of the pores. Applying the kinetic theory of gases to a single straight and cylindrical pore, the Knudsen diffusion coefficient can be defined as:

$$\mathcal{D}_{i,K} = \frac{\varepsilon \cdot d_{pore}}{3 \cdot \tau} \sqrt{\frac{8 \cdot R \cdot T}{\pi \cdot MW_i}} \qquad 2\text{-}20$$

Where ε = membrane void fraction, d_{pore} = pore diameter, R = universal constant, T = temperature, τ = tortuosity, η= viscosity and MW molecular weight.

Solution-diffusion mechanism. The transport mechanism in dense membranes is a solution-diffusion mechanism. An example is illustrated in Figure 2-9, where the H_2 diffusion through the membrane is a very complex process, which consists in:

(i) H_2 molecules adsorption from the side of the membrane at highest H_2 pressure;

(ii) dissociation of these molecules on the same surface;

(iii) reversible dissociative chemisorption of H_2 molecules;

(vi) reversible dissolution of atomic H_2 in the metal lattice of the membrane;

(v) diffusion into the metal of atomic H_2 proceeds from the side of the membrane at a higher H_2 pressure to the side at lower pressure;

(vi) re-association and atomic H_2 recombination;

(vii) Molecular H_2 desorption from the surface to the bulk membrane.

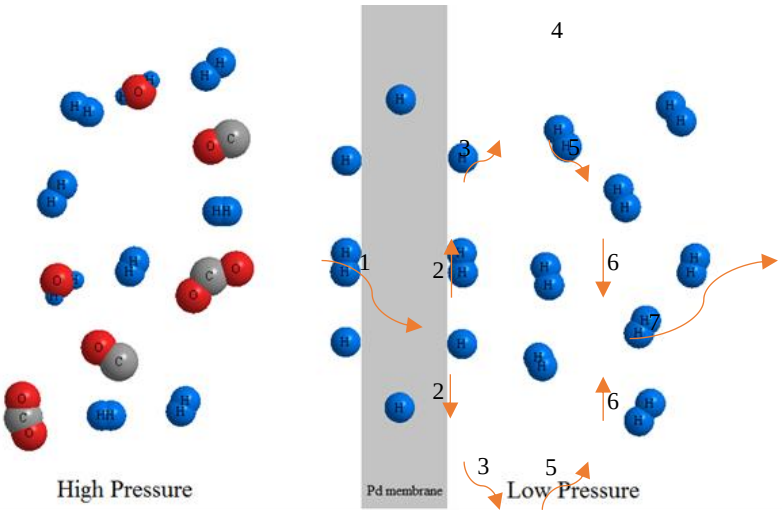

Figure 2-9. Solution-diffusion mechanism[91]

H_2 transport through the membrane is described by Fick's equation:

$$J_{H_2} = Pe_{H_2} \frac{\left(p_{H_2,1}^{n} - p_{H_2,2}^{n}\right)}{\delta} \qquad 2\text{-}21$$

Where Pe_{H2} is the H_2 permeability through the membrane, n represents the dependence of H_2 flux to H_2 partial pressure, this parameter can vary between 0.5 and 1. When n is

equal at 0.5, the transport resistance is H_2 dissociation into the Pd layer, the becomes Sieverts-Fick law [92]:

$$J_{H_2} = Pe_{H_2} \frac{\left(p_{H_2,ret}^{0,5} - p_{H_2,perm}^{0,5}\right)}{\delta} \quad 2\text{-}22$$

Regarding the temperature influence on the H_2 permeability, the relationship between the permeation rate of hydrogen and the temperature can be described by the Arrhenius law:

$$Pe_{H_2} = Pe_{H_2}^{o} exp\left(-\frac{E_a}{RT}\right) \quad 2\text{-}23$$

where Pe°H_2, Ea, R and T are pre-exponential factor, activation energy, universal gas constant and temperature.

2.5.1 Membrane reactor classification

McLeary et al.[93] classified the MRs according to their catalytic activity and membrane performance (Figure 2-10). The catalytic membrane reactor (CMR) is able to perform a permeo-selective action and to catalyse the reaction. In the CMR the membrane can be:

(i) intrinsically catalytic, given from catalytic sites;

(ii) presence of two layers, the first catalytically active and a subsequent permeable-selective layer;

(iii) the catalyst can be dispersed in the membrane.

The packed bed membrane reactor (PBMR), the catalyst, in pellet or powder, is located inside and/or outside of the membrane. While the catalytic not perm-selective membrane reactor (CNMR), the membrane with catalytic capacity is unable to perform a selective separation, acting as a reaction front, facilitating stoichiometric progression of reagents. A not perm-selective membrane reactor (NMR) simply acts as a reagent dispenser.

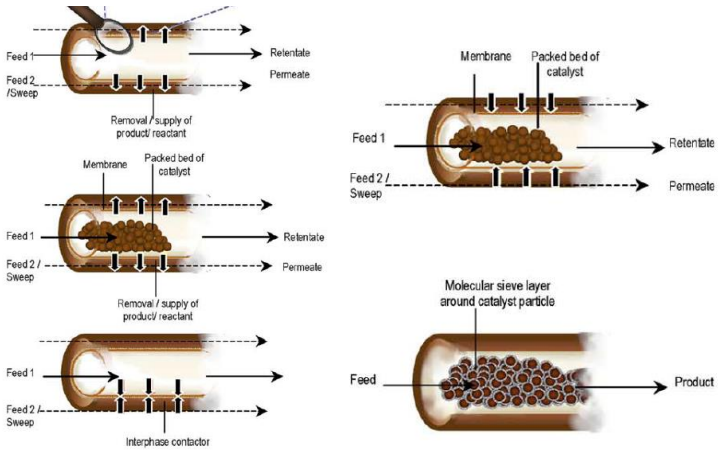

Figure 2-10. Membrane classification[93]

2.5.2 Membrane reactor and hydrogenation of bio-oil and its model compounds

The main disadvantage of hydrogenation reaction is represented by mass transport limitation, because the reaction takes place in contact with the gaseous, liquid and solid phase. The system has to have a high operating pressure, improving the gas solubility into the liquid system and high temperature to advantage the kinetic, but in the same time, the H_2 solubility decreases at under those conditions. One of the features of the MRs is to act as a contactor between the three phases. Furthermore, the membrane can have catalytic activity chancing the product distribution as reported by Miu et al.[94], who compared packed bed MR and catalytic MR for the hydrogenation of nitrobenzene in presence of Pd/γ-Al_2O_3 catalyst. The CMMR showed best performance in term of conversion and catalytic stability (~85% for 10 hours) as shown in Figure 10.

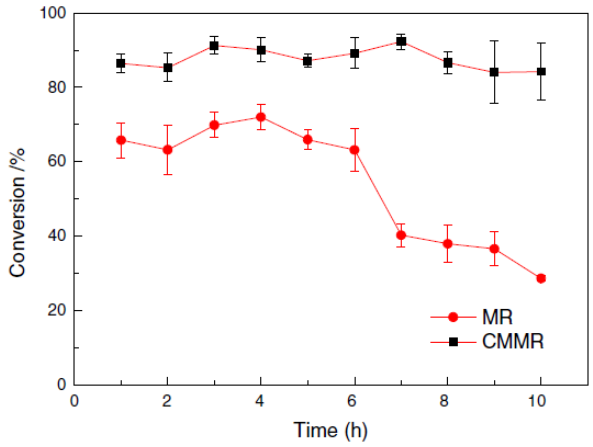

Figure 2-11. Comparison between CMR and PBMR [94]

Liu et al.[95] studied the selectivity hydrogenation of butadiene in butene at 40 ºC and 10 bar by CMRs, obtaining a butene selectivity higher than 99% and butadiene concentration in the output stream lower than 10 ppm. Other example of hydrogenation reaction are reported in Table 2-9. Despite the increasing interest in catalytic membranes, the HDO of bio oil in MR is a novelty, since in literature there is only one article[96] available on the topic, where the authors used a MR for the hydrogenation of levulinic acid (compound present in bio-oils) by a porous expanded polytetrafluoroethylene (ePTFE) membrane with Ru catalyst particles. Also, the same membranes were coated only in one side with a dense Matrimid layer, which was used to control the hydrogen flux through the membrane. The reaction was studied in a temperature and reaction pressure between 40-90°C and 0.7 and 5.6 bar, respectively. Furthermore, the authors compared the result obtained with a PBR as shown in Figure 2-12, where the kinetic rate is presented as ratio of gamma-valerolactone product (g/h) over grams of Ru. In particular, the MR without

the Matrimid layer obtained the best performance (4 time more than PBR) with conversion of 0.0065 %, while the MR with the control layer (Matrimid) showed a kinetic rate 2 time less than the PBR.

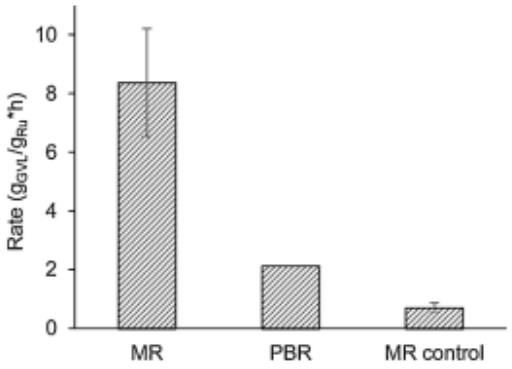

Figure 2-12. Kinetic rate of hydrogenation of levulonic acid using a MRs and PBR[96]

Analysing the membrane reactors studied in literature, part of the experimental campaign has been designed to develop a new catalytic membrane reactor, with the target to find a material compatible with the bio-oil, in term of stability. The membranes synthesised are based on polymer (PES and PEEK-WC) doped with Ru. The catalytic membranes have the task to facilitate the hydrogenation reaction, improving the surface contact among the reactants.

Table 2-9. MR for hydrogenation reaction

Hydrogenation of	catalyst	Support		Pressure [bar]	Temperature [25°C]	Ref.
3-hexyn-1-ol	Pd nanoparticles (4.6 nm)	zirconia/polyvinyl alcohol	Batch	5-10	25	[97]
Nitrite	Pd	γ-Al_2O_3	Continuous	1	25	[98]
Methylenecyclohexane (and isomerization)	Pt, Pd, Ru in γ-Al_2O_3	macroporous α-Al_2O_3	Continuous	1.5 liquid 2 gas	15-70	[99]
Methylenecyclohexane	Pd -PVDS PVP	macroporous α-Al_2O_3	Continuous		25-50	[100]*
Edible oil	Pd, Pt	porous polyamideimide (PAI)	Continuous	4	100	[101]
Nitrobenzene	Pd	zirconia/polyvinyl alcohol	Continuous	1-2	25	[102]
Nitrobenzene	Pd/γ-Al_2O_3	PDMS	Continuous	1-2	20	[94]
Butadiene	PVP-Pd, PVP-Pd, EC-Pd, AR-Pd, AR-Pd, PVP-Pd, PVP-Pd-0.5 $Co(OAc)_2$, PVP-Pd-0.5 $Co(OAc)_2$	CA, PSF, CA, CA, PSF, CA, CA, CA	Continuous	10	40	[95]**

* ceramic membrane showed a higher selectivity toward the hydrogenated product than the polymeric membrane but exhibited a lower TON (= converted moles in a second per gram of Pd) value.

**PVP-Pd-0.5 $Co(OAc)_2$ showed best performance. The presence of Co inhibited isomerization reaction

2.5.3 Recent work on technical economic assessment

The conversion of biomass in to hydrogen is largely study using different devices[103, 104], recently study estimated a cost of 1.77–2.05 per $/kg of hydrogen from the stem reforming reaction of biomass[105].

Pyrolysis is one of the most promising thermo-chemical conversion processes that converts biomass into bio-char, bio-oil and gas at temperatures close to 500˚C and in absence of oxygen. Mustapha et al.[106] compared the techno-economic feasibility of five forest-based biofuel conversion pathways (Hydrolysis and Fermentation, Mixed Alcohol synthesis, Fischer-Tropsch synthesis, Hydrothermal Liquefaction and Fast Pyrolysis) in the Nordic countries and fast pyrolysis and hydrothermal liquefaction were found to be the most cost-competitive pathways. Unrean et al. (2018) studied the TEA and environmental impact of rice husk-to-fuel conversion technologies, which suggested that hydrothermal carbonisation with palletisation could be cost-competitive with direct combustion [107]. They also highlighted that pyrolysis could be improved by exploration of process wastes for better economic benefits.

Magdeldin et al. [108] studied the TEA for a scale-up of non-catalytic hydrothermal liquefaction (HTL) plant for lignocellulose residues, with primary production of renewable liquid fuels. The authors set the operating condition of HTL reactor at 300 ºC and 210 bar, obtaining the minimum fuels price of 2.93 € gallon of gasoline equivalent, 2.46 €/kg for hydrogen and 51.4 €/MWh for biochar. Nie et a1.[108] evaluated the capital investment and operating cost for producing 105 m^3/year of biofuel from forest residues, reaching a minimum fuel selling prices (MFSP) between 0.82-0.90 $/L of gasoline equivalent. Wright et al. (2012) obtained a minimum fuel selling price (MFSP) of $2.48 per gallon from the bio-oil stabilisation and hydrotreating in a 1,440 tonnes per day plant and showed that hydrogen from bio-oil reforming resulted in lowest biofuel emissions, but is not always economical [109]. Carrasco et al. (2017) studied the TEA of converting forest residues by pyrolysis and the further bio-oil upgrading by hydro-treatment and simultaneous production of H_2 for a feed rate of 2,000 dry tonnes per day, obtaining a MFSP of $1.27 per litre [110].

Chapter 3- Methodology

This chapter summarises the materials, procedures and techniques applied to the research project, while specific techniques (or procedures) have been addressed into the relative chapters. In particular, this chapter is dived into three main sections, where the first one illustrates the protocol used for the catalysts synthesis and the description of the reaction set-up. While the procedure to develop the membrane reactor and the relative lab scale setup is summarised into the second section. At the end, the third section describes the approach used for performing the economical assessment of the hydrogenation process.

3.1 Catalyst preparation and characterisation

3.1.1 Chemicals

Furfural 99% (CAS Num. 98-01-1), furfuryl alcohol 98% (CAS Num. 98-00-0), vanillin (CAS Num.121-33-5), vanillin alcohol ≥ 98% (CAS Num. 498-00-0), D-glucose ≥ 99.5% (CAS Num. 50-99-7) sorbitol ≥ 98% (CAS Num. 50-70-4) were purchased from Sigma-Aldrich. Tetrahydrofuran for HPLC (THF, CAS Num. 109-99-9), di-*n*-butyl ether >99% (DBE, CAS Num. 142-96-1) Fisher Scientific.

The WBO was prepared from pine wood bio-oil (density: 1.17g/ml), supplied from Biomass Technology Group (BTG, Enschede, NL) [111], by adding water with weight ratio of 2/1 (bio-oil/ water). The mixture was then left to decant for 8 h and centrifuged for 3 h a 3500 rpm for separating the water bio-oil fraction.

3.1.2 Catalysts synthesis

Support synthesis: $Zr(OH)_4$ was prepared by the dropwise addition of required amount of aqueous $ZrOCl_2 \cdot 8H_2O$ (Aldrich, 99.5%) to water (100 ml). During addition, the pH was kept constant at 8.5 by the dropwise addition of an aqueous solution of ammonia (5 M). After addition, the suspension was aged 20 hours at 90 °C. The resulting $Zr(OH)_4$ was isolated by filtration and subsequently calcined in flowing air (30 mL/min) at 500 °C for 3 h to obtain the ZrO_2 support[112].

Catalyst synthesis: an incipient wetness impregnation method was applied to prepare the catalysts. The proper amount of an aqueous solution of the metal precursor ($PdCl_2$, $FeN_3O_9 \cdot 9H_2O$ or $Cu(NO_3)_2 \cdot 3H_2O$) were added to the ZrO_2 support to obtain the desired metal content on the support (5 wt% for Cu and Fe, 1 wt % for Pd). The catalysts were

dried in an oven at 110 °C for 15 h and calcined in flowing air (30 mL/min) at 500 °C for 3 h.

3.1.3 Catalysts characterisation

The metal amount on the catalyst was determined by Atomic Absorption Spectroscopy (AAS) using a Perkin-Elmer Analyst 100. The dried samples (50 mg) were dissolved in 5 mL of aqua regia under reflux for 5 h prior to analysis. TEM analysis were carried out using a CM12 microscope (Philips), operating at 120 keV. The imagines were made by a slow scanning CCD camera. The samples were prepared by adding a drop of a suspension of the catalyst in ethanol onto a carbon coated 400 mesh copper grids.

XRD was used to determine the crystalline structure and composition of the catalyst. The analyses was performed using a Bruker Nonius X8-Apex2 CCD diffractometer equipped with an Oxford Cryosystems Cryostream (typically operating at 100 K), an X-ray source with a Cu anode working at 40 kV and 40 mA and an energy-dispersive one-dimensional detector.

Moreover, Sherrer`s equation was used to calculate the zirconia support particles size. The instrumental line broadening calculated using a diffractogram from a well crystalline sample of Al_2O_3 with a 0.03 slit was accounted in the calculation and it was also assumed that the crystals had a spherical shape (k = 0.89 ~0.9).

TPR measurements were carried out using a home-made device. The catalysts (100 mg) were heated with a temperature rate of 10 °C/min from 25 °C to 900 °C in a 5% H_2/He flow (40 mL/min). The effluent gases were analysed by a TCD detector. Nitrogen physisorption analyses were performed to determine specific surface area and porosity of the samples. Surface areas and pore size distributions were obtained from N_2 adsorption/desorption isotherms obtained at -196 °C using a Tristal II Plus Micromeritics analyser.

The surface area was calculated from the N_2 adsorption isotherm using the BET equation, and pore size distribution was determined by the BJH method[113]. Total pore volume was taken at p/p0 = 0.99. TPO was applied to characterise the carbon species on spent catalysts. TPO measurements were carried out using a home-made device. Catalyst samples (100 mg) were heated with a temperature rate of 10 °C/min from 25 °C to 600 °C in a 5%O_2/He flow (40 mL/min). The surface acidity of the catalysts was determined using NH_3-TPD measurements on an AutoChem II system (Micromeritic, USA) and the

total acidity quantified. The samples were pre-treated at 600 °C for 1 h in presence of He (50 mL/ min), then cooled to 100 °C.

Subsequently, NH_3/He (1/99, 50 mL/min) was passed over the sample for 1 h to ensure acid site saturation. Finally, the sample was purged with He (50 ml min^{-1}) to remove the NH_3 adsorbed, using a temperature ramp of 10 °C/ min to 600°C. Weak and strong acidity was calculated by deconvolution method using Origin software. CO_2-TPD was run using a TA Q500. Firstly, the catalysts were heated in helium at 50 °C/min up to a final temperature of 550 °C and held at 550C for 20 minutes. CO_2 adsorption was then studied at 60 °C for 30 minutes, while CO_2 desorption was evaluated increasing the temperature to 600 °C at a rate of 10 °C/min.

XPS analysis were carried out using a Scienta XPS with Al Kα (1486.6 eV) monochromatized ($\Delta\varepsilon$ < 300 meV) source. The powder samples were mounted on the sample stub using conducting, double sided sticky tape and immediately transferred to the vacuum system.

3.1.4 Catalysts testing protocols

The hydrogenation reactions were carried out in a batch reactor (stainless-steel, 50 mL, Amar Equipments LTD, model no. 1233). The reactor was equipped with a heating jacket to allow operation at constant temperature. The reactor was loaded with 200 mg of catalyst and 30 mL of an aqueous solution of the model component (0.519, 0.204 and 1.07 mol/L for furfural, vanillin and glucose, respectively) and subsequently pressurised using H_2. All reactions were carried out at 100 °C, 50 bar, and under continuous stirring (600 rpm). Before each experiment, the catalyst was activated overnight in the presence of H_2 at 20 bar at 100 ºC (PdFe and Pd), 200 ºC (PdCu and Cu) or 300 ºC (Fe). The reduction temperatures were determined by TPD analyses. To evaluate the performance of the catalysts, the conversion and selectivity were calculated for the *i*- model compound as follows:

$$\text{Conversion}_i = \left.\frac{\text{mole reacted}}{\text{initial mole}}\right|_i 100 = [\%] \qquad 3\text{-}1$$

$$\text{Selectivity}_j = \frac{\text{mole produced}_j}{\text{mole reacted}_i}\left|\frac{\nu_i}{\nu_j}\right| 100 = [\%] \qquad 3\text{-}2$$

Where, ν_i and ν_j represent the stoichiometric coefficients of i- and j- compounds, and the moles of metal on the catalyst are the moles of Cu, Pd and Fe for the monometallic catalysts and the sum of the moles of metals for the bimetallic ones.

3.1.5 Product characterisation

The glucose concentration was determined by HPLC using a Hewlett Packard 1050 system equipped with a Bio-Rad Organic Acid column (Aminex HPX-87H), and a Waters 410 differential refractometer. Aqueous sulphuric acid (5 mmol/L) was used as the mobile phase (0.55 mL/min). The column was maintained at 60º C. Furfural and vanillin hydrogenation products were analysed by a Shimadzu GC-2010A gas chromatograph equipped with a FID detector using a CPWAX 57-CB column (25 m × 0.2 mm × 0.2μm). While for characterisation of WBO fraction different techniques have been used:

Gas chromatography (GC)

GC−TCD (HP5890 Series II) was used to analyse the gas composition resulting from the WBO experiments. The samples in presence of carrier gas (He) were fed at the injector, set at 150 °C, and separated with CP Porabond Q (50 m × 0.5 mm, with a film thickness of 10 μm) and CP-Molsieve 5A (25 m × 0.53 mm, with a film thickness of 50 μm) columns. The columns were maintained at 40 °C for 2 min, then the temperature was increased to 90 °C at 20 °C/min and kept at this temperature for 2 min. The gas phase was quantified using a reference gas (54.40% H_2, 20.70% CH_4, 2.99% CO, 17.90 % CO_2, 0.51% ethylene, 1.50% ethane, 0.51% propylene and 1.50% propane).

Two-dimensional chromatography (GCxGC)

The GCxGC technique was used to identify the chemical functional groups (e.g. ketones, guaicols, aromatics, etc.) and quantify them using an internal standard.

The samples were dried with Na_2SO_4 and diluted in a THF solution containing 500 ppm DBE, as internal standard, with a mass ratio WBO/THF= 1/1.

The analysis was performed by Trace 2D-GC system from Interscience, the auto-sampler injected the solution in presence of a carrier gas (Helium at 0.6 mL/ min) in two columns (30 m x 0.25 mm-i.d. and 0.25 μm-film sol–gel capillary column connected to a 148 cm x 0.1 mm-i.d. and 0.1 μm-film Restek 1701 column) connected in series through a dual-jet modulator (modulation time 6 s) cooled by cryogenic trap. The capillary columns placed inside an oven were maintained a 40 ºC for 5 min and heated with a rate of 3 ºC/ min until 250 ºC. At the exit of the second column, the compounds were identified by flame ionisation detector (FID).

The GCxGC chromatogram of WBO fraction is represented in Figure 3-1, where the X- and Y-axes represent the retention time of the first and second column, respectively. The

compounds were classified according their functional group and quantified following the method developed by Kloekhorst et al.[114].

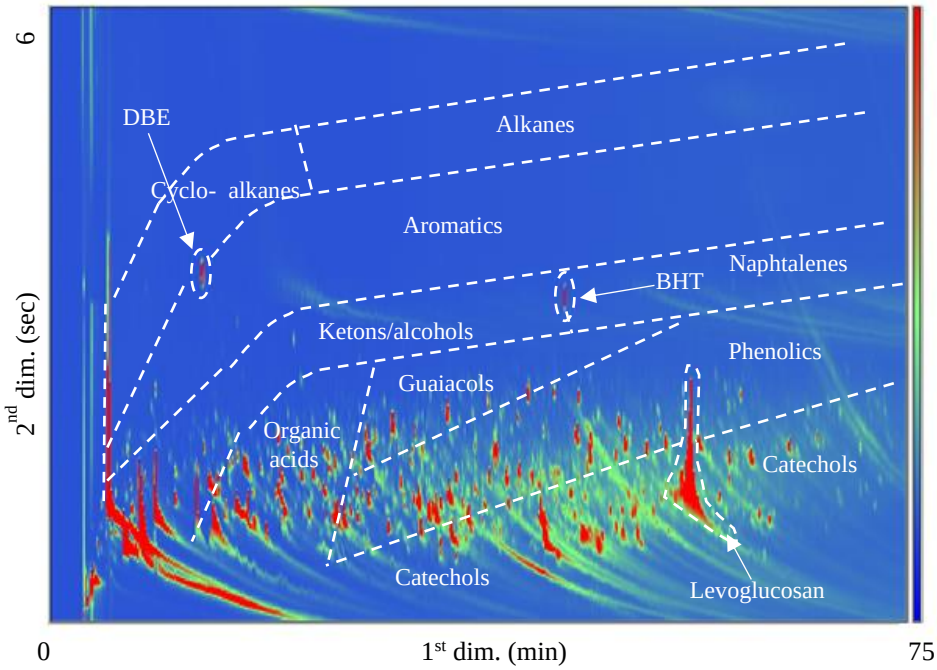

Figure 3-1. WBO fraction GCxGC analysis

Gas chromatography-mass spectrometry (GC-MS)

GC-MS analyses were performed on a HewlettPackard 6890 gas chromatograph combined with a Quadrupole Hewlett-Packard 5973 MSD. The samples were injected at 280 °C in presence of carrier gas (He, 1 mL /min), separated in a chromatographic column, Restek Rxi-5Sil capillary (30 m length, internal diameter of 0.25 mm; 0.25 µm thickness of stationary phase). placed in oven at 40 °C for 5 min, then the temperature was increased to 250 °C at a rate of 3 °C/ min, and finally held at 250 °C for 10 min. The spectrums were analysed by NIST MS Search program (Version 2.0) operating on the NIST/EPA/NIH Mass Spectral Database 2011 (NIST 11). The compounds detected by GC-MS analysis for WBO fraction are summarised in Appendix B.

Gel permeation chromatography (GPC)

The GPC analysis was performed using an Agilent HPLC 1100 system with three columns in series of mixed type E (length 300 mm, i.d. 7.5 mm). The GPC was carried out to identify the molecular weight distribution of the WBO samples, detecting the large MW compounds not recognised by GC-MS and GC-GC techniques. The samples was

prepared adding few drops of toluene as a marker. Average molecular weight calculations were performed using the PSS WinGPC Unity software from Polymer Standards Service.

Total organic carbon (TOC)

The TOC concentration of the WBO samples were analysed using a Shimadzu TOC-VCSH, diluting the WBO with water (2 drops of sample in 25mL of distillate water), in order to not exceed a TOC concentration of 0.01 mg/L.

3.2 Membrane preparation and characterisation

The membranes have been synthesized with different technique, to make clearer the thesis each membrane preparation have been reported into the specific chapter. While, the characterisation techniques have been described below.

3.2.1 Coating presence

The presence of the acrylic acid polymerized onto the membrane surface, after the UV-grafting, was identified by Frontier IR single- range system (Perkin Elmer).

Scanning Electron Mycroscopy (SEM)- The membrane morphology was observed by Scanning Electron Mycroscopy (Carl Zeiss SIGMA HD VP), studying the top layer and the cross section; the latter observed cutting the semple in liquid nitrogen. The samples were prepared for SEM analysis coating the one layer with carbon.

Ru content- The Ru quantification was evaluated by inductively coupled plasma optical emission spectrometry (ICP –EOS) analysis. The samples were dissolved in dimethyl formamide. The solvent was evaporated and added an acid solution of aqua regia (HNO_3 wt. 70% / HCl 36% = 3/1 v/v). The instrument (Perkin Elmer Optima 5300DV) dissociated the sample into atoms or ions, by ICP source, emitting them to radiation at a determinate wavelength, which are specific for each atom/ion.

3.2.2 Porosity

Membrane porosity was determinate by a gravimetric method, as reported in literature[115]. Dry membrane samples were weighed and impregnated in kerosene for 24h obtaining a completely filling of the voids. The total volume (V_{Tot}) is equal at:

$$V_{Tot} = V_m + V_v \qquad 3\text{-}3$$

Where V_m and V_v are membrane and void volume. Dividing for V_{Tot}, is possible to define the porosity, ε:

$$\varepsilon = \frac{V_{Tot} - V_m}{V_{Tot}} \qquad 3\text{-}4$$

Filling the void with kerosene the total volume will be the sum of volume of membrane and kerosene. By the density of each compound is possible to rewrite the eq. (0-2) as:

$$\varepsilon = \frac{(W_w - W_D)/\rho_m}{(W_w - W_D)/\rho_m + (W_D/\rho_K)} \quad 3\text{-}5$$

Where W_W, W_D, ρ_W and ρ_K are the weight of membrane dried and wet (filled with kerosene), density of membrane (1,37gr/cm^3) and kerosene (0.82 gr/cm^3) respectively.

3.2.3 Bubble point and pore size diameter

Bubble point, pore size distribution and diameter were determinate by PMI Capillary Flow Porometer (CFP1500 AEXL, Porous Material Inc, USA). Membranes sample were fully wetted with a solution of perfluorocompound Fluorinert-FC40 (16dynes/cm) for 24 hours[116]. The wet membrane allocated into a module at controlled N_2 pressurization; the method is based on gas permeation; at minimum Δp the N_2 starts to permeation through the membrane, emptying the pores from the liquid until full expulsion. The operating mode used was wet-up/dry-up and by the software Capwin the average pore size diameter is calculated via the interaction between the wet curve and the semidry curve, the last one obtained using the half slope of dry curve. By the Laplace equation [117] the pore size is possible to determinate:

$$\Delta p = \frac{2\gamma \cos\theta}{r} \quad 3\text{-}6$$

Where Δp, γ, θ and r different of pressure, surface tension, contact angle (assumed equal at 0º) and pore radius.

3.2.4 Contact angle

The contact angle measures the surface interaction with three phase system (membrane/ water /air) [118]. Measurements were performed using ultrapure water (5µL) and estimating the angle between the membrane surface and the droplet; a low contact angle value (<90º) denotes a hydrophilic nature of the membrane. At the contrary, a high contact angle (>90º) indicates a hydrophobic nature. The contact angle was determinate by CAM200 (KSV Instrument LTD, Finland).

3.2.5 Mechanical tests

The tensile test measures the resistance of a material to a static or slowly applied force. The test was carried by ZWICK/ROELL testing machine (model Z 2.5) gripping opposite ends of the samples, with initial length 30 mm, and stretched at a constant controlled tensile speed until a predetermined stress [119].

3.2.6 Lab scale plant and data evaluation

The experimental setup for the catalytic hydrogenation tests is shown in Figure 3-2. It consists of a catalytic reactor module, gas supply lines and a condensation set-up. The gas streams were controlled by Brooks mass flow controllers (MF-100 and MF-101), while the bio oil (or WBO, IBO) was fed by Eldex pump (P-100). Liquid and gas feeds were pre-heated before their entrance in the membrane reactor. The membrane reactor consists of a flat stainless steel module, where the catalytic membrane (120 x 60 mm) was allocated, the temperature was maintained constant by a temperature controller (TIC-2) connected with a heating tape. The pressure into the 2 membrane reactor zones (gas and liquid zones) were controlled by back-pressure regulators (BP-100 and BP-101). The output streams from the membrane reactor where passed through an ice trap system (S-100 and S-101), where the liquid phases were collected and then stored for further analysis.

After each reaction test the catalytic membrane was regenerated with a flow of H_2 and N_2, respectively 0.8 mL/min and 2.2 mL/min for 8 hours.

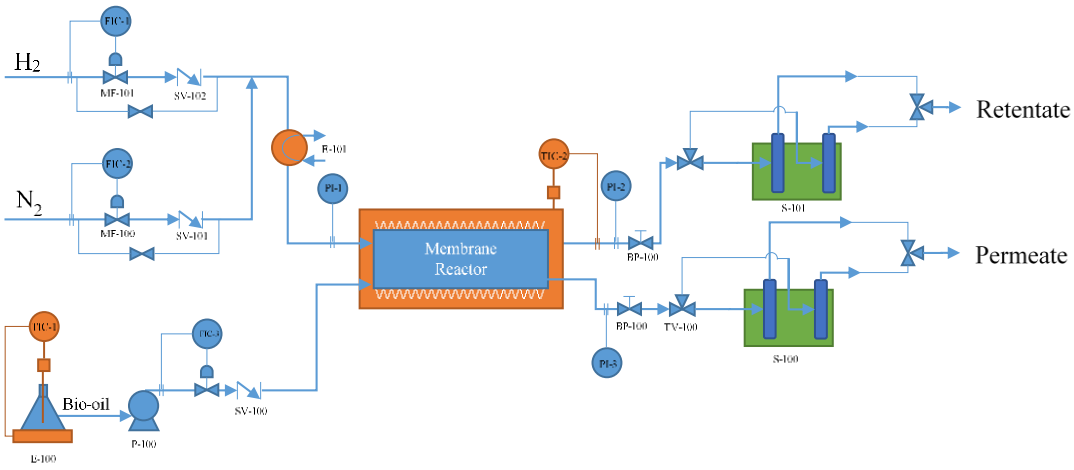

Figure 3-2. Lab-scale plant

3.2.7 Membrane reactor design

The membrane was placed inside a stainless steel module by means of a square steel gasket and one of PTFE to avoid the membrane to move. Two plates, provided with screws, allows the closure of the module ensuring the seal, which causes the expansion of the PTFE gasket that seals the two zones of the module. The module is schematised in Figure 3-3, where the catalytic membrane divides the intern reactor volume into two

zones, the liquid and phase zone. The two phases diffuse through the membrane reaching the catalytic layer where they react.

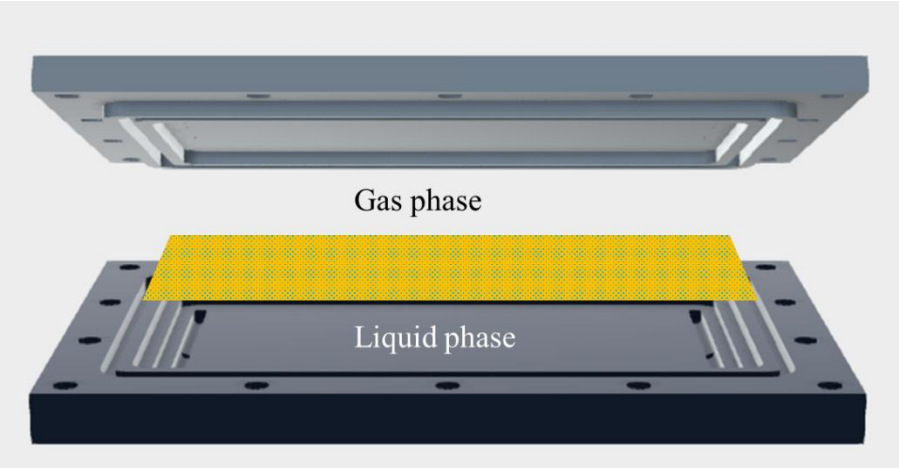

Figure 3-3. Membrane reactor module

3.3 Techno-economic assessment

The techno-economic assessment has been run using the software Aspen Plus for designing the relative operation units (reactors, compressors, heat exchangers, etc…), to calculate the project parameters for each unit and the relative costs.

The software has been able to calculate the chemical and physical proprieties of all the compounds by non-random two-liquid (NRT) model. While, the units have been sized by energy and material balance and applying the equilibrium (physical and chemical). After that, the TEA has been evaluated.

The TEA followed the heuristic method proposed by Douglas et al.[120], including the direct costs (equipment costs) and indirect costs (engineering, supervision), the working capital (funds required to operate the plant, pay the salaries etc.) and the cost of the land. The fixed capital investment (FCI) was obtained by the following equation:

$$FCI = direct\ cost + indirect\ cost \quad (3\text{-}7)$$

Direct cost is the sum of onsite cost (all reactors total costs) and offsite (main and auxiliary buildings, other equipment like electrical, plumbing, alarms, security etc.). In this simulation, the offsite cost was assumed at 20% of the onsite cost, because most reactors costing already include these costs (pyrolysis reactor, hydro-treater). This hypothesis led to the final direct cost:

$$Direct\ cost = 1.2 \cdot \sum Equipment\ cost \quad (3\text{-}8)$$

After that, the indirect costs (sum of the owner's costs such as engineering, supervision and construction expenses and the contingencies) were calculated by:

$$Owner's\ costs = 0.05 \cdot direct\ cost \quad (3\text{-}9)$$

$$Contingencies = 0.20 \cdot direct\ cost \quad (3\text{-}10)$$

(Values are approximations usually used for large-scale plants)

$$Indirect\ cost = Owner's\ costs + contingencies \quad (3\text{-}11)$$

$$Indirect\ cost = 0.25 \cdot direct\ cost \quad (3\text{-}12)$$

The working capital needed to operate the plant was estimated at 15% of the fixed capital investment (FCI). The land cost was estimated at 6% of the FCI [121]. Based on this, the total project investment was calculated with the following equation:

$$Total\ project\ investment = FCI + Working\ capital + Land \quad (3\text{-}13)$$

The annual operating costs are the costs associated with the production of the bio-fuel, such as feedstock (algae), the hydrogen purchased for hydrotreating, replacement of catalysts, all utilities used to cool or heat the reactor, electricity to pump air in the reactors, salaries, fixed charges and plant overhead. These costs were divided in manufacturing costs and general expenses (SARE) like the catalyst replacement:

$$Operating\ cost = Manufacturing + SARE \quad (3\text{-}14)$$

The manufacturing costs were calculated as follows:

$$Manufacturing\ cost = direct\ prod\ costs + fixed\ charges + plant\ overhead \quad (3\text{-}15)$$

Where the fixed charges include local taxes (~1-4% FCI), rents (~10% price of land and building), interest (0.7% TCI) and insurances (~0.4-1% FCI). For this study, the interests were assumed zero, the venture has been financed entirely from the company, and also the rents. These fixed charges were estimated at 3% of the FCI calculated, by:

$$Fixed\ charges = Tax + Insurance = 0.03 \cdot FCI \quad (3\text{-}16)$$

The plant overhead included seniors and director salaries, supervision and maintenance as follows:

$$Plant\ overhead = 0.72 \cdot labour + 0.024 \cdot FCI \quad (3\text{-}17)$$

Labour cost was determined by considering a plant with 250 employees paid with an annual salary of 40,000 $, leading to annual cost of 10 MM$. The number of employee was taken by comparing the Chevron Richmond refinery capacity (240,000 barrel per day) and its number of employee (1200) with this one[32]. The direct production cost included the feedstock, utilities and other factors as follows:

$$Direct\ prod\ cost = feedstock + utilities + maintenance + operating\ supply + labour + supervision + laboratory\ charges \quad (3\text{-}18)$$

Where the annual cost of feedstock was the unit price (66 $/metric ton) multiplied by the annual flowrate of wet algae (3.46 millions of metric ton), resulting in 228.3 MM$. The maintenance and operating supply costs were calculated by:

$$Maintenance = 0.04 \cdot FCI \quad 3\text{-}19$$

$$Supply = 0.15 \cdot maintenance \quad 3\text{-}20$$

Supervision and laboratory fees were respectively estimated at 20 and 15% of the labour cost. The utility cost is the sum of all utilities used in the process (steam, electricity and cooling water). Then, the general expenses SARE was calculated. In this project SARE included the purchase of hydrogen for hydrotreating and the replacement of catalysts (for pyrolysis and hydrotreating).

$$SARE = hydrogen\ purchased + catalysts\ replacement \quad 3\text{-}21$$

The final step of the economic evaluation was to determine the cost associated with the return on investment. In this study, average return on investment was fixed at 10%, based on previous works [121-123]. The annual cost of the return on investment is obtained by multiplying the rate of return by the total project investment (TPI):

$$Annual\ return\ on\ inv = 0.10 \cdot Total\ project\ investment \quad 3\text{-}22$$

Afterwards, the total operating cost was calculated with the following equation:

$$Total\ operating\ cost = Manufacturing + SARE + Return\ on\ investment \quad 3\text{-}23$$

While, specific parameters are going to discuss into the relative chapters.

Chapter 4- Bimetallic catalysts for biobased aldehyde hydrogenations

This chapter is under review on ACS Sustainable Chemistry & Engineering as: G. Bagnato, M. Signoretto, C. Pizzolitto, F. Menegazzo, X. Xi, G. ten Brink, B. Kooi, H. J. Heeres, A. Sanna, Bimetallic catalysts for mono-alcohols production by biobased aldehyde hydrogenation.

4.1 Abstract

The first experimental approach was using a batch reactor, where a series of mono- and bi-metallic metal catalyst (Pd, Cu, Fe, PdCu, PdFe) supported on ZrO_2 (6-8 μm) were synthesised and tested for the hydrogenation of bio-oil model compounds (furfural, vanillin, glucose) under 50 bar H_2 at 100°C. The catalysts were fully characterised and their properties related to their catalytic activity.

The bi-metallic PdFe and PdCu displayed enhanced catalytic performance compared to the monometallic catalyst for aldehyde hydrogenations (furfural, vanillin, glucose). For the best catalyst, 98% vanillin alcohol (VA) and 65.5% furfuryl alcohol (FA) yield were obtained for 80 min batch-times. PdFe showed a high selectivity towards sorbitol (74%) from glucose, though at low conversion (20%).

Overall, we have demonstrated that bimetallic Fe and Cu based catalysts promoted by Pd show significantly better performance for the hydrogenation for bio-oil model compounds than the corresponding monometallic ones. The better performance of the Pd doped Fe/Cu catalysts is most likely due to the presence of smaller and better dispersed Pd nanoparticles (TEM) and their lower acidity (~90 μmol/g cat) than for the corresponding monometallic ones (~ 167 μmol/g cat).

4.2 Introduction

Fast pyrolysis of biomass to bio-oil is an attractive technology due to its low environmental impact, scalability and cost-competitiveness. Bio-oil is a complex mixture of oxygenates including low molecular weight compounds like acids, alcohols, sugars, aldehydes, esters, ketones, phenols, as well as a range of higher molecular weight compounds[124]. The current manufacturing costs are estimated at about $300/t [111], which is higher than for typical fossil based energy carriers. As such, diversification routes towards high-value chemicals is highly desired. Bio-oil contains a large number of potential valuable compounds, such as furfural, vanillin and glucose, which can be

separated from the bio-oil and converted to valuable added-value chemicals by hydrogenation. For example, Yang *et al.*[125] showed that 70% of the furfural could be isolated from bio-oil by means of resin adsorption, while Gomes and Rodrigues[126] recovered 96% of vanillin from lignin derived bio-oil using chromatographic adsorption at basic conditions.

The selective hydrogenation of the carbonyl bond of (unsaturated) aldehydes to form the corresponding (unsaturated) alcohols has received high attention because the products are widely used in industry [62, 127]. Furfural is a compound derived from hemicellulose and its production is estimated at about around 300 kton per annum. Possible product from reactions of furfural with hydrogen in the presence of metal catalysts are shown in Figure 4-1 a)[128]. Partial hydrogenation leads to furfuryl alcohol (FA), which is an important chemical intermediate for the production of chemical products, such as vitamin C, lysine, plasticizers, dispersing agents and lubricants[129, 130]. Vanillin (VL) can also be partially hydrogenated to vanillin alcohol (Figure 4-1 b)), which finds application in foods, beverages, pharmaceuticals industries, and renewable polymers. VL current production is around 12-14 kton per year[131]. Moreover, bio-oil contain large amount of sugar derived compounds such as glucose, levoglucosan and cellobiose. Glucose represents a platform for the production of numerous chemicals (e.g. sorbitol) by hydrogenation reaction (Figure 4-1 c).

Numerous heterogeneous catalysts have been reported for the selective hydrogenation of furfural, vanillin and glucose. Typically, noble metals such as platinum, palladium, rhodium and ruthenium are used, which are expensive. Recent trends in nano-catalysis have shown that supported bimetallic catalysts show often improved performance compared to their monometallic analogues due to synergistic effects (electronic, geometric, other interfacial effects) [132].

When considering furfural hydrogenation to alcohols, the objective of the current study, Cu based catalysts have shown good performance [133]. Preferential aldehyde reduction is observed, without competitive hydrogenation of the C=C bonds. Improved bimetallic catalysts, notably with Cr (VI), have been reported, though the use of Cr(VI) is not considered green due to its carcinogenic properties. Recently, Pt, Pd, Ru, Re and non-noble Ni have been shown to be good alternatives to Cr [61, 134-136].

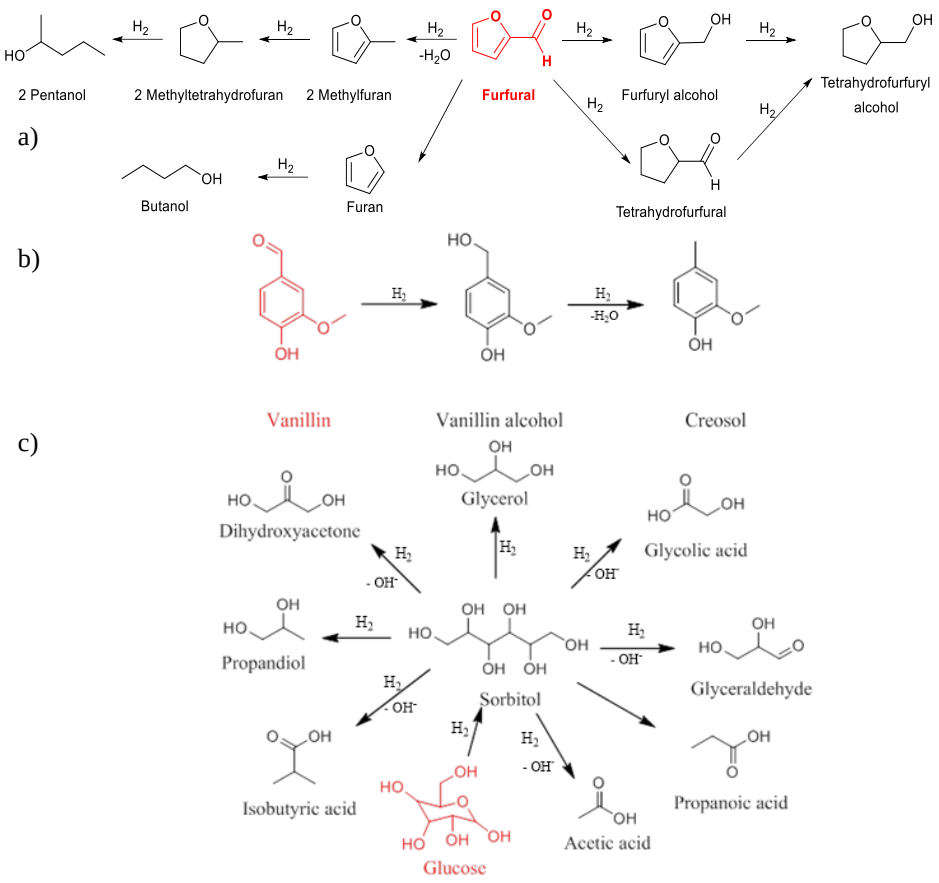

Figure 4-1. Catalytic hydrogenation products for a) Furfural, b) Vanillin and c) Glucose.

For instance, Fulajtárova *et al.* (2015) showed that furfural was quantitatively hydrogenated to FA with a selectivity of 86% using a bimetallic Cu (5%) - Pd (1%) catalyst supported on MgO (80 bar H_2, 130°C, 480 min). Selectivity was enhanced to 98% by adding more Pd (5%) in the catalyst formulation[61]. Du *et al.* reported studies on the hydrogenation of furfural using bimetallic Cu (2.66%) - Pd (0.25%) catalysts supported on carbon in 1,4-dioxane (170°C, 3 h) using formic acid as the H-donor and obtained high selectivity to FA (> 96%) at 100% furfural conversion [134].

Bimetallic Ni based catalysts have also been explored. Sitthisa et al. (2011) showed that the addition of Fe to Ni suppresses the decarbonylation activity of Ni [137], which is a major issue. Shi et al (2019) reported a 74% selectivity to FA at ~97% conversion using a $Fe_{50}Ni_{50}/SiO_2$ catalyst at 150 °C, 20 bar H_2 (2 h) and isopropanol as the solvent[138]. These studies clearly indicate that supported Fe and Cu based catalyst promoted with noble metals are of high interest for the hydrogenation of furfural to FA.

Hydrogenation of vanillin is typically perfromed using monometallic noble-metals (Ru and Pd) [139]. For instance, Tian *et al.*[140] investigated the catalytic properties of a single Ru atom supported on mesoporous graphitic carbon nitride. Vanillin was

effectively hydrogenated into VA, with a close to quantitative selectivity at 95% conversion (60 °C, 40 bar H_2, 72 h). Li *et al.* reported studies on vanillin hydrogenation over a Ni/CCNTs-4 catalyst at mild reaction (190 °C, 10 bar H_2, 3 h). Here, overreduction of the alcohol was observed and p-creosol was formed at 88% selectivity at 90% vanillin conversion [141]. A number of Pd NPs on different supports[142-144] have also been reported for vanillin hydrogenation to VA. It was found that their application is limited due to catalyst stability issues associated with leaching of metal nanoparticles. The use of bimetallic Cu-Pd catalysts has been reported recently[139]. CuPd catalysts on N-rich porous organic polymers were shown to be highly efficient catalyts compared to their monometallic counterparts, providing 99.3% conversion of vanillin with a selectivity of 93.6% for the hydrogenolysis product 2-methoxy-4-methylphenol at 140 °C, 10 bar H_2 in isopropanol [139].

When considering the selective hydrogenation of the aldehyde moiety in glucose to sorbitol, a number of monometallic catalysts have been developed. Commercially, sorbitol is obtained by the using Raney Ni. Ru/C has shown to be a very attractive alternative achieving yields close to 100%, however the latter is expensive and prone to coking and sulphur deactivation [145]. The addition of Cu NPs to Ru/C resulted in a 50% enhanced catalytic activity in glucose hydrogenation (100°C, 80 bar H_2, 3h, 30 mL of 40% glucose in water, 500 mg catalyst) [146]. Pd/C was less effective than Ru/C in the hydrogenation of glucose, achieving 40% conversion and ~43% sorbitol yield, compared to 100% conversion and 80% yield for the latter under same conditions (120°C, 30 bar H_2, 2 h)[147]. Pd activity can be enhanced adding Pt (Pd 50% Pt 50% /TiO_2), with conversion increasing from 82% to 98% and sorbitol selectivity from 60% to 96% (110°C, 15 bar H_2, 2h, 1% glucose in water, glucose: metal ratio= 600)[148]. However, Pt is an expensive noble metal and cheaper alternatives are highly desirable. Ro *et al.* [149] showed that the addition of Fe to (Pt) enhances the catalyst activity for the hydrogenation of aldehydes, with TOF passing from 7.8 min^{-1} (Pt), to 480 min^{-1} (PtFe), which was ascribed to stabilisation of adsorbed reactive intermediates on the Pt-Fe interface through bonding with C=O groups[149].

The above literature indicates that Fe and Cu based catalysts, which are 3 and 2 order of magnitude cheaper than Pd, are not very effective for aldehyde hydrogenation. However, little is known about the use of bimetallic Fe catalysts promoted with Pd for the hydrogenation of furfural and also only one paper is available for a Cu catalyst promoted by Pd for the hydrogenation of vanillin, while none are available for CuPd for glucose

and FePd for vanillin and glucose hydrogenation. We here report an experimental investigation on the use of novel bimetallic catalysts comprising of a cheap metal (Fe, Cu) combined with a noble metal (here Pd), for the aqueous phase hydrogenation of an aldehyde (furfural, vanillin and glucose), with the aim to obtain alcohols (FA, VA and sorbitol). Performance of the bimetallic catalysts was compared to that of the monometallic analogues. ZrO_2 was selected as the support as i) it is known to be stable in aqueous media at elevated temperatures[133], ii) is it less prone to deactivation (compared to TiO_2 and C) [150, 151]. The catalysts were characterised in detail and performance was tested in a batch set-up using aqueous solutions of the three model components

4.3 Experimental details

The experimental details is described on *3.1 Catalyst preparation and characterisation*.

4.4 Results and discussion

4.4.1 Catalysts characterisation

The textural properties of the catalysts and the actual metal contents are reported in Table 4-1. The Pd content is almost similar for all samples (around 1 wt %, in line with the nominal values). The concentrations of Fe and Cu in both mono- and bimetallic catalysts are, as expected based on intakes, around 5 wt%. Nitrogen physisorption was performed to determine the specific surface area, pore size distribution and pore volume of the catalysts (Appendix A, Figure A-1). The hysteresis loop is located for all catalysts at 0.7-0.9 relative pressure, indicating a similar distribution of pore diameters. Indeed, the pore size obtained by the BJH method (Table 4-1) are about similar (18-20 nm) for all the catalysts, indicating that the textural properties are not affected by the impregnation procedure. The surface areas for all catalysts are also very similar and in the range of 60 - 68 m^2/g (Table 4-1), in accordance with literature data for the ZrO_2 support [112, 127]. TEM images (Appendix A, Figure A-2), showed that the individual ZrO_2 crystals are present as elongated spheres with particle sizes in the range of 15-25 nm. The particles appear agglomerated, which was also confirmed by particle size analyses using a Malvern device (120-142μm). Individual metal nanoparticles were not clearly visible using TEM. Two of the catalysts (Pd/ZrO_2 and $PdCu/ZrO_2$) were characterised in more detail by STEM-EDX and the results are given in Figure 4-2 and Figure 4-3. Figure 4-2 shows that the Pd nanoparticles in Pd/ZrO_2 have a nanonoparticle size of about 5 nm. In

contrast, nanoparticles of Pd and Cu were not clearly visible in the bimetallic PdCu/ZrO_2 catalyst. EDX mapping shows that Pd and Cu are well dispersed, indicating that Cu stabilizes the nanoparticles and leads to smaller Pd nanoparticles than found for the monometallic Pd/ZrO_2. These distinct differences are expected to have impacts on catalyst performance (*vide infra*).

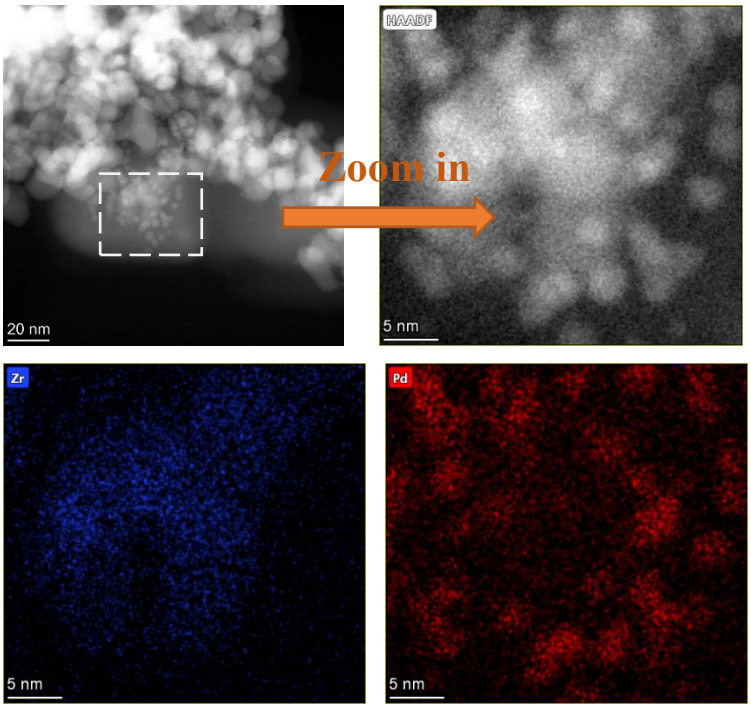

Figure 4-2. STEM- EDX image of the Pd/ZrO_2.

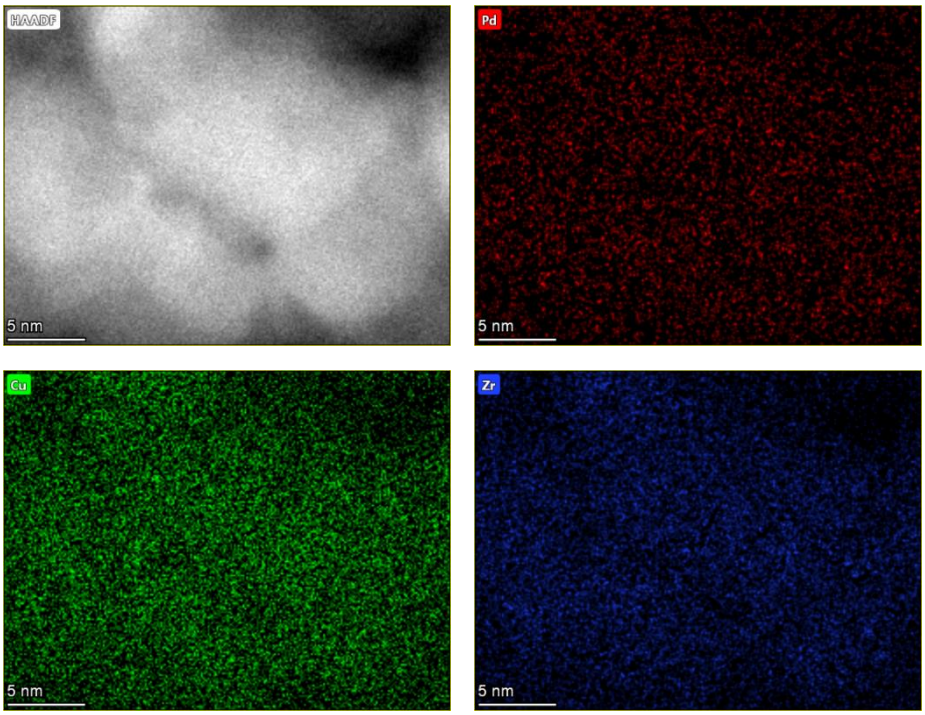

Figure 4-3. STEM- EDX image of the PdCu/ZrO_2.

Table 4-1. Relevant catalyst properties.

	Metal content[a] (%)			Specific surface area[b] (m^2/g)	Pore volume[c] (cm^3/g)	Mean support pore diameter[c] (nm)	Mean support particles diameter[e] (nm)	H_2 uptake, µmol/g	Weak acid sites [f,g] (µmol NH_3/g cat)	Strong acid sites [f,h] (µmol NH_3/g cat)	Total acidity (µmol NH_3/g cat)	Total basicity (mmol CO_2/g cat)
	Pd	Fe	Cu									
Pd/ZrO_2	1.11	-	-	66	0.27	19.9	7.3 ± 0.5	350	167	165	332	-
$PdFe/ZrO_2$	1.00	4.11	-	68	0.25	18.6	8.4 ± 0.6	98	91	78	169	0.19
$PdCu/ZrO_2$	1.05	-	4.68	60	0.26	18.3	6.1 ± 0.4	290	92	88	180	0.12
Fe/ZrO_2	-	5.05	-	64	0.24	18.8	7.4 ± 0.6	280	111	119	260	0.16
Cu/ZrO_2	-	-	4.28	61	0.25	18.4	8.0 ± 0.5	280	109	152	261	0.09

[a] From Atomic Absorption Spectroscopy analyses, [b, c] From N_2 physisorption analyses, [d]BJH, [e] From Sherrer`s equation [f] by peak's deconvolution from data obtained by AutoChem II system, [g]Weak acid sites temperature range 100-210 ºC, [h] Strong acid sites temperature range 210-400 ºC

A representative XRD spectrum is given in Figure 4-4a (Pd/ZrO_2). The reflections were identified by using the Crystallography Open Database [152]. In all the samples, reflections of the zirconia support were clearly detected and showed that presence of monoclinic, tetragonal and cubic crystallites. Application of the Sherrer`s equation for major ZrO_2 revealed a particle size range of about 6-8.4 nm (Table 4- 1), which is slightly smaller than found using TEM. The Fe and Cu nanoparticles were in the oxidic from, while the Pd was mainly in the oxidic form while minor amounts of Pd^0 was detected. Although not very clear, the presence of Pd-metal alloys was suggested by XRD (Figure 4-4b), as is evident from a shift of the Pd reflection in the range 37-42 °from 39.6° for the monometallic catalyst to 39.8° and 40.6° for the bimetallic PdCu and PdFe ones[61, 132].

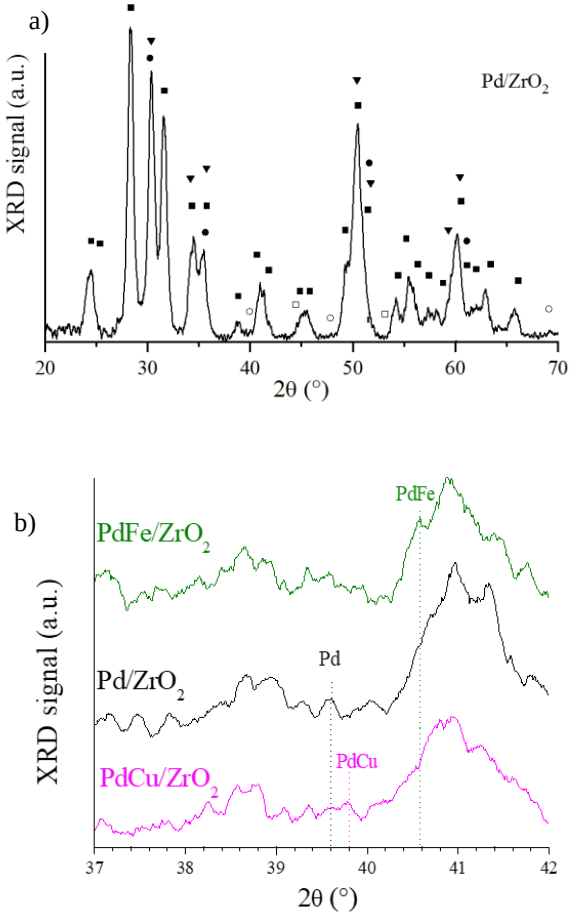

Figure 4-4. X-ray Powder Diffraction (XRD) for a) $PdZrO_2$ (■) ZrO_2 monoclinic, (▼) ZrO_2 tetragonal, (●) ZrO_2 cubic, (□) Pd_3O_4, (○) Pd and b) bimetallic catalyst in the range 37-42 °

H_2-TPR data for the different catalysts are provided in Table 1 and the supplementary information (Figure A-3). The studied catalysts present similar H_2 uptake (~280-350 µmol/g) excluding $FePd/ZrO_2$ (98 µmol/g). For the monometallic Pd/ZrO_2 catalyst, only one clear peak is observed at around 100 °C, which is attributed to Pd metal formation

from the oxide phase [153-155]. Zr^{4+} reduction does not take place in the measured temperature range (max 700°C), in line with literature data [156].

The monometallic Cu/ZrO_2 catalyst shows two peaks, one at about 200 °C assigned to the reduction of CuO to Cu_2O, and a broad peak between 250 and 400°C, assigned to the consecutive reduction of Cu_2O to Cu°. The presence of the two overlapping peaks can be attributed to the different CuO species that are differently interacting with the support[157, 158]. The H_2-TPR spectrum of the bimetallic $CuPd/ZrO_2$ shows one clear band from Cu (~230°C) and a shoulder (~300°C) assigned to reduction of Cu_2O to Cu°. The peak from Cu reduction is shifted to higher temperatures compared to monometallic Cu/ZrO_2, indicating presence of Cu-Pd alloy[134] .

The Fe/ZrO_2 catalyst shows clear peaks at about 300, 400 and 520 °C, associated with several reduction steps ($Fe_2O_3 \rightarrow Fe_3O_4 \rightarrow Fe$) [159]. In the bimetallic Fe-Pd catalyst, the main reduction peaks of Fe_2O_3 are shifted to lower temperature, indicating the formation of a PdFe alloy and a much stronger capability of $FePdZrO_2$ (compared to $FeZrO_2$) in adsorbing H_2 at low temperature. This is supported by the XRD (*vide supra*) [132]

Figure A-4 (Appendix A) shows the NH_3-TPD profiles of the catalysts studied in this work. All the samples there was noted an overlapping of weak and strong acid peak, recorded at range of 160-210 ºC and 240-340. ° C, respectively. Furthermore, the strength peak was shifted toward for Fe and Cu catalyst in presence of Pd, indicating an increment of strength acid site than the weak site. NH_3-TPD reveal that the bimetallic catalysts are less acidic than the monometallic ones (Table 4-1). The monometallic Pd/ZrO_2 catalyst was the most acidic, with 332 μmol NH_3/g_{cat} desorbed, while $PdFe/ZrO_2$ was the least acidic (169 μmol NH_3/g cat). XPS spectra for the monometallic Fe/ZrO_2 catalyst show two Fe 2p binding energy (BE) bands from Fe_3O_4 (711 eV and 715 eV) and one for Fe_2O_3 (725 eV). In the bimetallic $FePd/ZrO_2$ catalyst, these bands shift to higher BE's (Appendix A, Figure A-5), which suggest the presence of Fe-Pd interactions. XPS spectra for monometallic Cu/ZrO_2 (Appendix A, Figure A-6) indicate presence of Cu^{2+} species (934.4 and 944eV). For the bimetallic Cu based catalyst, the shake-up features of Cu $2p_{3/2}$ were very similar to those of the monometallic Cu catalyst, but the bonding energy less strong, suggesting interactions between Cu and Pd.

4.4.2 Furfural hydrogenation

The hydrogenation of furfural using the mono-and bimetallic catalysts was performed in a batch autoclave at 100 °C, 50 bar hydrogen and using water as the solvent. The

concentration of furfural was 0.519 M, the substrate-catalyst ratio was set at 7.48 g/g. The catalyst performance data are given in Table 4-3 and Figure 4-5. Some experiments were performed in duplicate and the error in the conversion was shown to be about 7%. All catalysts gave close to quantitative selectivity to FA and neither ring hydrogenation nor decarbonylation, well known by-products, were observed. The highest furfural conversion was obtained with the bimetallic $PdCu/ZrO_2$ catalyst (~70% after 80 min), which is considerably higher than for the monometallic Cu/ZrO_2, A similar trends, i.e. higher activity of the bimetallic PdFe catalyst compared the monometallic Fe one was found for the Fe based catalysts.

A possible explanation is the better dispersion of the metals for the bimetallic catalysts compared to the monometallic ones, as was illustrated using STEM- EDX for the Pd and Cu based catalysts (Figure 4-2).

Table 4-2. Hydrogenation of furfural at 100 ºC, 50 bar, furfural 0.519 mol/L; 200 mg catalyst after 80 min.

Catalyst	Furfural conversion (%)	Furfuryl alcohol selectivity (%)
5 wt.% Cu/ZrO_2	29.5	99
1/ 5 wt.% $PdCu/ZrO_2$	66.1	99
5 wt,% Fe/ZrO_2	26.1	99
1/ 5 wt.% $PdFe/ZrO_2$	54.7	99
1 wt.% Pd/ZrO_2	43.7	99

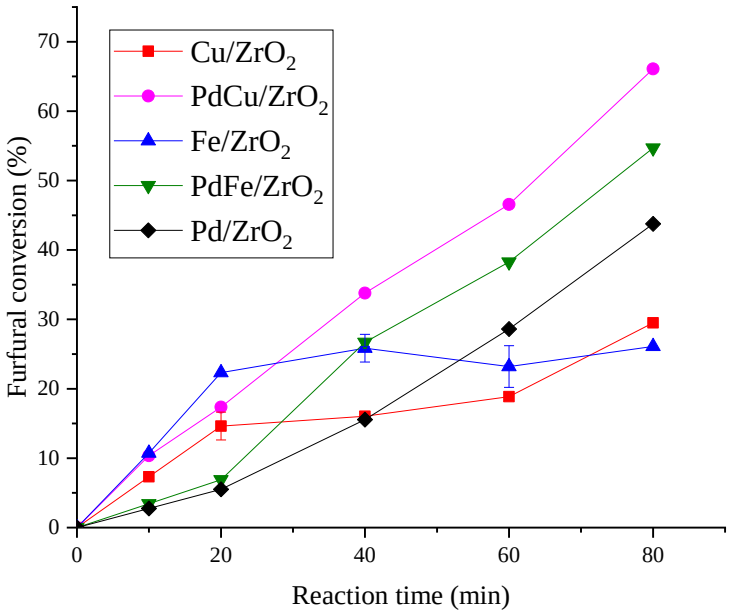

Figure 4-5. Hydrogenation of furfural at 100 ºC, 50 bar, 30 mL of furfural 0.519 mol/L, 200 mg of catalyst (furfural:catalyst wt ratio 7.48:1).

Since the furfural conversion showed deactivation for the mono-metallic catalysts, TPO was carried out. Figure 4-6 indicates that poisoning by organic species (in terms of mg O_2 consumed/g catalyst) occurred during the reaction and increased in the following order: $PdFeZrO_2$ (8.57 mg/g) < $FeZrO_2$ (10 mg/g) < $PdZrO_2$ (11.43 mg/g) < $CuZrO_2$ (17.15 mg/g) < $PdCuZrO_2$ (35.73 mg/g). However, if the TPO data are compared to the conversion ones (Figure 4-6), deactivation by coking can be excluded, since Fe/ZrO_2 and Cu/ZrO_2 do not present the highest organic deposits, which instead seem to be proportional to the catalysts' activity. This also suggest that other causes such as metal sintering (unlike at 100°C) or leaching could be linked to the mono-metallic deactivation.

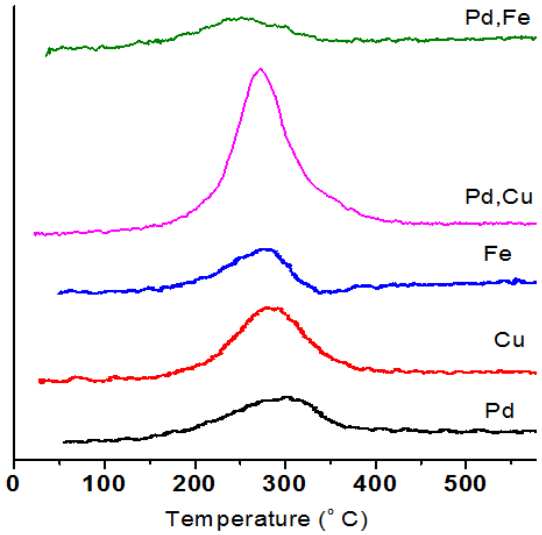

Figure 4-6. TPO analyses of spent samples after furfural hydrogenation.

4.4.3 Vanillin hydrogenation

The hydrogenation of vanillin was studied under the same conditions used for furfural, but with a concentration of 0.204 M and a substrate-catalyst ratio of 4.65 g/g. The catalysts performance is shown in Table 4-3 and Figure 4-7. Reproducibility was evaluated running two testes in triplicates with an average error of 2.15 %.

The catalysts show a 99% selectivity for partial hydrogenation to vanillin alcohol, since neither cresol (C-O bond cleavage) or guaiacol (C-C bond cleavage) by-products were detected. The largest conversion of VL was obtained for $PdFe/ZrO_2$ (99.2%) and $PdCu/ZrO_2$ (98.2%) after 40 and 80 min, respectively, which was 2-fold (Cu/ZrO_2) and 2.5-folds (Fe/ZrO_2) higher than mono-metallic zirconia catalysts. Therefore, a clear synergic effect is exhibited by the bi-metallic catalysts. A previous study reported that Fe surface serves as the catalytic site for the activation of phenolic compounds and Pd stabilise Fe by its electronic interaction with Fe surface atoms. The H_2-TPR (Appendix

A, Figure A- 3) suggest that the addition of Pd to Fe reduces the barrier to H_2 chemisorption of Fe (peaks at lower temperature). Furthermore, the addition of 1%Pd to 5%Cu (and possibly to Fe) is beneficial to the dispersion of the Pd nanoparticles and can be related to the enhanced hydrogenation activity of the bimetallic species (See Figure 4-3).

Table 4-3. Hydrogenation of vanillin at 100 ºC, 50 bar, 30 mL of vanillin 0.204 mol/L; 200 mg catalyst at 10 min.

	Vanillin conversion (%)	Vanillin alcohol selectivity (%)
5 wt.% Cu/ZrO_2	51.4	99
1/ 5 wt.% $PdCu/ZrO_2$	98.2	99
5 wt. % Fe/ZrO_2	39.3	99
1/ 5 wt.% $PdFe/ZrO_2$	99.2	99
1 wt.% Pd/ZrO_2	71.6	99

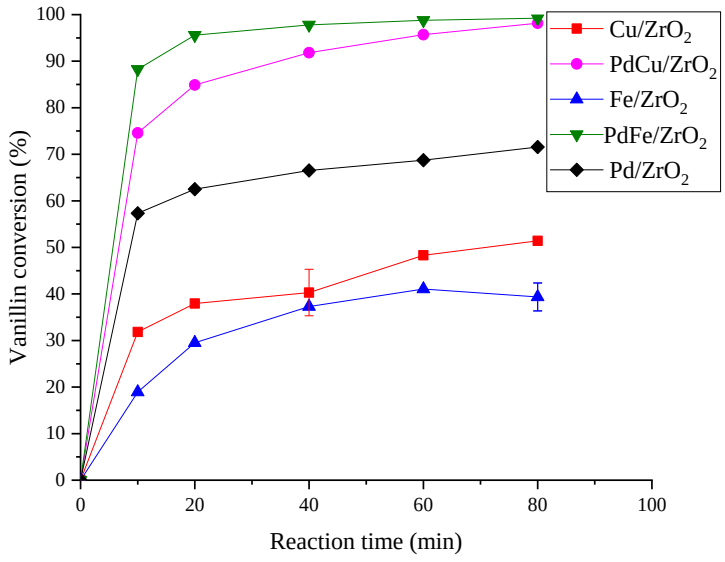

Figure 4-7. Hydrogenation of vanillin at 100 ºC, 50 bar, 30 mL of vanillin 0.204 mol/L; 200 mg catalyst (vanillin: catalyst wt ratio 4.65:1).

Previous works suggest that the partial hydrogenation of VL to VA is favoured in presence of basic sites[139, 142, 143]. All the ZrO_2 based catalysts possess basic sites as reported in Table 1, which can be linked to the high VA selectivity.

The comparison of the VL and FU conversion data indicates that the aldehyde group of vanillin is more reactive than the aldehyde group of furfural, due to a week bonding with

the C=C present in the furfural hetero-cyclic group, therefore a greater difficulty to desorbing.

The TPO analyses of spent samples clearly suggest deposition of organics on the catalyst surface, mainly for the bimetallic catalysts, which are the most active (Figure 4-8). The quantitative analysis resulted in the following organic deposits formation (in terms of mg O_2 consumed/g catalyst): $CuZrO_2$ (15.72 mg/g) < $FeZrO_2$ and $PdZrO_2$ (17.15 mg/g) < $PdCuZrO_2$ (20 mg/g) < $PdFeZrO_2$ (91.46 mg/g). However, these deposits did not lead to catalyst deactivation during the 80 min reaction time.

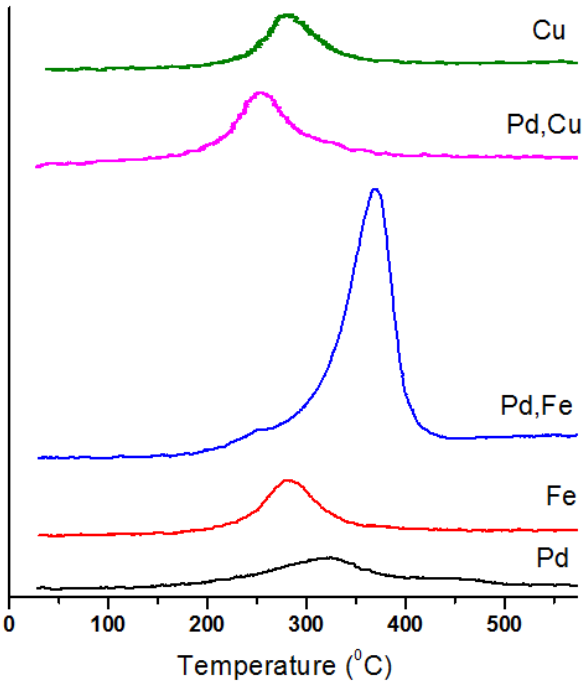

Figure 4-8. TPO analyses of spent catalysts after vanillin hydrogenation reaction

4.4.4 Glucose hydrodeoxygenation

The hydrogenation of glucose with an initial concentration of 1.07 M and a substrate-catalyst ratio of 28.9 g/g was studied in water phase under the same conditions used for FU and VL. The catalysts performances are reported in Table 4-4 and Figure 4-9.

The conversion of glucose was relatively low (16-20%) possibly due to the initial large concentration of glucose (20 wt. %) and high substrate- catalyst ratio used in comparison to previous works [160-162]. Similarly to FU and VL, the highest glucose conversion (~20%) was achieved with the bimetallic catalysts, even if the conversion difference with the monometallic counterparts was less marked for the glucose, which support the finding

that more dispersed Pd NPs (see Figure 4-2 and Figure 4-3) in the bi-metallic species benefit the bio-substrates conversion.

Table 4-4. Hydrogenation of glucose at 100 ºC, 50 bar, 30 mL of glucose 1.07 mol/L; 200 mg catalyst (glucose: catalyst wt ratio 28.9:1) at 120 min.

	Glucose conversion (%)	Sorbitol selectivity (%)
5 wt.% Cu/ZrO_2	18	34
1/ 5 wt.% $PdCu/ZrO_2$	20	52
5 wt. % Fe/ZrO_2	16	49
1/ 5 wt.% $PdFe/ZrO_2$	19	74
1 wt.% Pd/ZrO_2	18	58

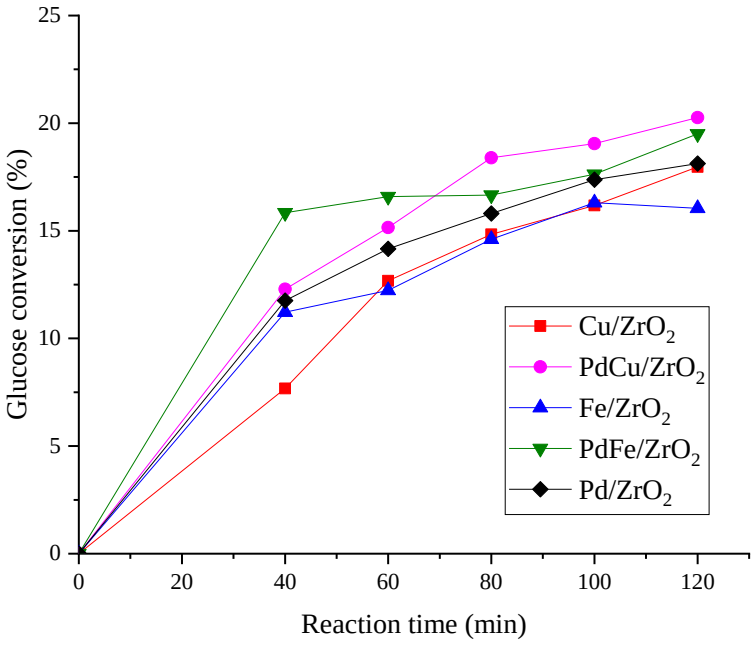

Figure 4-9. Hydrogenation of glucose at 100 ºC, 50 bar, 30 mL of glucose 1.07 mol/L; 200 mg catalyst (glucose: catalyst wt. ratio 28.9:1).

Contrary to FU and VL, the hydrogenation of glucose led to several products (Figure 4-10) denoting the co-existence of multiple reactions under the studied conditions. The aldehyde group of glucose was hydrogenated to produce sorbitol, achieving a selectivity around 74% for $PdFe/ZrO_2$, while the lowest value (about 34%) was detected for the Cu containing catalysts. The catalyst selectivity for sorbitol decreased in the order: $PdFe/ZrO_2$ > Pd/ZrO_2 > Fe/ZrO_2 > $PdCu/ZrO_2$ > Cu/ZrO_2 suggesting that the dispersion

of the Pd NPs in not linked to the product's selectivity. The different products distribution could be linked to the catalysts acidity[162]. Figure 4-11 shows the relation between the acidity of the catalysts and the selectivity towards sorbitol. As can be seen, excluding Pd, there is a clear trend, where the least acid catalyst (PdFe) resulted in the highest selectivity to sorbitol. Cu/ZrO_2 and in less extent $CuPd/ZrO_2$ favour the further hydrogenation or retro-aldol condensation of sorbitol to form glycerol and the hydrogenolysis to EG, PG etc and this explains its low selectivity towards sorbitol[162].

Zhang et al. (2016) obtained a 60 and 75% selectivity to sorbitol respectively at 40 and 60 bar at 140°C using 1.5% Pt-SBA-15 (calculated at 5% glucose conversion) [163]. In the same study, it was shown that the catalyst activity increased 3 folds when the temperature was increased from 100 to 140 °C. This latter data can be used to compare the conversion obtained in our work, since similar metal loadings and H_2 pressure were used. Despite Ru and Pt are typically employed for the hydrogenation of glucose [163], here we show that Fe promoted by Pd have a good selectivity towards sorbitol. The TPO analyses (Figure 4-12) show low oxygen consumption (10 mg/g for Cu and Pd; 11.47 mg/g for Fe; 15.72 mg/g for PdFe and 20 mg/g for PdCu), possibly correlated to the low activity of the catalysts in hydrogenating glucose.

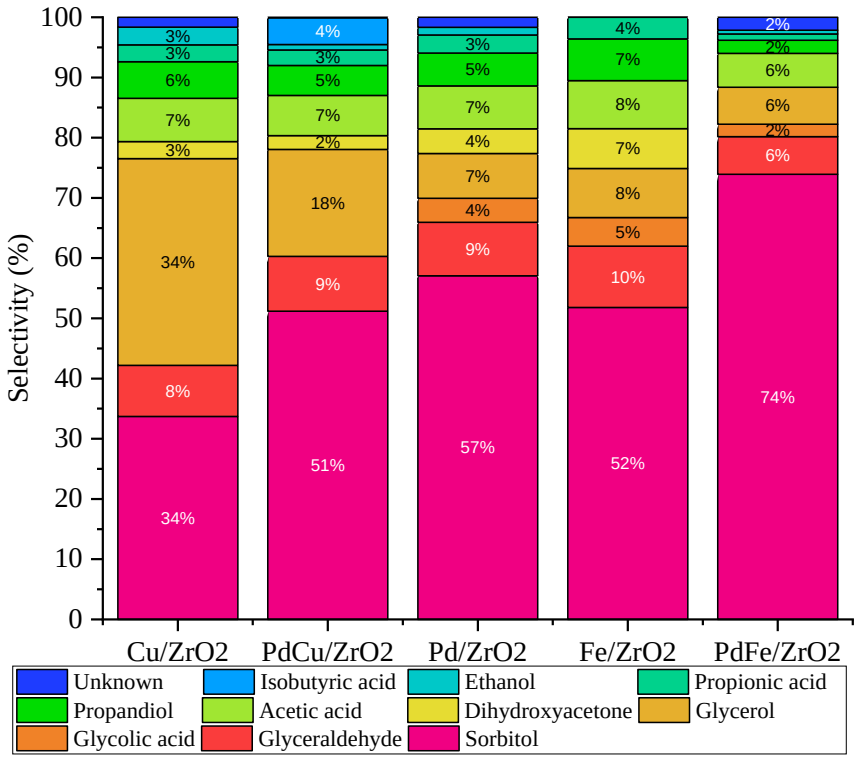

Figure 4-10. Selectivity of glucose hydrogenation at 100 ºC, 50 bar, after 120 min.

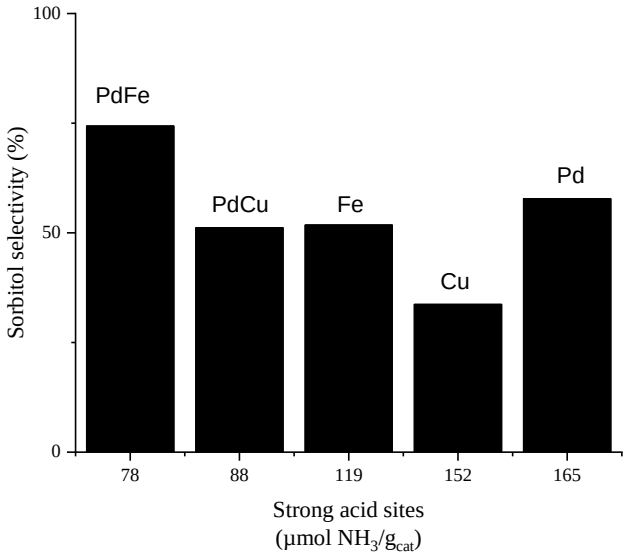

Figure 4-11. Sorbitol selectivity vs catalysts acidity at 40 min for hydrogenation of glucose at 100 ºC, 50 bar, 30 mL of glucose 1.07 mol/L; 200 mg catalyst (glucose: catalyst wt. ratio 28.9:1).

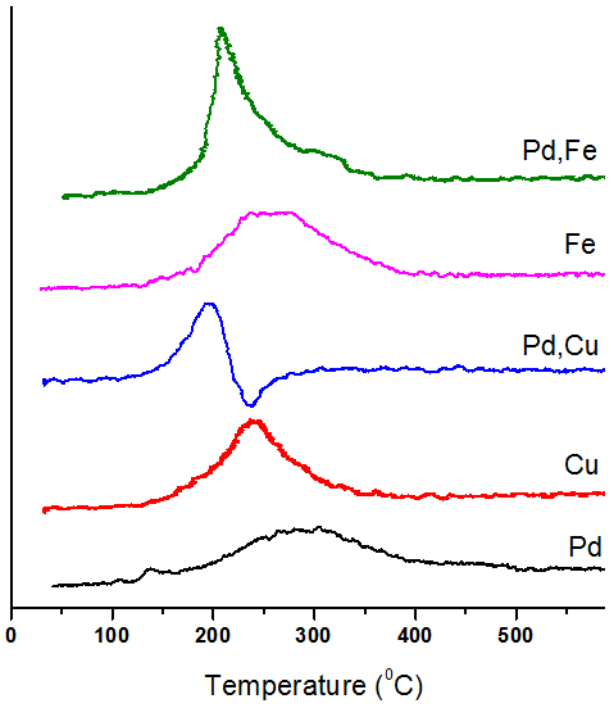

Figure 4-12. TPO analyses of spent catalysts after glucose hydrogenation reaction

4.5 Conclusions

The aim of this study was to investigate the effect of adding Pd as promoter to non-noble metals such as iron and copper for the hydrogenation of the aldehyde group of different model compounds representative of pyrolysis bio-oils. Therefore, Cu, Fe, Pd, PdCu, and PdFe supported on ZrO_2 were prepared by wetness impregnation technique, characterised by different techniques and studied in the partial hydrogenation experiments. For all the

catalysts, a 99% selectivity was obtained for the partial hydrogenation products (FA and VA).

The bi-metallic PdFe and PdCu displayed enhanced catalytic performance in terms of reactant conversion towards VA and FA and to a less extent sorbitol, compared to the monometallic catalysts. A better dispersion of the metals for the bimetallic catalysts compared to the monometallic ones, as was illustrated using STEM-EDX, is probably the main reason behind the higher conversion of the bimetallic catalysts. Moreover, presence of FePd and to less extent CuPd alloy was linked to their superior performance, due to enhanced H_2 adsorption at low temperature.

Based on the catalysts characterisation and reaction tests, it is concluded that the well-dispersed Fe-Pd and Cu-Pd bi-metallic catalysts possess an excellent aldehyde hydrogenation activity under mild conditions.

This work shows that non-noble metals such as Fe and Cu have high potential in the partial hydrogenation (or stabilisation) of bio-oil model compounds by the addition of a small quantity (1wt%) of Pd. Based on the promising results, future work should include the study of real bio oil solution to evaluate the effectiveness of the bi-metallic catalysts in stabilise wood derived bio-oils.

Chapter 5- Stabilisation of pine derived water-soluble bio-oil by zirconia-supported Fe/Cu/Pd nano-catalysts under mild operating conditions

5.1 Abstract

The previous catalysts have been tested with a real bio-oil mixture. Bio-oil is, which is a complex mixture of oxygenated compound, has a high potential for fuels and chemicals production when upgraded by catalytic hydrodeoxygenation (HDO).

The HDO of the soluble water bio-oil fraction (WBO) has been studied in presence of mono e bimetallic catalyst (Cu, Fe, Pd, PdCu and PdFe) on zirconia support. The WBO extracted was upgraded at 50 bar and 100 °C, in presence of 200 mg of catalyst, into a batch reactor for 360 min. The low operating condition was able for the bi-metallic catalysts (PdCu and PdFe) to maintain 90 % C of the starting organics in liquid phase after 360 minutes.

5.2 Introduction

In the last decade, stringent environmental regulations and the need to replace fossil fuels with renewable sources are pushing the development of lignocellulosic biorefineries, which involve a portfolio of technologies including fermentation, gasification, fast pyrolysis, reactive fractionation etc. The pyrolytic conversion of biomass to bio-oil is particularly attractive due to its low environmental impact, scalability and cost-competitiveness [164, 165]. Bio-oil is a complex mixture of oxygenates including acids, alcohols, sugars, aldehydes, esters, ketones, phenols, oligomers and it is known to be thermally and chemically unstable [164]. Nevertheless, the direct bio-oil application as fuel in conventional engines is not possible for the high content in water, acid pH, corrosiveness and high viscosity. Several bio-oil upgrading pathways have been proposed, such as hydrotreating, fluid catalytic cracking, supercritical fluids, solvent addition/esterification, emulsification, aldol-condensation and steam reforming and ketonization [127, 164, 166, 167].

Promising results have been reached by hydrodeoxygenation (HDO) reaction[168, 169], improving the proprieties of bio oil. HDO requires a metallic site for hydrogenation/dehydrogenation as well as a support that adsorbs the oxy compound and promotes alkylation and polymerization reactions. The reaction is catalysed in presence of noble metals as platinum, palladium, rhodium and ruthenium. The role of the metal support is also very important and different supports have been investigated as Al_2O_3,

SiO_2, ZrO_2 and carbon based [48, 49]. The control of the metal particle size and the selection of the support with appropriate properties may inhibit catalyst deactivation [170]. In spite of the research efforts, the development of an appropriate catalyst for HDO reaction is still an issue.

Most of the work on bio-oil HDO reactions have been performed using mono-metallic catalysts at high operating condition (10–20 MPa, 523–873 K). Bjelić et al. (2019) studied the hydrogenation and hydrodeoxygenation of aromatic lignin monomers over Cu, Ni, Pd, Pt, Rh and Ru catalysts supported on carbon at 275 °C and 5 MPa [171]. Both non-noble metals (Ni/C and Cu/C) exhibited negligible catalytic activity for regardless of loading, Pd/C had good hydrogenation but poor deoxygenation activity, while Ru/C had the best deoxygenation activity.

Mortensen et al.[48] screened 23 different catalysts at 100 bar H_2 and 275 °C, for HDO of phenol as a model compound of bio-oil, proposing a reaction path of two steps, from phenol to cyclohexanol and then subsequently to cyclohexane. The authors noted that the most active metals were Ru, Pd, Pt and Ni, and the support helped in improving their performance. The catalyst activity scale was: Ni/ZrO_2 > $Ni\text{-}V_2O_5/ZrO_2$ > $Ni\text{-}V_2O_5/SiO_2$ > Ru/C > Ni/Al_2O_3 > Ni/SiO_2 ≫ Pd/C > Pt/C.

Despite the addition of a second metal that can result in catalytic and adsorptive properties changes is currently of great interest [170, 172-174], there are only few studies regarding bimetallic catalysts for the HDO of real bio-oils [175, 176]. The presence of host metal can decrease the size of the ensemble, inhibiting the carbon formation and minimise the sintering process [170].

Nobel metal such as Pd, with the potential for high hydrogen uptake and high dissociation of hydrogen molecules, are effective metal as hydrogenation promoter, but its high price makes the use of Pd not suitable from economic point of view.

On the other hand, iron with their considerably lower price (~$90/t vs ~$63M/t for Pd) and hydrogenation activity comparable to that of Pd (based on hydrocarbon yield obtained from lignin HDO at 350°C 1bar H_2 in presence of Fe and Pd on $ReOx/ZrO_2$) can be considered as a potential hydrogenation metal for the catalytic conversion of bio-oils [172]. However, these more economic metals typically require more sever operating conditions than noble metals to be effective by their own and benefit from a Nobel-metal promoter [177].

Duan et al. (2017) reported a highly active HDO catalyst comprising highly dispersed Pd and ultrafine Mo phosphate nanoparticles supported on SiO_2 [175]. Using water-insoluble

fraction of wood and bark-derived bio-oil, the catalyst showed simultaneous HDO of lignin, cellulose, and hemicellulose-derived oligomers into liquid alkanes with total mass yield of 29.6 wt% under mild condition (523 K, 1 MPa H_2).

Gutierrez et al.[177] studied the hydrogenation of guaiacol at 100 and 300 °C with different catalysts, ZrO_2-supported noble metal (Rh and RhPt) and sulfided $CoMo/Al_2O_3$, showed a carbon deposition more accentuated for sulfided $CoMo/Al_2O_3$. Furthermore, at 100°C the conversion of guaiacol was complete when the ZrO_2-supported catalysts were used. Specifically, the combination of RhPt and RhPd had better hydrogen chemisorption than monometallic Rh, Pd and Pt. Pt and Pd on ZrO_2 resulted in higher yield than the Rh/ZrO_2 for the bio-oil hydrogenation, due at their sulphur tolerance.

Sun et al. [178] investigated the performance of carbon supported PdFe for HDO of guaiacol. PdFe/C exhibited higher activity to deoxygenated products (benzene/toluene) than monometallic catalysts [178]. The selective conversion of m-cresol to toluene over bimetallic silica supported Ni-Fe catalysts was also studied [178]. For the bimetallic catalyst, the presence of an oxophilic metal, such as the unreduced Fe species present in the $Ni\text{-}Fe/SiO_2$ catalysts enhanced the interaction with the carbonyl group, promoting the oxygen removal reaction pathway.

Hita et al. (2019) studied the HDO of bio-oil at 450 °C, 65 bar H_2 (space time, 0.15 gcat h g^{-1} bio-oil; 90 ml min^{-1} H_2; and time on stream up to 6 h) in presence of PtPd and a NiW catalysts supported on a phosphorus-containing activated carbon [174]. The NiW catalyst provided yields of 42.3 wt.% liquid carbon products (in a dry bio-oil basis), yielding 5.3 wt.% phenolic and 12.3 wt.% aromatic product yields, while PtPd catalyst showed a carbon liquid yield about half of NiW catalyst.

Han et al (2019) studied the HDO of lignin derived phenols at 250°C, 50 bar in presence of monometallic Ni and Fe and bimetallic NiFe catalysts [173]. The bimetallic Ni-Fe catalyst exhibited better performance for phenol HDO due to the formation of Ni-Fe alloy phase, which significantly enhanced the adsorption strength of organic HDO intermediates, where Fe-containing sites adsorb the hydroxyl species while Ni sites perform the H_2 activation, playing a synergistic effect. Furthermore, PdNi catalyst on cellulose nanocrystals (CNCs) has been synthesised by Li et al [179] for HDO of vanillin at mild condition (70°C, 10 bar), resulting in a complete conversion of the reactant to 2 methoxy 4 methyl-phenol after 2 h.

Our group studied mono and bimetilic catalyst (Cu, Fe, Pd, PdCu and PdFe) on zirconia for hydrogenation reaction of furfural, vanillin and glucose at 100 ºC and 50 bar [180].

The bi-metallic PdFe and PdCu displayed a conversion of 98% to vanillin alcohol and 65.5% to furfuryl alcohol after 80 min indicating a higher reactivity of vanillin aldehyde group than the aldehyde group of furfural. Moreover, the PdFe showed a high selectivity towards sorbitol (74%) from glucose at low conversion (20%), the presence of the noble catalyst was able to improve the performance of Cu and Fe catalysts, increase H_2 adsorption at low temperature onto the catalyst surface[180].

The catalyst support is also studied for minimising the carbon formation and stabilise the physical catalyst proprieties [49, 181-183]. Previous works exclude zeolites as HDO support for the high coke deposition and low activity [184, 185]. Ardiyanti et al.[49] studied Ni–Cu catalyst on several supports (CeO_2–ZrO_2, ZrO_2, SiO_2, TiO_2, rice husk carbon, and Sibunite) for HDO of bio-oil at 150 °C for 1 h, followed by 3 h at 350 °C, 200 bar. NiCu/ZrO_2, resulted in the lowest carbon deposition (2.7 wt.%), compared to the other catalysts. De Souza et al. [49, 182, 183] also studied the effect of the type of support (SiO_2, Al_2O_3, TiO_2, ZrO_2, CeO_2 and $CeZrO_2$) on the performance of Pd-based catalysts for the HDO of phenol at 300 ºC. Benzene was the major product over Pd/TiO_2 and Pd/ZrO_2, whereas Pd/SiO_2, Pd/Al_2O_3, Pd/ CeO_2 and Pd/$CeZrO_2$ produced mainly cyclohexanone. For Pd/ZrO_2, the oxophilic sites represented by incompletely coordinated Zr^{4+} cations near the perimeter of the metal particles favoured the interaction of the oxygen of the carbonyl group in the phenol intermediate with the catalyst surface, so that the carbonyl group was preferentially hydrogenated on the metal particles at the metal-support interface, leading to the formation of benzene. Then, oxophilic supports such as zirconia promote the production of deoxygenated products during HDO reaction [170]. Moreover, ZrO_2 has been shown to improve the mechanical strength and thermal stability [182, 183] and plays a role in achieving excellent catalytic HDO performance in aqueous media for compounds with hydrophilic groups (e.g vanillin), which make it hardly undergo HDO reaction over hydrophobic catalysts [170]. This could be linked to Lewis acid sites that may help catalyse the reaction through initial binding of the oxygenated substrates and subsequent cleavage of the C–O [176].

Acids in bio-oil are typically recalcitrant to HDO and require further study. The hydrogenation of light oxygenates in the aqueous fraction of bio-oil, real and model compounds (hydroxyacetone, acetic acid, and formic acid) was studied with Ru/TiO_2 and Ru/C catalysts by Bergem et al.[52]. For a temperature between 100 and 140°C at about 62 bar, for the model compound the reaction involved the conversion of hydroxy-ketones into diols and hydrogenation of ketones and aldehydes into mono-alcohols. A declining

of about 25% catalyst activity was observed after 90 hours a when processing a WBO fraction. Moreover, the authors noted a decrement of hydrogenation reaction as: formic acid > hydroxyacetone > acetic acid, whose main products were CO_2, ethanol and propylene glycol, respectively.

Sanna et al. [62] studied the HDO of a real WBO fraction in presence of Ru/C and Pt/Cat 75 and 100 °C and about 50 bar.

2-furanone, furfural, 5-HMF, hydroxy-acetaldehyde and methyl-cyclopentanedione were fully converted, while acetic acid was recalcitrant to hydrogenation/HDO under the studied conditions. Similarly, Yin et al. (2016) investigated the use of a bimetallic Ni–Cu based catalyst stabilized by SiO_2–ZrO_2 with high Ni loading prepared by a sol–gel method for the catalytic hydrotreatment of pyrolysis bio-oil [168]. Although, the sugar fraction was found to be reactive in the low temperature range (<200 °C), the lignin fraction was only converted at elevated temperatures (>300 °C) and the recalcitrant organic acids reacted only above 350 °C [168].

In this work we reported the hydrogenation reaction of WBO in presence of Fe, Cu,Pd mono and FePd and CuPd bimetallic catalyst supported on zirconia, for the conversion of aldehydes, ketones, sugars, phenols, etc. in more stable alcohols under mild operating condition. In addition, we are going to identify the effect of the mono- or bi- metal presence on the products distribution at different reaction time.

Also, the catalytic deactivation was determined by the carbon formation, influencing the activity of the metals. This paper increases the knowledge about the WBO stabilisation in presence of non-nobel metals for the production of added value chemicals.

5.3 Materials and Methods

Materials and methods are described on *3.1 Catalyst preparation and characterisation*.

5.4 Results and Discussion

5.4.1 Catalysts characterisation

ICP analysis were used to confirm the amount of metal loaded on the ZrO_2 surface, which corresponded to 1% Pd and around 5% Fe and Cu in both mono- and bimetallic catalysts [180]. BET surface area and mean pore diameter were previously calculated and resulted in the range 60-68 m^2/g and 18.3-19.9 nm, respectively, denoting similar surface properties for all catalysts [180].

TEM images (Appendix A, Figure A-2), showed that the individual ZrO_2 crystals are pseudo-spherical and with size between 10 and 30 nm. As in previous work, it was difficult to distinguish between the metal particles and the individual ZrO_2 crystallites in the TEM images, due to the low Pd content and the poor contrast between Pd, Fe and Cu and ZrO_2. Therefore, the size distribution analysis was not performed [170].

The XRD spectra of the catalysts (Figure 5-1), clearly show the patterns of the zirconia crystallites. Fe and Cu nanoparticles were found in the oxidic from, while Pd was mainly in the oxidic form (mostly) and a Pd^0.

The presence of Pd-metal alloys previously highlighted by our group[180] was further studied by Rietvel refinement, since the lines characteristic of Pd/Cu/Fe were not well defined under standard XRD analysis and the identification of alloys was not certain [170]. Figure 5-2 show the Rietvel refinement diffraction peaks for the PdFe and PdCu bimetallic catalysts. While monometallic FeO_x ($2\theta = 35.5°$, 43.0° and 62.7°) is not visible, CuO_x ($2\theta = 36.4°$, 43.2° and 50.4°) is present in the $PdCu/ZrO_2$ catalyst [170]. Moreover, from the expected diffraction peak for Pd (40.1 and 45.5) only the second is visible for both catalysts. In the bimetallic $PdFe/ZrO_2$ these diffraction peaks shifted to lower angles in presence of 1% Pd, which indicates the formation of Fe-Pd alloy for bimetallic $PdFe/ZrO_2$ catalysts [173, 186].

Therefore, the absence of the Fe diffraction peak observed at 39.86° and 44.9° are ascribed to the FePd alloy phase. For $PdCu/ZrO_2$, the evidence of the alloy is less marked, since Cu peak (43°) is well defined and there is overlapping with ZrO_2 at $2\theta = 40.98°$, where the possible PdCu diffraction peak could be [187]. However, the absence of the Pd peak at 40.1° could suggest presence of some PdCu alloy.

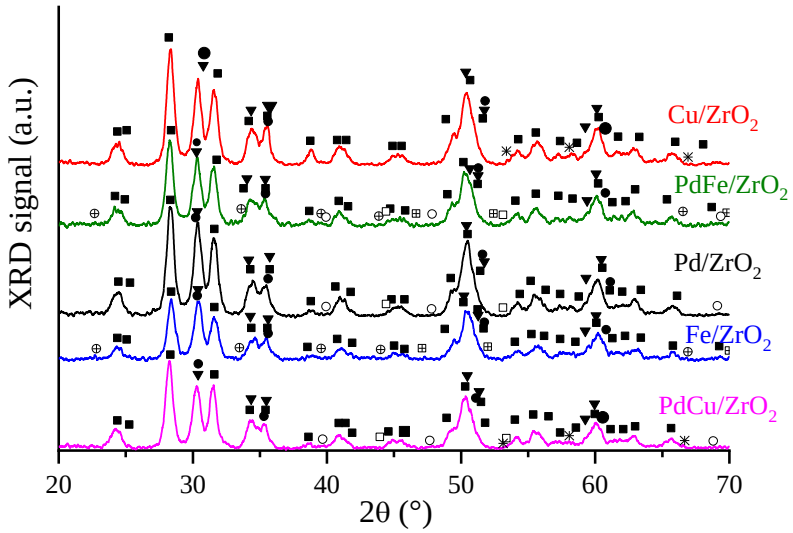

Figure 5-1. X-ray Powder Diffraction (XRD) spectra for the catalysts. (■) ZrO_2 monoclinic, (▼) ZrO_2 tetragonal, (●) ZrO_2 cubic, (⊞) Fe_2O_3, (⊕) Fe_3O_4, (□) Pd_3O_4, (○) Pd, (*) CuO.

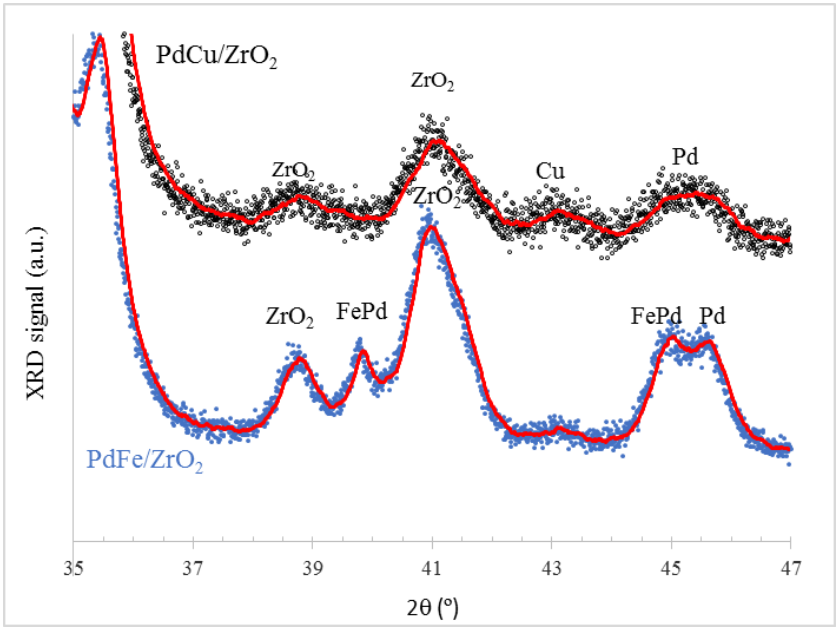

Figure 5-2. X-ray Powder Diffraction (XRD) Rietvel-refinement for the bimetallic catalysts.

H_2 reduction profiles for the different catalysts are shown in Appendix A, Figure A- 3. The single peak at around 100 °C for Pd/ZrO_2 can be assigned to the reduction of Pd oxide with homogeneous particle size [170]. From the H_2-TPR of the Pd/ZrO_2 can also be deduced that Zr^{4+} reduction does not take place in the measured temperature range, in line with literature data [156]. There is also the indication that only Pd oxide is reduced in the low temperature region (around 100°C), while Cu and Fe were completely reduced in the high temperature region. Cu/ZrO_2 catalyst shows two peaks, assigned to the

reduction of CuO to Cu_2O (~150 ℃), and a broad peak in the range 200-400°C, assigned to the reduction of Cu_2O to Cu°. The H_2 reduction profile of the bimetallic $PdCu/ZrO_2$ shows one clear band from Cu and a shoulder and a shoulder (~300°C) assigned to reduction of Cu_2O to Cu°. The peak from Cu reduction is shifted to higher temperatures compared to monometallic Cu/ZrO_2, indicating presence of Cu-Pd alloy[134].The presence of Pd also suggests interactions Pd-Cu. The Fe/ZrO_2 catalyst shows clear peaks at about 300, 400 and 520 °C, associated with several reduction steps ($Fe_2O_3 \rightarrow Fe_3O_4 \rightarrow Fe$) [159]. A gradual shift to lower reduction temperature and increment of H_2 consumption (for Pd) result from the addition of 1% Pd to 5%Fe point to the interaction between the two metals [173]. In other words, the efficient dissociation of H_2 by Pd accelerates the reduction of iron oxide. In our previous work we also showed that XPS supported the presence of strong interactions between Pd and Fe and Pd and Cu in the bimetallic catalysts [180]. Figure A-4 (Appendix A) shows the NH_3-TPD profiles of the catalysts studied in this work. The bimetallic catalysts resulted less acidic than the monometallic ones. The monometallic Pd/ZrO_2 catalyst (332 μmol NH_3/g_{cat} desorbed) was more acidic than the Cu (261 μmol NH_3/g_{cat},) and Fe (260 μmol NH_3/g_{cat}) monometallic, while $PdCu/ZrO_2$ and $PdFe/ZrO_2$ were the least acidic (180 and 169 μmol NH_3/g_{cat}, respectively).

5.4.2 Bio-oil hydrogenation

The core of the experimental campaign was to evaluate the catalytic behaviour of mono metals (5 wt.% Cu, 5 wt.% Fe and 1 wt.% Pd) and their combination (1-5 wt.% Pd-Fe and 1-5 wt.% Pd- Cu) on zirconia support. The catalysts shown similar distribution of support pore diameters (18-20 nm) and surface areas (60 - 68 m^2/g), while the metal particle size have a range of about 6-8.4 nm [180]. Moreover, monometallic Pd/ZrO_2 catalyst was the most acidic, with 332 μmol NH_3/g_{cat} desorbed, subsequently Fe/ZrO_2 and Cu/ZrO_2 (both ~260 μmol NH_3/g_{cat}) while bimetallic catalysts ($PdFe/ZrO_2$ and $PdCu/ZrO_2$) were the least acidic, 169 μmol NH_3/g cat and 180 μmol NH_3/g cat, respectively [180].

5.4.3 Gas phase composition

Figure 5-3 shows the gas composition of the upgraded WBO fraction, where only CO_2 and CH_4 were detected in gas phase. Their presence highlights decarboxylation and methanation reactions, respectively. The cited reactions are favoured in acidic environment, in particular for the elimination of CO_2 from organic acids such as formic

acid, which is present in pyrolysis liquids in significant amounts and is the most reactive organic acid, particularly when noble metal catalysts are present [169]. Methanation was detected only in presence of $PdCu/ZrO_2$, indicating a HDO onto methyl group and a rapid desorption from the catalyst surface [188, 189], or gas phase hydrogenation reactions of CO and CO_2 with hydrogen by methanation reaction [168]. Furthermore, the low amount of CO_2 and CH_4 in gas phase suggests that the catalysts were more selective for hydrogenation than HDO reactions. The amount of gas phase components for the monometallic catalysts (Pd,Cu,Fe) is much higher compared to that evolved by the bimetallic CuPd and in particular FePd. Thus, the use of the bimetallic Fe-Pd catalyst is advantageous when considering its lower formation rate of gas phase components and particularly methane.

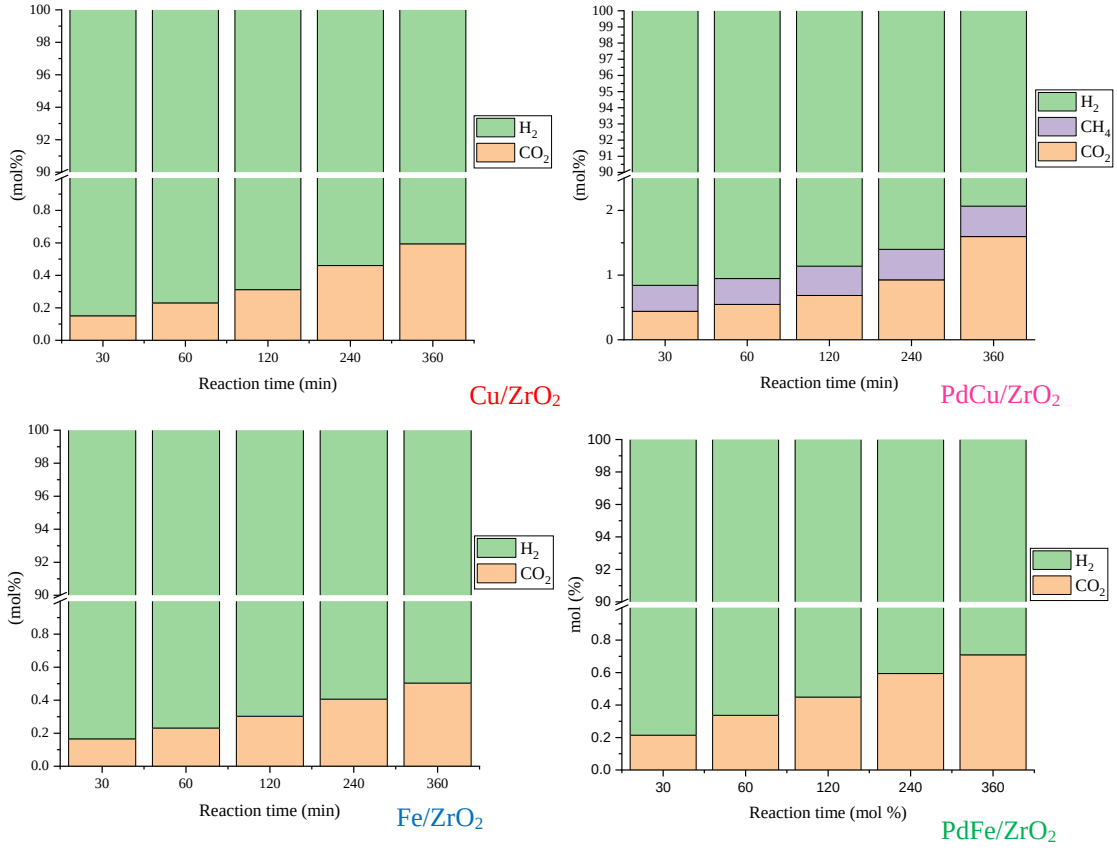

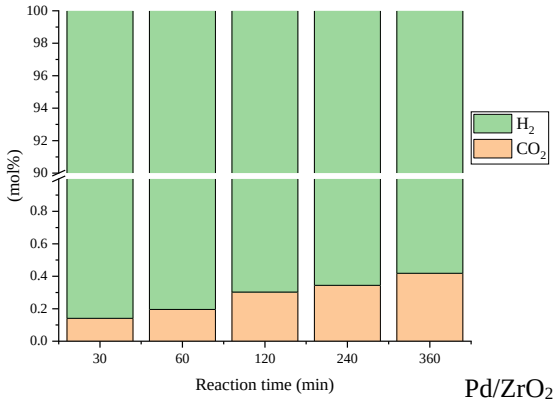

Figure 5-3. Gas composition

5.4.4 Liquid phase composition

The liquid phase was analysed by different techniques due the complexity of the mixture. GCxGC analysis was able to identify most of the functional groups present in solution, as reported in Figure 5-4, where the composition of the WBO at different reaction times and using different catalysts is shown. The main functional groups present in the upgraded WBO fraction were: acids, ketones, alcohols, levoglucosan, guaicols, phenolics and catechols. Furthermore, Figure 5-4 shows the percentage of carbon present in liquid phase (TOC) for the whole experimental campaign. As can be appreciated from the figure, for all the catalysts tested the carbon content in liquid phase decreased according to the reaction time, to a value around 85-90 wt.% after 360 minutes. This is consistent to the gas composition shown in Figure 5-3. The bi-metallic catalysts (PdCu and PdFe) were able to retain most of the starting organics in liquid phase, with only 3% C and 9-10 % C lost in gas phase after 60 and 360 minutes, respectively. PdFe in particular was able to minimise the C lost in gas up to 240 min (4%). Moreover, the different migration of C from the liquid to the gas phase is related to the ability of the (i) not noble metals to adsorb the organic molecule[190] and (ii) the desorption of the CO_2 (Cu>Fe) [191] from the catalytic surface, then not able to react. Overall, from the distribution of the functionalities in Figure 3, it can be seen that $PdFeZrO_2$ was the only catalyst able to maintain most of the organics in liquid phase during the whole hydrogenation experiment, denoting stability. The presence of acids compounds decreased with the reaction time, where about 45% of the acids were removed after 360 minutes. $FeZrO_2$ and $PdFeZrO_2$ resulted more efficient in reducing WBO acidity. Low acidity in bio-oils is a desirable product requirement, since can reduce corrosion rates of feed lines and storage vessels and increase the stability of bio-oil. Previous study showed that organic acids were almost unreactive until about 350 °C (P=200 bar) in continuous HDO and slight reduced (~15%)

when batch reactors were used at temperature between 150 to 250 °C in presence of Ni-Cu catalyst [168]. Therefore, Fe seems to be very effective in the HDO of formic and acetic acids even at low temperature. About 50% of levoglucosan was converted in HDO products by the catalysts after 360 min. HDO of levoglucosan to alcohols and ketones was previously described in literature under similar conditions [80, 192, 193]. The abundance of catechols, phenols and guaiacols increased after the HDO reactions, with $PdFeZrO_2$ being the most active in doing this, with catechols, phenols and guaiacols passing from 5, 5 and 2 wt% (in the starting WBO) to 13, 8 and 4 wt%, respectively. Furthermore, part of the ketones/alcohols and phenolics production were attributed at the HDO of guaiacols and catechols groups (see Figure 5-4). Phenolic groups can further react to alcohol and subsequently cyclo- and linear alkanes. Only $FeZrO_2$ and $FePdZrO_2$ were able to produce cyclohexanes suggesting the Fe is active on cyclic hydrogenation of their C=C bonds, leading to saturation of their aromatic rings into cyclohexanol and 1,2-cyclohexanediol and alkanes, due to C-O bond and C-C bond cleavage reactions.

It is known that, despite the fact that GCxGC analysis is able to give a good picture of the WBO composition for the low molecular weight compounds (up to 200 Da), the oligomers are not detectable, so that GPC analysis was used to evaluate the distribution of the high molecular weight compounds, as reported in Figure 5-5.

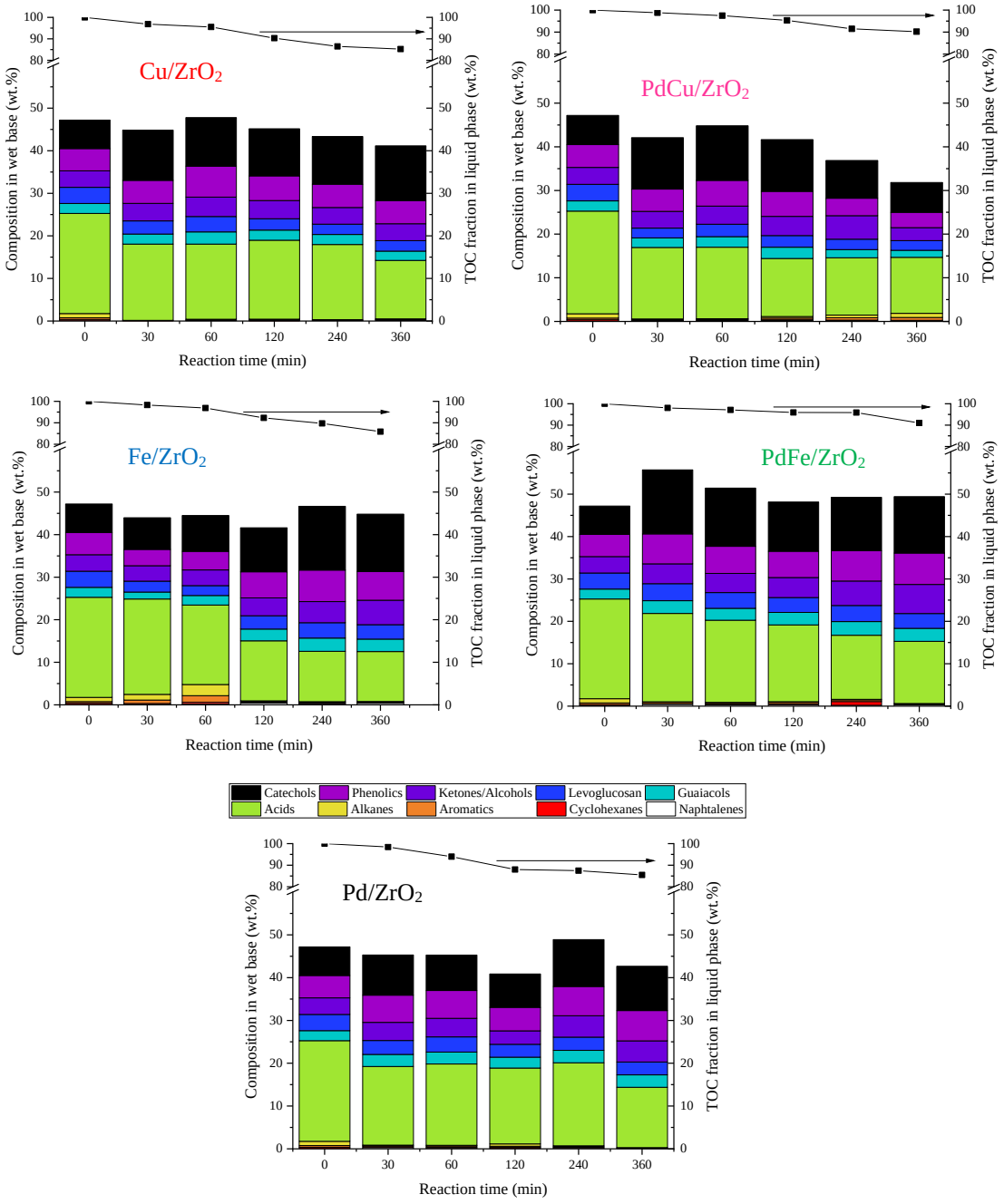

Figure 5-4. Products distribution for HDO of WBO

Overall, the molecular weight distribution analysis shows an increment of compounds with a MW larger than 800 g/mol, which generally increases with the reaction time. This trend was minimised by the presence of the bi-metallic catalysts, in particular for $PdFe/ZrO_2$. The formation of large MW compounds (1500-3000 g/mol) suggests polymerisation reactions. An opposite trend was noted for compounds with MW range about 100 - 300 g/mol, mostly due to HDO of glucose units (180 g/mol) to lower MW compounds.

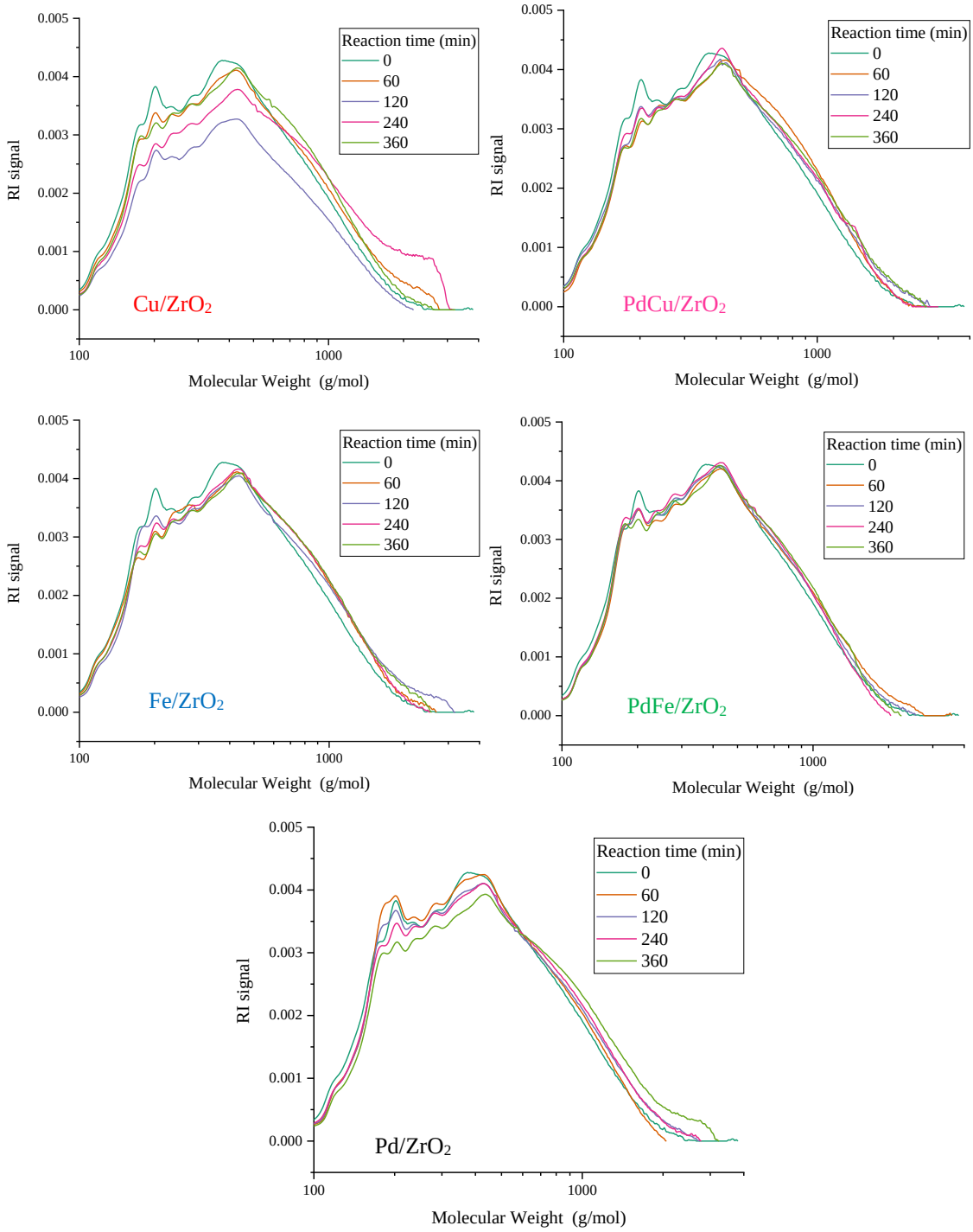

Figure 5-5. Molecular weight distribution (in dry base) for HDO of WBO

After 60 minutes reaction, the addition of Pd to the Cu/ZrO_2 catalyst resulted in a larger abundance of compounds with MW of 500-600 g/mol compared to the starting WBO and considerably reduced the presence of very large compounds (1500-3000 g/mol) compared to the catalyst containing only Cu. Fe/ZrO_2 had a much better capacity to limit polymerisation reactions when compared to Cu/ZrO_2 and this was further enhanced by the addition of Pd, with the $PdFeZrO_2$ showing reduced presence of large compounds

(1500-3000 g/mol) compared to all the other catalysts and even the starting WBO after 240 and 360 minutes, suggesting high and stable activity in depolymerising sugar oligomers. This is also supported by the increased abundance of compounds with MW at about 180 g/mol (glucose or sorbitol) and at 300-450 g/mol (cellobiose and 3-unit sugars). Analysing the performance of the noble metal alone, it can be seen that despite the high activity of Pd after 60 min in enhancing the production of MW compounds between 200 and 300 g/mol, the catalyst led to polymerisation reactions after 240 and 360 min, with enhanced presence of compounds with MW higher than 1000 g/mol. A qualitative analysis was performed by GC-MS, most of the detected compounds are reported in Table S1. Some key compounds were selected and studied qualitatively as their area percentage varied with the reaction time to study the reaction HDO mechanism (see Figure 5-6 and 8).The HDO of the main compounds derived from the cellulose fraction is reported in Figure 5-6. Glycero -d -galacto -heptose decremented according to the increase of the reaction time towards the formation of diols. Hydroxyacetaldehyde exhibited the highest grade of conversion, in term of area percentage reduction, in comparison to the other compounds examined. Ethandiol and ethyl alcohol where the main products from the HDO of glycolaldehyde.

Figure 5-7 shows some compounds related to the lignin fraction. In term of area percentage, the vanillin content increased according to the reaction time due to: (i) the depolymerisation of lignin oligomers. This is in agreement with the GCxGC data (see Figure 5-3) where guaiacols content also increased at the increment of the reaction time. Possible products from the hydrogenation/HDO of guaiacols are ethyl-cyclohexane, 2-methyl-cyclohexanol and cyclohexanone. Figure 5-8shows the percent variation of hemi-cellulose derived compounds in the experiments. Analysing the area percentages area of furfural, the highest decrement was noted for $PdCu/ZrO_2$ (~43%), confirming the previous work [180], while the decrement was of 36%, 21%, 36% and 33% respectively for Cu/ZrO_2, Fe/ZrO_2, $PdFe/ZrO_2$ and Pd/ZrO_2. One of the key components analysed was gamma butyrolactone, which content passed from 0.28 to 0.5 % for Cu/ZrO_2, $PdCu/ZrO_2$ and Fe/ZrO_2 after 360 min and to 0.65 and 0.75 % when $PdFe/ZrO_2$ and Pd/ZrO_2, were used respectively. According to Sanna et al. [62] the presence of gamma butyrolactone is related to the conversion of 2(5H)-furanone and hydroxymethylfurfural, both present in initial WBO fraction. Moreover, furfural was converted to butyrolactone in water thanks to the synergistic effect of metal and the mild acid sites in the catalysts[194].

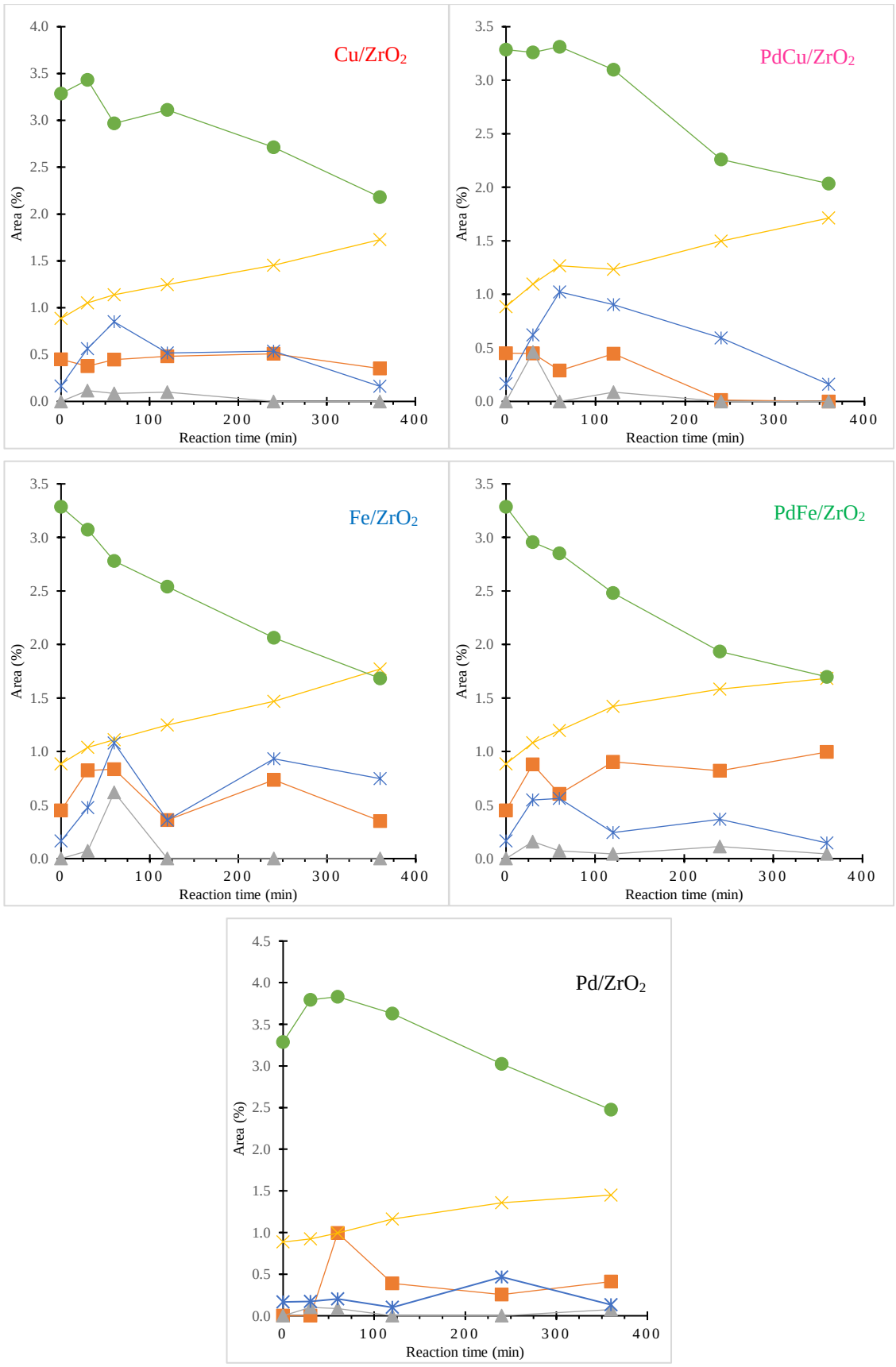

Figure 5-6. GC-MS qualitative analysis for cellulose fraction. Glycero -d -galacto -heptose, Butanediol, Ethanediol, Ethanol, Acetaldehyde, hydroxy-.

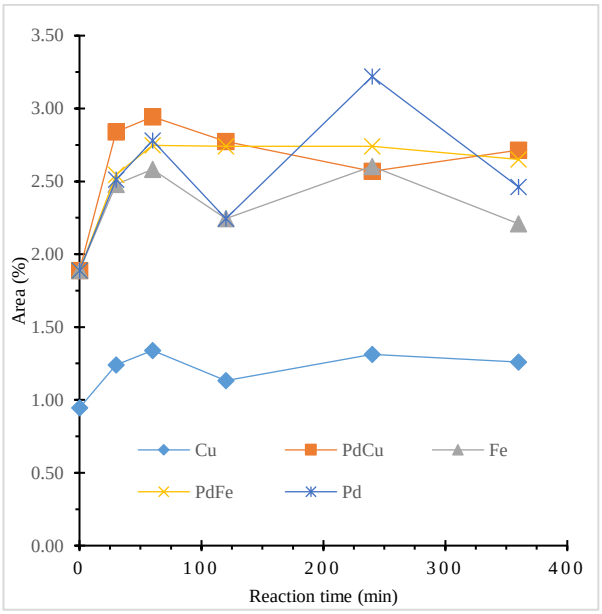

Figure 5-7. GC-MS qualitative analysis for Vanillin

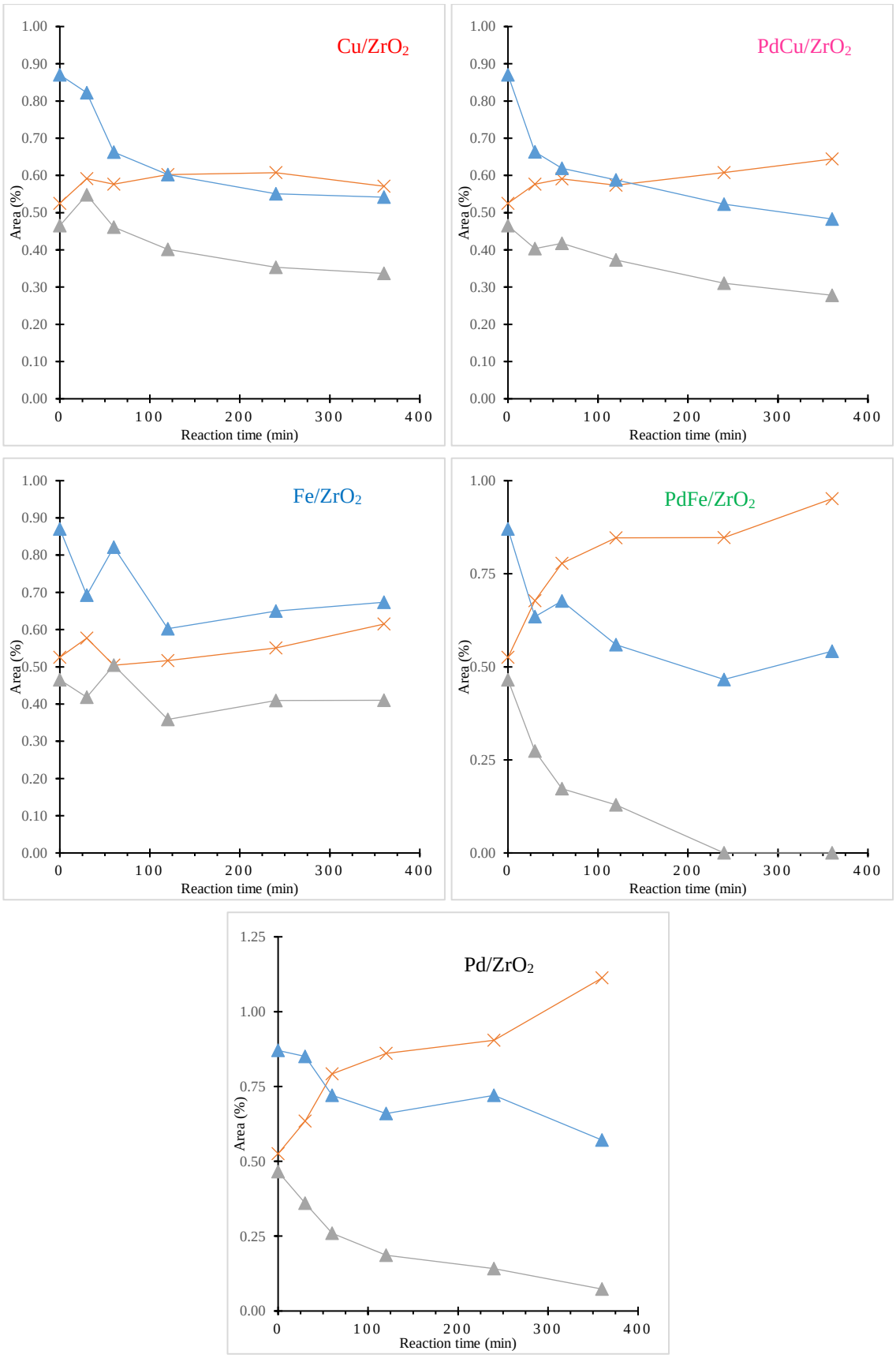

Figure 5-8. GC-MS qualitative analysis for hemicellulose fraction. γ Butyrolactone, 2-Cyclopenten-1-one, Furfural.

TPO was applied to determine the amount of carbonaceous deposits. Both Fe and Cu catalysts present TPO peaks between 250 and 400°C, although of different shape and intensity. This indicates that the nature of the carbonaceous deposits on the non-noble metal catalysts and the activities of the catalysts for the oxidation of carbonaceous species are about similar. Cu seems to be less prone to coking compared to Fe but this could also be linked to differences in HDO activity, with Fe being more active. Previous work showed that the slightly acidic ZrO_2, which is not very active in the hydrotreatment reaction can be partially responsible for repolymerisation reactions and deposition of high-molecular weight products at around 350-400 °C [190].The TPO of Pd shows an additional peak at 500 °C, which may correspond to the oxidation of more complex organic compounds with higher molecular weights than the ones oxidised at lower temperatures [190].

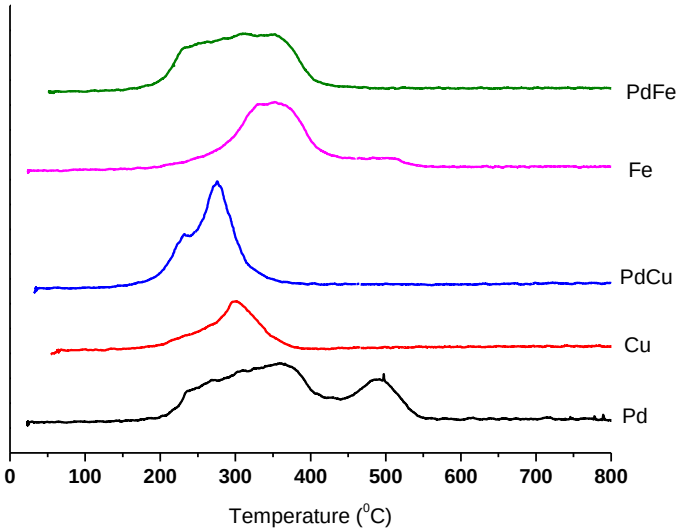

Figure 5-9. Temperature program oxidation

5.5 Conclusions

The catalytic hydrogenation of WBO was investigated in presence of mono- and bi-metallic on zirconia base at low operating condition. The experimental campaign was conducted in batch reactor in presences of 200 mg catalyst and 30 mL of WBO at 100°C and 50 bar. The bi-metallic catalysts (CuPd and FePd) were more effective than the monometallic ones in stabilising the organic phase and retain ~90% C in the liquid phase. Moreover, the catalysts with presence of Fe were able to convert the phenolic compound into hydrocarbon, reducing the acidity of WBO. Also, the synergic work of Pd and Fe shown the lowest presence of molecular compound higher than 1500 g/mol, relating to polymerisation reaction.

Chapter 6 -A novel Ru–polyethersulfone (PES) catalytic membrane for highly efficient and selective hydrogenation of furfural to furfuryl alcohol

This chapter has been published as: G. Bagnato, A. Figoli, C. Ursino, F. Galiano and A, Sanna, A novel Ru–polyethersulfone (PES) catalytic membrane for highly efficient and selective hydrogenation of furfural to furfuryl alcohol, J. Mater. Chem. A, 6 (2018), 4955-4965.

6.1 Abstract

In order to carry out the reaction at middle operating condition, a membrane e reactor has been proposed. A novel catalytic membrane has been synthesised, characterised and evaluated for the selective hydrogenation of furfural to furfuryl alcohol. Unlike conventional methods, involving high pressure and high H_2: feed ratios, this work proposes an innovative Ruthenium based Catalytic Membrane Reactor (CMR) to overcome mass transfer limitations, resulting in low H_2 requirements, high catalytic activity and high selectivity towards furfuryl alcohol. A UV-curable hydrophilic anionic monomer acrylic acid was used as coating material onto a commercial PES membrane and subsequently Ru nanoparticles have been added. The hydrogenation of furfural has been carried out in a customised catalytic membrane reactor under mild conditions: 70 ºC and 7 bar, exhibiting high catalytic activity towards furfuryl alcohol (selectivity >99%) with turnover frequency (TOF) as high as 48,000 h^{-1}, 2 orders of magnitude higher than those obtained so far.

6.2 Introduction

The production of bio-fuels or chemicals from biomass derivates, such us pyrolysis/liquefaction bio-oils or cellulose hydrolysis, is a promising pathway to reduce the dependence on fossil fuels and reducing the emission of greenhouses gases. Bio-oils are obtained from the fast pyrolysis from lignocellulosic biomass, marine biomasses and bio-wastes[195, 196]. Bio-oil is a brown dark liquid with a high viscosity and a high oxygen contents and water, which limits its use us fuel in common engines. To decrease the oxygen content and convert highly reactive functionalities in more stable ones, the bio-oil can undergo hydrogenation reactions [52, 62, 197, 198] resulting in compounds with a higher economic value that can be used for the production of polymers, cosmetics, food additives or drop-in fuels. Furfuryl alcohol is an important chemical intermediate

for the production of chemical products, such as vitamin C, lysine, plasticizer, dispersing agent and lubricants [199]. Furfuryl alcohol can be manufactured by the chemoselective hydrogenation of furfural, which is an aldehyde with a heterocyclic structure and a common product of lignocellulose pyrolysis and/or cellulose hydrolysis [200-202]. The production of furfuryl alcohol from renewable source has recently attracted great interest. Furfural, mainly derives from a variety of agricultural products, including corn, oats, wheat, bran and sawdust. Industrially, the hydrogenation of furfural is used to obtain furfuryl alcohol, intermediate product of industrial process for resin production[203]. Figure 6-1 shows the reaction pathway for the hydrogenation of furfural. The furfuryl alcohol formation is in competition with the tetrahydrofurfural via the saturation of different functional groups, aldehyde and the heterocyclic group, respectively.

Other undesirable products derive from the hydrogenation/ dehydration of furfural in 2 methylfuran and further hydrogenation to 2 methyltetrahydrofuran; with consecutive hydrogenation to pentanol. Furthermore, decarbonylation reaction are favoured at the same condition of the hydrogenation reaction, which lead to the formation of furan subsequently in butanol[204]. All these competing reactions render difficult to control the selectivity on a desired product.

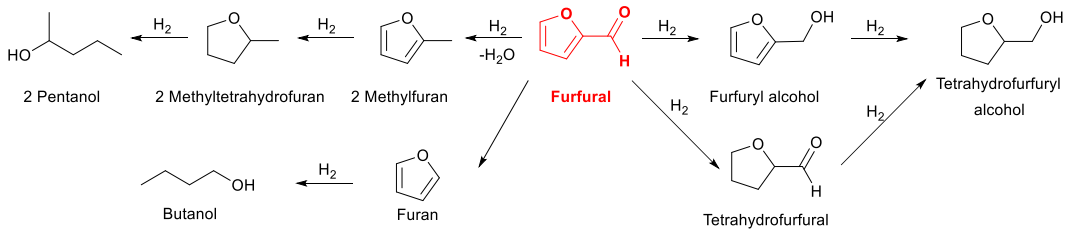

Figure 6-1. Reaction pathways

The hydrogenation of furfural has been studied in both gas and liquid phase [205-207], in presence of metal catalysts, in particular the elements of IX (Co, Rh, Ir) and X (Ni, Pt, Pd) groups and Cu, on supports such as SiO_2, C or Al_2O_3[205, 208-211].

O'Driscol et al. [212] synthesized Pt−Sn/SiO_2 catalyst to study the furfural hydrogenation at different reaction temperatures between 25 and 150 ºC at 20 bar and different solvents in a batch reactor. The authors obtained the complete conversion after 48 h at 100 ºC in presence of toluene. Chen et al. [206] achieved the complete conversion after 5 h at 100 ºC and 10 bar in presence of Pt supported on g-C3N4.

Rh and Pt nanoparticles stabilized by phosphine-functionalized silica for the hydrogenation of different bio-oil compounds were studied by Llop et al. for the hydrogenation of different bio-oil compounds [213] At 80 ºC and 40 bar, furfural was completely converted in furfuryl alcohol in presence of Pt, while the conversion was about 16% using Rh.

The above studies, indicate that high pressure (>10bar) and/or long residence time (hours) are required for the successful selective conversion of furfural in furfuryl alcohol, using traditional reactors (continuous and batch). The main disadvantage of hydrogenation reactions is represented by mass transport limitation, due to the reaction taking place in gaseous, liquid and solid phases. The system must operate under high pressure, which improves the gas solubility into the liquid system and at high temperature, which advantages the kinetic. However, the hydrogen solubility decreases under those conditions. The choice of temperature and pressure reaction are dictated by the conversion of the limiting reagent and the selectivity of desirable product. With the purpose to decrement the mass transfer limitation, the use of membrane reactor (MR) represents a valid choice [214-216]. According to the IUPAC definition, a MR is a device for simultaneously carrying out a reaction and a membrane-based separation, in the same physical enclosure[217]. The membrane can have extractor, distributor or active layer functionalities. For example, Bagnato et al.[218] used a dense Pd-Ag membrane to extract the H_2 from the reaction zone during the steam reforming of a model bio-ethanol in presence of Ni/CeO_2 catalyst. They compared the performance of a MR and a packed bed reactor (PBR) at 400 °C, a gas hourly space velocity (GHSV) of 800 h^{-1}, obtaining the best conversion and hydrogen yield by using the MR. Catalytic membrane reactors were recently proposed for the conversion of biomass substrates into bio-chemicals. The hydrogenation of levulinic acid was carried out using a porous expanded polytetrafluoroethylene (ePTFE) membrane with Ru catalyst particles by Stanford et al.[96]. Different membranes, with and without a dense Matrimid layer, were tested to evaluate the hydrogen flux through the membrane. The hydrogenation reaction was studied in the temperature and reaction pressure range of 40- 90 °C and 0.7- 5.6 bar, respectively. Furthermore, the authors compared the results obtained with a PBR considering the kinetic rate of gamma-valerolactone product over grams of Ru. The MR without the Matrimid layer resulted in the best performance (rate was 4 time higher than PBR), but with a low conversion of

0.0065 %; while the MR with the control layer (Matrimid) showed a kinetic rate 2 time less than the PBR. Two different MRs were studied by Miu et al. [94], who compared (i) a MR plus a catalytic packed bed, where the membrane acted as H2 distributor into the reaction zone (where the catalyst was allocated) and (ii) a catalytic MR, where the membrane was modified adding a catalytic layer. The two systems were tested for the hydrogenation of nitrobenzene in presence of Pd/γ-Al_2O_3 catalyst. The authors noted that, the membrane with the catalytic activity showed best performance in term of conversion and catalytic stability, ~85% for 10 hours. Instead, the MR with the separated catalytic packed bed achieved a conversion of about 20% and 60%, respectively after 4 and 6 hours. A limited number of works have been focused on the specific catalytic hydrogenation of furfural and all of them were done using batch reactors [206, 208, 209]. The outcomes of these works are discussed and compared to this work findings in the last part of this work. The aim of this work was to develop and test a novel catalytic membrane reactor in order to selectively hydrogenate bio-oil derived compounds reducing the amount of hydrogen used. To the best of our knowledge, Ru-functionalised PES membranes have never been synthetized and tested for hydrogenation reactions. Recently, Mengistie et al.[219] used a Pd-PES membrane for the hydrogenation of the -NO_2 group in the nitrophenol in a flow-through catalytic membrane reactor, denoting the stability of PES as support for Pd.

In this work, a novel catalytic membrane with an activity layer was synthesised modifying a commercial PES membrane by photochemical graft [220, 221], polymerization of acrylic acid and doping its surface with Ru nanoparticles. The modified membrane has been characterized in terms of morphology, porosity, pore size diameter, contact angle and Ru content. After that, the catalytic membrane has been tested for the hydrogenation of furfural under mild process conditions for evaluating its Turnover Frequency (TOF).

6.3 Method

The commercial PES membranes (supplied from Hangzhou Cobetter Filtration Equipment Co., China), with different pore size (from 50 to 800 nm), were dipped in grafting solution composed by 25 wt. % acrylic acid, 2.83 wt. % N,N′-methylene-bis acrylamide and 0.0753 wt.% 4-Hydroxybenzophenone in water. PES membrane exposed at UV light (two lamps by General Electric, UV output 2.2 Watt, gap from the samples 6

cm), and the presence of photo-initiators, led at dissociation in free radicals with consecutive polymerization of acrylic acid onto the membrane surface.

The irradiation time was between 5 and 30 min equivalent at 4.84-14.53 J/cm^2 energy flux. Subsequently, the grafted membranes were washed with distilled water removing the grafting solution excess and dried.

The PES modified membrane was dipped in hexaammine-ruthenium (II) chloride solution (0.01 M) for 18 hours at room temperature[219]. The solution reacted with the carboxyl group of acrylic acid onto the PES membrane (Figure 6-2).

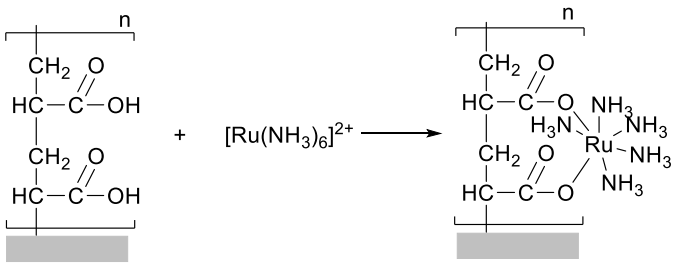

Figure 6-2. Precursor loading

A Na_2BH_4 0.1 M solution was added for reducing the Ru from ions to metallic form for 3 hours (Figure 6-3).

After that, the membrane was washed with distilled water and dried at 80 ºC. Three different commercial PES membranes (pore size of 50, 220 and 800 nm) were modified by different ʼJV light exposition, from 5 to 30 min.

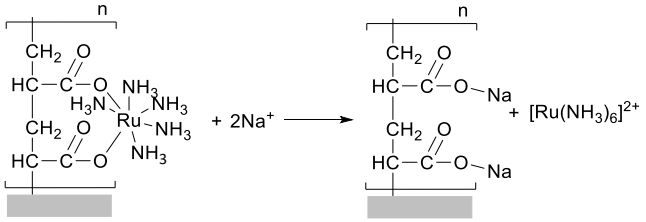

$$[Ru(NH_3)_6]^{2+} + 2BH_4^- + 6H_2O \rightarrow Ru^0 + 7H_2 + B(OH)_3 + 6NH_3$$

Figure 6-3. Redox reaction

6.4 Result and discussion

The modified membranes were then characterized by SEM analysis and the Ru was quantified. The catalytic membrane with an initial pore size of 220 nm, was selected to perform the furfural hydrogenation tests. In order to evaluate the effective presence of the acrylic layer and the Ru content on the PES membrane, different characterisations techniques were employed (Supplement material). The FTIR analysis was used for

measuring the effectiveness of the UV grafting, with the acrylic acid polymerization promoted by UV in presence of compound such as N,N methylenebis acrylamide and hydroxyben-zophenone. Figure 6-4 shows the mid IR spectrum of a modified and unmodified PES membrane with initial pore size of 50 nm. The presence of acrylic acid onto the membrane is highlighted by the peaks at 1720, 1620 and about 1100 cm^{-1}. The presence of acrylic acid onto the membrane is highlighted by the peaks at 1720, 1620 and about 1100 cm^{-1}. Those peaks represent the stretching of C=O, C=C and =C-O- bonds. The different time of exposition at UV light resulted in a different polymerization grade of acrylic acid onto the membrane. The presence of the acrylic layer led to different amount of Ru loaded onto the membrane and to different transport phenomena.

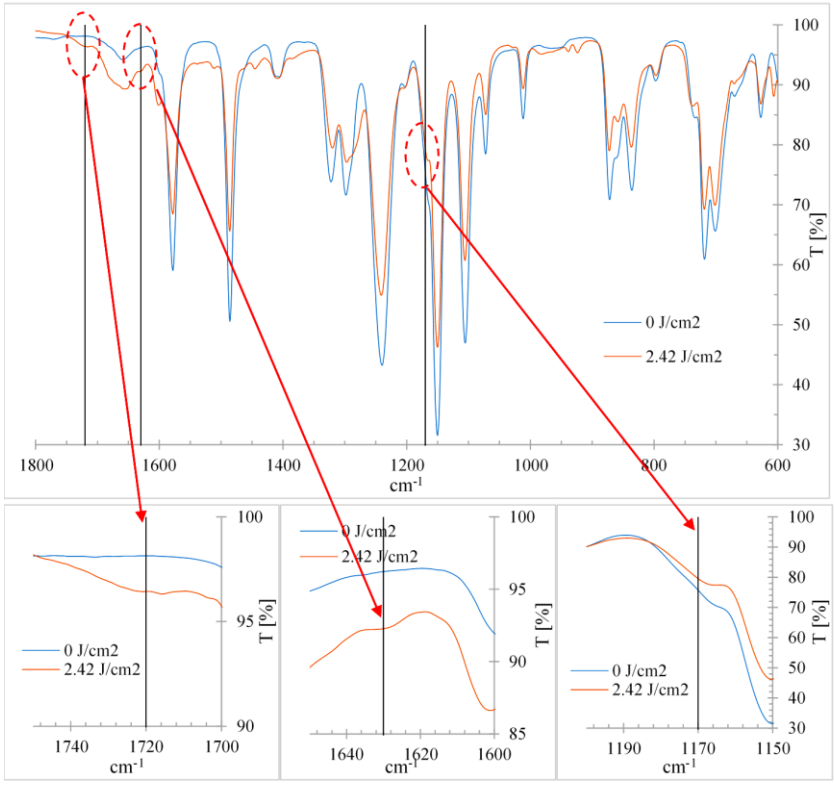

Figure 6-4. FTIR spectrum of PES modified

The morphological changes in the membrane and the formation of the activity layer was evaluated by SEM (see Figure 6 5). A longer UV light exposition involved a larger absorption of energy by the PES membrane, and the presence of photo-initiators, led at dissociation in free radicals with consecutive acrylic monomer addition.

Figure 6-5 shows the modified PES membrane using different UV light exposition. A thicker acrylic layer was obtained using an UV energy flux of 4.84 J/cm^2 (20 µm) than 2.42 J/cm^2 (15 µm), due to a major concentration of free radicals.

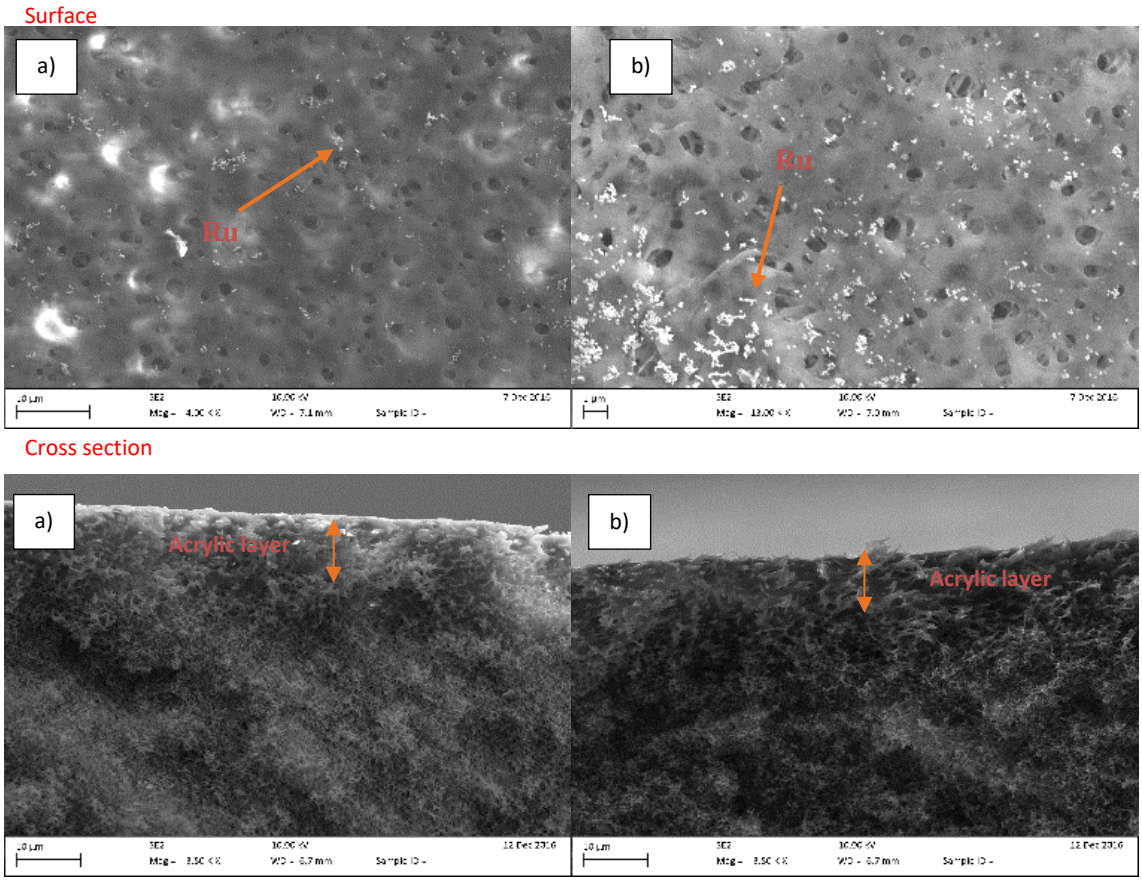

Figure 6-5. SEM surface and cross-section analyses for 220 nm PES modified a) UV= 2.42 J/cm^2 b) UV= 4.84 J/cm^2

The hydrophilic propriety of the modified membrane was quantified by the contact angle between the membrane surface and a water drop. The measurement confirmed the presence of a coated layer on the PES membrane results in changes in the contact angle, as shown in Figure 6-6. For the PES membrane 50 nm and for the bottom layer of PES membrane 200 nm, there was an increment of the contact angle (decrement of hydrophilic proprieties). This phenomenon is linked to presence of Ru nanoparticles onto the membrane surface and to their relative orientation[222, 223].The bubble point, pore size distribution and overall porosity were determined, as reported in the Supplement material, before and after the UV light exposition.

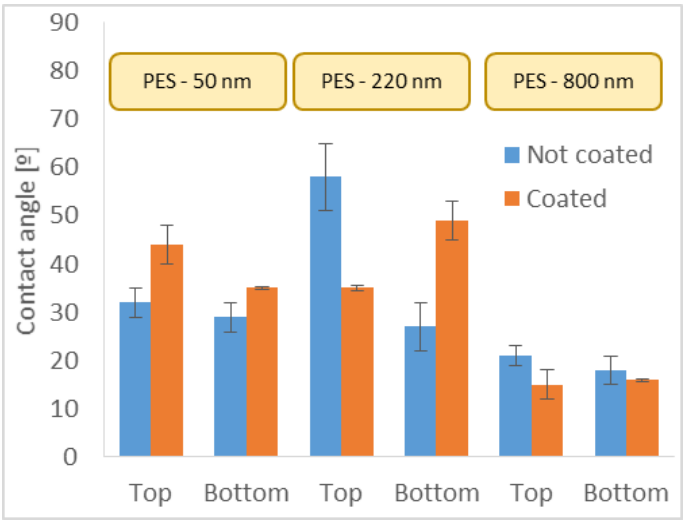

Figure 6-6. Contact angle for PES before and after the coating (UV light 7.26 J/cm^2)

The formation of the acrylic layer resulted in a slight decrement of the porosity from 83 to about 77 % and from 85 to about 81%, respectively for the PES membranes with 50 and 800 nm, as can be seen in Figure 7. Instead, the porosity did not change for the PES 220 nm. The distribution of the pores size is reported in Table 1, indicating that the presence of the coating layer has not a significant effect on the pore size for the PES 50 and 220, while has the contrary effect on the PES 800.

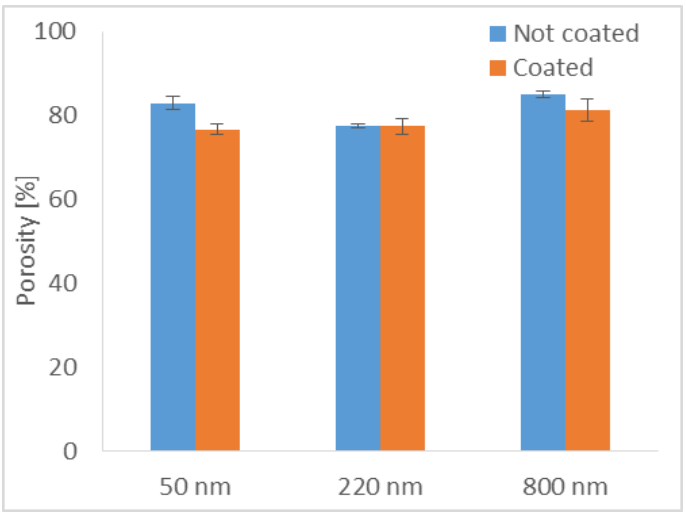

Figure 6-7. Porosity for PES before and after the coating (UV light 7.26 J/cm^2)

Table 6-1. Bubble point, pore size and maximum pore size distribution for PES before and after the coating (UV light 7.26 J/cm^2)

Membrane	Bubble point [bar]	Mean flow pore diameter [nm]	Diameter at maximum pore size distribution [nm]
PES 50 nm not coated	1.55	120	70
PES 50 nm coated	0.78	110	72
PES 220 nm not coated	1.14	280	240
PES 220 nm coated	0.62	240	220
PES 800 nm not coated	0.51	850	740
PES 800 nm coated	0.54	770	700

In order to study the effect of acrylic acid and Ru doping on the mechanical proprieties of the PES membrane structure, the tensile stress was analysed, calculating the Young's module, and the elongation at break, which resulted respectively in the range ≈150-250 N/mm^2 and 17-32 %. Figure 6-8 shows a considerable increment of Young's module after the coating for the membrane PES 220 nm, while was almost unchanged for the PES 50 nm and diminished after coating for the 800 nm PES membrane.

This different behaviour can be attributed to the different morphological structure of the pristine PES membranes, symmetric for the 50 and 220 nm ones and asymmetric for the 800 nm one.

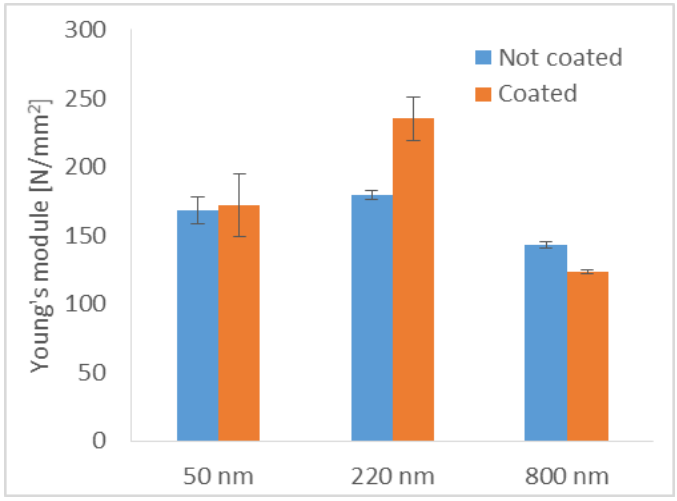

Figure 6-8. Young's module and after the coating (UV light 7.26 J/cm^2)

The PES 220 nm also presented an increase of the elongation at break compared to the other two membranes that showed a decrease of the elongation at break after treatment (Figure 6-9). The Young's module and the elongation break results have been used to assess how the mechanical membrane structure changed after the coating. A high Young's module for 50 and 220 nm membranes indicates a better resistance to deformation from stress, therefore a more rigid structure. The elongation at break instead indicates how the membrane absorbs deformation without breaking. For the membrane 50 and 800 nm there was a clear ductility reduction after coating.

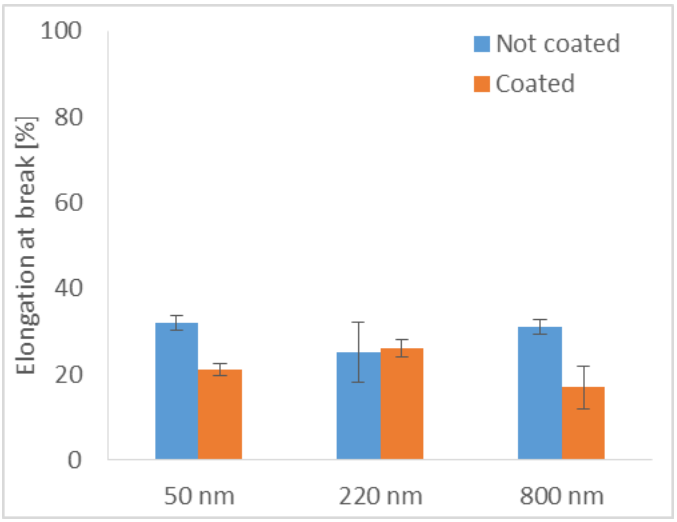

Figure 6-9. Elongation at break and after the coating (UV light 7.26 J/cm^2)

The inductively coupled plasma optical emission spectrometry (ICP –EOS) analysis was used to determine the Ru content loaded onto the coated PES membranes with different pore size. Figure 6-10 shows the concentration of the Ru for the tested membranes: 50, 200 and 800nm. A constant Ru content of about 9 μg/cm^2 was detected for the PES membranes with pores size of 800 nm at the different UV energy supplied (depending on the UV exposition time). An increment of Ru onto the PES membrane surface was noted for the PES membrane with pore size of 220 nm, with about 15 μg/cm^2 for the maximum exposition time of UV light (corresponding at the maximum energ y used).

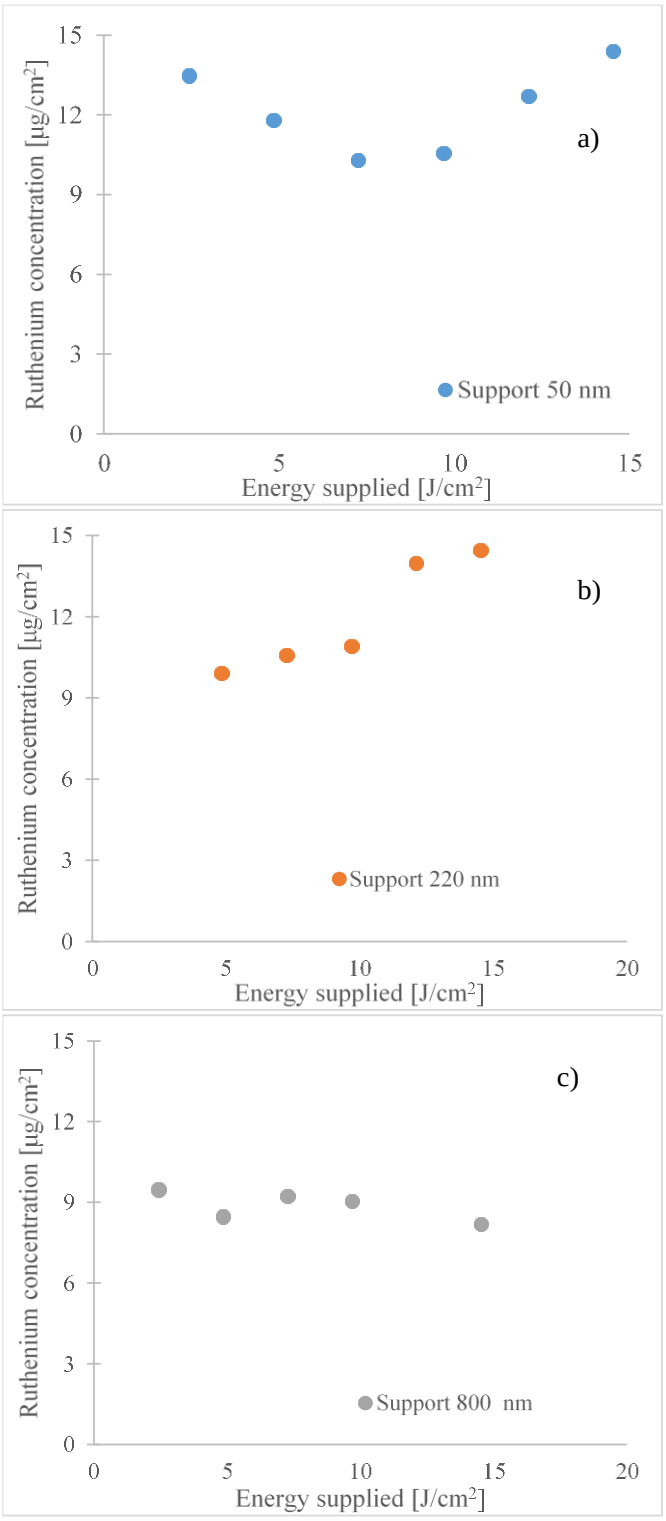

Figure 6-10. ICP analysis for modified a) PES 50 nm, b) PES 220 nm and c) PES 800 nm

An unusual trend was instead observed for the PES 50 nm, with an initial decrease of Ru deposited in the membrane up to an energy flux of about 10 J/cm^2 and an increment of the metal deposited at the longer UV exposition times up to 15 µg/cm^2. From the SEM analysis (see Figure 6-11), it is possible to note that for energy flux lower than 9.69 J/cm^2

(intermediate UV exposition time), the pores size on the membrane surface are relatively larger compared to those obtained with longer UV exposition times. At the longest UV exposition time, corresponding to an energy flux of 14.53 J/cm^2, the Ru content onto the modified membrane was almost equal to that obtained for an exposition of 2.42 J/cm^2, but the pores size distribution was different, five time bigger for the lower energy flux.

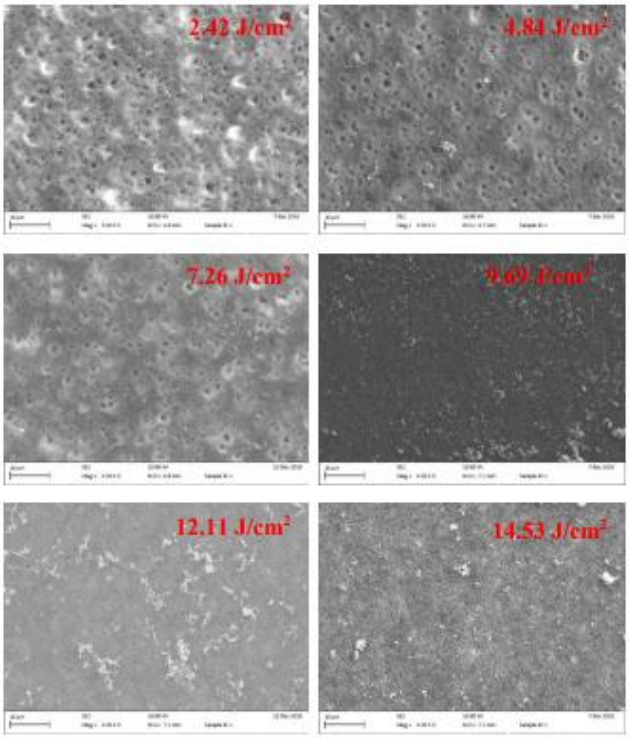

Figure 6-11. SEM PES membrane 50 nm at different energy flux

This difference was caused by the diverse exposition of UV light. The increased number of free radicals produced at high energy flux, influenced the amount of acrylic deposited and the final membrane structure. The pore size reflects on the capacity of the membrane to work as contactor among the phases. Small pores sizes increase the mass transfer resistance of the liquid phase, with consequent reduced contact of the organics in the liquid with the activity layer. On the contrary, large pores sizes lead to short contact into the reaction system (liquid/catalyst/gas), then a low conversion. The PES 220 nm modified membrane showed an intermediate pores size (maximum pore size distribution of 240 nm). More specific analyses were conducted about the Ru NPs on the PES membrane by Transmission electron microscopy (TEM) and X-ray photoelectron (XPS). The surface composition of the Ru-PES membrane was studied by XPS technique, as reported in Figure 6-14a. The survey-scan XPS spectrum shows all the framework elements of the Ru-PES membrane, in agreement with the SEM-EDS data. The high-

resolution XPS spectrum given in Figure 6-14b, shows two significant bands at 284.2 and 280.6 eV, which can readily be assigned of Ru(0) and Ru oxide, respectively[224].

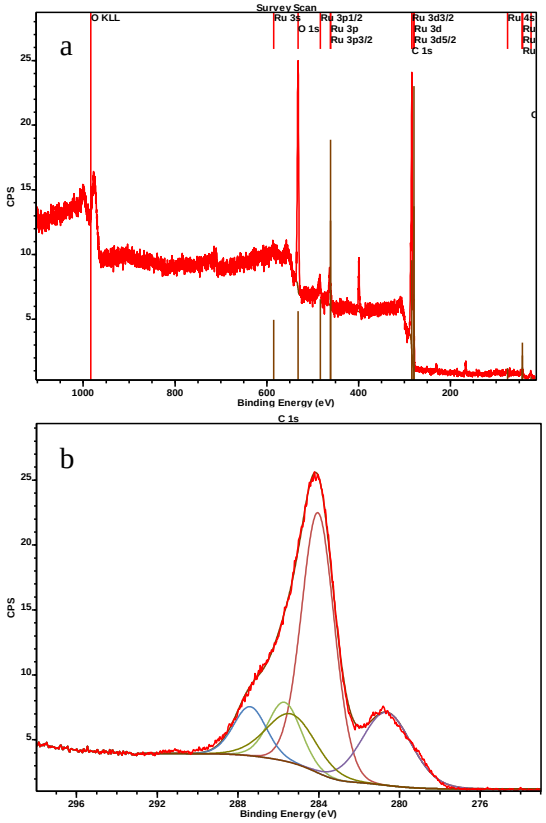

Figure 6-12. a)XPS spectrum for Ru-PES 220 nm, b) Ru 3d XPS spectrum for Ru-PES 220 nm

The presence of Ru oxide can be attribute to the Ru oxidation during the sample preparation for the XPS analysis[225]. TEM images show the internal structure of not coated and coated active layer of Ru-PES membranes. As reported in Figure 6-13, in all cases the presence of Ru nanoparticles is clearly visible, and the coating is homogeneous. In respect to the unmodified membranes, the coated membranes present a thin darker (electrondense) Ru-rich part of the skin and penetration of the Ru nanoparticles on the pores of the support, according to pore size and porosity measurements. Energy-dispersive X-ray analysis were also performed, using the coated and not coated membranes. Spectra demonstrate that the coated membranes are rich in Ruthenium. The additional peaks belong to Copper, used for TEM grid.

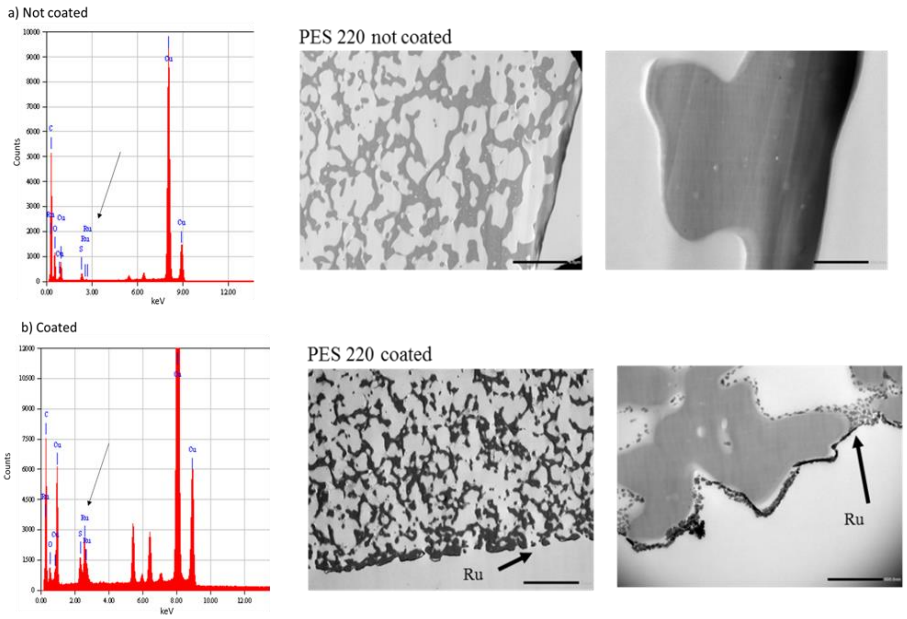

Figure 6-13. TEM and EDX analysis of PES 220 nm membrane a) not coated and b) coated. (Magnification x2000 and x20K, scale bare: left, 5µm- right, 500nm)

In order to evaluate its activity, once characterised, the PES 220 nm modified membrane (UV light grafting at 7.26 J/cm^2) was tested for the hydrogenation of furfural. The test was carried out in duplicate at 70 ºC with a pressure in the gas and liquid zones of 7 bar; a liquid flow rate of 0.497 mL/min, a water feed with 5 wt.% furfural and a hydrogen/ furfural molar ratio of 1. For a complete evaluation and comparison with previous studies, the conversion of furfural, the selectivity for the products (i-compound) and the turnover frequency (TOF) have been defined as:

$$\boldsymbol{x} = \left.\frac{\boldsymbol{Furfural_{in} - Furfural_{out}}}{\boldsymbol{Furfural_{in}}}\right|_{\boldsymbol{molar}} \times \mathbf{100}\ [=]\% \qquad 6\text{-}1$$

$$\boldsymbol{S_i} = \left.\frac{\boldsymbol{i\text{-}compound_{out}}}{\boldsymbol{Furfural_{in} - Furfural_{out}}}\right|_{\boldsymbol{molar}} \times \mathbf{100}\ [=]\ \% \qquad 6\text{-}2$$

$$\boldsymbol{TOF} = \frac{\boldsymbol{mole\ of\ furfural\ reacted}}{\boldsymbol{mole\ of\ catalyst \times reaction\ time}}\ [=]\boldsymbol{h^{-1}} \qquad 6\text{-}3$$

Among the potential reaction products reported in Figure 6-1, only furfuryl alcohol was detected under the tested conditions (selectivity >99%), with a furfural conversion of 26% after 30 minutes. The conversion and selectivity remained constant for 4 hours. Figure 6-14 shows the conversion of furfural for the whole reaction test, where the conversion achieved the steady state condition after 30 min. After 4 hrs, the conversion of furfural decremented to 17%. A potential contribute to the furfural conversion from homogeneous reactions in absence of catalyst at the studied conditions, was excluded a priori based on previous assessments. Chen et al. [206] did not observe any conversion (less than 1%) at 10 bar and 100°C without catalyst. Moreover, Sanna et al. [62], who investigated the

homogeneous (without presence of catalyst) continuous flow hydrogenation of furfural at 125°C, 51 bar H_2 for 36 h, did not observe any change at 125°C in the furfural concentration. In order to compare the hydrogenation reaction of the furfural with previous works, the operating condition, conversion of furfural, products selectivity and TOF present in literature, are summarized in Table 6-2. Since all the previous works were carried out using batch reactors, similar process conditions can be used to generally compare a PBR reactor vs a CMR. However, a precise comparison of the catalyst properties is difficult due to the different reactors set-up and the use of TOF should be preferred. By the eq. 4-3, the TOF represents the reactant converted per catalyst mole per unit time (typically the second), with the number being a function of the operating conditions. Analysing the TOF obtained in the available works on furfural hydrogenation, the highest value of 48,000 h^{-1} was obtained in this work, mainly due for different factors: (i) the high hydrogenation activity of Ru at low temperature; (ii) a good stability of Ru in aqueous phase and (iii) high hydrogenation selectivity on carbonyl group [208, 210, 211]. Ru catalyst is widely used for hydrotreating biomass derivate substrates at low temperature[224]. Tan et al.[225] studied the Ru activity on different supports for the hydrogenation of levulinic acid to γ–valoerolactone from -10 to 100 ºC, with a completely selectivity in γ–valoerolactone and a conversion of levulinic acid of about 70 and 100%, respectively. (iv) The enhanced contact between the H_2 and the Ru active sites due to the reduced mass transfer limitation[226] in presence of the modified PES membrane. Under the studied conditions, the presence of three phases is due at a series of mass transfer limitations, where the main limitation step is represented by the hydrogen absorption to the catalyst surface. A method to improve the driving force of the solubility process is an increment of the pressure, very common for hydrogenation reaction in liquid phase, or the enhancement of the contact surface between the liquid and gas phase. For a PBR, the contact surface is about 100 m^2 per m^3 of reactor, while contact surface is in the order 1500-7000 m^2 per m^3 of module for hallow fibres membrane[227, 228]. The PES was mainly used as enhanced contactor and for its chemical resistivity in presence of furfural at the used conditions. Since H_2 in gas phase has low solubility in the other phase, higher surface area contact between these phases decreases the need of higher pressure that could have been applied to less soluble component. Moreover, suppling the H_2 through a porous membrane, it allowed the hydrogen to be adsorbed directly onto the Ru surface, and part solubilised in the liquid phase. The catalytic MR favoured the reaction in term of TOF, 48,000 moles of furfural has been converted in 1 hour and using 1 mole of Ru catalyst.

The conversion of furfural obtained was about 26%, value that is lower than some data reported in literature, but reasonable if considered the low ratio of hydrogen/furfural (1:1) and that only about 780 μg (2-3 order of magnitude less than the literature data) of Ru were loaded into the membrane. Moreover, it has to be stressed that the residence time of the reactants in the membrane layer was very low, at about 1 s, compared to typical residence times > 1 hour in PBR. For comparison, Nakagawa et al. [56] reported a similar conversion (14%) using 2%Pd and 2%Ru on silica with 49% selectivity on furfuryl alcohol after 1 hr, but much higher pressure (80 bar) and H_2:furfural molar ratio (125) were used, resulting in a TOF of 337. In the same study and under the same conditions, 4%Ir/SiO_2 was the most selective to FOL (96%) with a conversion of 14% and TOF of 67. Fang et al.[210] loaded different amount of Ru nanoparticle, from 1 to 5 wt.%, on an acidic MOF material (MIL-101) obtaining a total conversion of furfural at 160 °C and 40 bar and in presence of 3 wt.% Ru/MIL-101, but with furfuryl alcohol selectivity of only 1 %. A complete conversion and selectivity to furfuryl alcohol was obtained by Yang et al.[211] at 20 ºC and 5 bar in presence of Ru on aluminium-based MOF (Al-MIL-53-BDC). However, the TOF in that case was 21 h^{-1}, indicating that a large amount of catalyst was used for converting the furfural (to convert 21 mol/h of furfural, 101.7 gr of Ru, which corresponds to 3.5 kg of 2.9 wt.% Ru/ Al-MIL-53-BDC). Chen et al. [11] also achieved a 99% selectivity to FOL at comparable temperature (80 ºC) and pressure (10 bar) with 32% conversion and a TOF of 120 using 5%Pt on g-C_3N_4 nanosheets, but using a H_2:furfural molar ratio of 2. In order to improve the furfural conversion, others reaction tests were carried out at the same temperature and reaction pressure, but varying the H_2/furfural feed molar ratio to 4:1. A maximum furfural conversion of 21% was obtained after 1 hour with a virtual complete selectivity to tetrahydro-furfuryl alcohol. This can be explained by the complete hydrogenation of the heterocyclic ring due to the H_2 excess. Moreover, the absence of tetrahydro-furfural among the products indicates that an increment of H_2 favoured the further hydrogenation of furfuryl-alcohol to tetrahydro-furfuryl alcohol, rather than the formation of tetrahydro-furfural and then its hydrogenation to tetrahydro-furfuryl alcohol, as showed in Figure 6-1.

Table 6-2. Hydrogenation of furfural (continue)

Catalyst	Operating conditions							Performance parameters					Ref.
								Selectivity [%]					
	Solvent	Reactor	Reaction/ Resident time	Temperature [°C]	Pressure [bar]	H_2/furfural Molar ratio [-]	Conversion [%]	THFA	FOL	THF	others	TOF [h^{-1}]	
2 wt% Pd/SiO_2	H_2O	batch	1	2	80	125	25	19	69	7	5	21	[208]
2 wt% Pd/SiO_2	H_2O	batch	1	2	80	125	63	27	33	28	13	53	[208]
2-2 wt% $Pd-Ir/SiO_2$	H_2O	batch	1	2	80	125	67	31	47	19	3	1690	[208]
2-2 wt% $Pd-Ru/SiO_2$	H_2O	batch	1	2	80	125	14	23	49	20	8	337	[208]
2-2 wt% $Pd-Rh/SiO_2$	H_2O	batch	1	2	80	125	5.7	13	77	3	7	137	[208]
2-2 wt% $Pd-Pt/SiO_2$	H_2O	batch	1	2	80	125	2.5	5	79	<1	16	63	[208]
4 wt% Ir/SiO_2	H_2O	batch	1	2	80	125	14	<1	96	<1	4	67	[208]
2 wt% Pd/SiO_2 2 wt% Ir/SiO_2	H_2O	batch	1	2	80	125	26	10	85	1	4	262	[208]
3-1 wt% $Pd-Ir/SiO_2$	H_2O	batch	1	2	80	125	30	27	47	21	5	522	[208]
1-3 wt% $Pd-Ir/SiO_2$	H_2O	batch	1	2	80	125	61	19	67	11	3	2783	[208]
2-2 wt% $Pd-Ir/SiO_2$	H_2O	batch	2	2	80	125	99	63	16	20	2	1250	[208]
2-2 wt% $Pd-Ir/SiO_2$	H_2O	batch	4	2	80	125	>99	80	<1	18	1	625	[208]
2-2 wt% $Pd-Ir/SiO_2$	H_2O	batch	6	2	80	125	>99	80	<1	18	2	415	[208]

continue

Catalyst	Operating conditions							Performance parameters					Ref.
								Selectivity [%]					
	Solvent	Reactor	Reaction/ Resident time	Temperature [°C]	Pressure [bar]	H_2/furfural Molar ratio [-]	Conversion [%]	THFA	FOL	THF	others	TOF [h^{-1}]	
2-2 wt% Pd-Ir/SiO_2	H_2O	batch	6	2	80	125	>99	91	<1	6	4	83	[208]
2-2 wt% Pd-Ir/SiO_2	H_2O	batch	6	2	80	125	>99	94	<1	1	5	28	[208]
Ir–ReO_x/SiO_2	H_2O	batch	8	40	60	1370	>99	0.5	96.9	n/a	2.6	22	[209]
Rh(0.66)–Ir–ReO_x/SiO_2	H_2O	batch	8	40	60	1370	>99	58.2	14.4	n/a	27.4	20	[209]
Pd(0.66)–Ir–ReO_x/SiO_2	H_2O	batch	8	40	60	1370	>99	66.8	0	n/a	33.2	20	[209]
Rh(0.66)–Ir/SiO_2 + Ir–ReO_x/SiO_2	H_2O	batch	8	40	60	1370	>99	6.6	86.6	n/a	6.8	15	[209]
Rh(0.66)–ReO_x/SiO_2 + Ir–ReO_x/SiO_2	H_2O	batch	8	40	60	1370	>99	21.3	55.7	n/a	23	13	[209]
Pd(0.66)/SiO_2 + Ir–ReO_x/SiO_2	H_2O	batch	8	40	60	1370	>99	1.9	81.7	n/a	16.4	20	[209]
5% Pt@CN	H_2O	batch	5	100	10	2	60.9	n/a	>99	n/a	n/a	45	[206]
0.5% Pt@TECN	H_2O	batch	5	100	10	2	32.1	n/a	>99	n/a	n/a	242	[206]
1% Pt@TECN	H_2O	batch	5	100	10	2	49.4	n/a	>99	n/a	n/a	186	[206]
2.5% Pt@TECN	H_2O	batch	5	100	10	2	95.9	n/a	>99	n/a	n/a	145	[206]
5% Pt@TECN	H_2O	batch	5	100	10	2	>99	n/a	>99	n/a	n/a	75	[206]

continue

Catalyst	Operating conditions							Performance parameters					
								Selectivity [%]					
	Solvent	Reactor	Reaction/ Resident time	Temperature [ºC]	Pressure [bar]	H_2/furfural Molar ratio [-]	Conversion [%]	THFA	FOL	THF	others	TOF [h^{-1}]	Ref.
5% Pt@TECN	H_2O	batch	1	80	10	2.11	31.8	n/a	>99	n/a	n/a	120	[206]
5% Pt@TECN	H_2O	batch	1	100	10	2	90.3	n/a	>99	n/a	n/a	340	[206]
5% Pt@TECN	H_2O	batch	1	120	10	1	90.5	n/a	99	n/a	n/a	341	[206]
5% Pt@TECN	H_2O	batch	1	100	5	1	61.2	n/a	>99	n/a	n/a	231	[206]
5% Pt@TECN	H_2O	batch	1	100	20	2.5	98.0	n/a	98.9	n/a	n/a	369	[206]
1 wt% Ru/MIL-101	H_2O	batch	2.5	160	40	2.25	46	n/a	22	n/a	n/a	n/a	[210]
2 wt% Ru/MIL-101	H_2O	batch	2.5	160	40	2.25	93	n/a	16	n/a	n/a	n/a	[210]
3 wt% Ru/MIL-101	H_2O	batch	2.5	160	40	2.25	>99	n/a	1	n/a	n/a	n/a	[210]
4 wt% Ru/MIL-101	H_2O	batch	2.5	160	40	2.25	95	n/a	2	n/a	n/a	n/a	[210]
5 wt% Ru/MIL-101	H_2O	batch	2.5	160	40	2.25	90	n/a	1	n/a	n/a	n/a	[210]
3 wt% Ru/C	H_2O	batch	2.5	160	40	2.25	72	n/a	46	n/a	n/a	n/a	[210]

continue

Catalyst	Operating conditions							Performance parameters					Ref.
								Selectivity [%]					
	Solvent	Reactor	Reaction/ Resident time	Temperature [°C]	Pressure [bar]	H_2/furfural Molar ratio [-]	Conversion [%]	THFA	FOL	THF	others	TOF [h^{-1}]	
2.9% Ru/Al-MIL-53-BDC 25	H_2O	batch	1	20	5	$1.81 \cdot 10^6$	12	n/a	>99.9	n/a	n/a	20	[211]
2.9% Ru/Al-MIL-53-BDC	H_2O	batch	1	20	5	$1.81 \cdot 10^6$	21	n/a	>99.9	n/a	n/a	18	[211]
2.9% Ru/Al-MIL-53-BDC	H_2O	batch	2	20	5	$1.81 \cdot 10^6$	100	n/a	>99.9	n/a	n/a	21	[211]
3.0% Ru/Al-MIL-53-ADP	H_2O	batch	1	20	5	$1.81 \cdot 10^6$	3.0	n/a	>99.9	n/a	n/a	4.9	[211]
3.0% Ru/Al-MIL-53-ADP	H_2O	batch	1	20	5	$1.81 \cdot 10^6$	5.0	n/a	>99.9	n/a	n/a	4.1	[211]
3.0% Ru/Al-MIL-53-ADP	H_2O	batch	2	20	5	$1.81 \cdot 10^6$	44	n/a	>99.9	n/a	n/a	8.9	[211]
10.9 μg/cm^2 Ru-PES *	**H_2O**	**MR**	**$3.13 \cdot 10^{-4}$****	**70**	**7**	**1**	**26.13**	**n/a**	**>99**	**n/a**	**n/a**	**$4.8 \cdot 10^4$**	**This work**
10.9 μg/cm^2 Ru-PES *	**H_2O**	**MR**	**$3.13 \cdot 10^{-4}$****	**70**	**7**	**1**	**20.83**	**>99**	**n/a**	**n/a**	**n/a**	**$4 \cdot 10^4$**	**This work**

THFA= tetrahydrofurfuryl alcohol, FOL= furfuryl alcohol, THF= tetrahydro furfural

*corresponding at 0.080 μg Ru/g PES

** calculated as: reaction volume (equal at membrane volume 6 cm x 12 cm x 130 μm)/ overall liquid flow rate (0.497 mL/min)

After 150 min from the beginning of the 4:1 test, the furfural conversion was reduced to 12%, suggesting that the modified Ru-PES membrane was not stabl e for the furfural hydrogenation. As can be seen in Figure 6-14, the furfural conversion was relatively stable for the first 3 hrs and then declined to 12% after 6.5 hrs. To understand the reason of the decreased conversion, the presence of Ru in both (i) the membrane (before and after the experiments) and (ii) the product-solutions was analysed.

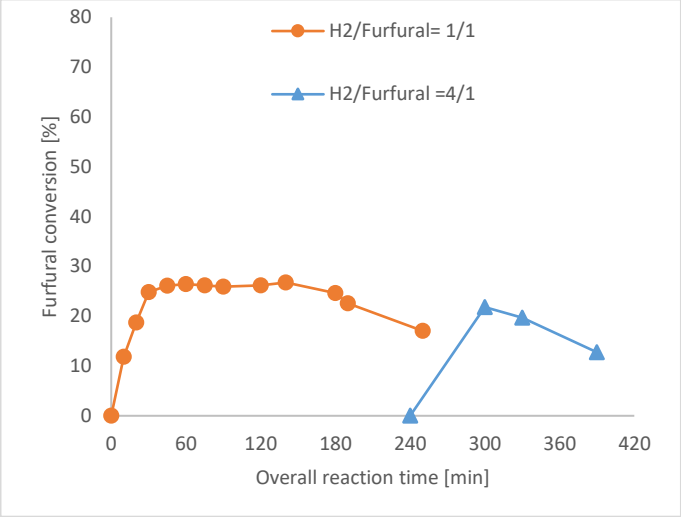

Figure 6-14. Furfural conversion vs time and Ru content before and after the reaction test

The Ru concentration was detected in the products stream for the whole experimental campaign by ICP-EOS and GC-MS analyses, as reported in Figure 6-15.

The highest Ru concentration of 40 μg/L was found in the product-solution after 30 min, while only half of that concentration (18 μg/L) was in the product after 180 min. In the same time, the GC-MS data did not show presence of Ru-Acrylic acid (AA) residue in the product-solution. Instead, Ru-AA residue started appearing from the product sampled after 240 min as shown in Figure 6-15.

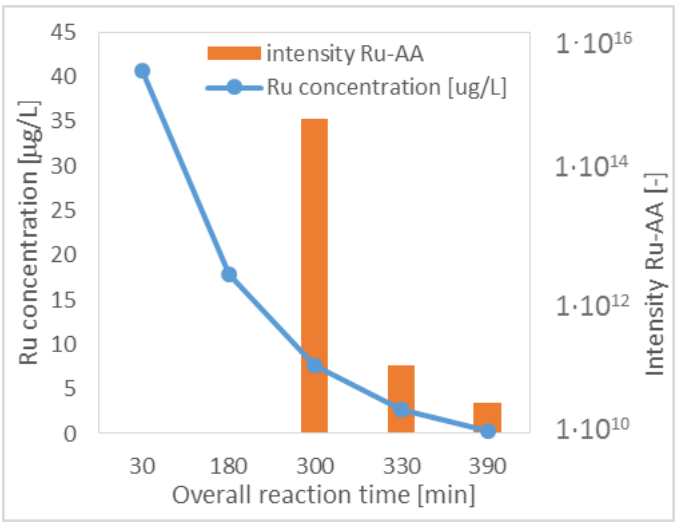

Figure 6-15. Ru concentration in products solutions

This suggest that the large presence of Ru in the product after 30 min (about 50% of Ru lost in solution) is most likely related to the removal of "Ru metal-clusters" not bonded to the AA that were not removed by the water pre-washing step under ambient conditions. This explains the stability of the catalytic membrane in the first three hours, while the appearance of Ru-AA residue from the forth hour suggests that also the activity layer (acrylic monomer and Ru) was partially removed in the liquid phase, so that a more resistant metal support rather than acrylic acid would need to be used for the furfural hydrogenation process. Moreover, from the TEM image after the hydrogenation test (Figure 6-16), is possible to see the presence of the Ru on the membrane, which appears to have preserved the homogeneity and dispersion of Ru in the coated layer. However, the EDX confirms that overall, the Ru is less than before the hydrogenation test. To further elucidate this, at the end of the hydrogenation tests, the metal onto the membrane was quantified before and after the reaction, confirming a decrement from 10.9 µg/m^2 to 5.76 µg/m^2, half of which can be linked to the activity layer degradation. In conclusion, Ru nanoparticle was added onto the surface of modified PES membrane by UV source.

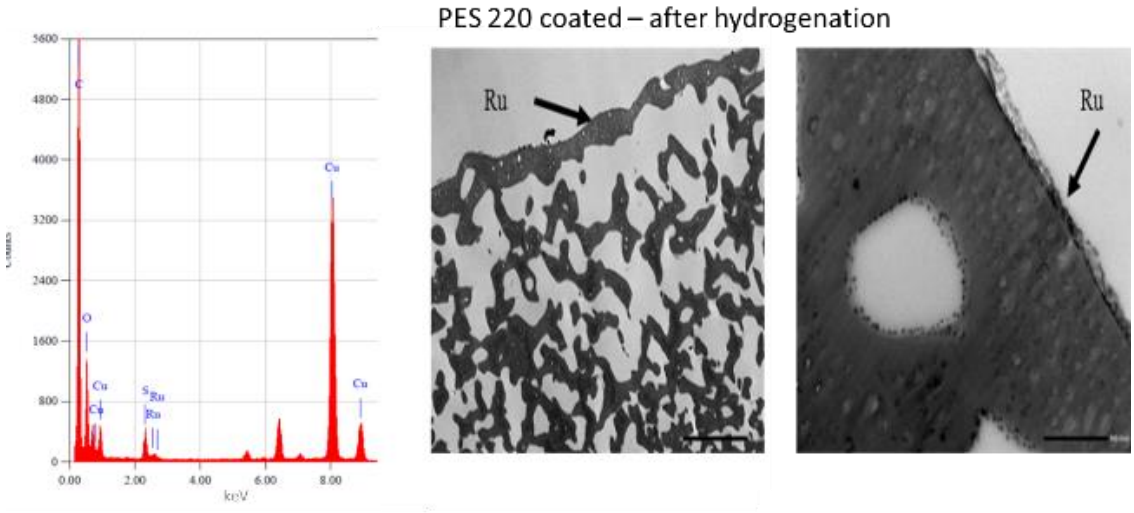

Figure 6-16. TEM image after the hydrogenation test. (Magnification x2000 and x20K, scale bare: left, 5µm- right, 500nm)

6.5 Conclusion

The catalytic membrane was characterized with different technique in order to evaluate the effective presence of the activity layer and of the Ru nanoparticles. The membrane with initial pore size of 220 nm and 10.9 µg/cm^2 of Ru catalyst was tested for the hydrogenation of furfural under mild conditions (7bar, 70°C) resulting in >99% selectivity towards FOL with a TOF of 48,000 h^{-1}, when a H_2/furfural molar ratio of 1:1 was used. The TOF resulted considerably higher than those reported in literature suggesting that the catalytic membrane reactor enhances the catalytic activity of the Ru in the selected reaction. While, a >99% selectivity to THF was obtained by increasing the H_2/furfural molar ration at 4:1 under the same process conditions. The use of the CMR also resulted in residence time of the reactants in the membrane layer of less than 2 seconds, compared to residence time higher than 1hr for conventional PBR. Therefore, this work indicates that selective hydrogenation of furfural to FOL can be successfully performed using CMR under mild conditions, but alternative support polymeric materials need to be developed/tested and the recyclability of the catalysts addressed for rending this pathway commercially viable.

Chapter 7- Development of Ru-PEEK-WC catalytic membrane using green solvent for stable hydrogenation reactions

7.1 Abstract

As a promising technique for multiphase catalytic reactions, the widespread applications of gas–liquid– solid microreactors are still limited by poor durability. Hence, in this work a novel catalytic membrane has been synthesised for carrying out the hydrogenation reaction of a simulated water bio oil fraction (WBO). A PEEK-WC membrane was obtained by VIPS/ NIPS technique using a green solvent (Tamisolve®), with subsequently surface solfanation and doped with Ru. The modified membrane has been characterised with different techniques and subsequently tested for WBO hydrogenation of the WBO at different temperature (65-85°C), pressure (11-18 bar) and H_2 flow rate (5 -25 mL/min.) achieving the highest conversion of furfural to about 75 %, at 85 ºC and 11 bar, and 57.53% furfuryl selectivity. While the vanillin hydrogenation for all the experimental campaign reached a total selectivity in vanillin alcohol. Finally, the Ru-PEEK-WC membrane was able to perform in a stable manner for about 90 hours.

7.2 Introduction

Biofuels are an alternative source of energy to conventional fuels. They are unique as they are the only renewable energy source capable of replacing fossil fuels in all energy utilisation sectors; heat, power and transportation [229]. Second generation biomass such as lignocellulose is non-edible biomass source that can be grown together with food crops or on non-agricultural land which is advantageous as it prevents food sources from being used for energy production. Besides, it eliminates the competition between the use of fertile land for food production and energy generation, which is the case with biofuels derived from first-generation biomass [230]. Biofuels can be synthesised via a variety of process routes, each with varying intermediates depending on the desired specific final product, including bio-routes (e.g. fermentation) and thermo-chemical routes (e.g. gasification, pyrolysis, liquefaction). Pyrolysis densifies lignocellulose into bio-oil (main product), gas and char under ambient pressure and short residence time (<3 s) at around 500°C in the absence of oxygen. Bio-oil via yield of up of 75 wt.% (dry feed) can be usually obtained by lignocellulose fast pyrolysis [231]. The produced liquid bio-oil mixture primarily contains oxygen-compounds, however over 400 different compounds are produced in the process [232]. Both the original bio-mass composition, in

combination with the process operating conditions, affects the specific bio-oil composition produced.

The fast pyrolysis production route is favoured in comparison to the other thermal, biological and physical processes as it is the simplest and most cost-effective way for processing lignocellulosic biomass, and thus produces the lowest cost bio-fuel [60].

Bio-oils require product upgrading before they can be used in current infrastructure unless they are to be used directly as boiler fuel [233]. This is due to their unfavourable physical and chemical properties such as thermal and chemical instability [234], high oxygen content (30-40 wt%) which significantly lowers their energy content and increases both the acidity and corrosiveness of products [233], high viscosity and ash content [4] and high water (~ 20 wt%) [232]. This high water content results in a polar nature and thus, the bio-oil is immiscible with crude oil [235]. A two-step process comprising of a low-temperature hydrogenation step, for the stabilisation of the bio-oil, followed by a high-temperature hydrodeoxygenation step for oxygen removal has therefore been developed for the production of the final value-added products[236]. Noble metal catalysts such as Pd, Ru and Pt tend to be used for this stage due to their increased hydrogenation activity [236]. However, the Ru catalyst, supported on carbon, has been selected due to its superior activity in aqueous-phase hydrogenation [224].

Moreover, changing the operating condition and solvent, different selectivity can be achieved. For example Alibegovic et al.[237] were able to synthesise Pt-and Pd-containing magnetite nanoparticles (NPs) stabilized by polyphenylquinoxaline and hyperbranched pyridylphenylene polymer for hydrogenation of furfural, achieving a conversion of about 98% and selectivity about 85%, at 120 ºC 60 bar in presence of isopropanol. Furthermore, the same group stabilised the NPs using use of hypercrosslinked polystyrene, able to maintain constant reaction performances for 7 cycles [238].

Based on previous studies undertaken, the main challenges facing the commercialisation of this hydrogenation step is the large hydrogen requirement for maintaining a high product selectivity [62]. Furthermore, due to this large hydrogen requirement, the process is expensive [239], mainly due to the mass transfer limitations which is a result of the limited solubility of H_2 in water.

Catalytic membrane micro-reactors have been recently proposed to overcome this limitation in the production of bio-chemicals and in hydrogenation reactions [94, 96, 129, 219, 240]. Catalytic membrane micro-reactors combine chemical reactions with

membrane separation and provide a more compact and less capital-intensive system design, along with achieving improved selectivity and/or yield.

The membrane provided to improve the contact between the reactants and the catalyst which should improve the reaction efficiency. The membrane functionality was to create an active contact surface between the liquid bio-oil, solid catalyst and gaseous hydrogen, as all three phases must be in contact for the reaction to take place. By incorporating the Ru catalyst into the membrane allows for optimisation of the product distribution, thus reducing undesirable side reactions [241]. The hydrogen and bio-oil streams can be sent counter currently along the membrane with the catalyst position determining where the reaction takes place [242].

The hydrogenation of levulinic acid was studied using Ru-expanded polytetrafluoroethylene (ePTFE) membrane in the range 40–90 °C and 0.7–5.6 bar, showing an hydrogenation rate 4 times higher than that of using a PBR [96]. Liu et al. (2016) studied the hydrogenation of nitrobenzene in the presence of a Pd/γ-Al_2O_3 coated polytetrafuoroethylene film modified by dopamine [94]. The authors noted that the membrane with the catalytically active layer showed the best performance in terms of conversion and stability (compared to conventional MR) as a result of enhanced mass transport of hydrogen.

Zhu et al. (2018) developed a gas–liquid–solid microreactor with a polydopamine functionalized surface coated with highly-active palladium nanocatalysts by the electroless deposition plus using hydrogen as a reducing agent [243]. This method increased both the utilization efficiency of the Pd ions and the durability of the microreactor compared to Pt/CNT, Pd/Al_2O_3 and Pt/TiO_2 active layer membranes.

Mengistie et al. [219] used a Pd–PES membrane for the hydrogenation of the –NO_2 group in nitrophenol in a flow-through catalytic membrane reactor, denoting the stability of PES as a support for Pd. Recently, our group has proposed an innovative Ru-PES composite membrane for hydrogenation reactions [129]. The Ru doped PES membrane was able to selectively convert furfural into furfuryl alcohol with high TOF (48,000 h^{-1}) under mild operating conditions (70 °C and 7 bar), but the Ru-PES membrane showed instability over time due to Ru leaching under acid conditions.

Unfortunately, the durability of the existing catalyst layers inside the membrane microreactor fabricated by the conventional methods is still poor [94, 129, 244, 245]. Therefore, facile methods are needed for preparing catalyst layer with good durability and activity in membrane microreactors for this technology to be commercially viable.

Modified poly ether ketone (poly(oxa-p-phenilene-3,3-phthalido-p-phenylene-oxyphenylene) (PEEK-WC: WC refers to cardo group) is a polymer containing a spirolacton group with good thermal stability, mechanical property and high resistance to chemicals due to its high glass transition temperature (225 °C) [240]. Due to these properties, PEEK-WC membranes find wide applications in different fields such as in biomedical engineering, fuels cells, liquid-liquid extraction and pervaporation [240, 246, 247]. Presence of WC increases solubility enabling techniques such as nonsolvent-induced phase inversion to be used in their preparation allowing for a larger range of membrane characteristics to be achieved [248]. Also, the PEEK-WC membrane has an high chemically and mechanically stability in acid environment than other polymeric membranes and an high permeability [249, 250].

Sulfonation can be used to increase the hydrophilicity of PEEK by introducing charged sulfonate (-SO_3-) groups into the polymer backbone. Sulfonation of PEEK can be applied before or after polymerization, where the former can achieve a high degree of sulfonation, but the resultant material has poor mechanical stability [251]. Hence, post-polymerization sulfonation is preferable in hydrogenation applications, where thermal and chemical integrity is critically important.

The aim of this work was to develop and test a novel and stable catalytic composite membrane in order to hydrogenate bio-oil derived compounds. To the best of our knowledge, Ru-functionalised PEEK-WC membranes have never been synthesized and tested for hydrogenation reactions.

For the preparation of PEEK-WC membranes, Tamisolve® NxG (identified from now on as Tamisolve®) was explored, for the first time, as an alternative non-reprotoxic and biodegradable solvent[252]. Tamisolve® is a polar aprotic solvent with high boiling point (241°C). The similar solubility parameters with those of traditional toxic solvents such as dimethyl formamide (MDF), N-methyl pyrrolidone (NMP) and dimethyl acetamide (DMA) and its completely miscibility with water, make Tamisolve® an ideal candidate for the preparation of PEEK-WC membranes, by phase inversion techniques, in a more sustainable way.

Therefore, this work focuses on the implementation of a sulfonated PEEK-WC membrane to overcome stability limitations shown by Ru-PES membrane on aldehydes groups' hydrogenation in aqueous media. Particular focus was on the use of green solvent in the PEEK-WC synthesis and the sulfonation stage towards durable membranes.

7.3 Materials and methods

7.3.1 Polymeric Membrane preparation

The membrane was prepared at room temperature via vapour induced phase separation / non-solvent induced phase separation (VIPS/ NIPS). The polymer used was PEEK-WC (13 wt.%) with Tamisolve® (87 wt.%) as a greener solvent . The polymer solution was cast on a glass plate into a climatic chamber using a manual casting knife with a set thickness of 0.35mm and let to evaporate for the 7 minutes and humidity of 55%, before the immersion in a water coagulation bath. The membranes were removed from the coagulation bath after 3h and washed in hot water (60°C) for 3 times to remove all the solvent. Finally, the membranes were dried in the oven for 4 hours at 40°C.

The PEEK-WC membrane was immersed into H_2SO_4 solution at different concentrations (from 50 to 80 wt.%) and time of exposition at 60 °C, in order to evaluate the sulfonation grade of the membrane surface. Subsequently, the modified PEEK-WC membrane was washed and dried and doped with Ru. The PEEK-WC modified has been placed into a bath of Sodium Mercapto Sulphonate (3.40 g salt in 200mL H_2O) and added 2.39 g Ru (III)Cl_3 x H_2O solution (2.39g of salt into 200mL H_2O). After 30 minutes, the reduction solution has been added (4.36g $NaBH_4$ in 200mL water) and left for 2 hours.

A simulated bio-oil was made, by mixing the following key compounds: vanillin (3.75 wt.%), acetic acid (4.2 wt.%), furfural (5.32 wt.%) and glucose (30.62 wt.%) in water for a total organic content of 43.89 wt.%. the pH of the solution as measured by a pH indicator paper and resulted acidic (pH=2- 3) as typical bio-oil.

7.3.2 Membrane characterisation

The membranes were then tested using a Thermogravimetric Analysis (TGA) (TA Q500), to determine the membrane performed more favourably at various temperatures and at which point the membrane structures change. The temperature rate was imposed to 10 °C/min until 550°C, feeding 22mL/min of nitrogen.

Fourier Transform Infrared (FTIR), Pore size and bubble point, contact angle, mechanical tests, SEM test and Ru content have been described on 3.2 Membrane preparation and characterisation.

7.3.3 Reaction test

The bench scale hydrogenation set-up consisted to a first stage where the liquid was fed by Eldex Pump (P-100), while the hydrogen stream was supplied by the Brooks mass flow controllers.

Both streams were heated up and sent into the second stage for carrying out the reaction into the catalytic membrane reactor (active surface 120x60 mm). The membrane reactor consisted in two stainless steel plates where the catalytic membrane was placed between them (see Figure 7-1), dividing the liquid and vapour zone. The presence of the catalytic membrane had the function to improve the contact among the phases.

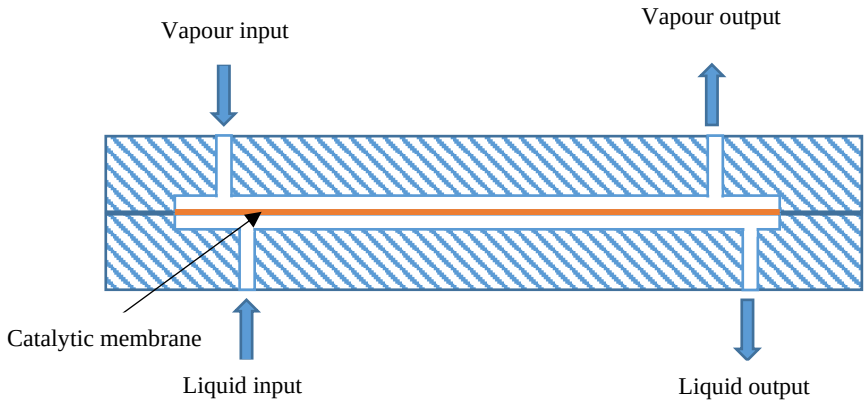

Figure 7-1. Membrane reactor layout

In the last stage, the output of catalytic membrane reactor was collected in a Dreschel bottle in an ice trap system and the liquid composition was analysed by HPLC Agilent 1200 series with MS hook-up. After each reaction test the catalytic membrane was regenerated with a flow of H_2 and N_2 respectively 0.8 mL/min and 2.2 mL/min for 8 hours [129].

During the experimental campaign, the operating condition such as the reaction temperature, reactor pressure and hydrogen flowrates were evaluate their effect on the simulated WBO hydrogenation. In particular:

- Pressure: 11 bar, 16 bar and 18 bar.
- Temperature: 65 °C, 75 °C and 85 °C.
- Hydrogen flowrate: 5 mL/min, 18 mL/min and 25 mL/min.

7.4 Results and discussion

7.4.1 Membrane characterisation

PEEK-WC membranes have been sulfonated superficially dipping them into an acid bath at different concentration of H_2SO_4. After the sulfonation procedure, the membranes immediately changed colour from white to orange/yellow becoming brittle, thus suggesting that these H_2SO_4 concentrations were effective on altering the PEEK-WC structure.

The TGA analysis (Figure 7-2), shows that the weight loss depended on the degree of sulfonation, with the higher weight losses corresponding to the higher degrees of sulfonation, which is represented clearly by the 70% and 60% sulfonic groups [253]. Moreover, the decrease in weight at approximately 450°C for all membrane types, is the point at which the polymer begins to degrade.

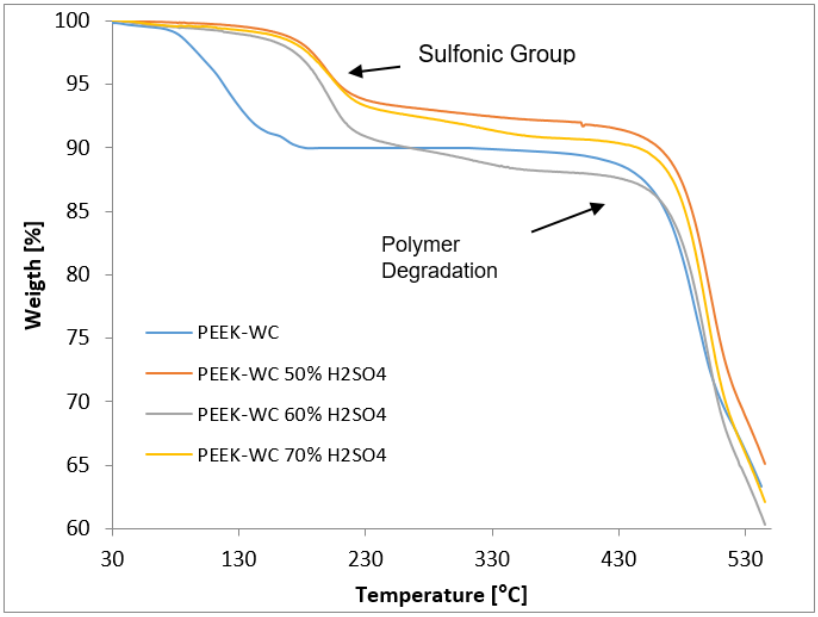

Figure 7-2. TGA Analysis for membranes sulfonated using varying concentrations of sulphuric acid solutions

FTIR analysis was carried out to determine which sulphuric acid concentration provided the optimal degree of sulfonation. The FT-IR spectra were recorded in the range of 4000-800 cm^{-1} with the relevant ranges shown below in Figure 7-3 and Figure 7-4. To verify that the sulfonation of the PEEK-WC membranes had taken place and that sulfonic groups were present, the S-PEEK-WC membrane spectra results were again compared to those of a non-sulfonated PEEK-WC membrane. In the results relating to S-PEEK-WC's, the band at 3394cm^{-1} (Figure 7-3) corresponds to the stretching vibrations of the S-O-H

functional group, which is due to the large volume of water bonded to the sulfonic groups. No water absorption was observed for the non-sulfonated membrane. Figure 7-4 demonstrates the S-O-C stretching vibrations. It is clear when compared to the non-sulfonated membrane, that sulfonic groups are present in the modified membranes. Also, the degree of sulfonation generally increases hand in hand with the sulfonic group band intensity and the amount of water bonded to the membrane. The membrane in which was sulfonated using the 60% solution, however, shows a higher peak in comparison to the 70% solution. This may be due to a variation in membrane thickness [253]. Due to the damage experienced by the membrane when exposed to the 70% mass and 80% mass solutions, the 60% mass solution was found to provide the most favourable results.

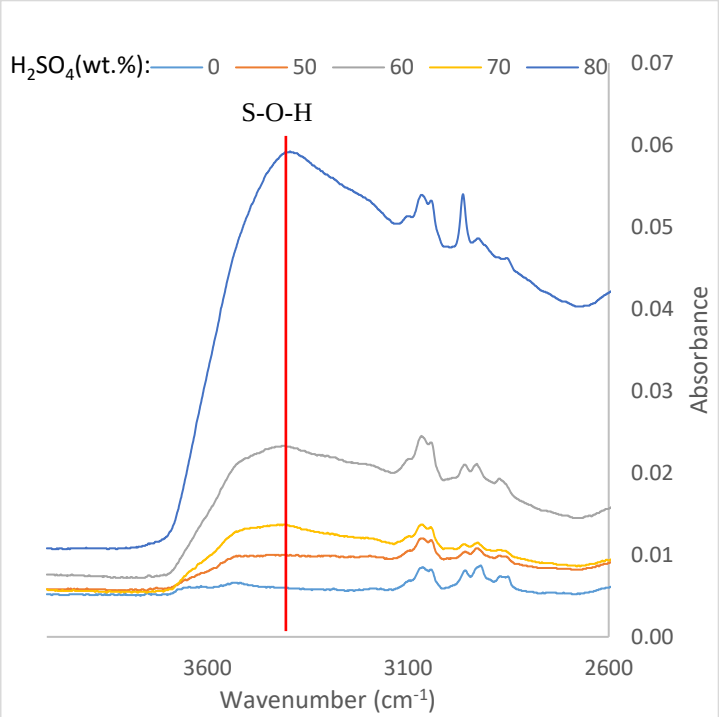

Figure 7-3: FT-IT Analysis results for membranes sulfonated using varying concentrations of sulphuric acid

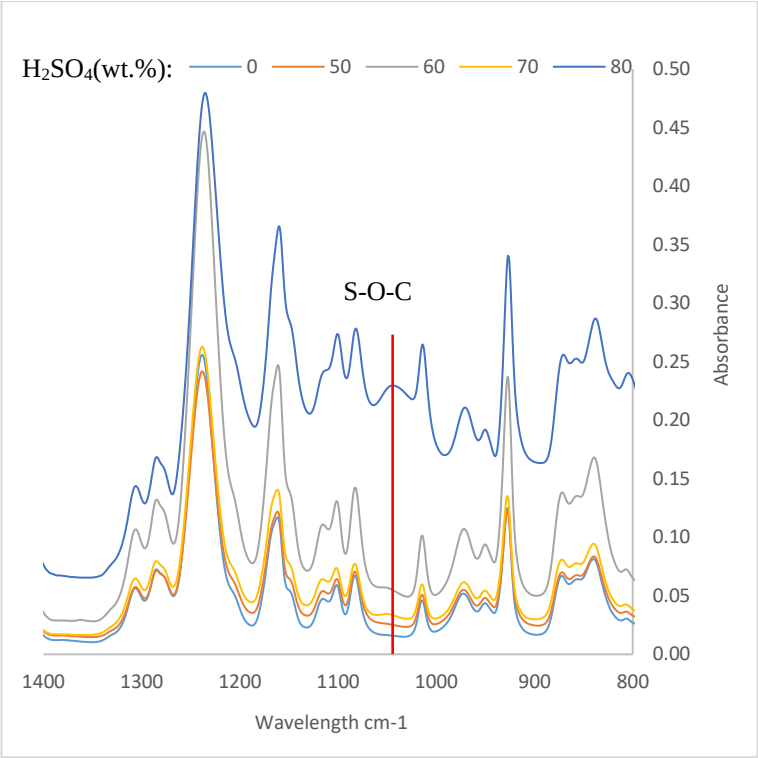

Figure 7-4. FT-IT Analysis results for membranes sulfonated using varying concentrations of sulphuric acid

The effect of the sulfonation duration was then investigated using the 60% solution, which demonstrated the most favourable sulfonation results. Therefore, 5 membranes were prepared and each exposed to a 60wt. % H_2SO_4 solution for one the following time durations: 30 mins, 1 hour, 2 hours, 4 hours and 6 hours. A non-sulfonated membrane was also analysed for comparison purposes.

Figure 7-5 shows that as the sulfonation period increases, the degree of sulfonation also increases. The only exception to this trend is the result for the 60-minute sulfonation period, which presents a peak higher than that of the 120 minute sulfonation period. This could possibly be due to a variation in membrane thickness or perhaps due to the damage the membranes experienced when exposed to the H_2SO_4 solutions for periods of over 60 mins. Due to the damage the membranes experienced when subjected to the solution for time periods over 60 mins, a 60-minute sulfonation period was determined to be most favourable.

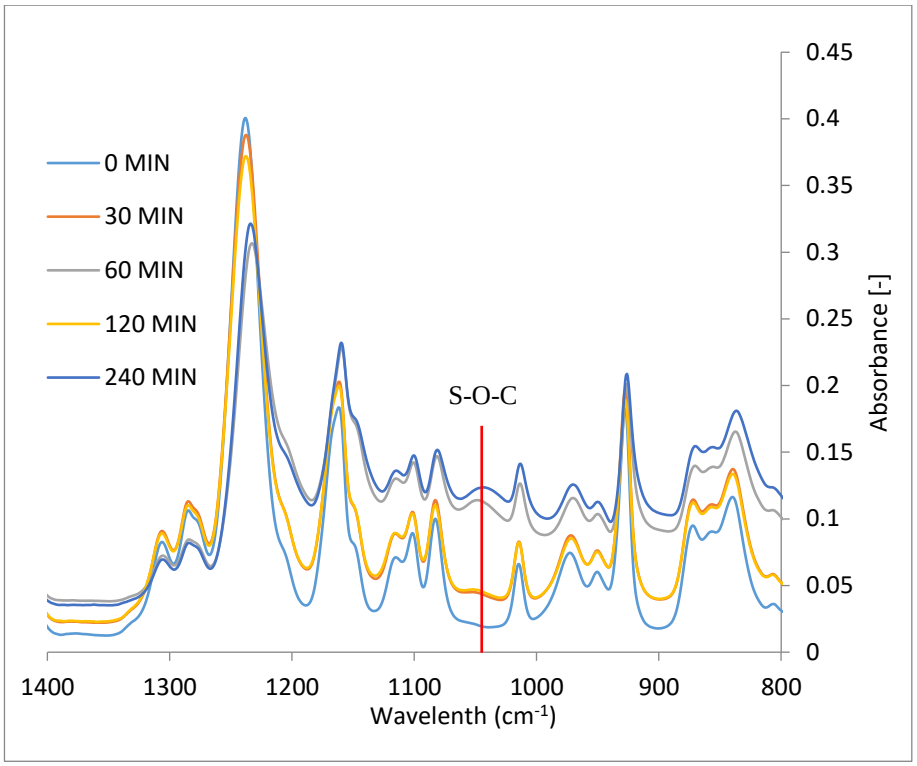

Figure 7-5. FT-IR Analysis for PEEK-WC membranes sulfonated using the 60% sulfuric acid for varying time periods

Furthermore, the membranes were characterized in terms of mechanical tests, porosity and contact angle. As reported in Table 7-1, the addition of the Ru catalyst the membrane had improved strength (Youngs modulus) from 19 to 74 N/mm^2, indicating a rigidity of the material, due mainly to the surface sulfonation, embrittlement the membrane.
Previous work shows that the sulphonation of PEEK-WC results in a decrease of Young's modulus [254]. However, the doping with Ru could have promoted the rigidity of the material as observed for other catalysts [255]. Both membranes showed a hydrophilic nature (Table 7-1) with a surface contact angle value between 72-75°, in line with literature data [256].

Also highlighted by the elongation at break test, was a reduced ability to resist changes of shape without crack formation. Both membranes showed a hydrophilic nature, displayed by the contact angle test being below 90° (Figure 7-6, Table 7-1).
If compared to the Young's modulus with the Ru-PES membrane (≈150-250 N/mm^2), PEEK-WC membrane shows good mechanical features[129].

Table 7-1: Characterization of the PEEK-WC membrane with and without Ru

		Membrane (blank)	Membrane (with Ru)
Mechanical tests	Young modulus (N/mm^2)	19 ± 2	74 ± 5
	Elongation at break (%)	23 ± 4	5 ± 1
Contact angle (°)	Top	72 ± 3	75 ± 3
	Bottom	61 ± 4	84 ± 4
Pore size	Bubble point (bar)	1,53±0,20	0,30±0,03
	Mean pore size(μm)	0,07±0,00	0,14±0,06

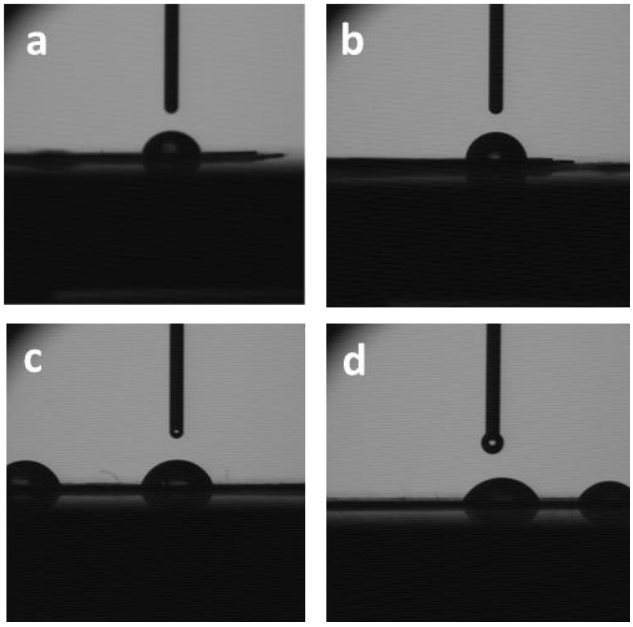

Figure 7-6. Contact angle a) Membrane + Ru (Top); b) Membrane C+ Ru (Bottom); c) Membrane blank (Top); d) Membrane blank (Bottom).

The membrane morphology was evaluated before and after the modification by SEM-EDS (see Figure 7-7), in term of pore size as confirmed from Table 7-1, the modified membrane has pore size diameter two times bigger than the blank membrane, 0.07 μm. The SEM surface morphology of non-doped and doped membranes is shown in Figure 6a and 6b, respectively. The modified membrane clearly presented a roughest surface characterised by a larger pore size of round and ellipsoidal shape surrounded by relatively round fibrils as pore walls. Enlarged porosity was also confirmed by pore size measurements reported in Table 7-1. The Ru doped membrane showed a pore size diameter (0.14 μm) two times bigger than the blank membrane (0.07 μm), while the porosity slightly increased after treatment due to the concurrently sulphonation and

dissolution of the PEEK-WC membrane, which is expected to correspond with an increase in roughness and surface nano-topography [251]. Presence of Ru and S on the Ru-S-PEEK-WC membrane surface was confirmed by EDS. The Ru is clearly visible as bright areas on the surface of sulphonic groups on the treated membrane and it is expected to be found also in the internal surface of the open pores [129]. The figure clearly show that the distribution of the Ru particles is not homogeneous, and the size varies from ~30 nm to ~200 nm. Moreover, larger agglomerates as big as 1 µm are shown in the magnified picture. The Ru detected by SEM-EDS of the selected area was 0.95 at%, while the overall Ru content in the Ru-S-PEEK-WC membrane was quantified by ICP-OES, resulting in 25.5 µg/cm^2.

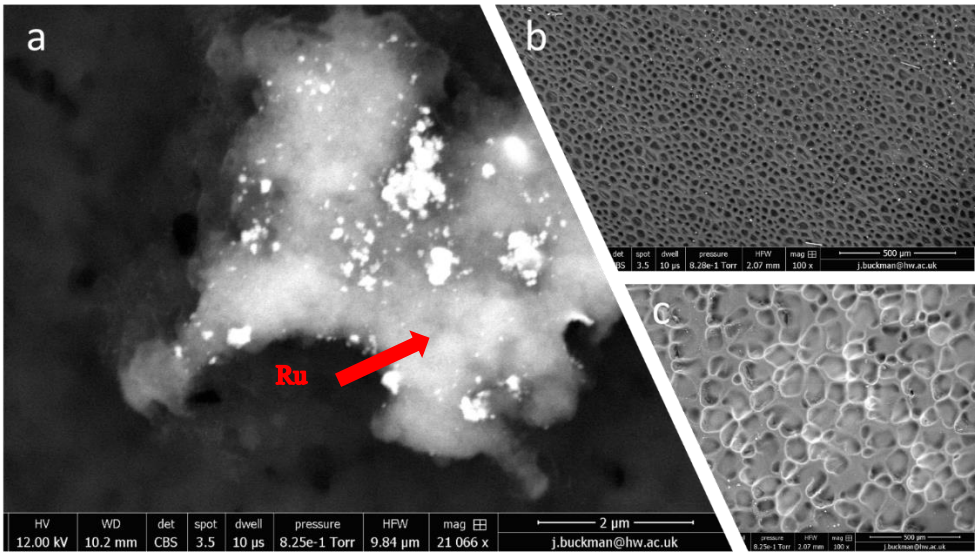

Figure 7-7. SEM-EDS analysis a) doped membrane 21066x resolution b) doped membrane x100 resolution c) not doped membrane x100 resolution.

7.4.2 Hydrogenation reaction test

The modified membrane was tested for the hydrogenation reaction of a simulated water bio-oil fraction studying the effect of pressure, temperature and hydrogen flow rate. For whole experimental campaign, there was not clear conversion of acid acetic and glucose due the low operating condition used, which is in agreement with previous studies [160, 257]. Therefore, the hydrogenation of furfural and vanillin were studied more in detail.

Effect of reaction temperature

The temperature effect was studied between 65 -85 °C, for a reaction pressure of 11 bar, 25 mL/min of hydrogen and 0.005 mL/min of liquid feed, As reported in Figure 7-8, the

temperature for the hydrogenation reaction plays a positive role incrementing the reactants conversion, then also the kinetic rate. The highest feedstock conversion was achieved for the highest temperature analysed, with 16.5 and 76.6 % for vanillin and furfural, respectively. The selectivity of furfural to tetrahydro furfuryl alcohol improved with the temperature from 42.47 to 74.59%. While the vanillin was converted to vanillin alcohol.

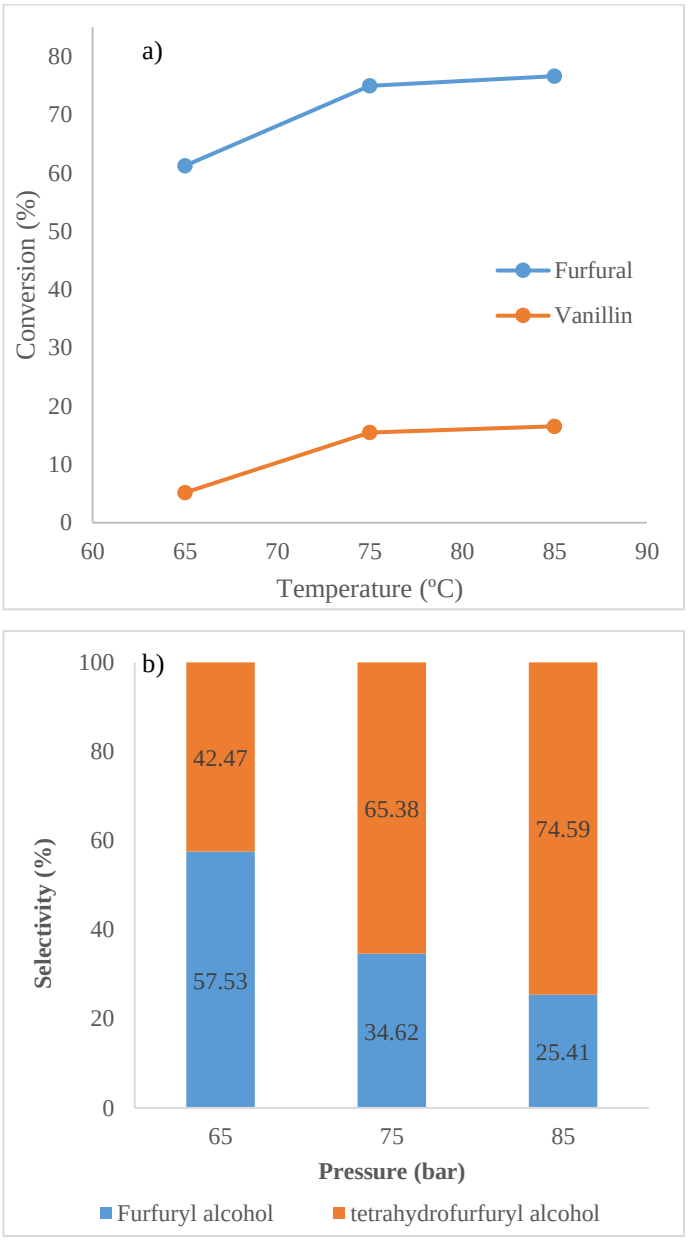

Figure 7-8. Effect of reaction temperature at 11 bar, 25 mL/min of hydrogen and 0.005 mL/min a) reactants conversion and b) products selectivity.

Effect of reaction pressure

The reaction pressure was varied from 11 -18 bar, at 75 °C, 5 mL/min of hydrogen and 0.003 mL/min liquid feed. Using the membrane as active contactor among the 3 phases,

the pressure favoured the hydrogen solubility into the liquid phase. Figure 7-9 indicates that the vanillin and furfural conversion increased with reaction pressure, from about 70 % (11 bar) to 75.3 % (18 bar), with a the furfuryl alcohol selectivity decremented due a better solubility of H_2 into the liquid phase, facilitating the hydrogenation reaction into the Ru surface. While the vanillin conversion to vanillin alcohol increased from 22 % to 32.8 % at the highest pressure.

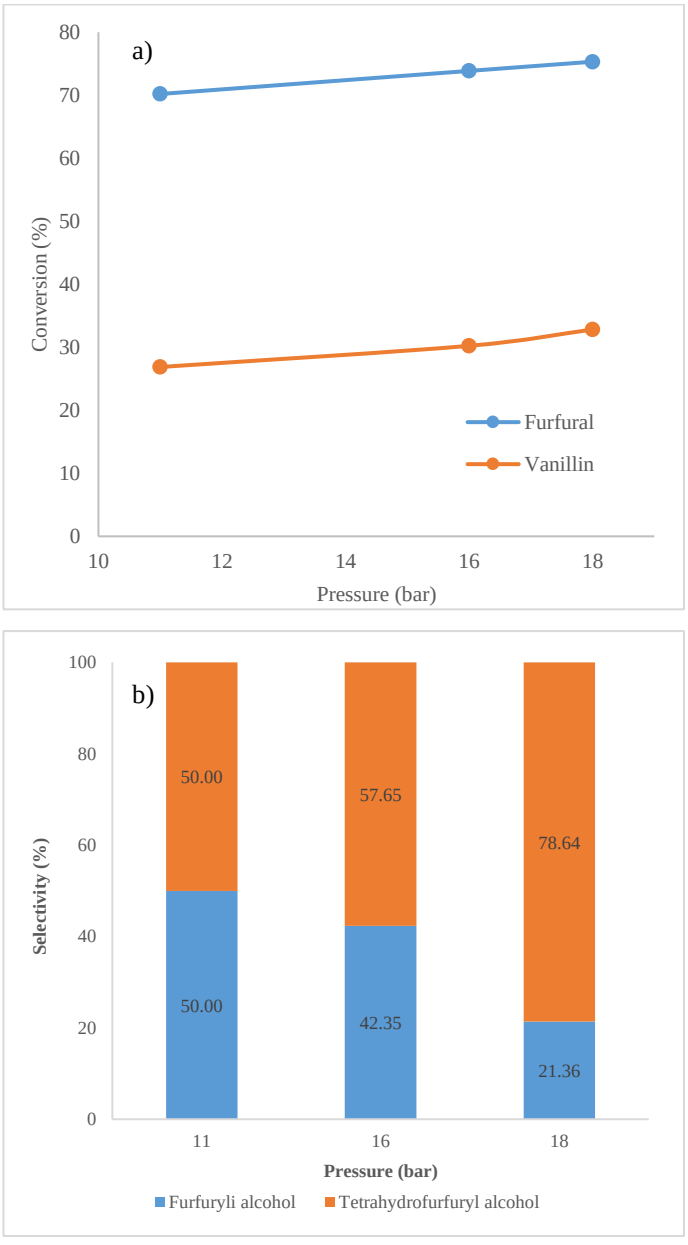

Figure 7-9. Effect of reaction pressure at 75 °C, 5 mL/min of hydrogen and 0.003 mL/min a) reactants conversion and b) products selectivity.

3.3 Effect of H_2 Flowrate on Conversion

The investigation of H_2 flowrate was carried out from 5 mL/min to 25 mL/min at 75 ºC and 11 bar, as shown in Figure 7-10, where the furfural conversion was steady at about

73%. The selectivity to furfuryl alcohol decreased from 21.36 to 0.83%, by increasing the H_2 flow rate, while tetrahydro furfuryl alcohol production increased. Furthermore, the lager hydrogen flowrate increased the vanillin conversion from ~1 to ~15 %, maintaining a complete selectivity to vanillin alcohol.

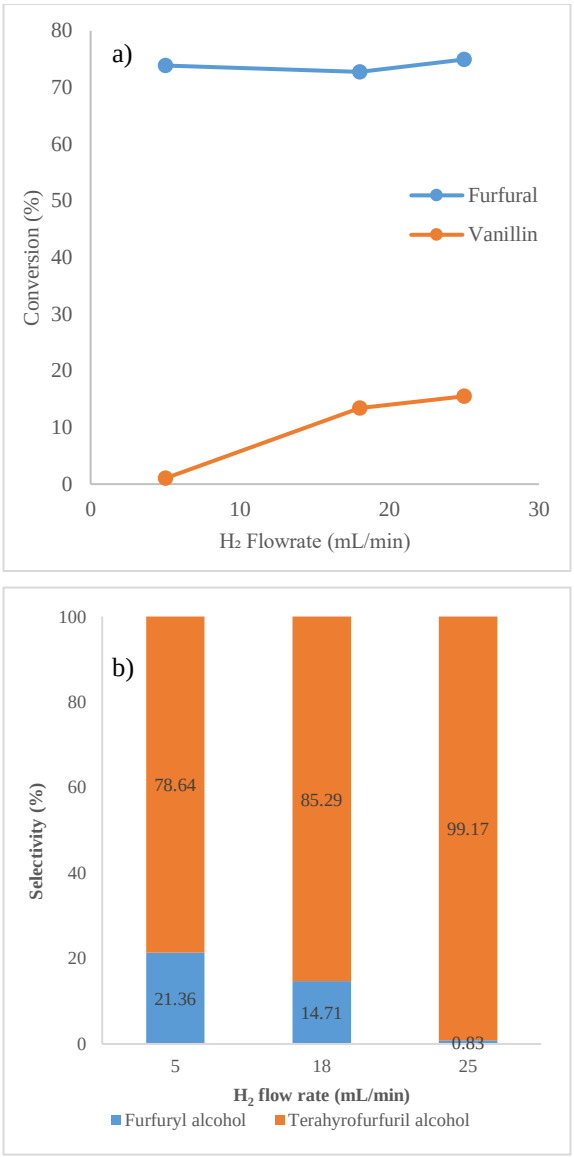

Figure 7-10. Effect of H_2 flowrate at 75 °C and 11 bar and 0.003 mL/min a) conversion and b) selectivity.

Membrane stability

The membrane stability was studied by evaluating the Ru leached in the product solution from the membrane by ICPS-EOS. As reported in Figure 7-11, the Ru content in the liquid product was about 3.2 µg/L after 16 hours, while dropped to 0.3 µg/L after 28 hrs and then remained constant up to 88 hours, suggesting stability. The initial Ru leaching can be attribute to some contamination left from the membrane Ru-doping step. A low amount of Ru was leached when compared to previous work [129], where Ru-PES membrane lost

most of the activity surface after just 6.5 hrs. The results achieved in this work suggest the Ru PEEK-WC membrane is more resistant to wear due to the chemical reaction. Moreover, based on the data present in Figure 7-11, the Ru lost was estimated to be 1.61μg after 88 hr, which is very low compared to the initial amount of Ru loaded on the membrane surface was 2.14 mg. Therefore, the Ru-PEEK WC membrane showed a better stability than Ru-PES due mainly to: (i) the nature of the support, with the PEEK-WC having a higher chemical resistance and (ii) the method used for the membrane coating, where the Ru-PES membrane grafted by acrylic UV exposition resulted in a high Ru leaching than the sulfonation method used for the PEEK-WC membrane.

.

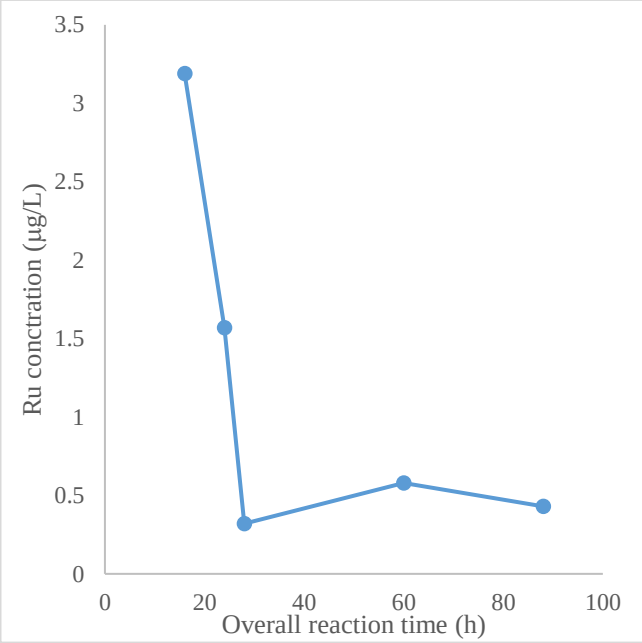

Figure 7-11.Ru concentration in product solutions.

7.5 Conclusion

The hydrogenation reaction of a simulated WBO was studied using a catalytic membrane reactor. A PEEK-WC membrane was synthesised by VIPS/ NIPS technique in presence of Tamisolve®, solvent with low carbon foot print. Afterward, the PEEK-WC membrane was sulfonated superficially, studying the effect of different concentration and time of exposition of H_2SO_4 onto the membrane. Subsequently, the membrane was doped with Ru, obtaining a concentration of 25.5 μg/cm^2. Comparing the PEEK-WC membrane before and after the Ru doping, the main differences consisted in an increase of the mean pore size from 0.07 to 0.14 μm and the Young's module form 19 to 70 N/mm^2, while the membrane hydrophilic nature did not have significant changes. The WBO hydrogenation

using the PEEK-WC catalytic membrane resulted in: (i) 75% furfural and 30% vanillin conversion at 18 bar, 75 °C, 5 mL/min of hydrogen, while the glucose and acid acetic were not successfully converted and (ii) the Ru-PEEK-WC membrane was stable for about 90 hours and outperformed a previously tested Ru- PES membrane.

Chapter 8- Effect of Li-LSX zeolite, NiCe/Al_2O_3 and NiCe/ZrO_2 on the production of drop-in bio-fuels by pyrolysis and hydrotreating of Nannochloropsis and Isochrysis microalgae Energy

This chapter has been published as: G. Bagnato, F. Boulet, A. Sanna, Effect of Li-LSX zeolite, NiCe/Al_2O_3 and NiCe/ZrO_2 on the production of drop-in bio-fuels by pyrolysis and hydrotreating of Nannochloropsis and Isochrysis microalgae Energy, Energy, 179 (2019), 199-213.

8.1 Abstract

The last part of the experimental campaign involved to evaluate the economic potential of the HDO reaction for a transition to a low carbon footprint industry.

The purpose of this work was to investigate the viability of a microalgae catalytic pyrolysis/hydrotreating plant to kerosene, diesel and gasoline using Aspen Plus. A series of 2000 dry tonne per day scenarios were simulated with the final goal of determine the price in USD per litre of the drop-in fuels produced and the economic feasibility of the technique at a large-scale. Different scenarios (mechanical, solar and thermal drying), microalgae (Nannochloropsis and Isochrysis) and catalysts (Li-LSX zeolite, Ni-Ce/Al_2O_3, Ni-Ce/ZrO_2). For this work, a systematic design approach by Douglas was considered and the whole process was actualised with the Marshall and Swift Cost Index of 2016. The lowest minimum fuel selling price (1.418 $/L) was found for Isochrysis and Li-LSX-zeolite. Finally, the sensitivity analysis showed that the bio-oil yield was the most influent factor, leading to a variation of the fuel price between 1.158 $/L to 1.751 $/L assuming a 20% of variation.

The techno-economic assessment and sensitivity analysis indicated that Isochrysis and Li-LSX-zeolites are promising for the production of drop-in fuels, but further research is required to further reduce the price of the feedstock production and drying to be competitive with lignocellulosic materials.

8.2 Introduction

Since biomass is carbon neutral, its use as a renewable energy source can reduce the dependence on fossil fuels and help to reduce emissions of greenhouse gases in the atmosphere [258]. Since biofuels can be produced through a variety of processes, the techno-economic analysis of producing bioenergy is an essential aspect to evaluate their

performance. Most of the work has been dedicated to lignocellulosic materials. For example, García-Velásquez and Cardona (2019) addressed the TEA, energetic and environmental of ethanol by fermentation and syngas by gasification from pine wood [259].

The production of bio-fuels from third-generation microalgae are recently receiving increasing attention, but there still is a lack of studies to assess their economic viability. Okoli et al.[260] studied the techno-economics of a microalgae to butanol via thermo-chemical route. The lowest minimum butanol selling price (MBSP) of 1.97 $/L was obtained for the S. Korean natural gas import plant and the sensitivity analysis showed that changes in gasoline prices could have an impact on the plant configuration in the South Korean, but not in the US market [260]. In the 1970s, the U.S. Department of Energy extensively researched the growth and conversion of microalgae for transportation fuels [261]. The most common fuels derived from microalgae are bio-ethanol and biodiesel produced by fermentation and solvent extraction [262, 263]. Microalgae with high lipid content are good feedstock for biodiesel production but still too expensive (6-10 $/L) [264]. Only fatty acids from microalgae can be used for biodiesel production, which moreover require costly organic solvents extraction [265, 266]. Thermo-chemical conversion (liquefaction, pyrolysis, gasification) pathways instead allows full conversion of the microalgae components to bio-fuels, which represents an economic advantage over bio-routes [121, 267]. Today, in spite of innovative approaches to microalgae growth and conversion into biofuel have renewed interest in algae biofuels [261, 268], the question of their economic feasibility remains. Despite the increase in algae-related publications, few papers effectively address the key question of translating the proposed technical approaches for producing algae biofuels to their economic costs. The cost estimates given in the literature vary greatly in their level of detail. Some provide single value estimates and others give complete process and economic analyses. It was found that at 10% Internal Rate of Return, thermal drying and mechanical dewatering scenarios resulted in MFSP of 1.80 $/L and $1.49 $/L, respectively the production of a mixture of BTX (25.9 gal/MT), diesel (4.2 gal/MT), and gasoline (2.5 gal/MT) from 2000 dry million t /day processed microalgae [121]. The same group updated the minimum fuel selling price of gasoline and diesel fuel produced via fast pyrolysis and hydro-processing of cellulosic biomass to 0.56/L, from the previously estimated 0.46 $/L, which was found to be competitive with petroleum and lower than competing technologies such as cellulosic ethanol and gasification with combined Fischer–Tropsch synthesis [122]. The

above MFSP suggests that pyrolysis-hydrotreating of microalgae is still not competitive with cellulosic biomass. However, several different combinations of microalgae drying and catalysts have been proposed for the pyrolysis of microalgae, which can affect the process costs.

In this work, in order to evaluate the economics of microalgae pyrolysis and bio-oil upgrading using a number of different catalysts, the energy cost and the carbon footprint of the techniques required have been investigated and modelled in Aspen Plus. For the microalgae drying step, three different system have been considered: (1) traditional thermal drying, which is energy intensive; (2) a partial mechanical drying of the algae before the thermal drying; (3) a drying system based on solar power [269]. For the production of microalgae, the use of wastewater has been investigated by Xin et al. [270] to reduce the cost of both treatment of wastewater and growth of microalgae. This system has been considered in this simulation.

The pyrolysis of the different microalgae species can be greatly affected by presence of catalysts and despite the number of works focusing on the development of catalysts for microalgae pyrolysis, the evaluation of their techno-economic feasibility is rather limited. Therefore, in this work, the effect on the final fuel price of a number of catalysts (Li-LSX zeolite, $NiCeZrO_2$, $NiCeAl_2O_3$) previously tested by our group, has been investigated with the purpose to establish which of the above mentioned catalysts could have a role in converting microalgae to drop-in fuels in industrial scale [271-273]. To have a precise estimation of the final price of kerosene (C_{10} to C_{14}), diesel (C_{21}) and gasoline (C_4 to C_{12}), an Aspen Plus model of the overall process including the hydrotreating and distillation stages was simulated [62].

8.3 Method

The simulation was built on Aspen Plus considering 2000 metric ton per day of dry biomass flow rate (10% wt. water). Figure 8-1 shows the complete flow chart of the simulated process, while the mass flow rates are reported Table 8-1. The plant size was selected to be comparable with previous works [121, 122, 274]. The goal of this simulation was to have the final flow rates of fuels, biogas and char produced by the catalytic pyrolysis, in order to size all the reactors and determine the utilities costs (electricity, cooling water). After the equipment sizing, it was possible to determine the capital cost (CAPEX) and the annual operating cost (OPEX) by using Aspen process economic analyser integrated in the Aspen software.

Figure 8-1 shows the PFD for the simulated process. The simulated process starts with the microalgae drying stage (H100) followed by the catalytic pyrolysis reactor (R100). The solid produced during the reaction (bio-char) was assumed to be separated in a cyclone (S100) and combusted (B3) at high temperature (800 ˚C), in order to regenerate the catalyst and to generate the heat required in the pyrolysis reactor. Then, the bio-oil produced was condensed (E-102) and upgraded by hydrotreatment (R-102). The bio-oil was assumed to be hydrotreated at 250 ˚C, at a pressure of ~50 bar, consuming about 0.12 kg of H_2 per kg of bio-oil to be treated [121]. The hydrogenation reaction resulted in paraffins, cyclo-alkanes, aromatics etc., which were further fractionated into kerosene, diesel, heavy and light gasoline and other chemical compounds by using a distillation tower (S-103) containing 23 plates, in order to separate the compounds by their respective boiling point. The simulation was carried out with the following flow rates and temperatures obtained in literature:

Temperature:

- Drying: 80˚C (hot air)
- Catalytic pyrolysis: 500˚C
- Char combustion: 800˚C
- Hydro-processing: 250˚C
- Final products: 35˚C

Material flow rate:

- Wet microalgae (80 % moisture): 9475 metric ton/day
- Dry microalgae (10% moisture after drying) : 2000 metric ton/day
- Ni-Ce/Al_2O_3 and Ni-Ce/ZrO_2 catalyst, 30 wt. % of dry biomass
- Li-LSX zeolite catalyst, 50 wt. % of dry biomass
- Hydrogen for hydrotreatment : 0.12 kg hydrogen per kg of bio-oil [121]

The microalgae composition (wt%) was obtained by Aysu and Sanna [271]. Nannochloropsis sp.: protein 62 %, carbohydrates 9 %, lipids 18 %; Isochrysis sp: protein 44 %, carbohydrates 25 %, and lipids 19 %. The microalgae have been simulated in Aspen Plus defining them by the proximate and ultimate analysis.

Four different scenarios were considered: Thermal drying, Mechanical drying, Thermal and solar drying and thermal and mechanical drying. For each of the scenarios, five different microalgae-catalysts were modelled in Aspen Plus:

- Nannochloropsis algae with Ni-Ce/Al_2O_3 catalyst
- Isochrysis algae with Ni-Ce/Al_2O_3 catalyst
- Isochrysis with Li-LSX zeolite catalyst (LSX : low silica x type)
- Isochrysis with Ni-Ce/ZrO_2 catalyst
- Isochrysis without catalyst

The Aspen model was divided in four parts, namely: (1) the drying stage; (2) pyrolysis and combustion of char; (3) bio-oil hydrotreatment; (4) separation system.

8.3.1 Drying stage

Before the pyrolysis process, the microalgae must be dried because of their large water content (~80 wt. %). 40,350 kg/hr of microalgae (F-101) were dried using 1,413 kg/hr air (F-102). This content must be lower than 10 wt. % in order to reduce parasitic energy required to heat water during pyrolysis. Reducing the energy consumption and thus the annual operating cost of this stage could make a great difference in the final cost of the plant; therefore, three types of drying methods have been entered in the simulation:

Thermal drying [121, 261, 270]**:** typical drying method where air at 35˚C is heated to 80˚C by steam, this steam is obtained by heating water with electricity or with natural gas. The dryer simulated was a tray dryer.

Solar drying [269, 275]**:** The biomass is also dried with hot air, but the steam to heat is produced by solar power tower. This solar system is heated by thousands of sun-tracking mirrors called heliostats that concentrates the power of the sun and permits to heat water and thus to produce steam. This method has a higher equipment cost and has geographical constrains, but in the same time does not use electricity.

Mechanical drying [121, 263]**:** This is a two steps drying, the first one is to reduce the moisture from 80% to about 60% with a belt dryer technique with pressurized air, then the algae with 60% moisture is fed to a classic drying step with air at 80˚C. The initial mechanical drying permits to reduce greatly the amount of energy needed to dry the microalgae.

The drying step modelling was carried out considering two different microalgae algae species, but since the energy requirement and costs resulted almost the same, a unified price was used for assessing the different drying processes.

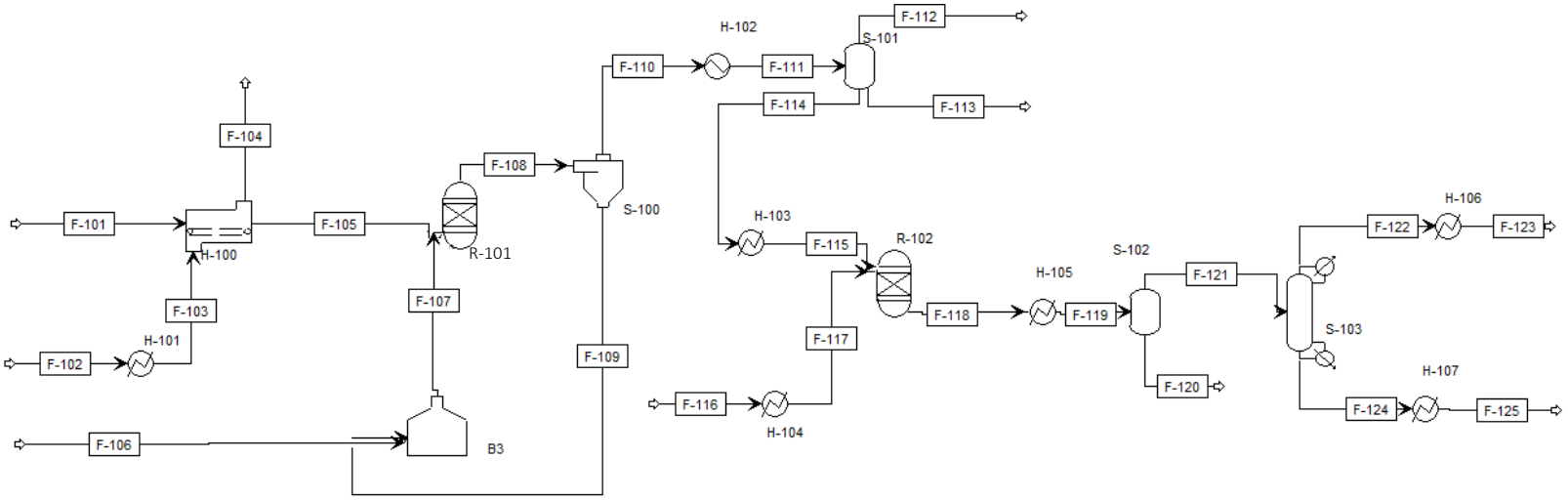

Figure 8-1. Process flow diagram

Table 8-1. Material balance using Isochrysis algae and Li-LSX zeolite catalyst.

	F-101	F-102	F-103	F-104	F-105	F-106	F-107	F-108	F-109	F-110	F-111	F-112	F-113	F-114	F-115	F-116	F-117	F-118	F-119	F-120	F-121	F-122	F-123	F-124	F-125
Mass flow rate [ton/h]	403.5	14.1	14.1	22.1	83.3	29.6	58.5	119.6	28.9	90.7	90.7	59.0	8313	23.3	23.3	2.50	2.50	25.8	25.8	2.83	23.0	13.6	13.6	9.42	9.42
Temperature [ºC]	25	35	175	80	80	35	800	500	500	500	35	35	35	35	100	25	100	100	35	35	35	113	35	193	32
Pressure [bar]	1	1	1	1	1	2	2	1	1	1	1	1	1	1	1	50	50	50	1	1	1	1	1	1	1
Composition [wt.%]																									
Moisture	80				10																				
Biomass	20				90																				
Bio-char								20.69	85.59																
Bio-gas								22.56		29.76	29.76	45.74													
Bio-oil								19.50		25.72	25.72			100	100										
H_2O		79	79	36.2		79	39.95	6.95		9.17	9.17		100					10.96	10.96	100					
N_2		21	21	50.4		21		19.50		25.76	25.76	39.58													
O_2				13.4												100	100								
H_2								7.23		9.56	9.56	14.68													
CO_2							7.12	3.57	14.41																
Catalyst																									
5-Methyl-3-Methylethyl-Phenol																		6.59	6.59		7.40			17.78	17.78
O-Ethylstyrene																		8.81	8.81		9.90			24.78	24.78
O-Xylene																		14.17	14.17		15.91	23.86	23.86		
n-Hexadecane																		4.73	4.73		5.31			8.46	8.46
2,3Dimethyldecane																		7.76	7.76		8.72				
2-Ethyl-1-Hexene																		1.36	1.36		1.53	2.19	2.19		
Cyclohexane																		28.67	28.67		32.20	60.97	60.97		
Butylcyclohexane																		16.38	16.38		18.40			48.98	48.98
n-Octane																		8.28	8.28		9.30	12.98	12.98		

8.3.2 Pyrolysis and char combustion

After the drying stage, 2000 t/day of dry algae (F-104, with only 10 wt. % of water) are sent to the pyrolysis reactor. Pyrolysis temperature was fixed at 500˚C, which is the temperature that resulted in the highest bio-oil yield [272].

The reactor operates at atmospheric pressure. The catalyst/algae mass ratio was set to 30% of catalyst per kg of algae for Ni-Ce/Al_2O_3 and Ni-Ce/ZrO_2, and 50% of catalyst for Li-LSX zeolite, based on the experimental results [271]. The experimental data used for bio-oil, bio-char and bio-gas yields for the Nannochloropsis and Isochrysis sp. algae pyrolysis have been experimentally obtained by our group in previous works [271-273]. Pyrolysis of *Nannochloropsis* microalgae in presence of NiCe/Al_2O_3 was selected as a comparison for *Isochrysis* microalgae. However, due to the larger content in proteins (which lead to gas products) of the former (62%) compared to the latter (44%), we selected *Isochrysis* for the catalysts' comparison study. In Table 8-2 are summarized the products yields (wt%) of the five different scenarios.

Table 8-2. Product yields for Isochrysis and Nannochloropsis catalytic pyrolysis assuming 10% water in bio-oils fed to reactor.

Algae	Catalyst	Bio-char	Bio-oil	Gas	Ref.
Nannochloropsis sp	Ni-Ce/Al_2O_3	27.8	21.0	41.2	[272]
Isochrysis sp	Ni-Ce/Al_2O_3	28.8	22.1	39.2	[271]
Isochrysis sp	Ni-Ce/ZrO_2	22.5	22.9	44.6	[271]
Isochrysis sp	Li-LSX-zeolite	29.7	27.9	32.4	[273]
Isochrysis sp	No catalyst	28.8	20.7	40.5	[271]

The bio-oil chemical composition was obtained from GC-MS [271-273]. Bio-oils compounds were divided in functionalities such as alcohols, ketones, esters, aliphatics, aromatics, carboxylic acids and nitrogen compounds. The main components of bio-oils from Isochrysis algae were aliphatics (25-42%) such as undecane, tridecene or pentadecene and aromatics (13-22%) like P-Cresol and 1-heptenyl-benzene. The third most abundant category was represented by nitrogen compounds (6-17%) such as hexadecane-nitrile, pyrindine and indole. These compounds need to be hydrotreated in order to make lighter chains of aliphatics, aromatics and alcohols (main components of fuels) by removing nitrogen and oxygen.

After pyrolysis has occurred, the stream product F-108 is sent to a cyclone separator in order to separate the fluid part from the solid part (bio-char and catalyst), F-110 and F-109 respectively.

After the cyclone separation, the stream F-109 containing the bio-char and catalyst is sent to the combustion reactor, where the catalyst is regenerated, and then, the bio-char is combusted in order to supply heat to the pyrolysis reactor, so it can be auto sufficient. Combustion occurs at 800 ˚C and atmospheric pressure, air is used to supply the combustion with oxygen. The simulation of the combustion process in Aspen included the addition of the elemental analysis of the bio-chars gas products and the correct flow rate of air to be fed to the combustor, in order to have an output feed without oxygen and a temperature of 800 ºC. The required heat was supplied burning all bio-char and part of bio-gas produced. The bio-gas weight fraction used to produce heat varied from 50 to 96%, depending on the elemental composition of the bio-char and gas, leading to a more or less efficient combustion.

8.3.3 Hydro-treatment

The here simulated bio-oils (F-115) contains a number of compounds that do not need upgrading (aliphatic, cyclo-alkanes or alcohols). Instead, nitrogenates, carboxylic acids, ketones and aromatics require treatment. Hydrotreating takes place at temperatures between 125 and 400°C and pressures between 50 to 280 bar. Hydro-processing allows to remove nitrogen and oxygen from organic compounds, open rings of aromatics and break C-C bonds in order to break heavy chains ($>C_{20}$) in lighter compounds that can be used in fuels, typically alkanes from C_6 to C_{18} and alcohols from C_1 to C_{18}.

Catalysts such as Pt/C, Ru/C or Ni-Mo/Al_2O_3 are typically added to improve the production of liquid, reduce the production of coke (solid with high content in carbon), decrementing oxygen and nitrogen in bio-oil. In this simulation, Ni-Mo/Al_2O_3 catalyst was the 5 wt% of the bio-oil treated, with a catalyst lifespan of 0.2 years were considered [62, 276]. The hydrogen required for the hydrotreating was assumed to be 0.12 kg of hydrogen per kg of bio-oil [121], at a price of $1.33/kg [122].

To determine the fraction of bio-oil to be treated, the composition of each bio-oil from the experimental works was considered [271, 272]. All nitrogen compounds, aromatics, ketones and carboxylic acids were considered as intermediate-products to be upgraded. The bio-oil obtained with Nannochloropsis algae and Ni-Ce/Al_2O_3 was rich in alkanes and alkenes and only 22 wt% had to undergo upgrading (benzene-propane nitrile, indole

and benzoquinoline-2,4-dimethyl). A larger fraction (~70 wt%) of Isochrysis based bio-oils obtained by catalytic pyrolysis needed treatment, with nitrogen compounds (pentadecane-nitrile), N-heterocyclic compounds (indole), ketones (pentadecanone) and aromatics (p-cresol) being in the bio-oils. About 75 wt% of the bio-oil obtained from Isochrysis without catalyst also required upgrading, where the main undesirable components were nitrogen compounds (28%) and ketones (16%).

8.3.4 Separation system

The water phase (F-120) was separated from the hydrotreating outlet stream by a decanter unit, after that, a distillation tower was used to recover the diesel (F-125) and gasoline (F123) products. The distillation tower was modelled by a shortcut method in order to calculate the operating parameter to build it. To separate the products by Boiling Point (BP) in Aspen, o-xylene (T_{bp}=144.4°C) and butyl-cyclohexane (T_{bp}=181°C) were chosen as key components. Properties and flowrates were used to calculate the price of all equipment of the separation process in the simulation. The column price was determined by its height and diameter, the price of condenser and reboiler are related to their heat duty. Cooling water was used to cool the final products and to supply the condenser, steam was used to heat the reboiler. The distillation tower was designed determining the high and diameter and subsequently the cost for whole separation unit (distillation tower, reboiler, condenser and utility). Douglas et al.[120] calculated the diameter imposing a vapour velocity between 60-80% of the flooding velocity:

$$D = 0.0164 * \sqrt{V} * \left(\frac{MW}{\rho_m}\right)^{\frac{1}{4}} [=] ft \qquad 8\text{-}1$$

Where, MW is molecular weight of the upper stream (gasoline) (lb/lbmol), V the molar flowrate of vapour (lbmol/hr) and ρ_m the molar density of vapour (lbmol/ft^3). The number of trays was obtained with the following equation, assuming a tray efficiency (η) of 0.5:

$$Number\ of\ trays = ideal\ number\ of\ trays/\eta \qquad 8\text{-}2$$

The height of the column (in feet) was then determined as follow:

$$H = 2 \cdot number\ of\ trays + 15\ [=]\ ft \qquad 8\text{-}3$$

In the simulation, the average density of gasoline produced was 0.776 g·cm^{-3} and 0.825 g·cm^{-3} for the diesel products. Their respective boiling points were 112.6°C and 192.9°C, which are classic values for gasoline and diesel transportation fuels.

8.3.5 Economic assessment of the plant

When possible, equipment costs were taken by previously published works, such as for the pyrolysis reactor [121], the mechanical dryer [263], thermal dryer and combustion reactor [120] the solar drying system [269] or the hydro-processing reactor [14, 62], due to their specificity and difficulty in determine their size using Aspen. Otherwise, were calculated in Aspen plus. The obtained values were then used in a discounted cash flow rate of return (DCFROR) spreadsheet analysis, in a similar way as done in previous techno-economic assessments [121, 261, 263, 270]. The total operating costs were determined in order to calculate the minimum fuel product selling price (MFSP) in $/L and compare it with the fossil fuel prices and bio-derived fuels.

Stream and product prices:

- Biomass (wet) : 66 $/ metric ton [121]
- Natural gas : 0.142 $/m^3 [277]
- Gasoline : 18.16 $/GJ [28]
- Diesel : 12.26 $/GJ [28]

Dryer unit- A temperature of 80˚C was used to dry 9500 metric ton/day of wet biomass obtaining an output of 2000 metric ton/day of dry biomass (10% moisture). The heat duty needed to dry the quantity of biomass specified was used to size the equipment (total area in m^2) in order to calculate the equipment and installed cost according to Turton et al [278].

Three different cases have been tested with low, medium and high-pressure steam, in order to determine an average price of the total drying step in dollars per year, including capital costs (equipment and installed costs) and utility costs (steam to heat the air). These three cases are:

- Low pressure steam: 2-3 bar at 125˚C
- Medium pressure steam: 9 bar at 175˚C
- High pressure steam: 36 bar at 245˚C

Pyrolytic and combustion reactor- The total cost of the pyrolytic and combustion reactor was calculated as suggested by Douglas et al.[120]. Once the heat supplied (Q, 10^6 Btu/hr) by the reactor is known the final price can be calculated by the following equations:

$$F_c = F_d + F_m + F_p \quad \text{8-4}$$

Where Fc is a factor of correction for depending on the type of reactor F_d (1 and 1.10 for combustion and pyrolytic reactor, respectively), the raw materials F_m, in this case carbon steel and the operating pressure.

$$Purchased\ cost = \frac{M\&S}{280} * (5.52 \cdot 10^3) \cdot Q^{0.85} \cdot F_c \qquad 8\text{-}5$$

$$Installed\ cost = \frac{M\&S}{280} \cdot (5.52 \cdot 10^3) \cdot Q^{0.85} \cdot (1.27 + F_c) \qquad 8\text{-}6$$

Where M&S is the Marshall and Shift index for 2016 (1582.3) and Q is the heat. This correlation is applicable for pyrolysis reactor with heat flow between 20 and 300 10^6 Btu/hr.

Cyclone separator- The cost of the cyclone separator depends on the flow of matter (P) that needs to be separated (in standard cubic feet per minute, SCFM) [279]. The purchased cost and installed cost were calculated with the following equations:

$$Purchased\ cost = 2.422 * P^{0.96}\ [=]\ k\$ \qquad 8\text{-}7$$

$$Installed\ cost\ (k\$) = 1.4 * purchased\ cost \qquad 8\text{-}8$$

Hydrotreating reactor- The hydrotreating price was calculated based on the flowrate of the bio-oil to be upgraded (in thousand barrels per day) as suggested by Gary et al.[280], this cost included preheater (from 35 to 250°C), hydrogen circulation facility, central control system, cooler (from 250 to 35°C) and initial catalyst charge. Ni-Mo/Al_2O_3 catalyst was considered for the simulation and was priced at an average value of 2750 $/metric ton.

Distillation column- By the technical analysis, the distillation column diameter (D, ft) and height (H, ft) have been calculated, equations 9 and 10 allows determining its purchased and installed costs:

$$Purchased\ cost\ = \left(\frac{M\&S}{280}\right) \cdot 101.9 \cdot D^{1.066} \cdot H^{0.82} \cdot F_c\ \ [=]\ \$ \qquad 8\text{-}9$$

$$Installed\ cost = \left(\frac{M\&S}{280}\right) \cdot 4.7 \cdot D^{1.55} \cdot H \cdot F_c\ \ [=]\ \$ \qquad 8\text{-}10$$

The condenser price was then determined by the following equation:

$$Condenser\ price = \left(\frac{M\&S}{280}\right) \cdot 328 \cdot \frac{\Delta Hv}{3000} \cdot \ln\left(\frac{T_{bp}-90}{T_{bp}-120}\right)^{0.65} \cdot V^{0.65}\ [=]\$ \qquad 8\text{-}11$$

Where, ΔH_v is the heat of vaporization of the upper stream (gasoline) in Btu/lbmole, T_{bp} the boiling point of upper product (°F) and V the molar flowrate (lbmole/hr) of vapour. Finally, the reboiler price was calculated with equation 12 as follows:

$$Reboiler\ price\ = \left(\frac{M\&S}{280}\right) \cdot 328 \cdot \left(\frac{\Delta Hv}{11250}\right)^{0.65} \cdot V^{0.65}\ [=]\$ \qquad 8\text{-}12$$

Where, ΔH_v is the heat of vaporization of the bottom product (diesel) in Btu/lb.mole and V the molar flowrate of diesel (lb.mole/hr).

Once the equipment was priced, the annual operating costs were determined. These operating costs are due to the utilization of water to cool the products and steam to heat the reboiler. Cooling water is priced at $2.12 \cdot 10^{-7}$ \$/kJ on Aspen and high-pressure steam at $2.5 \cdot 10^{-6}$ \$/kJ. The heat duty of the condenser and reboiler (in kJ/hr) were obtained by the software.

The annual cost was determined by multiplying the unit price of utility (steam or water) in \$/kJ by the duty in kJ/hr and then by the number of operating hours per year.

8.3.6 Economic evaluation

The economic evaluation has been is described on *3.3 Techno-economic assessment*.

8.4 Result and discussion

The techno-economic evaluation is shown hereafter for the bio-fuel production from fast pyrolysis and hydrotreating of microalgae. Different feedstocks, catalysts and drying systems were evaluated and compared in terms of minimum fuel selling price, with subsequent sensitivity analysis. At the end, the energy demand of the process has been optimised, in order to minimise the utility costs.

8.4.1 Dryer

Thermal drying

According to Aspen, the energy calculated for the drying was 22.6 MW. The total area of the dryer was 1226 m^2 and the average cost for steam production was 179.2 \$/hr, being about 1.60 MM\$/year, if the plant is continuously working. Based on 1226 m^2, the equipment cost was 3.68 MM\$. The installed cost was assumed to be a factor of 1.25 for this type of vessel resulting in 4.6 MM\$. The steam generator total cost was calculated by Aspen in 168 k\$. Table 8-3 shows the total cost associated with the thermal drying method.

Table 8-3. Total cost associated with the thermal drying process

Type	Cost
Dryer equipment cost	3.68 MM\$
Dryer installed cost	4.67 MM\$
Steam generator total cost	0.168 MM\$
Utility cost [\$MM/yr]	1.6 MM\$/yr

Solar assisted drying

In this scenario, the dryer was the same as in the thermal drying process, but the steam to heat air from 35˚C to 175˚C was assumed to be produced by a molten-salt solar power tower. The here adopted solar dryer shown in is Figure 8-2 was tested in Daggett, Colorado (USA)[281]. The total cost of the solar power tower was calculated following the economic assessment for a 200 MW plant [282]. This price is given in $/kW to facilitate the calculation of the total cost once the energy needed is known.

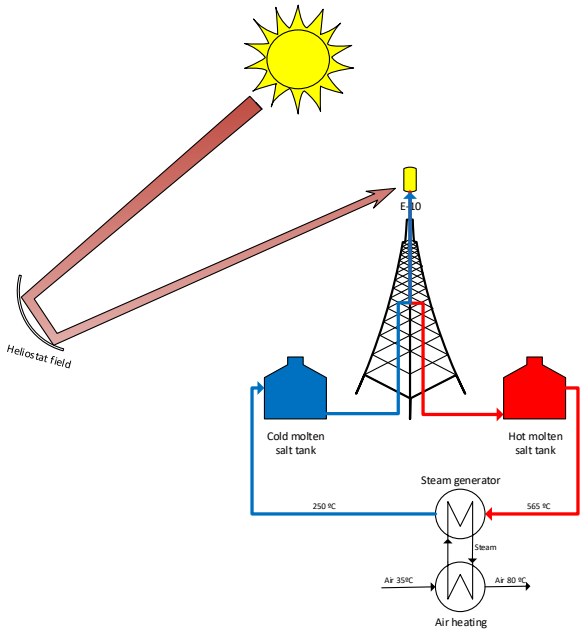

Figure 8-2. Solar power tower plant

The hot air (125˚C,175˚C or 245˚C) was then used to heat the dryer at 80˚C. The energy needed to produce steam was calculated at 22.60 MW, the steam generator equipment cost resulted in 173 k$ and its installed cost at 331 k$. These values were divided by the assumed 30 years of life-time for the equipment, which led to a final total cost of the steam generator of 17 k$/yr. The other equipment costs were calculated by multiplying the energy needed by the equipment costs given of 2.50 $/kW [282]. The operations and maintenance (O&M) cost was assumed to be 30$/kWh, resulting in 681 k$/yr. The final cost associated to this scenario as showed in Table 8-4, was about 1 MM$ higher than the thermal drying using gas or electricity. The advantage of this scenario is the avoidance of emitting 47,000 metric ton CO_2/yr (equal to the annual CO_2 emissions of approximately 10,000 cars) [38]. Furthermore, a future implementation of the carbon tax in more and more countries (currently between 2 and 40 $/metric ton of CO_2[283]), could result in

savings varying from 100 k$/yr to 1.88 MM$/yr, which would offset the cost difference with the thermal drying. Although, this potential cost reduction was not considered in the calculations.

Table 8-4.Total cost associated with the solar drying of algae

Type	Cost
Capital cost of the solar plant[MM$]	1.89
Steam generator[MM$]	0.02
Dryer[MM$]	8.28
Operations and maintenance [MM$/yr]	0.68

Mechanical dewatering

Mechanical drying was used to reduce the moisture content from 80 to 60 wt. %. The selected technique was previously employed by Humbird et al.[263], for lignin dewatering previous its further conversion to ethanol. This system includes filter and belt presses, membrane technologies, pressurized air and vacuum system to drive away moisture The cost of the mechanical dryer divided by 3 years of amortisation was assessed in 7 MM$/yr, inclusive of utilities and cost of energy. In addition, the cost of the classic dryer for decreasing the moisture from 60 to 10 wt% was estimated in 8.28 MM. The utility cost associated to the production of steam to heat the air was calculated at 0.62 MM$ and the steam generator total cost at 0.11 MM$, as reported in Table 8-5.

Table 8-5. Total cost associated with the partial mechanical drying

Part	Cost [MM$]
Mechanical dryer	7.00
Utility cost (2nd step, thermal drying)	0.62
Steam generator	0.11
Classic dryer	8.28
Total cost	16.01

This price resulted two times higher than the other two techniques, due to the high cost of the mechanical dryer. Therefore, at the current stage of development, this scenario does not seem to be economically viable. Thermal and solar drying resulted the most cost-effective methods. Thermal drying has lower CAPEX but larger OPEX, due to the

production of steam. Solar drying has a higher equipment cost due to the limited number of large scale solar power plant developed at the moment and is limited by weather conditions, but it permits to avoid CO_2 emissions of a great amount and it does not need electricity or gas to heat the air, so the annuals operating costs associated are lower.

Furthermore, the environment impact of the drying units in terms of CO_2 emissions in relation to the fuel used for heating the utilities was evaluated, as shown in Figure 8-3. The units with the highest environmental impact were the classic and thermal units, in order to satisfy the energy demand, while the CO_2 level was drastically reduced using solar dryers. In particular, the CO_2 produced was 107.8 metric ton/yr owing to build the drier solar unit, considering the useful life equal at 30 years.

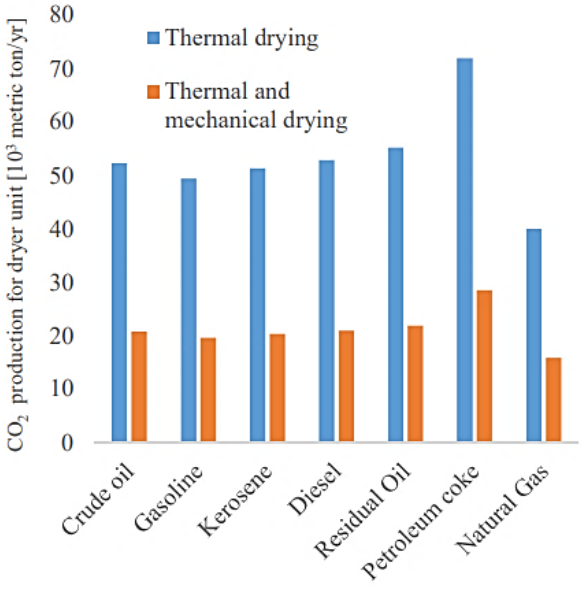

Figure 8-3. CO_2 production for drying unit

8.4.2 Pyrolysis and combustion of char

The pyrolysis catalytic reactor was priced at 158 MM$ and accounted for most of the total facility cost. This cost was determined based on the cost of the Evergent circulating bed pyrolyzer [284]. The catalysts prices were determined by considering 30 wt. % of Ni-Ce added on alumina or zirconia and by multiplying the price of each component by its weight percentage. The components costs were determined by considering very big orders to cut prices (>10 metric ton for Ni and Ce and >100 metric ton for the others). The output flow from the pyrolytic reactor was sent to a cyclone separator 8.02 m^3/s of fluid flow had to be separated from the solid phase, involving a purchase and installed cost of 42.30 k$ and 59.30 k$, respectively.

Table 8-6. Prices of the different catalysts used for pyrolysis.

Catalyst	Element	Wt. %	Price [k$/metric ton]	Final price [k$/metric ton]
Ni-Ce/Al_2O_3	Ni	1.5	9.04	0.74
	Ce	1.5	1.30	
	Alumina	97	0.60	
Ni-Ce/ZrO_2	Ni	1.5	9.04	9.86
	Ce	1.5	1.30	
	Zirconia	97	10.00	
Li-LSX/zeolite	Li	11.6	9.10	1.94
	LSX zeolite	88.4	1.00	

As shown in Table 8-7, the largest fraction of bio-gas used was 95.5% with Isochrysis algae and Li-LSX zeolite catalyst, due to the low amount of gas produced during the pyrolysis (32.4%, the lowest of all algae/catalysts). The combustor cost resulted the lowest for the system Isochrysis - Li-LSX-Zeolite with 33.5 MM$, while the presence of $NiCeZrO_2$ with Isochrysis had the highest cost (48.9 MM$).

The operating cost of the reactor came only from electricity, required to compress air from atmospheric pressure to 2 bar. An isentropic compression was modelled in Aspen Plus in order to calculate the annual operating costs. Table 8-8 shows that the lowest annual electricity cost was obtained in presence of the system Isochrysis - Li-LSX-Zeolite with 2.9 MM$/yr.

After the pyrolysis step, the obtained products (bio-oil, gas and water) were separated. Water was evacuated in the form of steam and the bio-gas not used during the combustion assumed to be sold at the price of natural gas (0.0114 $/ft^3 or 0.403 $/m^3) [276]. Since the bio-oil obtained from pyrolysis of algae contains a lot of nitrogen compounds and heavy compounds (more than 18-20 carbon atoms), hydrotreating was required for its upgrading to drop-in fuels.

Table 8-7. Results obtained for the combustion model in Aspen Plus.

Combustion					
Algae	Nannochloropsis	Isochrysis	Isochrysis	Isochrysis	Isochrysis
Catalyst	Ni-Ce/Al_2O_3	Li-LSX-Zeolite	Ni-Ce/Al_2O_3	Ni-Ce/ZrO_2	No catalyst
Bio-gas used [metric ton/day]	592	611	438	630	409
Bio-gas used [wt. %]	71.8	95.5	56.2	70.7	50.5
Air flowrate [metric ton/day]	$6.50 \cdot 10^3$	$6.85 \cdot 10^3$	$3.77 \cdot 10^3$	$3.95 \cdot 10^3$	$3.98 \cdot 10^3$
Combustion heat duty [MW]	72.62	60.57	64.96	94.35	64.89
Purchased cost [MM$]	11.97	10.25	10.88	14.95	10.87
Installed cost [MM$]	27.16	23.28	24.71	33.93	24.68
Total cost [MM$]	**39.1**	**33.5**	**35.6**	**48.9**	**35.6**

Table 8-8. Annual operating cost associated with the compression of air for the combustion reactor

Compression of air					
Algae	Nannochloropsis	Isochrysis	Isochrysis	Isochrysis	Isochrysis
Catalyst	Ni-Ce/Al_2O_3	Ni-Ce/Al_2O_3	Ni-Ce/ZrO_2	Li-LSX zeolite	No catalyst
Air to be compressed [metric ton/day]	$6.50 \cdot 10^3$	$6.85 \cdot 10^3$	$3.77 \cdot 10^3$	$3.95 \cdot 10^3$	$3.98 \cdot 10^3$
Annual electricity cost [MM$/yr]	**4.9**	**5.2**	**2.9**	**3.1**	**3.1**

8.4.3 Hydrotreatment

Table 8-9 shows the total cost of the reactor and the annual operating costs associated (hydrogen supply and catalyst replacement). The catalyst make-up per year was determined by dividing 5% of the bio-oil to be treated by the catalyst life span, assumed to be 0.2 year [276]. As expected, Nannochloropsis led to the cheapest total hydrotreating cost (9 MM$ for the reactor and 5.43 $MM/yr of operating costs) due to the low fraction of bio-oil to be upgraded. The largest cost was associated to Isochrysis with Li-LSX zeolite, due to the high amount of bio-oil produced in this scenario. A part the scenario with Nannochloropsis, the operating costs of the hydrotreater resulted larger than the capital expenditure, due to the hydrogen high cost. H_2 could be obtained via steam reforming of the gas generated during the pyrolysis. This option was studied by Wright et al. [123] for the same plant size as in this work, but the hydrogen production scenario was not conclusive and therefore a purchasing scenario was assumed here.

8.4.4 Separation system

The capital costs of the separation system obtained by the Aspen simulation are summarised in Table 8-10 for the different scenarios.

While, Table 8-11 shows the operating costs for the separation process. As can be seen in Table 8-10and Table 8-11, both capital and operating costs resulted higher for the scenario “Isochrysis, Li-LSX zeolite”, with $1202 k and $265.4 k, respectively. The largest CAPEX can be ascribed to the larger quantity of fuel to be separated (23,012 kg/hr), which led to a larger separation plant. Similarly, the larger OPEX are mostly due to the higher cost of the steam (261.7 k$).

Table 8-9. Hydrotreating costs.

Hydrotreating total cost					
Algae	Nannochloropsis	Isochrysis	Isochrysis	Isochrysis	Isochrysis
Catalyst	Ni-Ce/Al_2O_3	Ni-Ce/Al_2O_3	Ni-Ce/ZrO_2	Li-LSX zeolite	No catalyst
Bio-oil to be treated [%]	22	70	70	70	75
Total bio-oil flowrate [metric ton/hr]	17.46	18.75	19.12	23.34	17.25
Total bio-oil to be treated [metric ton/hr]	3.84	13.12	13.38	16.34	12.94
Catalyst needed [metric ton/year]	23.0	78.8	80.3	98.0	77.6
Hydrogen purchased [MM$/yr]	5.37	18.35	18.71	22.84	18.09
Catalyst replacement [MM$/yr]	0.06	0.22	0.22	0.27	0.21
Hydrotreater price [MM$]	**9.00**	**14.00**	**14.00**	**16.00**	**14.00**
Annual operating costs [MM$/yr]	**5.43**	**18.57**	**18.93**	**23.11**	**18.30**

Table 8-10. Total capital costs of the distillation process

Distillation system cost					
Algae	Nannochloropsis	Isochrysis	Isochrysis	Isochrysis	Isochrysis
Catalyst	Ni-Ce/Al_2O_3	Ni-Ce/Al_2O_3	Ni-Ce/ZrO_2	Li-LSX zeolite	No catalyst
Fuels to be Separated [kg/hr]	17218	18492	18854	23012	17013
Column purchased cost [k$]	444	461	466	518	441
Column installed cost [k$]	96	102	103	121	95
Condenser total cost [k$]	257	269	272	310	255
Reboiler total cost [k$]	211	221	223	254	209
Total equipment price [k$]	**1007**	**1052**	**1064**	**1202**	**1000**

Table 8-11. Annual operating costs of the distillation process

Distillation cost					
Algae	Nannochloropsis	Isochrysis	Isochrysis	Isochrysis	Isochrysis
Catalyst	Ni-Ce/Al_2O_3	Ni-Ce/Al_2O_3	Ni-Ce/ZrO_2	Li-LSX zeolite	No catalyst
Cooling water annual cost [k$/yr]	2.8	3.0	3.0	3.7	2.7
Steam annual cost [k$/yr]	195.8	210.2	214.3	261.7	193.5
Annual operating costs [k$/yr]	198.6	213.2	217.4	265.4	196.2

The final flowrates of gasoline and diesel that were obtained in the simulation are shown in Figure 8-4. The scenario with Isochrysis algae and Li-LSX zeolite was the one that produced the highest amount of transportation fuels, with 183.95 million L/year of gasoline and 120.39 million L/year of diesel. The lowest was obtained with Isochrysis algae without catalyst, with 29.9 millions of gallons/year of gasoline and 19.6 of diesel.

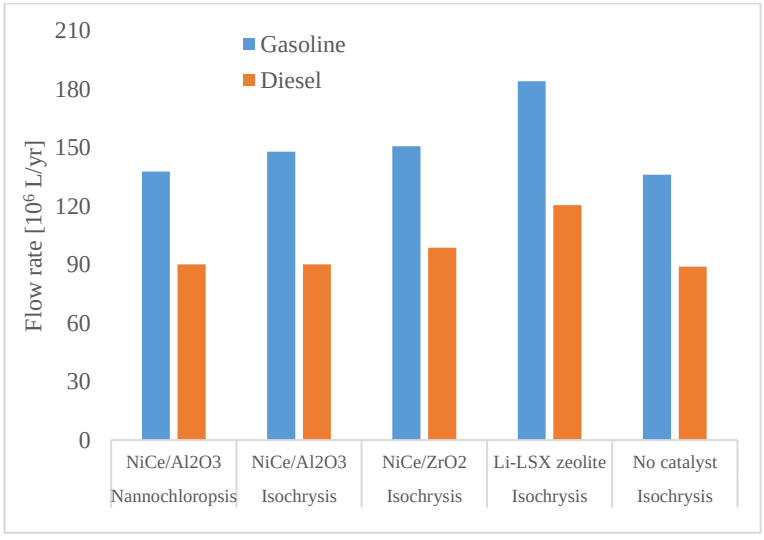

Figure 8-4. Flowrates of gasoline and diesel obtained with this facility.

After completing the simulation of all the steps involved in the conversion of microalgae to drop-in fuels, the total cost of the plant, the operating costs associated and the minimum fuel selling price (MFSP) in $/L were calculated.

8.4.5 Minimum selling price and sensitivity analysis

Using the data obtained from Aspen Plus, the CAPEX and OPEX were calculated for all the scenarios and reported in Table 8-12. A minimal difference in CAPEX was found after the two different algae species were pyrolysed in presence of $NiCe/Al_2O_3$ undergoing the same drying and hydrotreating Instead, the OPEX resulted 5% (solar) or 12% (other drying systems) lower for Nannochloropsis compared to Isochrysis under same conditions, mainly due to the different bio-oil yield and composition, which required more or less hydrogen for the downstream upgrading. As can be seen in Table 8-12, drying affects the CAPEX. If we consider the most representative scenario (Isochrysis/Li-LSX-zeolite), it can be seen that the CAPEX increase from ~$399 to $408 million when the drying system includes mechanical aid. No major difference were instead noticed for the OPEX at the variation of the microalgae drying system. The data reported in Table 12 were used to estimate the price of the fuel. In this study, gasoline and diesel were assumed to be sold at the same price as if they were the same fuel. The final price of the fuel was calculated as follows:

$$\boldsymbol{Minimum\ selling\ price} = \frac{\boldsymbol{Annual\ operating\ costs}}{\boldsymbol{Annual\ flowrate\ of\ fuels}} [=]\$/\boldsymbol{L} \qquad 8\text{-}13$$

This price was calculated in $/L considering the flowrate in millions of litres per year. The catalyst used in the pyrolysis stage affected the MFSP, which decreases as follow: Li-LSX-zeolite << $NiCe/Al_2O_3$ < $NiCe/ZrO_2$ < No Cat. The lowest MFSP was equal at 1.43 $/L obtained for the thermal dryer scenario using Isochrysis algae and Li-LSX zeolite catalyst, which produced the largest gasoline and diesel output, with 183.95 10^6 L/yr and 120.39 10^6 L/yr, respectively. The plant without catalyst showed the least favourable MFSP, about 30% higher than the MFSP obtained with Li-LSX zeolite catalyst.

Table 8-12. Economic evaluation of the different selected scenarios (N= Nannochloropsis, I=Isochrysis)

		Thermal drying					Solar drying					Mechanical and thermal drying					Mechanical and solar drying				
Algae		N	I	I	I	I	N	I	I	I	I	N	I	I	I	I	N	I	I	I	I
Catalyst		$NiCe/Al_2O_3$	$NiCe/Al_2O_3$	$NiCe/ZrO_2$	Li-LSX zeolite	No catalyst	$NiCe/Al_2O_3$	$NiCe/Al_2O_3$	$NiCe/ZrO_2$	Li-LSX zeolite	No catalyst	$NiCe/Al_2O_3$	$NiCe/Al_2O_3$	$NiCe/ZrO_2$	Li-LSX zeolite	No catalyst	$NiCe/Al_2O_3$	$NiCe/Al_2O_3$	$NiCe/ZrO_2$	Li-LSX zeolite	No catalyst
CAPEX [MM$]	Direct costs	260.9	262.7	278.7	262.9	262.7	261.9	263.8	279.7	263.8	263.6	268.1	269.9	285.9	270.0	269.8	268.5	270.3	286.3	270.4	270.2
	Indirect costs	65.24	65.69	69.68	65.72	65.67	65.49	65.95	69.94	65.97	65.92	67.04	67.49	71.48	67.52	67.46	67.13	67.58	71.57	67.61	67.55
	FCI	**326.2**	**328.4**	**348.4**	**328.6**	**328.3**	**327.5**	**329.7**	**349.7**	**329.9**	**329.6**	**335.2**	**337.4**	**357.4**	**337.6**	**337.3**	**335.6**	**337.9**	**357.8**	**338.0**	**337.8**
	Working capital	48.93	49.27	52.26	49.29	49.25	49.12	49.46	52.45	49.48	49.44	50.28	50.62	53.61	50.64	50.60	50.34	50.68	53.68	50.70	50.66
	Land	19.57	19.71	20.90	19.72	19.70	19.65	19.78	20.98	19.79	19.78	20.11	20.25	21.44	20.25	20.24	20.14	20.27	21.47	20.28	20.27
	TPI	**394.7**	**397.4**	**421.6**	**397.6**	**397.3**	**396.2**	**399.0**	**423.1**	**399.1**	**398.8**	**405.6**	**408.3**	**432.4**	**408.5**	**408.1**	**406.1**	**408.9**	**433.0**	**409.0**	**408.7**
OPEX [MM$/yr]	Direct production costs	265.6	263.7	264.9	265.7	263.8	263.9	261.95	263.2	263.9	262.4	264.9	262.9	264.2	264.9	263.1	264.3	262.3	263.6	264.3	262.5
	Fixed charges	9.79	9.85	10.45	9.86	9.85	9.82	9.89	10.49	9.90	9.89	10.06	10.12	10.72	10.13	10.12	10.07	10.14	10.74	10.14	10.13
	Plant overhead	15.03	15.08	15.56	15.09	15.08	15.06	15.11	15.59	15.12	15.11	15.24	15.30	15.78	15.30	15.30	15.26	15.31	15.79	15.31	15.31
	Manufacturing costs	**290.4**	**288.6**	**290.9**	**290.6**	**288.8**	**288.7**	**286.9**	**289.3**	**288.9**	**287.1**	**290.2**	**288.4**	**290.7**	**290.3**	**288.6**	**289.6**	**287.8**	**290.1**	**289.7**	**287.9**
	SARE	6.91	20.04	38.64	32.80	18.30	6.91	20.04	38.64	32.80	18.30	6.91	20.04	38.64	32.80	18.30	6.91	20.04	38.64	32.80	18.30
	Return on investment	39.47	39.74	42.16	39.76	39.73	39.62	39.90	42.31	39.91	39.88	40.56	40.83	43.24	40.85	40.81	40.61	40.88	43.30	40.90	40.87
	Total operating cost	**336.8**	**348.4**	**371.8**	**363.2**	**346.8**	**335.3**	**346.9**	**370.3**	**361.6**	**345.3**	**337.6**	**349.2**	**372.6**	**363.9**	**347.7**	**337.1**	**348.7**	**372.1**	**363.4**	**347.1**
	MFSP [$/L]	**1.78**	**1.76**	**1.79**	**1.43**	**1.85**	**1.77**	**1.75**	**1.78**	**1.43**	**1.84**	**1.78**	**1.76**	**1.79**	**1.44**	**1.86**	**1.78**	**1.76**	**1.79**	**1.43**	**1.85**
Sells & profits	**Total fuel sales** [MM$/yr]	**337**	**348**	**372**	**363**	**347**	**335.3**	**346.9**	**370.3**	**361.6**	**345.3**	**337.6**	**349.2**	**372.6**	**364.0**	**347.7**	**337.1**	**348.7**	**372.1**	**363.4**	**347.1**
	Bio-gas total sale [MM$/yr]	**4.6**	**8.1**	**5.2**	**0.7**	**7.9**	**4.6**	**8.1**	**5.2**	**0.7**	**7.9**	**4.6**	**8.1**	**5.2**	**0.7**	**7.9**	**4.6**	**8.1**	**5.2**	**0.7**	**7.9**
	Total revenues [MM$/yr]	**341**	**356**	**377**	**364**	**355**	**339.9**	**355.0**	**375.4**	**362.3**	**353.2**	**342.2**	**357.3**	**377.8**	**364.6**	**355.6**	**341.7**	**356.8**	**377.2**	**364.1**	**355.0**

8.4.6 Heat exchanger network

In the last part of this analysis, the design of the exchanger network was done, which requires knowledge on all the process streams and for this reason represents the final step of design process. The exchanger network has been optimized by minimizing its energy utility.

Table 8-13 summarises the streams that required a heat treatment, classified as hot streams that must be cooled (hot), and the cold streams that must be heated (cold).

Table 8-13. Thermal energy balance

Stream	Condition	F·Cp [kW/ ºC]	Temperature inlet [ºC]	Temperature outlet [ºC]	Heat available [kW]
F-102	Cold	3.93	35	175	-549.62
F-110	Hot	9.57	500	35	4,451.12
F-114	Cold	13.38	35	250	-2,876.18
F-116	Cold	9.93	25	250	-2,235.00
F-118	Hot	14.10	250	35	3,031.49
Condenser	Hot	1425.84	114	113	1,425.84
Reboiler	Cold	914.50	192	193	-914.50
F-122	Hot	6.56	113	35	518.05
F-124	Hot	6.67	193	35	1,053.92
					3,905.13

Summing algebraically the different heat rates, the energy released at the external environment was 3.905·GW, which makes the process exothermic. In order to exchange the thermal energy, the streams need to have a ΔT among them. As result, in Figure 8-5, the different streams are represented together with their enthalpy and temperature range. The streams are shown as arrows, with origin at the input temperature of the exchangers and end at the outlet temperature. The hot and cold streams have shifted scales of 5 °C, which represents the minimum driving force. On the left scale of the figure, the hot streams are cooled, while on the right, the cold streams are heated. Furthermore, the temperature interval of the streams where they can exchange the thermal energy is reported. The cumulative enthalpy for the cold and hot streams have been plotted with

the temperature (Figure 8-6), to identify possible pinch points' temperature (temperature difference between the streams of less of 5 ºC). In this case, the pinch point was not detected, which does not restrict the design of the heat exchange network.

Having defined all the streams and identified the minimum amount of the process utility, the heat exchange networks has been determinate and represented in Figure 8-7. The hot streams (red arrows) achieving their target temperature suppling thermal energy by cold utilities (black dot) or from the cold streams (blue arrow connected by a black line). Moreover, the heat exchange networks was designed, imposing $(F \cdot c_p)_{hot} \leq (F \cdot c_p)_{cold}$.

In particular, the gaseous stream from the outlet of the cyclone (F-110) was cooled by the energy supplied from the distillation tower reboiler. Afterwards, the stream was split to two stream, exchanging thermal energy for preheating the air for the drier unit (F-102) and the hydrogen (F-116).

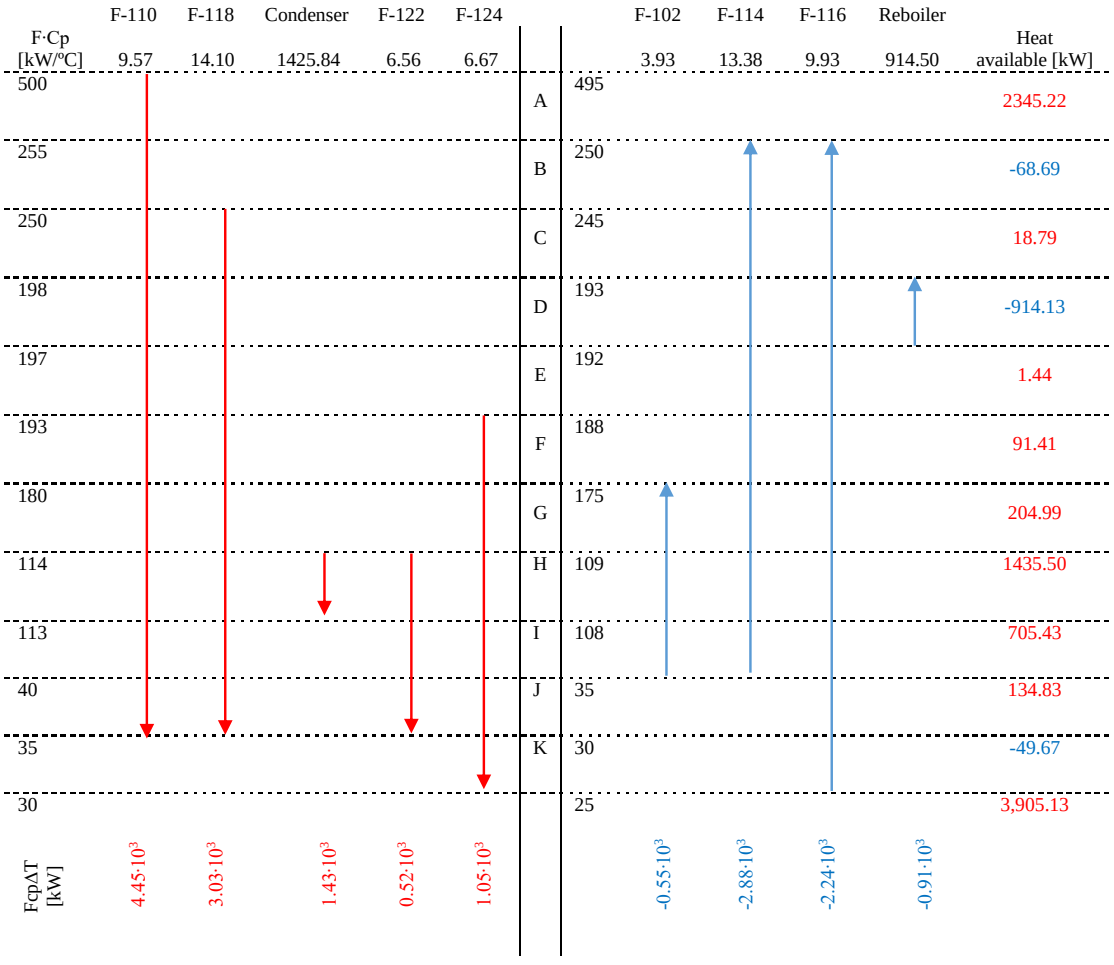

Figure 8-5. Temperature interval diagram

At the end, the stream F-110 did not achieve the temperature target, for this reason a cold utility has been expected. As it is possible to note from Figure 8-7 the stream F-102, the air supplied at the drier unit, the thermal energy was satisfied from the streams present in

process, achieving a significant energy/cost reduction. The stream exiting the hydrotreater (F-118) was cooled using part of the air stream entering the drier unit (F-102) and the hydrotreater (F-114). While, the cold utilities have been used for cooling the diesel stream in output of the reboiler (F-124) and gasoline streams, in input of the condenser and the stream F-122. The heat exchange network was designed for minimising the energy required for the process for the best case scenario (LiLSX zeolite), resulting in a decrement of OPEX and CAPEX of 359 MM$/yr and 393 MM$, respectively, as reported in Table 8-14. The MFSP achieved a value of 1.418 $/L, which represents a decrement of 0.012 $/L compared to the non -optimised process.

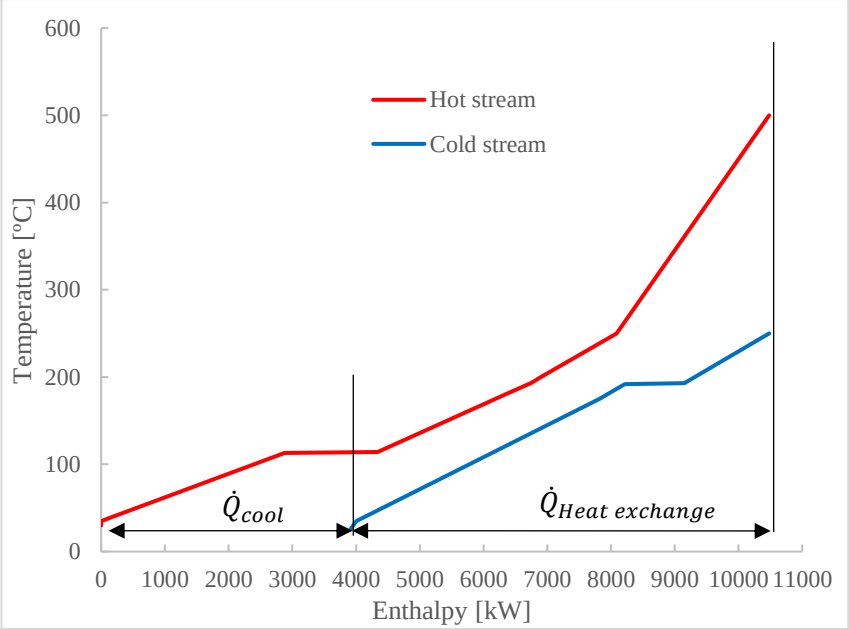

Figure 8-6. Composite curves for hot and cold streams

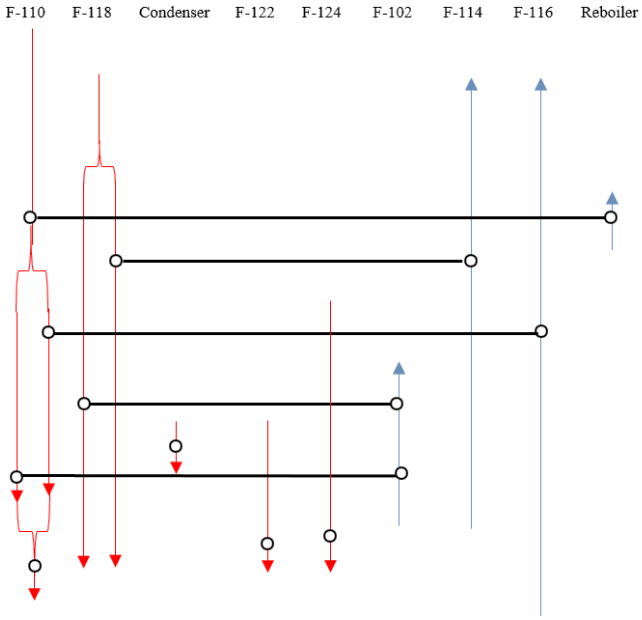

Figure 8-7. Heat exchange network

Table 8-14. Economic evaluation after heat exchange network

Algae		Isochrysis
Catalyst		Li-LSX zeolite
CAPEX [MM$]	Direct costs	260
	Indirect costs	65
	FCI	**325**
	Working capital	49
	Land	20
	TPI	**393**
OPEX [MM$/yr]	Direct production costs	262
	Fixed charges	10
	Plant overhead	15
	Manufacturing costs	287
	SARE	33
	Return on investment	39
	Total operating cost	**359**
	MFSP [$/L]	**1.418**
Sells & profits	**Total fuel sales** [MM$/yr]	**359**
	Bio-gas total sale [MM$/yr]	**0.0114**
	Total revenues [MM$/yr]	**0.7**

8.4.7 Sensitive analysis

In order to identify the components and properties that affect most the final price of the fuels, a sensitivity analysis was carried out, by varying of ±20 % the following sensitivity factors: Bio-oil yield, feedstock cost, rate of return on investment and price of pyrolysis reactor. This sensitivity analysis was carried out with Isochrysis as feedstock and Li-LSX zeolite for the thermal dryer scenario, since the fuel price determined was the lowest (1.418 $/L). The main results are reported in Table 8-14, where it can be seen that the bio-oil yield and the feedstock cost were the most important factors. For the latter, by varying the price of algae from 52.8 $/metric ton to 79.2$/metric ton, the fuel price increased from 1.237 $/L to 1.1593 $/L. These two properties were also found to be the key factors in most of the previous studied [121-123]. Therefore, the techno-economic success of producing drop-in fuels from microalgae is strictly dependent on the future development of cost-effective processes for microalgae cultivation. Figure 8-8 shows the operating costs for the best scenario (Isochrysis – Li-LSX-zeolite).

Feedstock, annual return on investment and hydrogen purchased were the main operating costs associated with the plant. Regarding the equipment costs, the pyrolysis reactor was

the most expensive component of the integrated facility, representing about 60% of the total equipment cost, as can be seen in Table 8-14. This base fuel price calculated in this work for the system Isochrysis-LiLSX-zeolite was lower than that found in a previous algae pyrolysis study as reported in the introduction section [121], but resulted higher than in Xin et al. (0.59 $/L) [270], where wastewater was used to grow microalgae, leading to a lower price of the feedstock, which as we have shown, is a key factor affecting the overall conversion costs.

Despite the fact that the fuel price of 1.418 $/L resulted less expensive than those obtained by processing microalgae by other methods, such as solvent extraction of lipid fraction, leading to fuel prices between 2.60- 5.42 $/L [285] and other assessments indexed in a recent review [286]; fuel price obtained using lignocellulosic material (corn stover) (0.68 $/L) in similar conversion processes [122], suggests that micro-algae to biofuels through pyrolysis-hydro-treatment still require improvements in particular concerning to the microalgae production cost.

Table 8-15. Sensitivity analysis for Isochrysis as feedstock and Li-LSX zeolite as catalyst.

	Property/component			Fuel price ($/L)		
Key component/ process	-20%	Base case	+20%	-20%	Base case	+20%
Bio-oil yield (wt. % of dry biomass)	24.8	31	37.2	1.751	1.418	**1.158**
Feedstock cost [$/metric ton]	52.8	66	79.2	**1.237**	1.418	1.593
Return on investment [%]	8	10	12	1.385	1.418	1.445
Catalytic pyrolysis reactor [MM$]	126.4	158	189.6	1.366	1.418	1.455

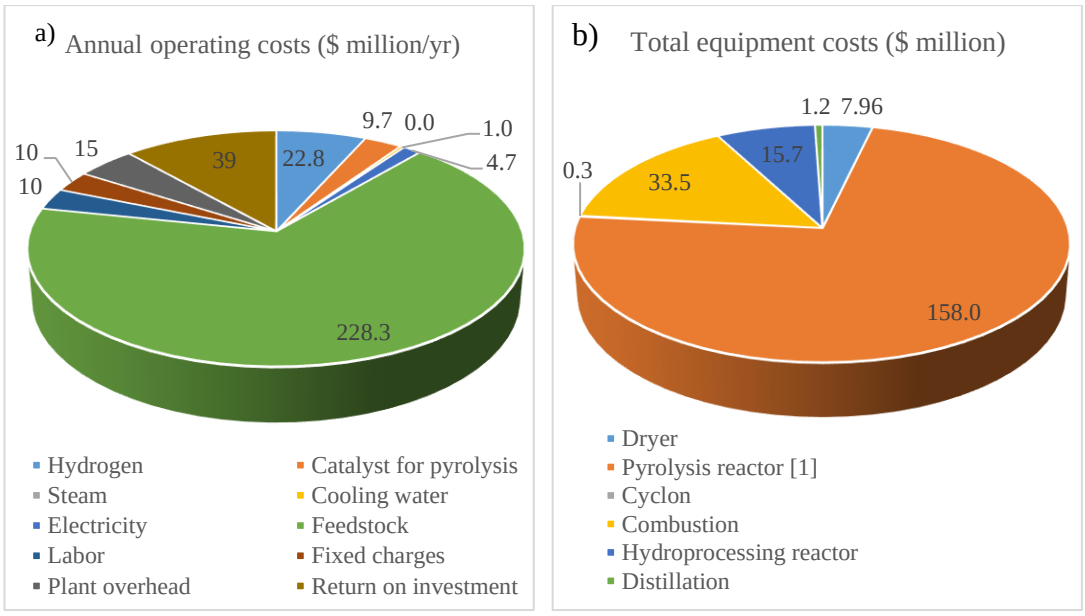

Figure 8-8. Repartition of the (a) annual operating costs and (b) equipment costs for Isochrysis as feedstock and Li-LSX zeolite (thermal drying scenario).

8.5 Conclusion

This techno-economic study explored the cost of producing drop-in fuels from microalgae via catalytic pyrolysis and bio-oil upgrading. Microalgae drying, pyrolysis, biochar combustion and bio-oil/bio-gas refining process were simulated in Aspen environment. Capital expenditure and operational expenditure were obtained comparing the running costs with the fuel selling price, thus giving more understanding to the costs associated with the overall process. In order to determine their impact on the final cost of the fuels, different scenarios were considered including three types of microalgae drying, due to the known impact of drying on microalgae based biofuels, two microalgae species (Nannochloropsis and Isochrysis) and a number of different catalysts. Fuel prices determined in this project varied from 1.43 $/L to 1.84 $/L, resulting similar to those calculated in previous work using Chlorella microalgae as feedstock (1.49 $/L to 1.80 $/L). In this study, Isochrysis as feedstock with Li-LSX zeolite as catalyst was the most promising scenario (1.43 $/L), mainly due to the higher bio-oil yield obtained by using Li-LSX-zeolite for the microalgae pyrolysis. The best scenario (Li-LSX zeolite) was then optimised, in terms of energy demand, reaching a MFSP equal to 1.418 $/L. Finally, the sensitivity analysis showed that the bio-oil yield was the most influent factor, leading to a variation of the fuel price between 1.158 $/L to 1.751 $/L assuming a 20% of variation. The fuel price determined in this study for the Isochrysis and Nannochloropsis microalgae based process is promising, but requires to be lowered to a more favourable price to be

competitive with lignocellulosic based processes. In particular, further research is required to drastically reduce the price of the feedstock production and drying and the development of catalysts able to maximise both the yield and quality of the bio-oils produced.

Chapter 9- Process and techno-economic analysis for fuel and chemical production by hydrodeoxygenation of bio-oil

This chapter has been published as: G. Bagnato, A. Sanna, Process and techno-economic analysis for fuel and chemical production by hydrodeoxygenation of bio-oil, Catalysts 2019, 9(12), 1021.

9.1 Abstract

The catalytic hydrogenation of lignocellulosic derived bio-oil has been assessed from the thermodynamic simulation perspective, in order to evaluate the economic potentiality of bio-oils as feedstock for chemicals and drop-in fuels production. The aim of this work was to design a hydrodeoxygenation (HDO) process for pyrolytic oil from pinewood by a heuristic method, in order to evaluate the economic feasibility.

A preliminary economic evaluation was first run to identify the conditions where the process is profitable, while a full economic analysis evaluated how the operating conditions affected the reaction in terms of yield. The results indicate that the bio-oil should be separated into water-soluble and insoluble fractions previous hydrogenation, since very different process conditions are required for the two portions.

The maximum economic potential resulted in 38,234 MM$/y for a capacity of bio-oil processed of 10 Mton/y, processing the insoluble bio-oil fraction for biofuels production with a cost of of 22.22 and 18.87$/GJ for light gasoline and diesel, respectively. While, the water soluble bio-oil fraction was able to produce 51.43 ton/day of chemicals, such as sorbitol, propanediol, butanediol, etc., for a value equal to the market price. The feasibility of the plan was also evaluated by return of investment (ROI) of 69.18%, a pay-out time of 2.48 years and discounted cash flow rate of return (DCFROR) 19.11% considering a plan cycle life of 30 years.

9.2 Introduction

In 2018, fossil fuels' share in global energy production was 136,580 TWh (93.6 % of the total) [287] contributing to the increase in greenhouse gases (GHG) in the atmosphere, which are gradually raising the global temperature, thus causing a series of problems to our planet [288, 289]. Currently, the scientific community in sync with national and international policies (e.g. COP21) are seeking into alternative source of clean energy for

reducing GHG emissions. Renewable energy represents energy derived from renewable sources such as solar energy, wind power, hydroelectric power, geothermal energy, tidal power and biomass [290]. Among them, biomass is the only renewable source that can cover all three aspects of energy uses: electricity, heat and transportation fuels. In particular, its densification in liquid bio-oils through thermochemical processes such as pyrolysis and the further upgrading of the oils using crude oil refineries is attractive due to the possibility to carry on using existing infrastructures. The bio-oils obtained from lignocellulosic biomass are dark brown organic liquids with the presence of many different organic compounds such as aldehydes, ketones, sugars, carboxylic acids and phenols. However, the potential of these liquids for direct substitution of petroleum fuels is limited due to their high viscosity, high water and oxygen contents, low heating value, instability and high acidity (corrosiveness) [291, 292].

The catalytic hydrodeoxygenation (HDO) of biomass-derived fast pyrolysis oil represents a fascinating route for the production of liquid transportation fuels and commodity chemicals. The path for the conversion of biomass into the petroleum-compatible product through pyrolysis/HDO can be dived into a series of steps including feed purification, chemical modification and products separation. In refineries, the hydrogenation reactions are common operations to limit the presence of oxygen, nitrogen, sulphur, olefins and aromatics[293]. The reaction is catalysed by molybdenum together with Ni or Co supported by γAl_2O_3. The operating conditions depend on the type of feed: Liquid hourly space velocity (LHSV) ranges from 0.2-to 8.0, H_2 flow from 50 to 675 Nm^3 / m^3, H_2 pressure between 14 and 138 bar and temperatures between 290 and 470 ºC [40].

According to the feed processed and the desired products, different metals can be used. The metals reactivity scale:

$$\text{Olefin: Rh, Ru, Pt, Pd} > \text{Ni, Ir} > \text{Co, Fe} \qquad 9\text{-}1$$

$$\text{Aromatic: Pt} > \text{Rh, Ru} > \text{Pd, Ni} > \text{Co, Fe} \qquad 9\text{-}2$$

Noble metals are able to hydrogenate olefins and aromatics compound compared to conventional metals. Acid support is present favouring the isomerisation reactions but also promoting coke formation. The acid support reactivity decreases as follow:

$$\text{Zeolite} > SiO_2 / Al_2O_3 > H_3PO_4 / SiO_2 > Al_2O_3 \qquad 9\text{-}3$$

Noble catalysts supported on C (Ru/C, Ru/TiO_2, Ru/Al_2O_3, Pt/C, and Pd/C) have been studied for the hydrotreating of bio-oil by a number of authors. For example, Wildschut et al.[21] studied the bio-oil hydrogenation at different temperatures (250 and 350 °C) and pressures (100 and 200 bar) and compared carbon-supported catalysts with

conventional hydrotreatment catalysts (sulfided NiMo/ Al_2O_3 and CoMo/Al_2O_3). The authors obtained best performance with Ru/C catalyst in term of oil yield (up to 60 wt %) and deoxygenation level (up to 90 wt %). Ardiyanti et al.[183] tested different noble mono and bimetallic catalyst (Pt, Pd, Rh) supported on zirconia at 350 °C and at 200 bar. The yields of the upgraded bio-oils resulted in 37 and 47 wt% oil (based on the feed), the remainder being an aqueous phase (30–42 wt% based on feed), a gas phase (6–10 wt% on feed) and some coke (2–7 wt% on feed). Furthermore, the noble catalyst showed higher activity than CoMo/ Al_2O_3 under the same condition. Furthermore, Ardiyanti et al.[23] proposed a reactivity scale for the bimetallic catalysts for bio-oil HDO, as follow:

$$Pd/ZrO_2 > Rh/ZrO_2 > RhPd/ZrO_2 \approx PdPt/ ZrO_2 > RhPt/ZrO_2 > Pt/ZrO_2 > CoMo/Al_2O_3 \quad 9\text{-}4$$

Pucher et al.[294] tested the performance of noble (Ru, Pt and Pd) and Ni catalysts at moderate (250 °C and 100 bar) and severe (at 300 °C and 150 bar) condition in bath reactor. Pt/C showed good results in term of increasing the calorific value of the upgraded bio-oils and reduction of coke formation; also, the water content was reduced of about 86 % and 73-79 % of the starting energy was transferred into the oil phase. Instead, the use of Ru/C catalysts resulted in a higher H_2 consumption up to about 200°C. After this temperature, the polymerization reactions were favoured and the H_2 consumption remained constant[295]. NiMo/γ-Al_2O_3 has been studied[296] at 390 °C and 70 bar. In this study, the bio-oil was heated inside the reactor injecting hot hydrogen, resulting in a decrement of coke and the formation of aromatic ring compounds. To reduce the acidity value of bio-oil, Parapati et al.[297, 298] added 0.5 mg KOH/g bio-oil carrying out the bio-oil hydrotreating with sulfided CoMo/γ-Al_2O_3 and KOH treated reduced CoMo/γ-Al_2O_3 (2 mg KOH/g bio-oil) at 375 ºC and 100 bar. In each test, they obtained an oxygen content around 0.1%, and the higher heating value (HHV) increased to about 44 MJ/kg. Moreover, the products of the reduced catalyst resulted in 50% gasoline, 30% jet fuel and 20% diesel, while the sulfided catalyst produced 90% gasoline, 5% jet fuel and 5% diesel. The bio-fuel obtained in literature have been presented as Van Krevelen plot in Figure 9-1, where the bio-fuel proprieties in term of O/C and H/C molar ratios are compared. A bio-fuel with the same proprieties of the diesel should have O/C and H/C molar ratios that tend to zero and greater than one, respectively. The bio-fuels obtained by Parapati et al.[297, 298] resulted comparable to diesel, thanks to the strong deoxygenation obtained using the reduced catalysts in presence of a strong base.

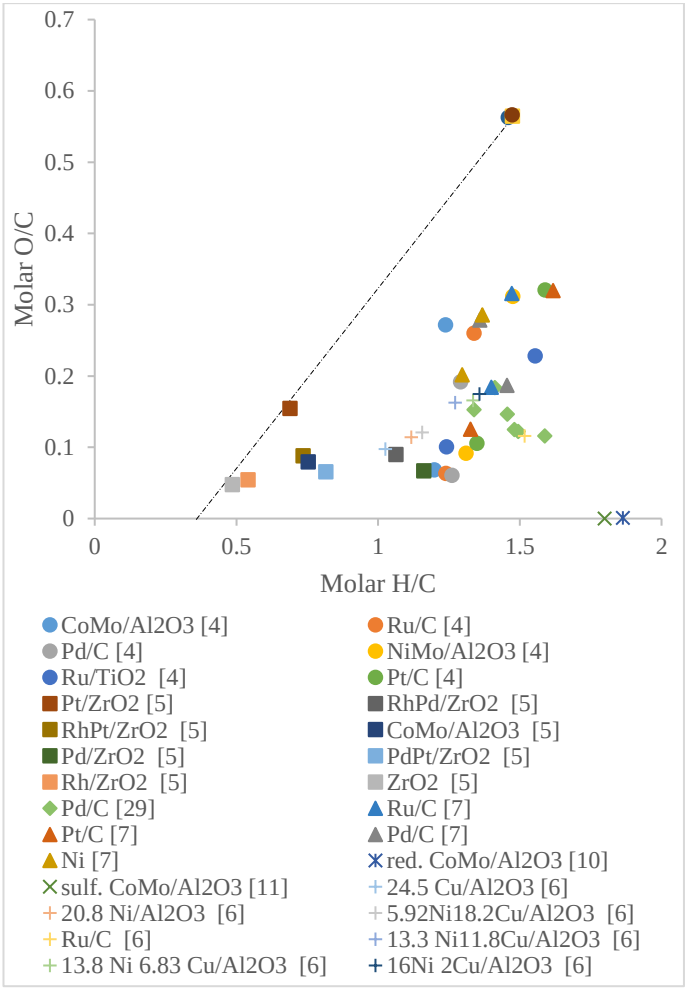

Figure 9-1. Van Krevelen plot [299]

Recent works analysed the techno-economics of hydrotreating bio-oil to biofuels [109, 110, 300-302]. Bagnato et al. [300] simulated the pyrolysis of 2000 dry tonne per day of *Isochrysis* sp. microalgae in presence of Li-LSX-zeolite, producing biogas, bio-oil and bio-char. Subsequently, the bio-oil was upgraded by hydrotreating reaction into fuels, achieving a minimum fuel selling price of 1.418 $/L. The main economic concerns were linked to high CAPEX and feedstock cost and short hydrotreating catalyst lifetime. Finally, Zhu et al. (2014) designed a process for the high thermal liquefaction of 2000 dry metric tonne per day wood biomass derivate, estimating a MFSP equal to 0.98 $/ litre-equivalent [302]. The studies above show high variability of the MFSP and are mostly focused on producing transport fuels, while little is reported on producing added-value chemicals from the bio-oil. Therefore, this study aims to evaluate the overall performance of a bio-oil hydrotreating process to both transportation fuels and chemicals and explore the appropriate operation variables by the economic criteria suggested by Douglas et al. [303]. This work is performed using Aspen Plus software based on the simulation of the

hydrogenation reactions of the water soluble and insoluble bio-oil process system, with a feedstock processing capacity of 10Mt/y.

9.3 Methods

Therefore, a suitable simulation model for an industrial bio-oil hydrogenation plant was developed in order to predict the reactions behaviour during the upgrading process. In this regard, first, a reaction network responsible for the hydrogenation of the bio-oil is proposed and then, physical and empirical correlations are applied.

To design the hydrogenation of bio-oil the heuristic method described by Douglas et al.[303] was used. This method provides solving the problems by different detailed layers, starting from a basic level to a level where more specific knowledge is required. Each level has been evaluated using the Economic Potential (EP) that indicates the annual profit of the process, depending on the variable of projects and the specific required of the level:

Level 0: Preliminary information. The target of this level is to find all the information present in literature about the process, including the reactions involved, the catalysts studied and operating condition at which the products can degrade. In order to evaluate the system, the following variables have been defined:

$$\boldsymbol{Yield_i} = \frac{\boldsymbol{mass\ flow\ of\ i{-}component}}{\boldsymbol{mass\ flow\ of\ Bio{-}oil}}\ [-] \qquad 9\text{-}5$$

$$\boldsymbol{MR} = \frac{\boldsymbol{molar\ flow\ of\ H_2\ feed}}{\boldsymbol{molar\ flow\ of\ Biooil\ fraction}}\ [-] \qquad 9\text{-}6$$

$$\boldsymbol{R_1} = \frac{\boldsymbol{malar\ flow\ rate\ of\ vapour\ recyvcled}}{\boldsymbol{malar\ flow\ rate\ of vapour\ reactor\ output}}\ [-] \qquad 9\text{-}7$$

$$\boldsymbol{R_2} = \frac{\boldsymbol{malar\ flow\ rate\ of\ liquid\ recyvcled}}{\boldsymbol{malar\ flow\ rate\ of liquid\ reactor\ output}}\ [-] \qquad 9\text{-}8$$

Level 1: Batch vs continuous process. This level the process is defined how to operate, continuous or batch.

Level 2: Input-output structure. At this level, the process is considered as a black box, with input and output streams. By the material balance, the products have been calculated using the thermodynamic data.

Moreover, level 2 corresponds to the maximum EP obtainable calculated as:

$$\boldsymbol{EP_2 = Product\ value + Byproduct\ values - Raw\ material\ cost}\ [=]\$/\boldsymbol{yr} \qquad 9\text{-}9$$

The cost of each compound is reported in Table 9-1.

Table 9-1. Chemical price of main reactants and products from bio-oil HDO

Compound	Unit	Price	Ref.	Compound	Unit	Price	Ref.
Acetic acid[§]	$/kg	0.839	[304]	Hydroxyacetone[§]	$/kg	1.25	[304]
Benzendiol[§]	$/kg	1.50	[304]	Hydroxypropionic acid[§]	$/kg	10.12	[304]
Bio-Oil*	$/GJ	16.84	[12]	Kerosene*	$/GJ	11.92	[35]
Butyric acid[†]	$/kg	1.21	[304]	Levulinic acid[§]	$/kg	5.80	[304]
Butanediol[§]	$/kg	1.71	[304]	Light Gasoline*	$/GJ	14.44	[35]
Diesel*	$/GJ	12.26	[35]	Methanol[§]	$/kg	0.315	[304]
Ethanol[§]	$/kg	0.67	[304]	o-Methoxyphenol[§]	$/kg	1.50	[304]
Ethylene glycol[§]	$/kg	1.43	[304]	Propanediol[§]	$/kg	1.27	[304]
Fuel gas*	$/GJ	3.72	[35]	Residual fuel*	$/GJ	6.82	[35]
Glucose[§]	$/kg	0.309	[304]	Sorbitol[§]	$/kg	1.72	[304]
Heavy Gasoline*	$/GJ	21.88	[35]	Methoxy-Hydroxybenzaldehyde[§]	$/kg	12.0	[304]
Hydrogen*	$/GJ	12.50	[305]	Vanillin alcohol[§]	$/kg	44.46	[304]
Hydroxyl acetaldehyde[§]	$/kg	1	[304]	γ- Valero lactone[§]	$/kg	14.43	[304]

*2015, [†]2001, [§]2006

Level 3: Recycle structure. By using the kinetic rates, it was decided how the reactor has to work and the possibilities in terms of recycle streams. The EP_3 is composed of EP_2 plus the addition of the reactions cost:

$$\boldsymbol{EP_3 = EP_2 - L_3\ cost}[=]\$/\boldsymbol{yr} \quad (9\text{-}10)$$

$$\boldsymbol{L_3\ cost = reactor\ cost|_{L_3} + compressor\ cost|_{L_3} + heat\ excange\ cost|_{L_3} + utitlities\ cost|_{L_3}}[=]\$/\boldsymbol{yr} \quad (9\text{-}11)$$

The reactor cost was calculated by Guthrie's correlation, where all the equipment costs were actualised at 2016 by Marshall and Shift index (M&S).

Level 4: Separation system. The most suitable equipment to obtain the desired products and to recover them with a purity that is as high as possible were found out. To determine the general structure of the separation system, the phase in output of the reactor was specified. The separation system was split into two sections, vapour and liquid phase, which affected the EP4:

$$\boldsymbol{EP_4 = EP_3 - L_4\ cost}[=]\$/\boldsymbol{yr} \quad (9\text{-}12)$$

$$\boldsymbol{L_4\ cost = liquid\ sep.cost|_{L_4} + \ vapour\ sep.cost|_{L_4} + product\ lost|_{L_4} + utitlities\ cost|_{L_4}[=]\$/yr} \quad 9\text{-}13$$

Cost estimating. Defined all the part of the process, the economic evaluation was done following the guideline of Douglas et al.[120] and Peters et al. [306], as summarised in Table 9-2 and Table 9-3 (described on *3.3 Techno-economic assessment*). Those values were then used to calculate the return of investment (ROI), able to measure the profitability of the overall process:

$$\boldsymbol{ROI = \frac{Annual\ Profit}{Total\ Investiment}}[\%] \quad 9\text{-}14$$

The pay-out time, a parameter able to indicate the years for recovering the initial investment:

$$\boldsymbol{Payout\ time = \frac{Fixed\ Cap.+Start-up}{Profit\ after\ Taxes+Deprec.}} \quad 9\text{-}15$$

Table 9-2. Estimation of capital investment cost

Direct costs:	**32,839 MM$**
Purchased equipment (22.9% FCI)	10,758 MM$
Installation, including insulation and painting (8.3% FCI)	3,899 MM$
Instrumentation and controls, installed (6.4% FCI)	3,007 MM$
Piping, installed (7.3% FCI)	3,430 MM$
Electrical, installed (4.6% FCI)	2,161 MM$
Buildings, process and auxiliary (4.6% FCI)	2,161 MM$
Service facilities and yard improvements (13.8% FCI)	6,483 MM$
Land (1-2% FCI)	940 MM$
Indict costs:	**13,765 MM$**
Engineering and supervision (9.2% FCI)	4,322 MM$
Construction expense and contractor's fee (12.8% FCI)	6,013 MM$
Contingency (7.3%FCI)	3,430 MM$
Fixed-capital investment (FCI) = direct costs + indirect costs	**46,980 MM$**
Working capital (15% TCI)	**8,291 MM$**
Total capital investment (TCI)= fixed-capital investment + working capital	**55,271 MM$**

Table 9-3. Estimation of the total product cost

Manufacturing cost = direct production costs + fixed charges + plant overhead costs	**55,910 MM$**
Direct production costs:	**42,847 MM$**
Raw materials (35% TPC)	22,861 MM$
Operating labour (10% TPC)	6,532 MM$
Direct supervisory and clerical labour (10-25% of operating labour)	653 MM$
Utilities (15% of total product cost)	9,797 MM$
Maintenance and repairs (2-10% of fixed-capital investment)	810 MM$
Operating supplies (0.5-1% FCI)	235 MM$
Laboratory charges (10-20% of operating labour)	653 MM$
Patents and royalties (0-6% TPC)	1,306 MM$
Fixed charges:	**6,5320 MM$**
Depreciation (10% FCI)	4,698 MM$
Local taxes (3%FCI)	1,409 MM$
Insurance (0.7%FCI)	329 MM$
Rent (10% of value of rented land and buildings)	94 MM$
Plant-overhead costs (10% TPC); includes costs for the following: general plant upkeep and overhead, payroll overhead, packaging, medical services, safety and protection, restaurants, recreation, salvage, laboratories, and storage facilities.	**6,532 MM$**
General expenses:	**9,406 MM$**
Administrative costs (15% operating labour)	980 MM$
Distribution and selling costs (11% TPC)	7,185 MM$
Research and development costs (5% TPC)	3,266 MM$
Financing (5% TCI)	3,266 MM$
Total product cost= manufacturing cost + general expenses	**65,316 MM$**
Gross earnings cost = total income - total product cost amount of gross earnings cost depends on amount of gross earnings for entire company and income-tax regulations; a general range for gross-earnings cost is 30-40% of gross earnings)	**38,428 MM$**
Profit before Taxes= Revenue-Total Production Cost	**20,833 MM$**
Profit after tax= 0.52 Profit before Taxes	**9,406 MM$**
Cash Flow=Profit after Taxes+ Depreciation	**19,423 MM$**

Also, the discount of cash flow rate of return (DCFROR), a parameter to estimate the profit as interest index (*i*), gave a direct comparison with bank interest. The DCFROR was calculated equating the value of the investment value (IPV) to build-up the plant (calculated in 3 years) and the return value (RPV), calculated in N-years equal to the process service life, assuming different case:15, 20, 25 and 30 years.

$$\boldsymbol{IPV = \sum_{j=0}^{3}\{Work.Cap. + Start\_up + [a_j \cdot TCI \cdot (1+i)^j]\}} \quad 9\text{-}16$$

$$\boldsymbol{RPV = \frac{Work.Cap.+Salv.Val.}{(1+i)^N} + \sum_{j=1}^{N}\left[\frac{b_j \cdot CashFlow}{(1+i)^j}\right]} \quad 9\text{-}17$$

Where a_j is the fraction of TCI for different year, a_1= 0.1, a_2= 0.4, a_3= 0.4 and a_4= 0.1; while b_j used to correct the annual cash flow, considering constant after the third year (b_1=0.6 b_2 =0.9 b_3= 0.95, j>4 b_j=1)

9.4 Result and Discussion

The designed simulated process for the HDO of biomass-derived fast pyrolysis oil is schematised in Figure 9-2 and 3 for WBO and IBO fraction, respectively. For both fractions there is a "preparation zone", where the reactants are heated up and the gas streams are compressed; a "reaction zone" where the reactants are converted into the desired products. This zone consists to a series of adiabatic reactors with intermediate cooling system. The last part of the plant is the "separation zone", which is divided into a vapour and liquid recovery for the WBO and a distillation tower for the IBO.

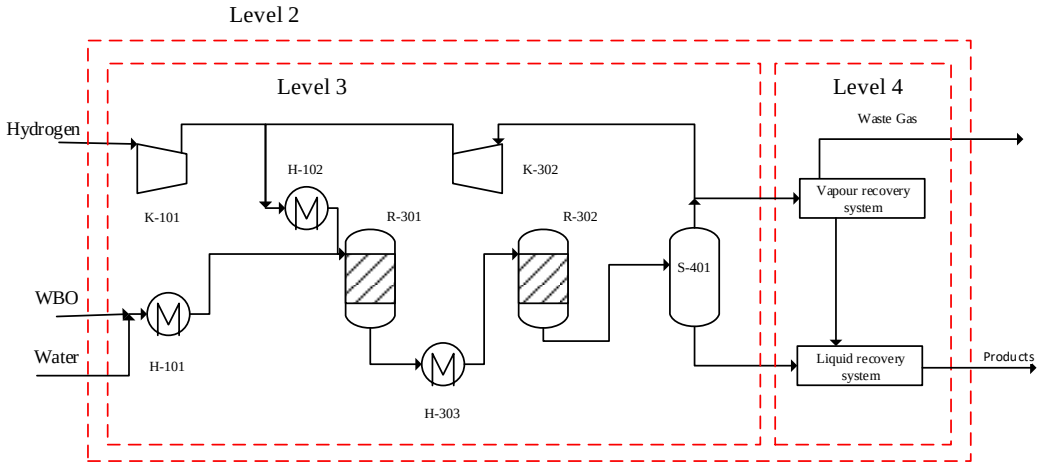

Figure 9-2. HDO- WBO process

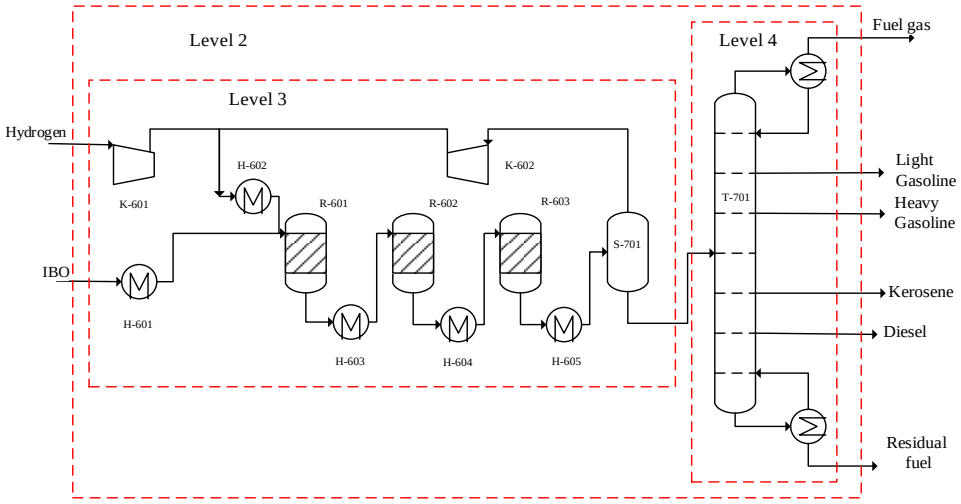

Figure 9-3. HDO- IBO process

9.4.1 Level 0: preliminary information

The bio-oil composition of the feed considered in this work was simplified using only the most representative compounds of the different pinewood bio-oil functionalities (see Table 9-4**).** Also, it was assumed that (1) the fresh feed does not contain impurities such as ash and solid particles; (2) the bio-oil is separated in two phases, a water-soluble bio-oil (WBO) and a water-insoluble bio-oil (IBO).

To design the HDO process, experimental data from literature were taken into account. The reaction pathways considered for the WBO hydrogenation are represented in Figure 9-4, while the reaction mechanisms of the IBO fraction hydrogenation can be seen in Figure 9-5[307]. For the WBO fraction, the equation kinetics for the hydrogenation reaction were identified in literature [79, 80, 308-311], using as catalyst 5 wt% Ru/C. Polymerization reactions that are favoured at temperature higher than 200 ºC, were also taken into consideration in the model [8].For the IBO fraction, the kinetic equation of Yu-Hwa et al. was considered for the simulation [83], where the IBO was divided into six groups (heavy non volatiles, light non-volatile, phenols, aromatics, alkanes, coke + H_2O + outlet Gases) and CoMo/γ-Al_2O_3 was the selected catalyst. To simplify the evolution of the data, the HDO products were separated in specific streams according to their temperature boiling point (TBP): (1) fuel gas stream (up to 35 ºC); (2)(3) light gasoline (35-90 ºC); (4) heavy gasoline – excluding water (90-180 ºC); (5) kerosene (180-250 ºC); (6) diesel (250-350 ºC) and finally, (7) residual fuel (more than 350 ºC).

Table 9-4. Bio-oil composition

Compound group	Model compound	Formula	%wt dry base	Ref.
	Water-soluble			
Acids	Acetic acid	$C_2H_4O_2$	3.90	[312]
	Levulinic acid	$C_5H_8O_3$	1.67	
Alcohols	Tyrosol	$C_8H_{10}O_2$	3.48	[312-314]
	Glycerol	$C_3H_8O_3$	3.49	
Ketones	Hydroxyacetone	$C_3H_6O_2$	8.29	[312-314]
Aldehydes	Hydroxyacetaldeyde 3-Methoxy-4-Hydroxybenzaldehyde	$C_8H_8O_3$	6.97	[312, 314-316]
Guaiacols	o-Methoxyphenol	$C_{10}H_{12}O_2$	4.98	[312, 313, 317, 318]
Low MW sugars	Levoglucosan	$C_6H_{10}O_5$	5.97	[313, 314, 317, 319]
High MW sugars	Cellobiose	$C_{12}H_{22}O_{11}$	33.86	[317]
	Water-insoluble			
Low MW lignin-derived compounds	Dimethoxy stilbene	$C_{16}H_{16}O_2$	10.95	[319]
	Dibenzofuran (representing diphenyl compounds)	$C_{12}H_8O$	2.21	[320]
Extractives	Dehydroabietic acid	$C_{20}H_{28}O_2$	2.99	[317-319]
High MW lignin-derived compounds	Oligomeric compounds with β-O- 4 bond	$C_{20}H_{26}O_8$	9.15	[307]
	Phenylcoumaran compounds	$C_{21}H_{26}O_8$	1.99	[320]
Nitrogen compounds	2,4,6- trimethylpyridine	$C_8H_{11}N$	0.070	[321]
Sulfur compounds	Dibenzothiophene	$C_{12}H_8S$	0.025	[314]

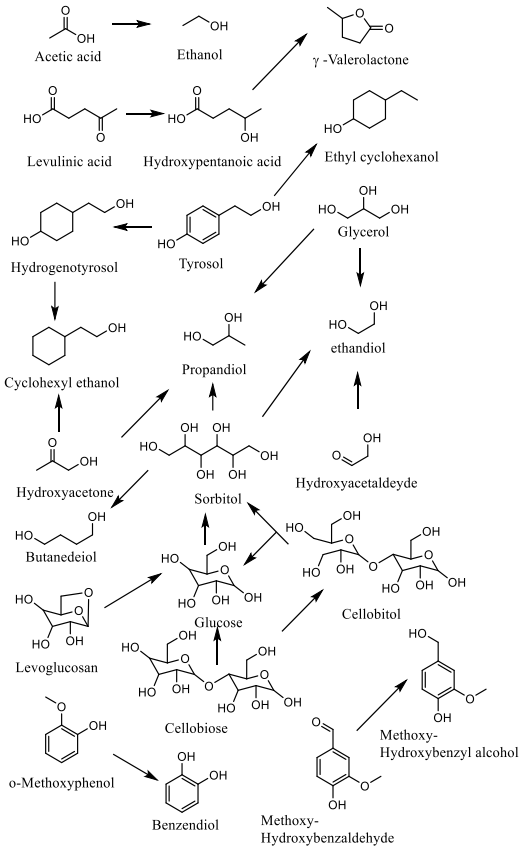

Figure 9-4. HDO reaction pathways for the WBO

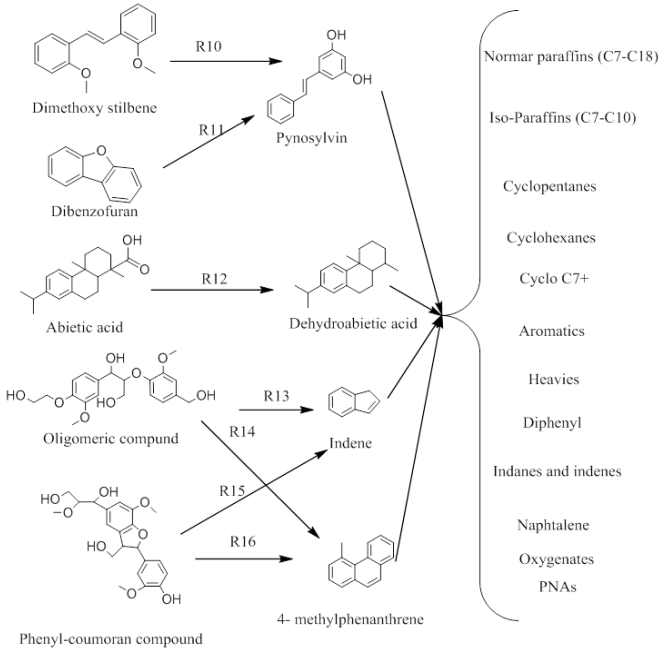

Figure 9-5. IBO HDO reaction scheme for the IBO (modified form [307])

9.4.2 Level 1: batch versus continuous

Continuous processes are designed to be operational 24 hours per day, without interruption, contrary for batch process. The criterion to be used to choose a continuous or batch process depend of the plant capacity, if the plants have a capacity greater than 4,500 tonnes/y are usually continuous[120]. In our case, the process capacity was assumed to be 10 million tonnes per year, which is similar in terms of raw material processed (215 thousands barrel per day) to the Valero Refining New Orleans LLC[322]. Therefore, the plant was simulated in continuous mode. Furthermore, the process was divided so that the (i) WBO fraction (representing 75% of the organic phase) was evaluated for the production of chemicals and fuels, and (ii) the IBO fraction (12.5% of the whole bio-oil, equal to 4,300 m^3/day) for fuels production.

9.4.3 Level 2: input-output structure

The HDO of the bio-oil was studied in terms of product yields, by varying the reaction temperature between 50 and 500 ºC, at pressures from 10 to 150 bar and changing the H_2/bio-oil feed molar ratio from 1 to 4. Furthermore, the sorbitol yield was separately investigated, as the reaction is strongly thermodynamic limited.

Water bio-oil fraction- The HDO reaction for the WBO involves multiple reactions, of which, three of them with thermodynamic equilibrium. In particular:

$$\boldsymbol{Hydroxyacetone + H_2 \leftrightarrow Propanediol \ \Delta H < 0} \quad \text{9-18}$$

$$\boldsymbol{Cellobiose + H_2O \leftrightarrow 2\ Dextrose\ \Delta H > 0} \quad \text{9-19}$$

$$\boldsymbol{Dextrose + H_2 \leftrightarrow Sorbitol \quad \Delta H < 0} \quad \text{9-20}$$

being the reactions exothermic, eq.s 7-19 and 7-20 are favoured at low temperature and high pressure due and a negative variation of moles number (Δν) [323, 324]. On the contrary, reaction 9-19 is favoured at high temperature, but the pressure is not of influence because the Δν =0. One of the most important steps in the HDO of bio-oils is the conversion of levoglucosan and glucose to sorbitol, which represent the limiting step of the WBO HDO process. From sorbitol, a number of shorten chain hydrogenation/hydrodeoxygenation products can be then obtained by varying the process conditions [325]. Therefore, a better understanding of the effect that the operating conditions have on the sorbitol yield is crucial to design a tuneable bio-oil HDO process. Figure 9-6 shows the yield variation of (a) sorbitol, (b) cellobiose and glucose (c) in function of temperature, pressure and H_2/WBO molar ratio. The maximum sorbitol yield was obtained at the minimum temperature, maximum reaction pressure and feed molar

ratio studied (50 ºC, 150 bar and H_2/WBO=4). Analysing Figure 9-6(a-c), it can be seen that the yield variation is minimal when the H_2/WBO molar ratio is changed from 2 to 4 up to about 80 bar. Furthermore, the cellobiose yield is very low in all the cases analysed, where it is mostly converted in glucose. Analysing the glucose distribution (Figure 9-6 c), a pressure higher than 40 bar and temperature up to 90 ºC favoured the conversion of glucose in sorbitol, this is possible to evaluate from the sorbitol distribution. The difference in yield at the different feed molar ratios enlarges when the temperature is higher than 120°C. To maximize the sorbitol yield, the cellobiose and glucose yields must be reduced, since their yield is inversely proportional to that of sorbitol. Previous work shows that 91.4% of glucose can be converted to sorbitol in presence of Ru-carbon nanotubes at 130°C, 20 bar in aqueous phase with 98.2% selectivity [326]. Based on the thermodynamic calculations, in presence of a dimer as cellobiose, which must be hydrolysed before its hydrotreating, the formation of sorbitol is favoured at lower temperatures (< 60°C) and higher pressure (> 40 bar). Another work showed that hydrolysis of cellobiose does not occur in a neutral environment such as water and that the simultaneous hydrolysis (in $ZnCl_{24}H_2O$) and hydrogenation (in presence of H_2 and Ru/C) is favoured at 125 °C and 40 bar, since at lower temperatures there is not hydrolysis[327]. However, since bio-oil has a pH < 5, bio-oil-water solutions can be directly hydrolysed/hydrogenated at lower temperatures, as shown by Sanna et al.[62]. In summary, the thermodynamic simulation suggests that temperatures of about 60-90 °C and pressures in the range 40-70 bar would maximise the production of sorbitol from sugars.

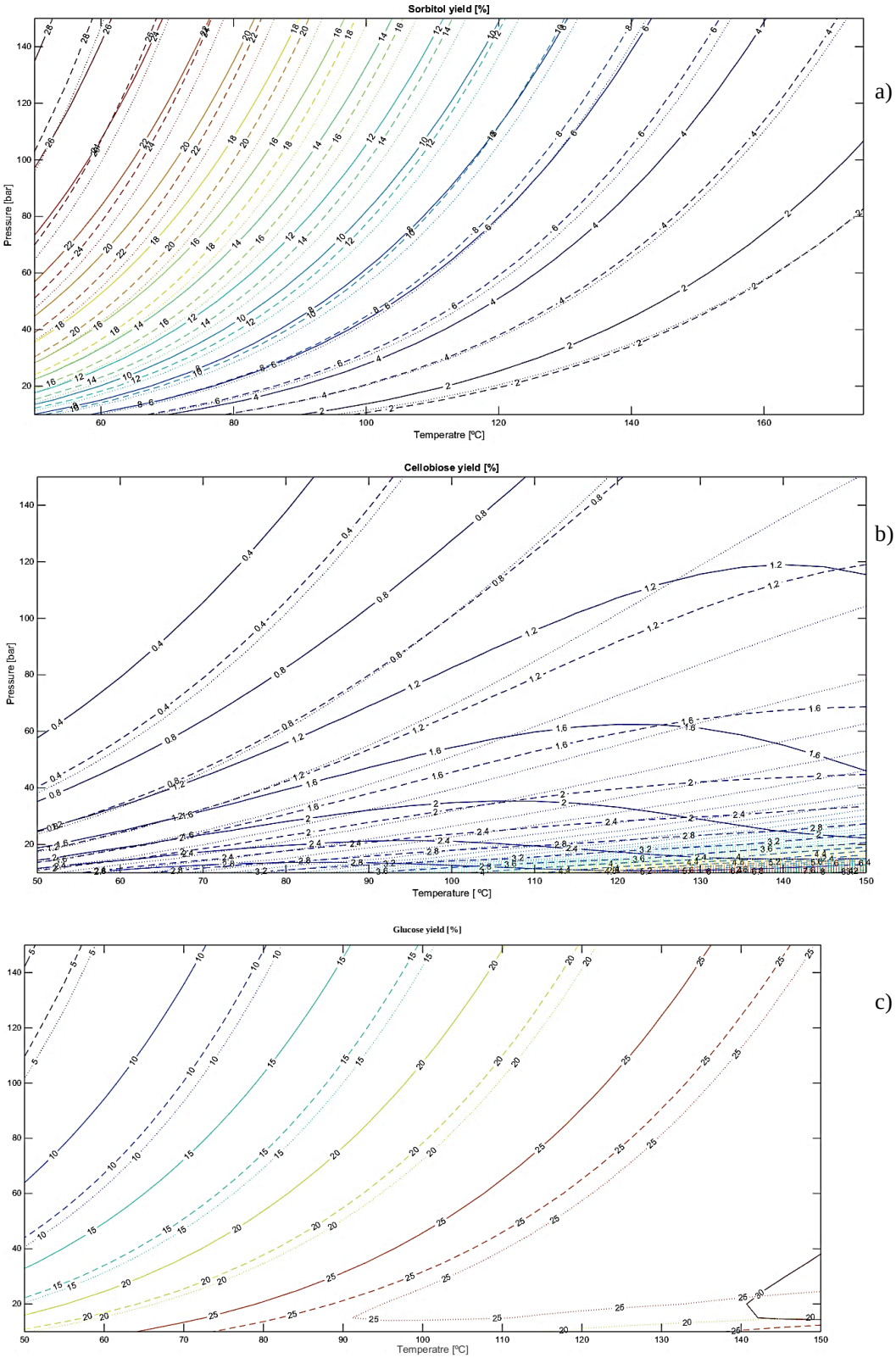

Figure 9-6. Influence of temperature, pressure and H_2/WBO molar ratio on a) Sorbitol yield, b) Cellobiose yield and c) Glucose yield

Insoluble bio-oil fraction- For the HDO of IBO there was not a clear reaction pathway, so that the thermodynamic equilibrium was calculated using a Gibbs reactor, able to calculate the composition of the reactor output minimising the ΔG. In order to study the temperature effect in terms of product yield, the reaction temperature was varied between 50 and 500 ºC at 10 bar selecting a H_2/IBO molar ratio = 1. Figure 9-7 shows the yields of the IBO HDO products. The residual fuel yield decreases according to the increase of temperature, favouring diesel, kerosene and heavy gasoline yield up to about 300°C, where the diesel yield increases to the expenses of the other products. At 300°C also corresponds the lowest yield of fuel gas. Interestingly, at about 150°C, the residual fuel can be completely converted, in the same time the maximum yield in term of kerosene and light gasoline are achieved.

The effect of pressure (10-150 bar) to the HDO of the IBO was instead studied at 100 ºC and using a H_2/IBO molar ratio = 1. In that specific set of operating condition, pressure has little influence in terms of products yield as can be seen in Figure 9-8. As main products, at 10 bar, the process yields about 13% diesel and about 6% fuel gas. Instead, the influence of the feed/H_2 molar ratio at 20 bar and 240 ºC (Figure 9-9) was more evident, in particular for the diesel and kerosene yield. An increment of H_2/IBO molar ratio promoted the HDO reactions towards more kerosene at expenses of diesel. This is related to the higher presence of H_2, which improves the breaking of C-C bond of compounds with higher molecular weight, aromatic rings and double C-C bonds [320]. In fact, at feed molar ratio of 4, the diesel yield is at its minimum (8%), while the kerosene (8%) and light gasoline (3.5%) yields are at their maximum.

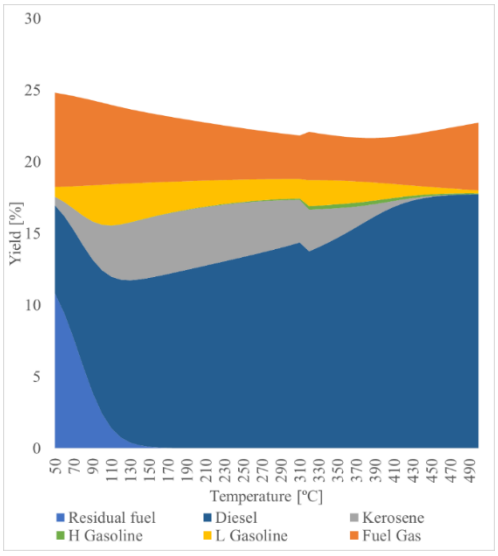

Figure 9-7. Influence of temperature (at 10 bar and feed molar ration H2/IBO = 1) on the HDO products yield.

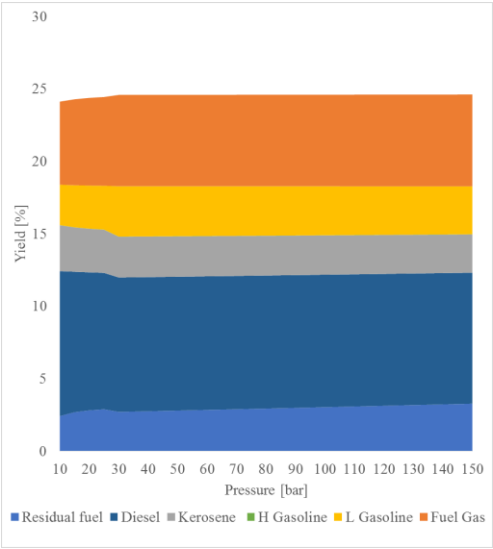

Figure 9-8. Influence of reaction pressure 100 ºC and feed molar ratio H_2/IBO =1 on the HDO products yield.

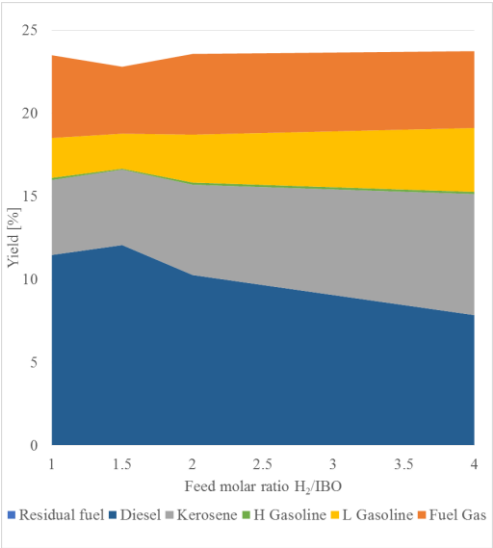

Figure 9-9. Influence of feed molar ratio H_2/IBO at 20 bar and 240 ºC on the HDO products yield.

9.4.4 Economic Potential of 2nd level

The success of a chemical process depends from its EP_2, since the objective is to have products with high added economic value than the raw material. Usually, the raw materials purchase represents from 33 to 85 % of total processing costs [303]. The EP_2 was dived in two parts, each of which addresses the economic feasibility for the WBO – HDO and IBO-HDO processes, respectively.

Figure 9-10 and Figure 9-11 evaluate the EP_2 (MM$/y) varying the pressure, temperature, H_2/WBO molar ratio (MR), liquid and vapour (R_1, R_2) recycle. As shown in the first line of the Figure 9-10, the R_1 and R_2 were maintained constant and equal to 0, while the other

parameters varied. The EP_2 did not change drastically with the reaction pressure, whereas there was a decrement of EP_2 when the temperature increased; trend explained by the exothermicity of the reactions involved.

Varying the WBO/H_2 MR from 1 to 10 the EP_2 value varied from ~32,000 MM$/y to ~38,000 MM$/y, indicating that very large H_2 presence promotes full conversion (or equilibrium), incrementing the EP_2 value. The highest value (EP_2 ~48,000 MM$/y) was obtained for a MR= 2. The decrement of EP_2 from 48,000 to 38,000 MM$/y for a MR 2 and 10, respectively was due mainly to the increment of the H_2 cost.

Maintaining the same operating condition and varying R_2 from 0 to 1, as reported in Figure 9-10 and Figure 9-11, the EP_2 improved. The increment of EP_2 for the highest liquid recycle stream caused the shift of the equilibrium reaction toward the products.

For the IBO-HDO, the operating condition, for having a positive EP resulted to be the following: temperature from about 150 to 275 ºC, reaction pressure between 40-150 bar and H_2/IBO MR = 1-1.5 with EP_2 between 5.5-6 M$/y (Figure 9-12). Furthermore, Figure 9-12 clearly suggests that a temperature lower than 150 ºC is undesired in terms of EP_2.

EP_2 for WBO-HDO resulted in 5.5 ± 0.5 MM$/y at pressure between 55-150 bar, temperature from 50 to 150 ºC and H_2/WBO molar ratio between 1 and 2. The above mentioned EP can be only obtained if the reactions products (diols, mono-alcohols etc.) are separated from the water solution and not considered as drop-in fuels, but sold as chemical commodities. Also, the EP does not take into consideration separation costs, which can be considerable. Remembering that the data were calculated by thermodynamic analysis, the catalyst and the utilities cost were not considered at this point and the products' distribution was the maximum possible, this preliminary EP_2 represented the maximum profit per year of the process.

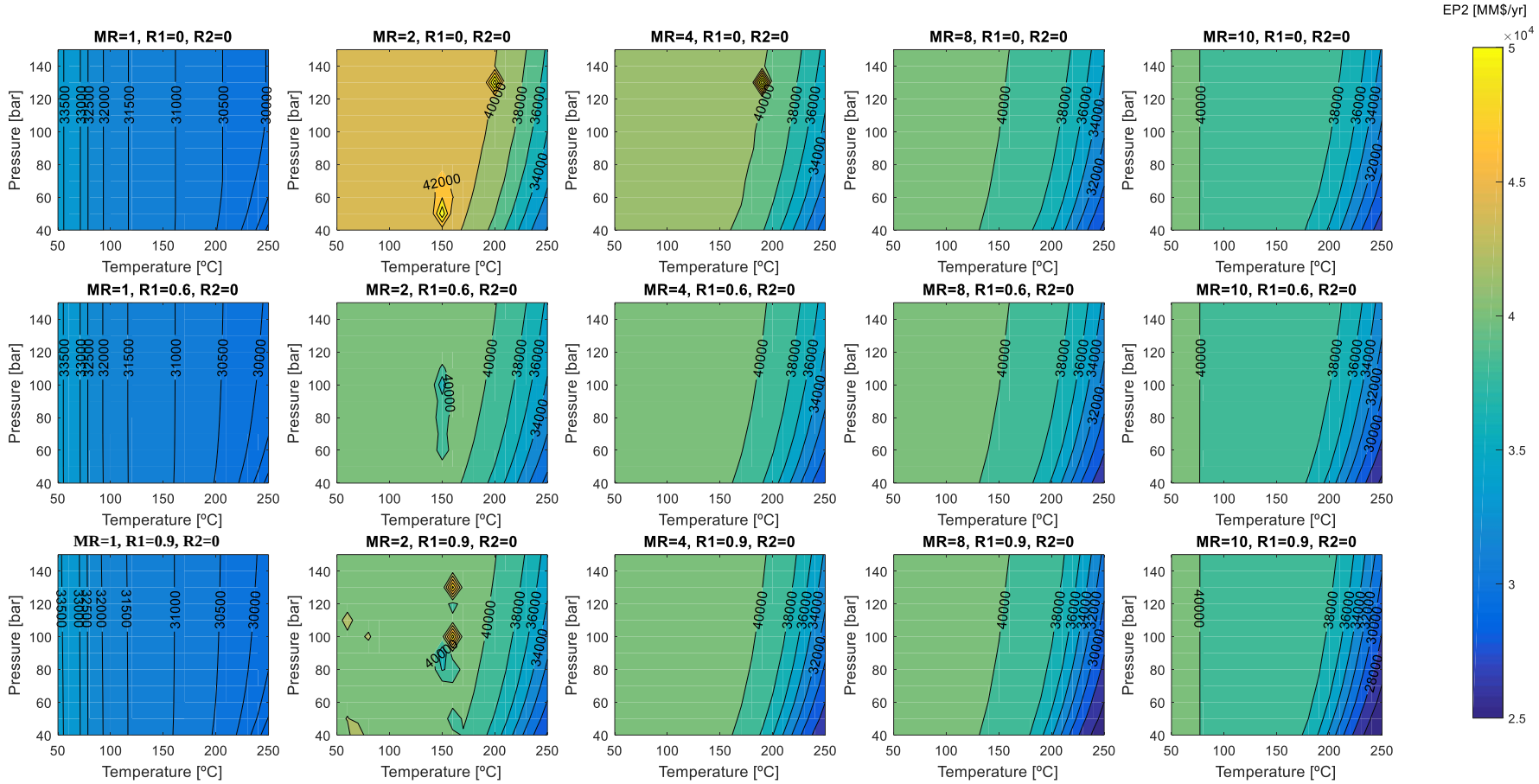

Figure 9-10. Economic Potential of the second level [MM$/y] HDO- WBO, varying the operating conditions. 1

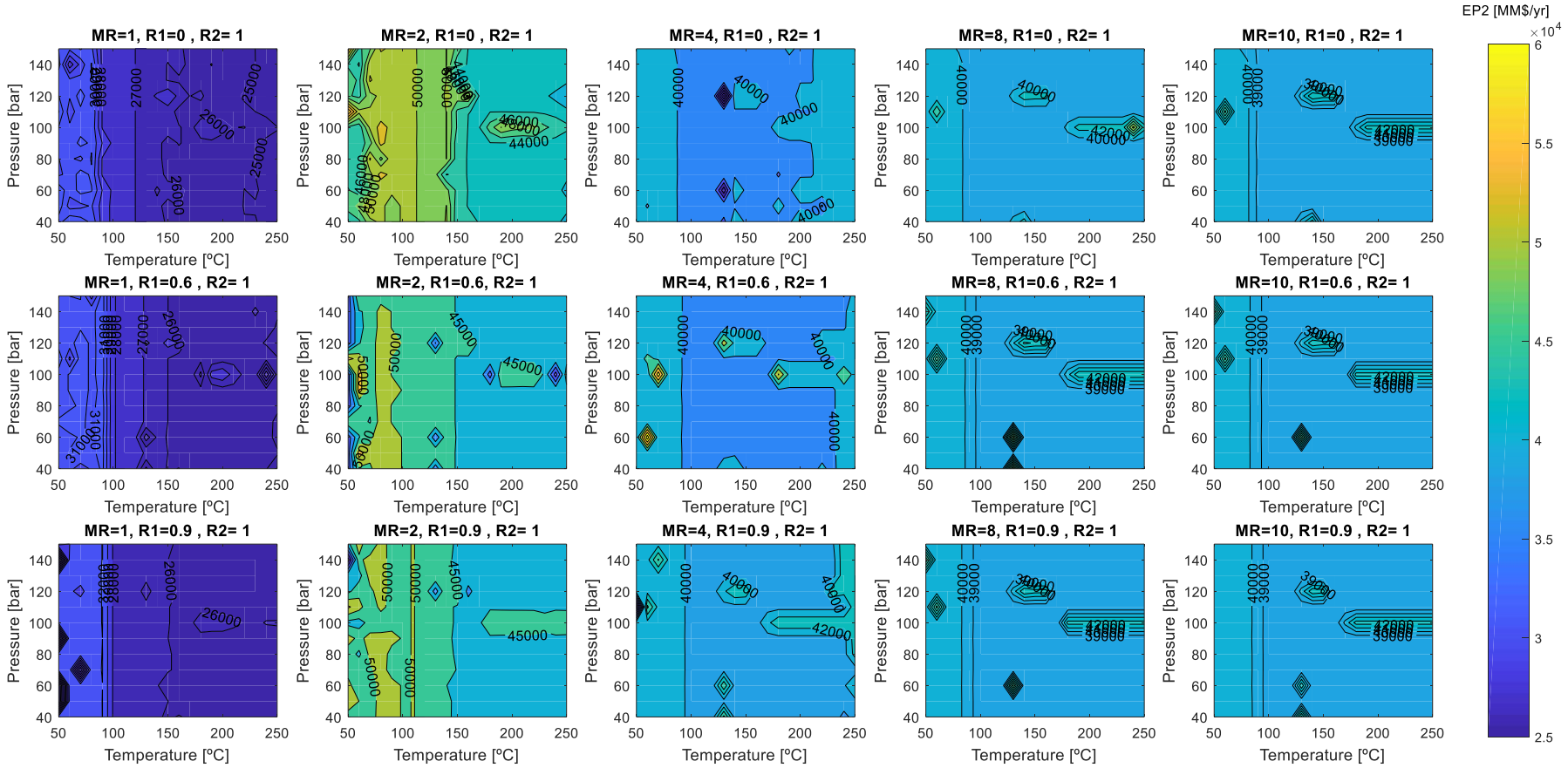

Figure 9-11. 2nd level Economic Potential of the second level [MM$/y] for the HDO- of WBO, varying the operating conditions. 2

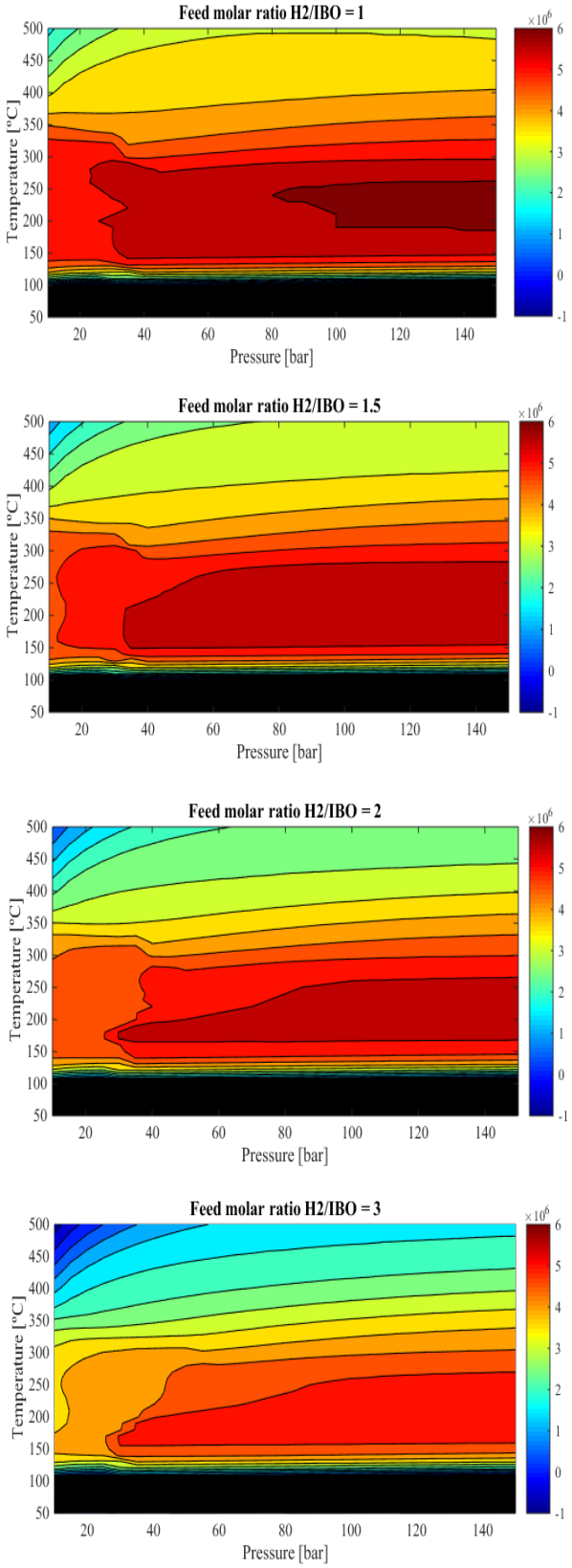

Figure 9-12. 2nd level Economic Potential of the second level [$/y] for the HDO - of IBO, varying the operating condition

9.4.5 Level 3: recycle structure

Having solved the input-output structure, the simulation passed to a further level of detail in which the necessary recycle streams, the cost of a hypothetical compressor, the reactors number, the possibility to operate them adiabatically and the reactors cost was evaluated in terms of economic potential of third level.

Compressor effect

The compressor cost was calculated using the Guthrie's correlation function of power supplied, while the electricity cost was assumed constant. The H_2 was considered supplied at 40 bar from a steam reforming of methane plant[328], Figure 9-13 shows the relation among the cost to compress the H_2 feed varying the reaction pressure (50-150 bar), and the H_2/WBO MR (1-10). It is worth to note that there was no reaction pressure limitation for a H_2/WBO MR up to 8.

The vapour recycle (R_1) was evaluated in order to improve the products yield without penalising the EP_3. For maintain the same feed pressure into the, recycle stream, a compressor system is expected, due to (i) pressure drop inside the system; (ii) or/and a deliberate pressure decrement in order to separate the liquid from the gas phase.

In our case the compressor into the recycle stream is due at the presence of the flash unit to separate the mixture into two phases. Figure 9-14 shows the cost related to recycle the vapour and liquid phase varying the pressure difference (ΔP) between the R_1 and the liquid recycle stream (R_2). Maintaining R_2 constant, for $R_1 > 0.8$ and $\Delta P > 10$ bar, the compressor cost are equal to the EP_2, not admissible for the realisation of the process.

While, varying only R_2, there is a decrement of compressor cost, due a decrement at a low amount of vapour recycle stream.

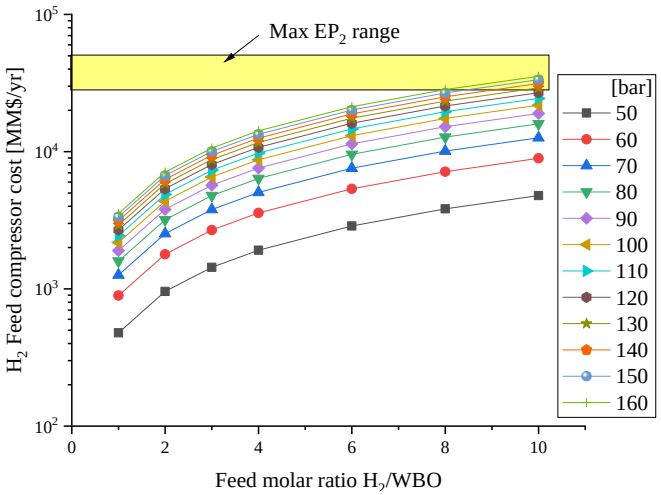

Figure 9-13. Compressor feed cost, varying the reaction pressure and H_2-WBO feed molar ratio

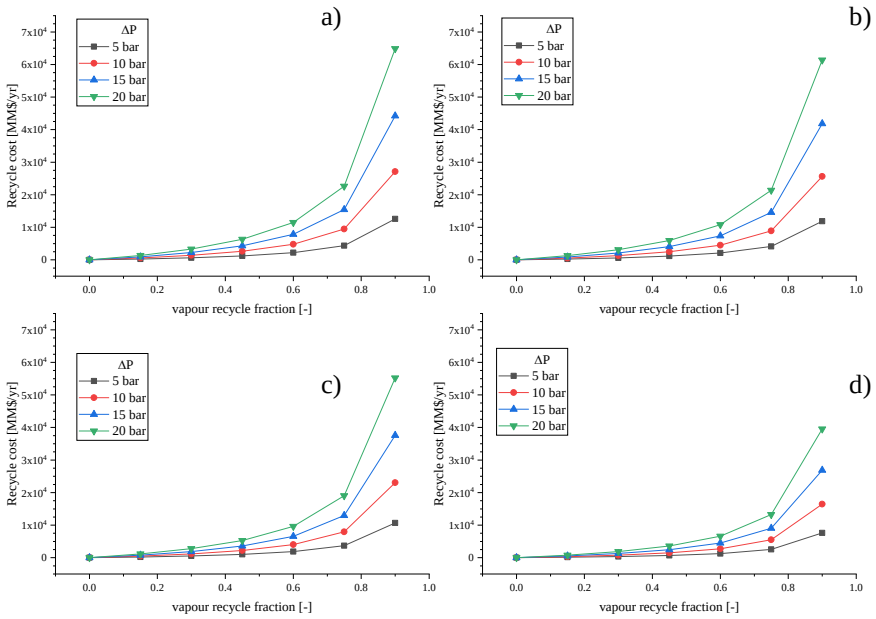

Figure 9-14. Recycle cost for HDO- of WBO for MR=2 in function of vapour recycle fraction, varying Δp and the liquid recycle fraction (R_2) at a) R_2=0, b) R_2=0.3 c) R_2=0.6, d) R_2= 0.9

Reactor heat effect

This analysis was carried out to decide whether the reactor had to be operated adiabatically, with direct heating or cooling, or whether a diluent or heat carrier was needed. The process is average exothermic for HDO-WBO and the presence of a recycle could be improve drastically the reaction temperature as reported in Figure 9-15, for and a reactor inlet temperature of 100 ºC, a H_2/WBO MR = 2 and 50 bar. The cited figure shows how the temperature into the reactor output stream changed varying the sorbitol yield, liquid and vapour recycle. For all the case, an increment of R_1, improved the reaction temperature and decremented the sorbitol presence due, then R_1 improving the diols production. While an increment of R_2 decreased the temperature into the reactor and also increased the sorbitol yield. Then, R_2 had the principally function of a thermal carrier. To remedy at the high temperature into the reactor adding water as thermal carrier has been taken in consideration.

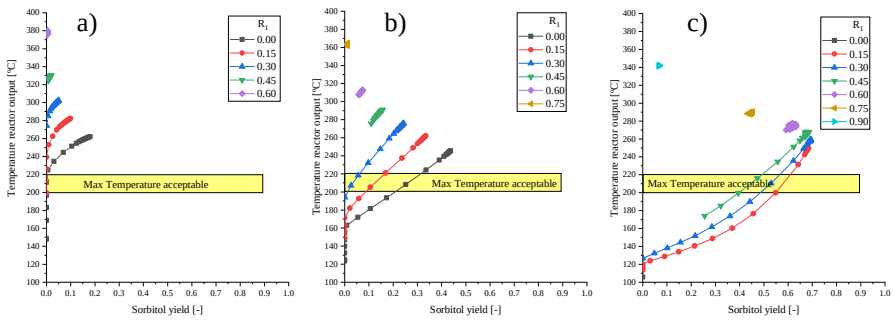

Figure 9-15. Reactor exit temperature vs sorbitol yield, varying the vapour recycle fraction (R_1), at a) R_2=0, b) R_2=0.6 and c) R_2=0.9

9.4.6 Economic Potential of 3rd level

To obtain the EP_3, EP_2 data were updated using eq.7-10 and 7-11, by including the cost related to the reactor, compressor and heat exchange units, with the relative utilities to achieve the operating condition.

For the WBO-HDO the reactor system consisted into two adiabatic packed bed reactors in presence of 5 wt% Ru/C as catalyst (void bed fraction equal to 0.40) with intermediate cooling. The inlet stream was preheated up to 175 ºC using water as thermal carrier, imposing a max temperature in the outlet of 200 ºC. Figure 9-16 shows the EP_3 for the WBO-HDO varying H_2/WBO MR, reaction pressure and also gas (R_1) and liquid (R_2) recycle fractions.

Analysing the effect of R_2 into EP_3, there was an evident decrement of the profit, mainly due to an increment of the reactor size and also the utility relate to preheating R_2.

An increment of the EP_3 was noted by increasing the H_2/WBO MR up to 2, where the EP_3 achieved the maximum value. For MR> 2, the cost related to the compressor unit downstream of the reactor increase resulting in a decrease of the EP_3. Furthermore, an increment of the reaction pressure enhanced the EP_3 in all the cases studied except for R_2= 0.9; while a drastic decrement of EP_3 was noted for R_1> 0.4.

The 3rd level of WBO-HDO fraction resulted in an EP_3 of 40,600 M$/y, for a temperature of 250 ºC at 100 bar, R_1=0.4 and in absence of R_2.

The stages number in the IBO-HDO process was imposed equal to 3, with the target to minimise the catalyst (Co-Mo/γAl_2O_3) amount loaded. The process condition were 250ºC and 50 bar. The output stream was cooled down to 35 ºC. The separation systems were considered ideal and evaluated at fourth level. For the IBO-HDO section the cost were calculated using the guideline from Gary et al. [329], achieving a 5.99 M$/y.

The EP_3 for the IBO-HDO section resulted negative (-0.19 M$/y), suggesting that this section of the process is not competitive with the actual fuel price based on market price. With the target to achieve the break-even point for IBO-HDO, the minimum fuel selling price (MFSP) was instead assessed:

$$\boldsymbol{MFSP_i = \frac{Annual\ plant\ cost}{EP_2}\Big|_{IBO} \cdot Fuel\ price_i} \qquad 9\text{-}21$$

Then, to be economically competitive, the fuel market price should be higher than the MFSP.

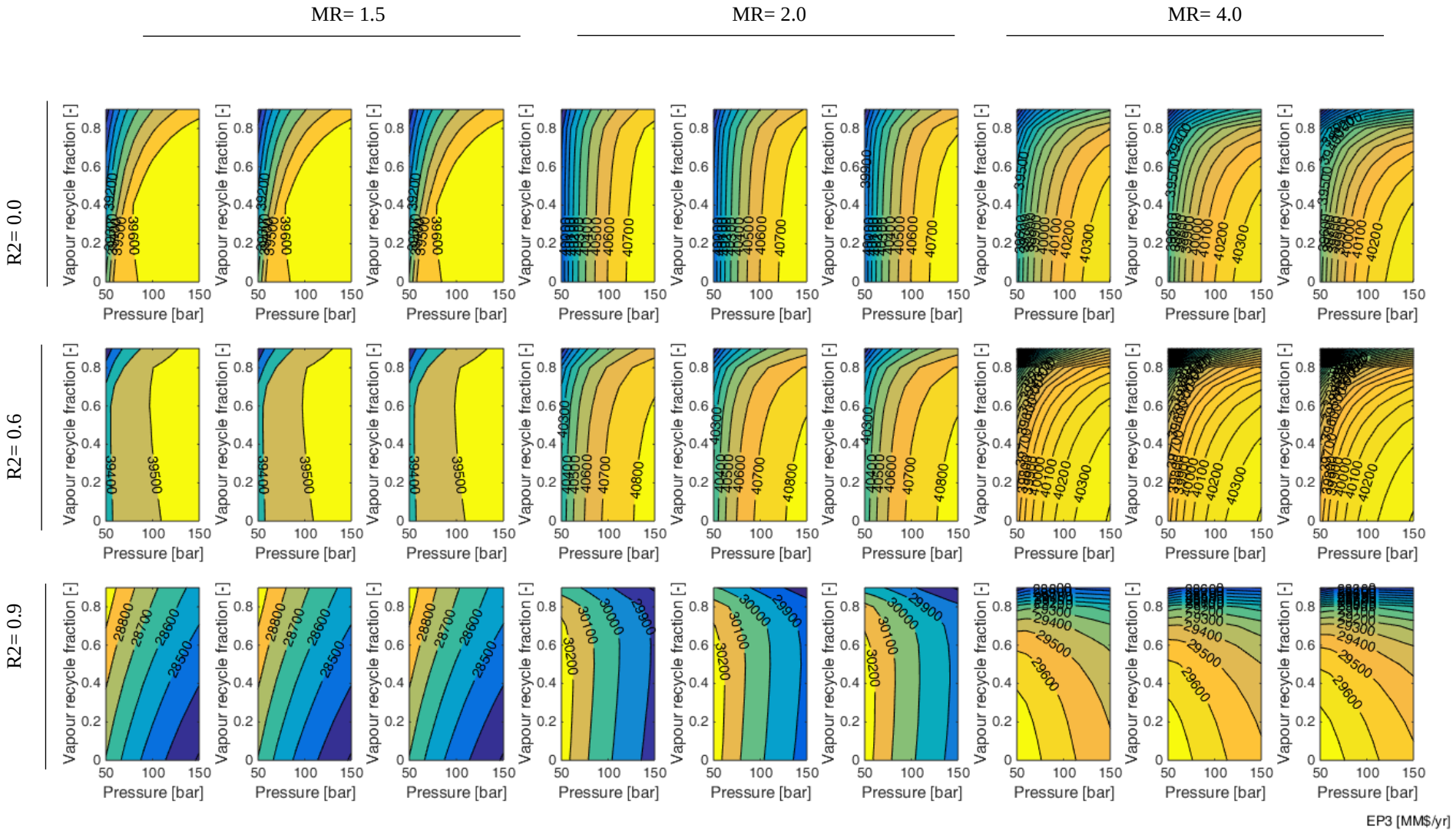

Figure 9-16. Economic Potential of the third level WBO varying the operating condition

9.4.7 Level 4: Separation system

In level 4 the separation system required to recover products with high purity was designed. For the WBO, the outlet stream of the reactor system (see Figure 9-17) was initially separated by a flash unit (S-401) able to split the two phases (vapour and liquid phases) and allow their purification by different methods.

The vapour stream (F-402) was cooled down to 35 °C using cooling water as utility stream. Since a simple cooling is not able to guarantee an efficient recovery of the products in the vapour phase, solvent absorption was considered. The solvent was based on cost, affinity and volatility difference with the solute. Simplifying hypotheses were made: (i) the thermal effects were neglected operating at a temperature equal to that of the gas to be treated and at approximately atmospheric pressure; (ii) hydrogen and methane were assumed to remain in the gas phase; (iii) the absorbing recovery of methanol was set at 99.5%, (iv) the absorber system was designed according to Kremser [330]. Therefore, to recover the condensable products from F-405, a water based absorber unit (S-403) was used.

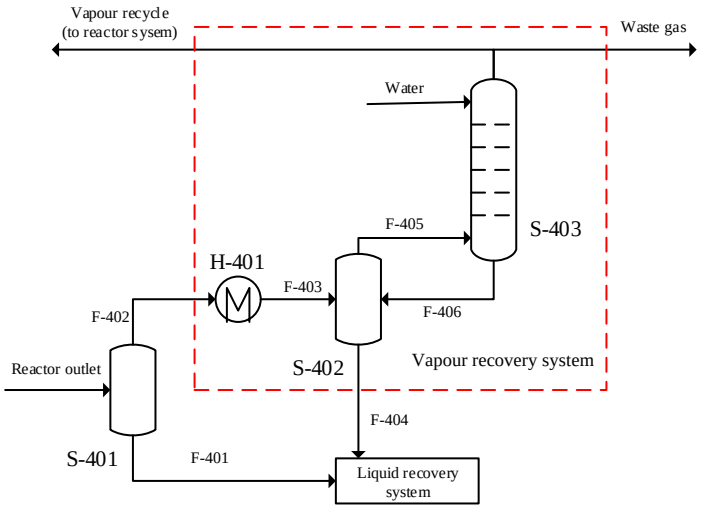

Figure 9-17. Recovery vapour system

The use of an absorber minimises the products lost into the vapour phase. The choice of a vapour recovery unit derives from a compromise between the recovery efficiency and the economy of the process. As reported in Table 9-5, the presence of the vapour recovery system results in a cost decrement of than 50% for all the scenarios.

Table 9-5. Absorber system cCost at various inlet and outlet pressures.

		Absorber system cost + product lost [k$/y]		Products lost w/o absorber system [k$/y]	
		Pressure outlet [bar]		Pressure outlet [bar]	
		10	20	10	20
Pressure inlet [bar]	100	1050	564	2820	1770
	110	950	547	2740	1650
	120	880	474	3180	1340
	130	1040	531	2850	1630
	140	100	522	2590	1600
	150	1010	606	2560	1830

The liquid phase from the flash S-401 and the liquid stream from the vapour recovery system (F-402) were sent to a liquid separation system. Heuristic rules were followed for the design: (i) the first separation targeted the components in greater quantity and with higher volatility; (ii) the most difficult separations were carried out at the end.

A total of 77.46 ton/day was fed the liquid recovery system, which consisted in a water and complex mixture of organic compounds (see Table 9-6). For the first separation, the distillation system was rejected due to the glucose TBP being higher than its realistic polymerisation temperature.

Table 9-6. Composition (wt. %) input stream to liquid recovery system

	Mass Fractions	TPB [ºC]
Ethanol	0.027	78
Water	0.336	100
Hydroxyacetaldeyde	0.003	145
Ethyl cyclohexanol	0.029	191
Ethylene glycol	0.046	197
Cyclohexane		210
ethanol	0.001	
Propandiol	0.127	214
Benzendiol	0.042	222
Butanediol	0.015	227
Hydroxypropionic		285
acid	0.015	
Vanillin alcohol	0.029	290
Glucose	0.018	344
Sorbitol	0.310	431

Therefore, a simulated moved bed (SMB), a typical applications in the sugar processing industry, was considered to separate glucose from the stream F-407 [331]. Eight packet columns filled with silica simulating the movement by a system valves, as represented in

Figure 9-18. In the system, it is possible to define a first zone (from SMB-1 to SMB-3), where the sorbitol was recovered from the solid phase into the extract stream. In the second zone (SMB-4 and SMB-5), the solid phase absorbed the sorbitol coming from the feed, while in the third zone (from SMB-6 to SMB-7), the stream was enriched in glucose. All the four fluid streams were periodically switched forward one column position, causing stepwise movement of the zones. The SMB system was able to separate the totality of the glucose and recover 98% sorbitol (45% purity) into the extract stream. The cost of the SMB system was estimate equal to 34 $/kgfeed [332].

The stream rich in sorbitol (without glucose) was then purified by a distillation system (see Figure 9-19, Table 9-7), which resulted in an overall cost of 704.8 M$/y.

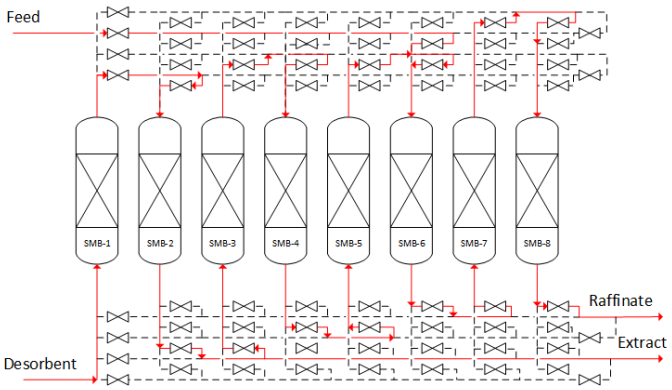

Figure 9-18. Liquid recovery system- Simulated moving bed for liquid recovery system.

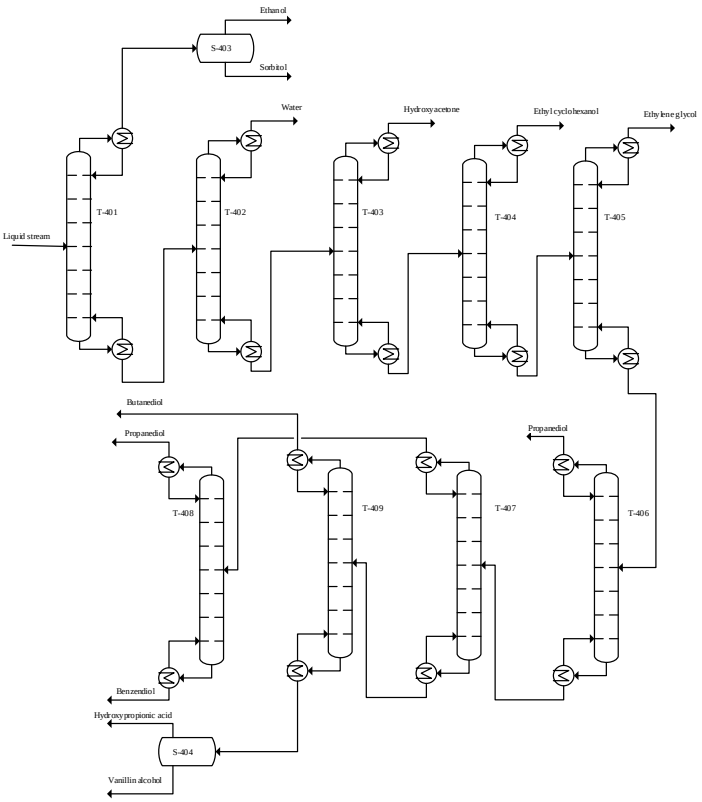

Figure 9-19. WBO-HDO dDistillation system for the separation of WBO products from HDO.

Table 9-7. Distillation columns specification

	T-401	T-402	T-403	T-404	T-405	T-406	T-407	T-408	T-409
Reflux ratio [-]	0.525	0.405	0.434	92.1	6.95	5.59	11.5	11.6	0.60
Nº stages [-]	100	20	92	230	146	224	816	442	52
Feed stage [-]	58	22	66	146	94	142	624	132	34
Reboiler heating required [Gcal/h]	334.9	92.8	2.1	387.8	146.0	239.4	208.9	82.5	9.0
Condenser cooling required [Gcal/h]	246.2	18.87	0.02	124.8	126.7	202.5	191.3	91.35	7.70
Distillate temperature[ºC]	117.0	100.0	138.3	166.0	196.6	213.6	218.6	213.6	227.4
Bottom temperature [ºC]	125.3	208.2	211.7	213.3	220.2	230.4	257.5	222.3	312.8
Capital cost [M$/y]	3.92	0.70	0.68	14.70	7.02	14.32	52.17	28.26	0.42
Utility cost [M$/y]	131.51	32.44	0.70	139.30	58.90	96.16	85.09	34.88	3.62

Water Insoluble fraction

The distillation was the separation technique used to achieve the commercial standard of purification of HDO-IBO products. The separation sequence was designed removing first of all the compounds with lower BP. The distillation tower was imposed a plate efficiency equal at 50% and for mechanical stability the height/ diameter ratio considerate was between 20-30, and the greater height 50 m. The overall cost of this plant section was equal 2.94 M$/y, based on Gary et al.[329] correlation.

9.4.8 Economic evaluation

The cost of the separation system was the final stage for allowing the calculation of the final EP (or EP_4). The EP_4 for the HDO-WBO was obtained subtracting from the EP_3 (40,070 M$/y) the cost related to the vapour recovery system (1M$/y), the SMB unit (704.8 M$/y) and the distillation system (1,130 M$/y). The EP_4 of the WBO resulted positive and equal to 38,234 M$/y, indicating that the HDO-WBO process would be competitive for the production of chemicals. Furthermore, an advantage of converting the WBO to chemicals is related to the large number of products, with the possibility to orientate the production through the compounds demand. The actual plant produces 24.0 ton/day of sorbitol, but and increment of its yield could be further achieved converting the 1.39 ton/day of unconverted glucose. Also, this work was able to produce 9.84 ton/day of propanediol at the actual market price, 1.27$/kg [304], which resulted more economically feasible than other bioprocesses such as the microbiological conversion of glycerol, with an estimated price of 2.43/kg [333]. Instead, the EP_4 calculated for the HDO of the IBO resulted negative and equal to – 3.13 M$/y, which is not economically competitive based on market fuels price. By eq. 9-21 has been calculated the MFSP (and reported in Table 9-8) in order to have a HDO-IBO process profitable. The MFSP varying from 0.406 to 1.465 $/kg for the different fuels produced, 53.9% higher than the fossil fuel. The MFSP obtained did not differ from the data of Carrasco et al. [110] estimating a MFSP equal to 1.38 $/L from hydrotreatment process of pyrolytic oils, for a capacity of 2000 tonnes per day of residual forest biomass. With a total cost of investment (TCI) equal to 171.5 MM$ Furthermore, Wright et al.[301] hydro-processed 1440 tonnes per day bio-oil, able to produce 5182 barrels per day of naphtha and diesel range blend fuel the MFSP was 0.546 $/L, same range of MFSP obtained in this work. The EP result is able to represent the profit of the whole process, taking in consideration the cost of all the operation units, the utility streams, and feeds. Furthermore, the EP has been used to

calculate the costs associated to the plant (piping, instrumental control, maintenance and repairs, etc.), as reported in Table 9-3.

Table 9-8. Minimum fuel sell price for HDO-IBO

Compound	Price from fossil fuel [$/GJ]	Mass flow [ton/day]	MFSP	
			[$/GJ]	[$/kg]
Fuel gas	3.72	$1.73 \cdot 10^{-4}$	5.71	0.685
Light Gasoline	14.44	125.38	22.22	0.966
Heavy Gasoline	21.88	42.3	33.69	1.465
Kerosene	11.92	20.8	18.35	0.791
Diesel	12.26	130.7	18.87	0.816
Residual fuel	6.82	9.08	10.50	0.406

The HDO process of pinewood bio-oil was designed to process 10 Mton/y with a TCI of 55,271 MM$ and profit after the tax equal to 9,406 MM$ per year. Since the parameters cited above do not give a real potential of the plant, the ROI and the pay-out of the investment were evaluated. In particular, a ROI of 69.18% and a recovery of the initial investment after 2.48 years was obtained. To further evaluate the economic feasibility of the plant, the DCFROR for a plant life of 20, 25 and 30 years was calculated, resulting in a rating of 18.75%, 19.02 and 19.11%, respectively. This is 3.95 times the interest if TCI was deposit in the bank (4.75%)[334].

9.4.9 Conclusions

In this work the HDO of bio-oil process was designed by the method proposed by Douglas et al.[303]. The HDO thermodynamic simulation of lignocellulosic biomass was investigated towards the production of chemical compounds and fuel with a higher added value than the raw material. The thermodynamic data were used to evaluate how the products yield varied with the operating condition (temperature, pressure an H_2/ bio-oil molar ratio). Furthermore, the kinetic data have been used to design, then estimate the reactor units and relative utility cost. Finally, the separation system cost was added to calculate the TCI, equal to 55,271 MM$, and the EP equal to 38,234 M$/y, given the possibility to have a flexible process, in term of chemicals and fuels production. The HDO process was designed to convert 215 thousand barrel/day into fuels with an MFSP of 0.406 to 1.465 $/kg (53.9% higher than the fossil fuels) and chemicals of high added value, such as sorbitol, propanediol, butanediol, ethanol, etc. at the actual market price. The process guaranteed a ROI of 69.18%, with pay of time of 2.48 and DCFROR for a plant life of 30 years was rating 19.11%.

Conclusions and future work

The aim of the present research project was for making competitive process for the hydrogenation of bio-oil. A comprehensive literature review focused on the bio oil HDO and efficient technologies for hydrogenation reaction was carried out.

The technology proposed were focused onto the evaluation of catalysts on zirconia support and also on a new approach for the hydrogenation, by using catalytic membrane reactor.

The first part involved to synthesise Cu, Fe, Pd, PdCu, and PdFe on ZrO_2 support for the hydrogenation of the aldehyde group of different model compounds representative of pyrolysis bio-oils. For all experimental campaign a total selectivity toward one single compound has been reached for furfural (to furfuryl alcohol) and vanillin (to vanillin alcohol). Furthermore, the catalysts have been tested using a real mixture of WBO fraction at 100°C and 50 bar, retaining ~90% of the starting organic phase into the liquid phase. The catalyst in presence of Fe converted the phenolic compound into hydrocarbons, reducing the acidity of the WBO.

The membrane reactor has been used as the alternative technology for the HDO reaction, in order to carry out the reaction at mild condition and maintaining high conversions.

The presence of the membrane constituted a variable for the design of the reactor unit, since the catalysts needed to be integrated in the membrane matrix and a good contact with the reactants must be guarantee, object of the second part of the research project.

The selection of the polymeric membrane and the choice of catalyst was driven by the operating temperature, pressure, chemical compatibility and catalyst activity.

The Ru-PES membrane has been syncretised and characterised for the hydrogenation of furfural under mild conditions (7 bar, 70 °C) showing >99% selectivity towards FOL with a TOF of 48,000 h^{-1}, when a H_2/furfural molar ratio of 1:1 was used.

Due to the low stability of the cited membrane, the research was diverted for using PEEK-WC as support and doped with Ru, converting 75% furfural and 30% vanillin at 18 bar, 75 °C, 5 mL/min of hydrogen. Ru was almost entirely retained on the PEEK-WC membrane during the 88 hours test, showing high stability of the Ru-PEEK-WC membrane.

In the third part of the project, the HDO process has been investigated in term of process developing by different feedstocks. The techno-economic study for the production of bio-

fuels from microalgae via catalytic pyrolysis and bio-oil upgrading was studied. Fuel prices determined was from 1.43 $/L to 1.84 $/L, 50 % more than the fossil fuel price.
While, The HDO process of lignocellulosic biomass was investigated towards the production of chemical compounds and fuel with a higher added value than the raw material, considering a plant processing 10 Mton/y of bio -oil. The TEA reached an EP equal to 38,234 M$/y, converting 215 thousand barrel/day into fuels with an MFSP of 0.406 to 1.465 $/kg and chemicals of high added value, such as sorbitol, propanediol, butanediol, ethanol, etc. at the actual market price. The simulated process guaranteed a ROI of 69.18%, with pay of time of 2.48 year and DCFROR for a plant life of 30 years was rating 19.11%.
The future prospective of this research field will be:

(i) The good result obtained of $PdFe/ZrO_2$ catalyst, suggest to continue the research using middle-high operating condition, in order to improve the sugar conversion to sorbitol and also study the effect on the compounds with high molecular weight.

(ii) Moreover, the kinetic study of hydrogenation of model compounds could be helpful for understanding the reaction mechanism onto the surface catalyst and/or proposing a new model approach to link the conversion and operating condition, i.e. an artificial neural network;

(iii) Continuing the research about polymeric catalytic membrane, in order to find the best connexion polymer – bio-oil environment, in term of membrane stability, also including the inorganic membrane (ceramic or metal).
The Ru-PEEK-WC membrane shown a higher stability than Ru-PES membrane, encouraging the future research for different coating method for a higher Ru content;

(iv) The TEA data for HDO plant given us as an idea about the process limitation, in terms of profit, if the target is fuels production. For this reason, the future research should be focused on different separation method at low energy demand and also provide the use of membrane reactors, for improving the yield toward desirable products.

Appendix A. Supplement material: Bimetallic catalysts for biobased aldehyde hydrogenations

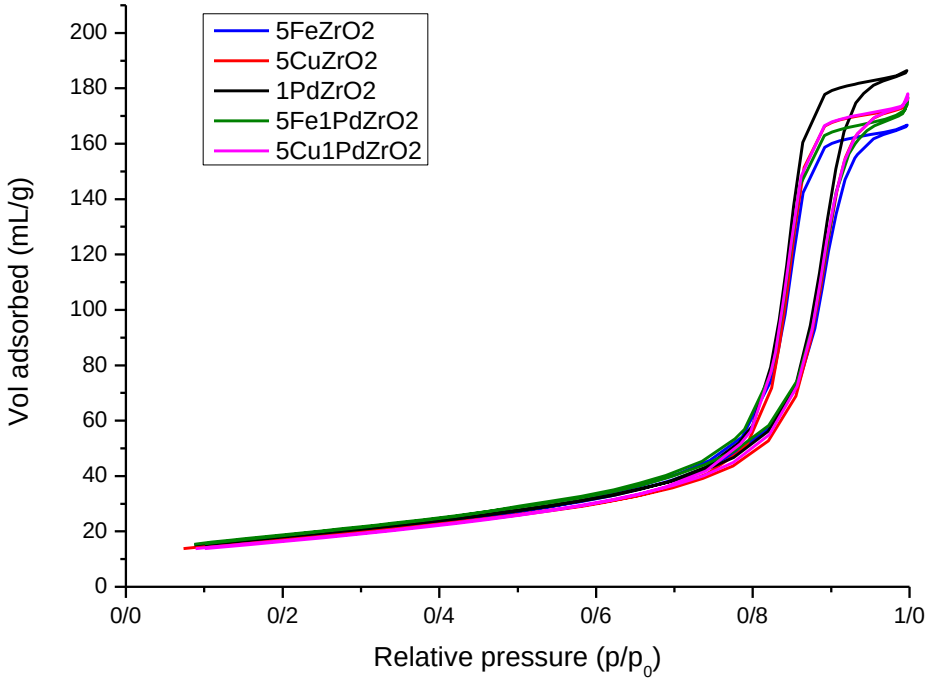

Figure A-1. Adsorption Isotherms of all catalysts.

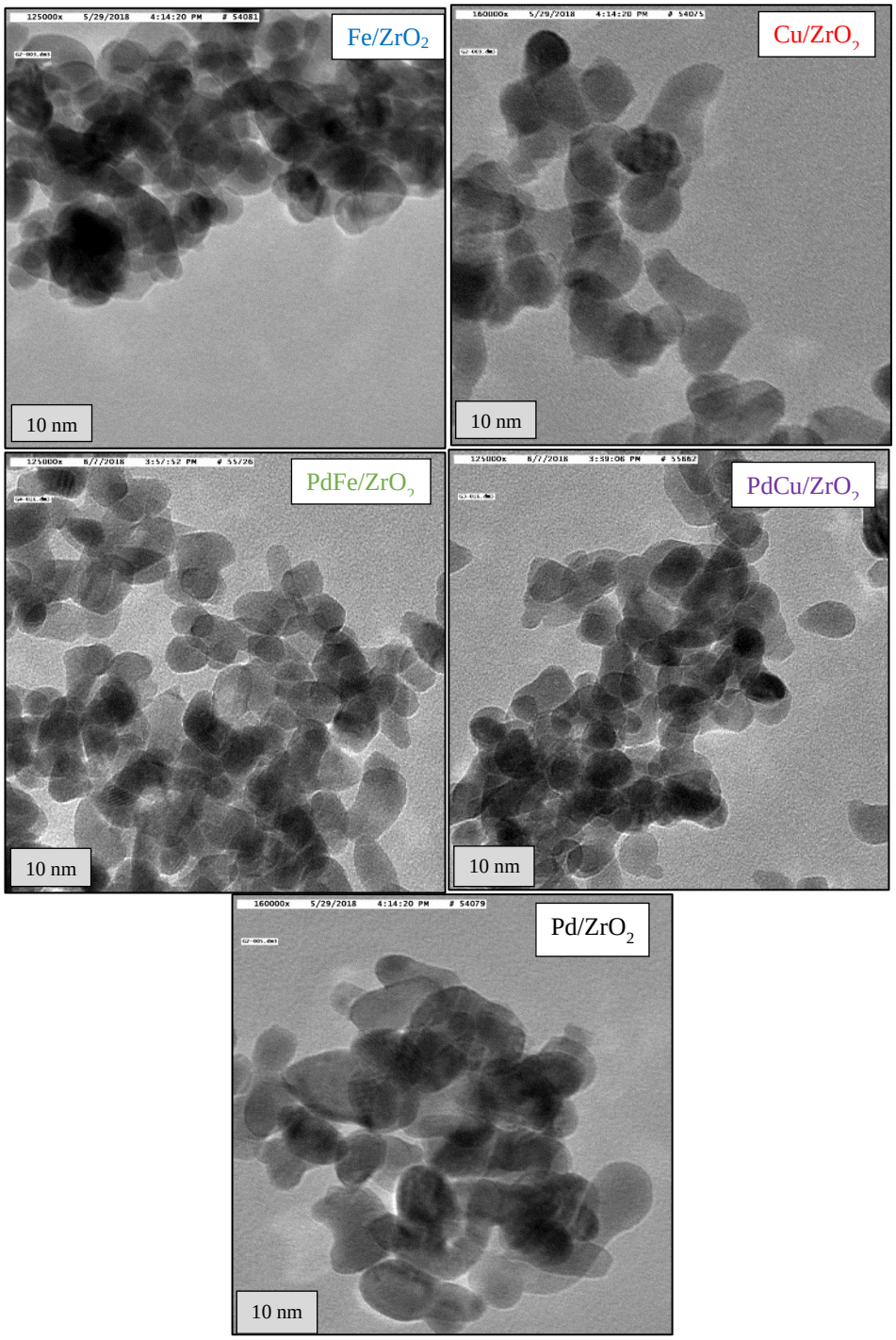

Figure A-2. Transmission electron microscope (TEM) images for the various catalysts

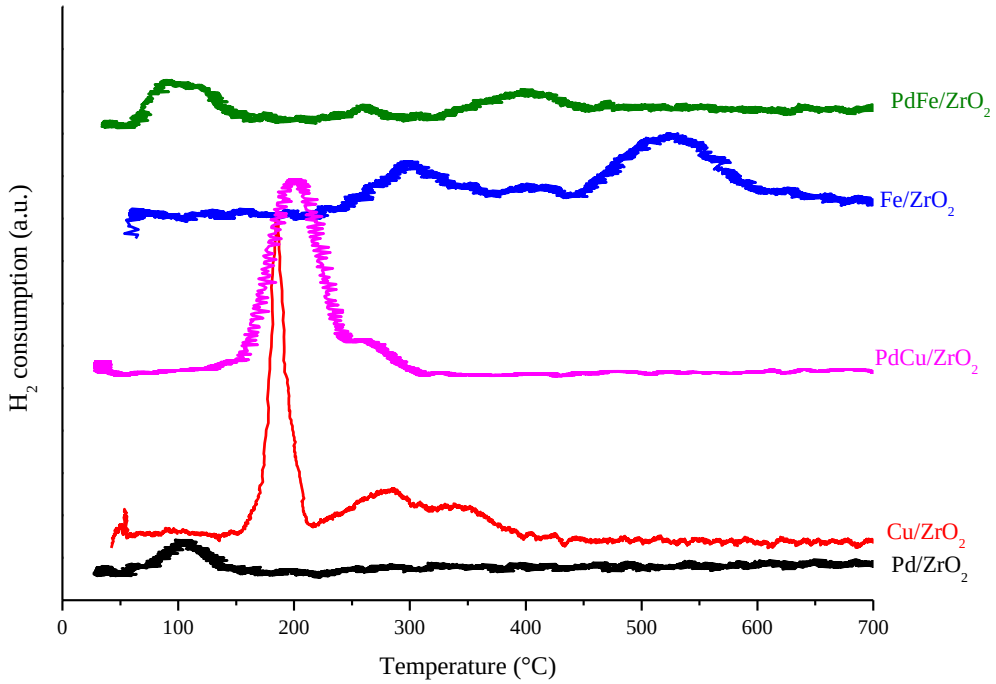

Figure A-3. H_2-Temperature-programmed reduction (TPR)

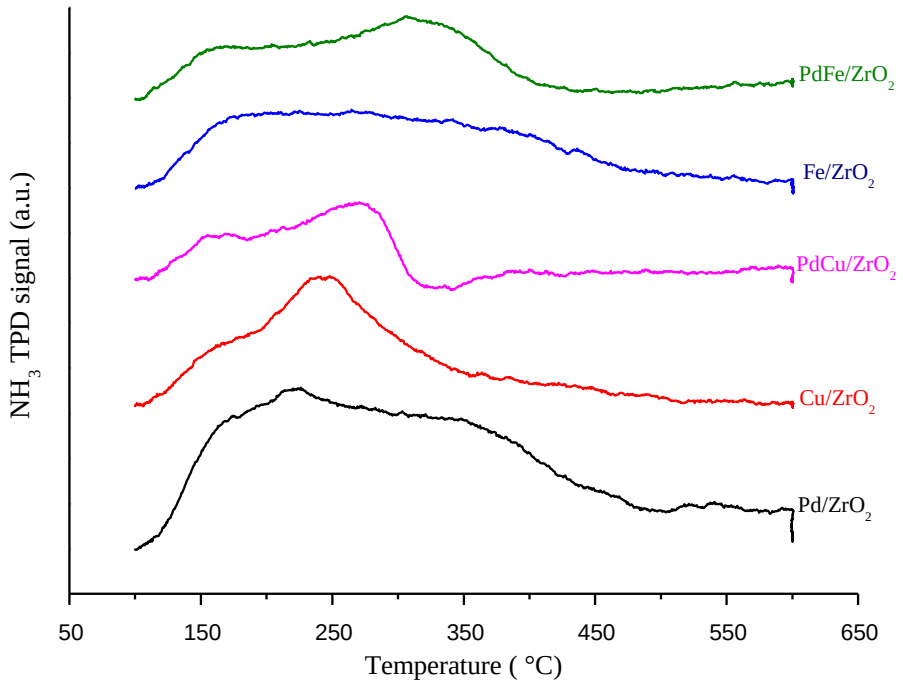

Figure A-4. NH_3 temperature programmed desorption (TPD) spectra for all catalysts

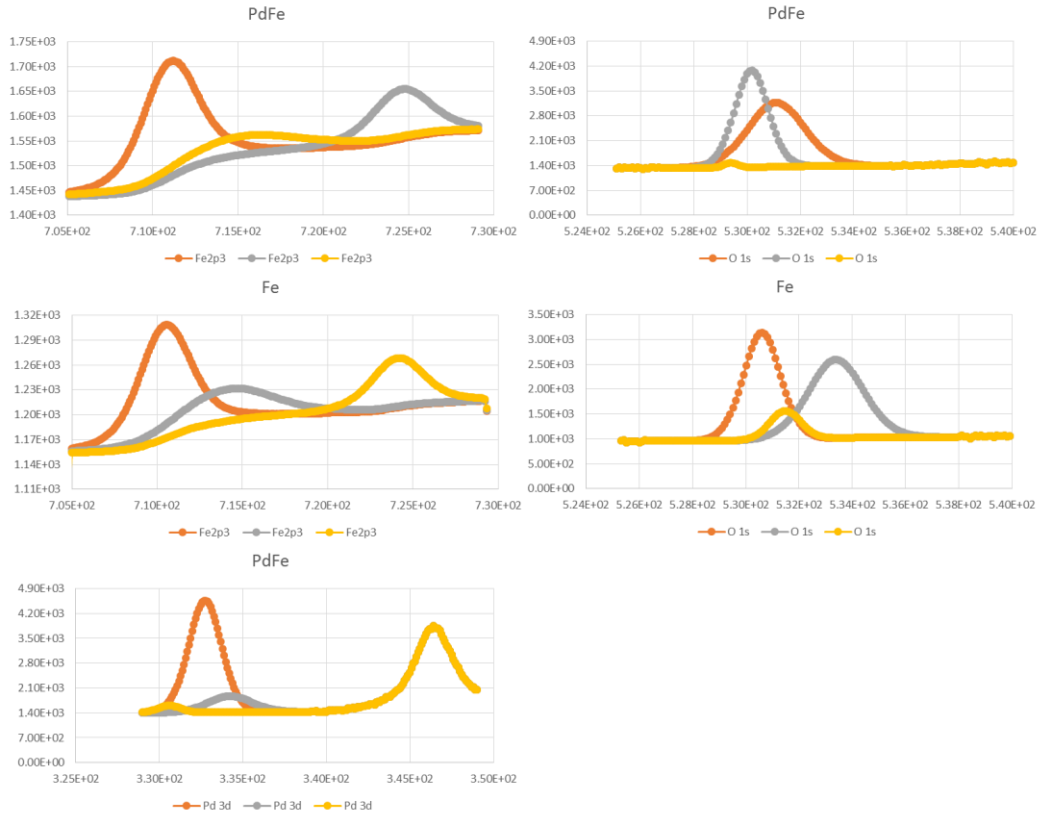

Figure A-5. XPS of the Fe and PdFe catalysts.

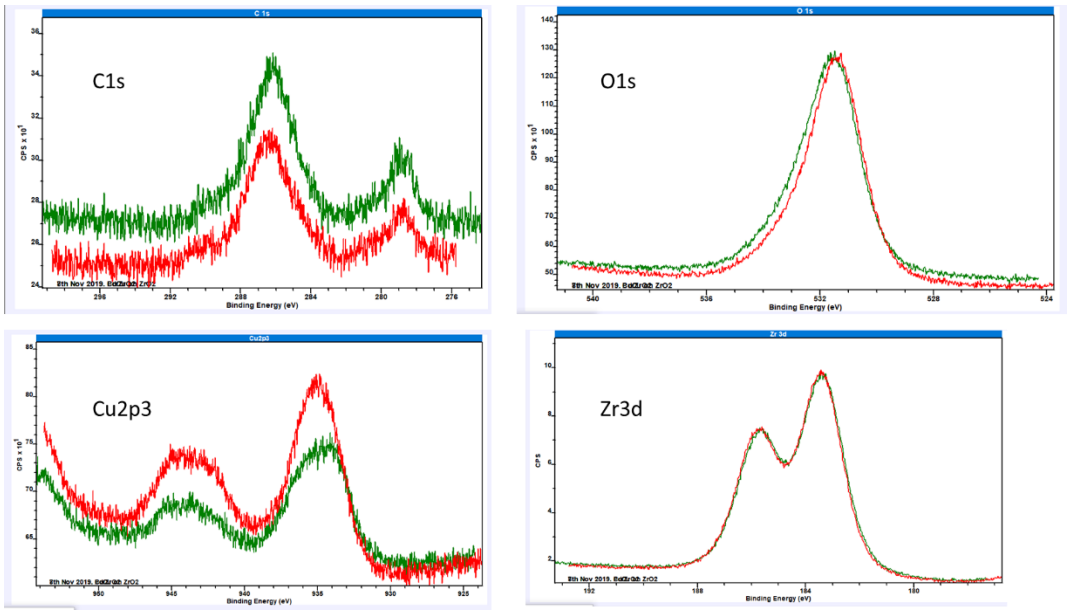

Figure A-6. XPS of the Cu (red line) and PdCu (green line) catalysts.

Table A-1. Selectivity for HDO of glucose at 100 ºC, 50 bar in presence of Cu/ZrO_2

Compounds	Reaction time (min)				
	40	60	80	100	120
Sorbitol	33.89	30.09	31.27	33.19	33.72
Glyceraldehyde	8.03	5.51	8.26	8.42	8.48
Glycerol	36.37	39.87	37.31	35.25	34.32
Dihydroxyacetone	0.00	0.00	0.00	2.67	2.83
Acetic Acid	0.00	7.43	6.11	6.08	7.19
Propandiol	7.72	9.15	7.81	6.72	6.07
Propionic Acid	7.35	4.53	4.01	3.62	2.81
Ethanol	4.41	2.43	3.48	2.68	2.95
Unknown	2.22	0.99	1.75	1.37	1.63

Table A-2. Selectivity for HDO of glucose at 100 ºC, 50 bar in presence of $PdCu/ZrO_2$

Compounds	Reaction time (min)				
	40	60	80	100	120
Sorbitol	47.45	48.39	46.31	51.06	51.20
Glyceraldehyde	10.30	11.95	10.14	10.02	9.10
Glycerol	15.20	15.71	17.17	17.54	17.76
Dihydroxyacetone	0.00	0.00	0.00	2.18	2.28
Acetic acid	10.20	7.42	7.47	7.72	6.70
Propandiol	10.91	6.44	6.74	5.78	4.97
Propionic acid	4.00	3.95	3.60	2.77	2.56
Ethanol	0.00	4.15	5.69	0.68	0.91
Isobutyric acid	0.00	0.00	0.00	5.68	4.45
Unknown	1.95	1.98	2.88	2.25	0.08

Table A-3. Selectivity for HDO of glucose at 100 ºC, 50 bar in presence of Pd/ZrO_2

Compounds	Reaction time (min)				
	40	60	80	100	120
Sorbitol	56.63	56.08	59.09	59.36	57.81
Glyceraldehyde	8.77	8.61	6.84	7.74	9.00
Glycolic acid	2.73	4.08	3.16	4.02	4.06
Glycerol	8.17	8.07	6.92	7.17	7.54
Dihydroxyacetone	5.94	4.94	3.03	3.30	4.13
Acetic acid	4.90	5.36	7.52	6.68	7.24
Propandiol	6.82	6.61	6.07	5.19	5.53
Propionic acid	4.72	3.82	3.40	3.08	3.02
Ethanol	0.00	1.62	1.75	2.75	1.30
Unknown	1.33	0.81	2.21	0.72	1.69

Table A-4. Selectivity for HDO of glucose at 100 ºC, 50 bar in presence of Fe/ZrO_2

Compounds	Reaction time (min)				
	40	60	80	100	120
Sorbitol	55.68	55.18	50.97	48.83	51.80
Glyceraldehyde	8.69	9.09	8.51	8.36	10.18
Glycolic acid	2.84	4.22	3.58	4.90	4.76
Glycerol	6.78	6.72	6.39	7.09	8.15
Dihydroxyacetone	6.03	5.14	4.92	5.88	6.61
Acetic acid	5.63	5.44	9.06	7.74	7.98
Propandiol	8.70	9.16	9.65	7.03	6.92
Propionic acid	5.19	4.36	4.55	4.23	3.59
Ethanol	0.00	0.00	1.86	3.91	0.00
Unknown	0.46	0.70	2.37	5.94	0.01

Table A-5. Selectivity for HDO of glucose at 100 ºC, 50 bar in presence of $PdFe/ZrO_2$

Compounds	Reaction time (min)				
	40	60	80	100	120
Sorbitol	72.93	72.16	74.72	73.48	74.39
Glyceraldehyde	8.03	6.24	4.80	6.25	6.27
Glycolic acid	0.00	1.64	1.82	1.90	2.07
Glycerol	7.04	7.04	6.68	6.50	6.18
Dihydroxyacetone	3.57	3.35	0.00	0.00	0.00
Acetic acid	2.22	2.88	5.57	5.96	5.67
Propandiol	3.11	3.26	2.95	2.23	2.19
Propionic acid	1.66	1.24	1.30	1.22	1.06
Ethanol	0.00	0.63	0.57	0.75	0.61
Unknown	1.44	2.19	2.15	2.47	2.17

Appendix B. Supplement material: Bimetallic catalysts for bio-based aldehyde hydrogenations

Table B-1. GC-MS compounds

N	Compound	N	Compound	N	Compound
1	(3-Methyl-oxiran-2-yl)-methanol	36	2- Hydroxy octanoic acid	71	Acetic acid
2	(S)-(+)-1,2-Propanediol	37	2-Hydroxy-3,5-dimethylcyclopent-2-en-1-one	72	Acetic acid, decyl ester
3	(S)-(+)-2',3'-Dideoxyribonolactone	38	2-Isobutoxyethyl acetate	73	Ethanol, 2-(pentyloxy)-, acetate
4	1-(2-Ethoxyphenyl)acetone	39	2-Pentanone, 5-(acetyloxy)-	74	Ethanol, 2-(vinyloxy)-
5	1,2-Benzenediol	40	2-Pentenoic acid	75	Ethanone, 1-(2-furanyl)-
6	1,2-Cyclopentanediol, trans-	41	2-Propanone, 1,3-dihydroxy-	76	Ethanone, 1-(4-hydroxy- 3-methoxyphenyl)-
7	1,2-Dimethoxy-4-n-propylbenzene	42	2-Propanone, 1-hydroxy-	77	Ethanone, 1-oxiranyl-
8	1,2-Epoxy- 3-propylacetate	43	2-Propenoic acid, 2-methyl-, ethyl ester	78	Ethene, ethoxy-
9	1,2-Ethanediol	44	3,3-Dimethyl- 2, 4-pentanedione	79	Ethyl alcohol
10	1,2-Ethanediol, monoacetate	45	3,3-Dimethyl- 2-pentanone	80	Ethyl ether
11	1,2-Propanediol, 3-methoxy-	46	3,4-Altrosan	81	Ethyl hydrogenoxalate
12	1,3,6-Trioxocane	47	3,4-Anhydro- d-galactosan	82	Eugenol
13	1,3-Butanediol, diacetate	48	3,4-Dihydroxy- 5-methyl-dihydrofuran- 2-one	83	Formaldehyde
14	1,3-Dioxane, 4-methyl-	49	3,5-dimethyl-2(5H)-furanone	84	Formic acid
15	1,3-Dioxane-4,6-dione, 2,2-dimethyl-	50	3,6-Dimethylperhydro-1,3-oxazine	85	Formic acid, 1-methyl ethyl ester
16	1,3-Dioxepane, 2-methyl-2-propyl-	51	3,7-Benzofurandiol, 2,3-dihydro-2,2-dimethyl-	86	Formic acid, ethenyl ester
17	1,3-Dioxolane, 2,4,5-trimethyl-	52	3-Butene-1, 2-diol	87	Furan
18	1,3-Dioxolane, 2-methyl-	53	3-Butenoic acid	88	Furan, tetrahydro-
19	1,4- Butanediol	54	3-Cyclobutene-1 ,2-dione, 3,4-dihydroxy-	89	Furfural
20	1,4- Diacetoxy butane	55	3-Cyclohexen-1-carboxaldehyde, 3-methyl-	90	Furyl hydroxyl methyl ketone
21	1,4:3,6-Dianhydro-a-d-glucopyranose	56	3-Heptanol, 2-methyl-	91	Galacto-heptulose
22	1,4-Benzenediol, 2-methyl-	57	3-Hexanone	92	Galactosan triacetate
23	1,4-Butanediol, diacetate	58	3-Mercaptohexyl hexanoate	93	Glycidol
24	1,4-Dioxane, 2-ethyl-5-methyl-	59	3-Pentanol	94	Guanidineacetic acid
25	1,4-Pentadiene	60	4-Methyl- 2-tert-octylphenol	95	Hexane, 2,3,5- trimethyl-
26	1,4-Pentanediol	61	4-Methyl- 5H-furan- 2-one	96	Hexanoic acid
27	1,6-Anhydro- b-D-glucopyranose (levoglucosan)	62	5- Hydroxy methyl dihydrofuran-2-one	97	Hexanoic acid, 3-hydroxy -5-methyl-, methylester
28	1-Hepten- 4-ol	63	5,9-Dodecadien-2-one, 6,10-dimethy	98	Hexanoic acid, 5-oxo-, ethyl ester
29	1-Heptene	64	5-Hydroxymethyldihydrofuran-2-one	99	Homovanillyl alcohol
30	1-Hydroxy- 2-butanone	65	5-Methylfurfural	100	Hydroquinone
31	1-Hydroxy- 2-pentanone	66	6,6,7-Trimethyl- octane- 2,5-dione	101	Hydroxymethylfurfural
32	1-Pentanol, 2,3-dimethyl-	67	6-Dodecanone	102	Isocrotonic acid
33	1-Propanol	68	7-Decen-2-one	103	L-Mannose, 6-deoxy-
34	1-Propanol, 2-methyl-	69	Acetaldehyde	104	Maltol
35	1-Propene, 3-methoxy- 2-methyl-	70	Acetaldehyde, hydroxy-	105	Methyl a d-rhamnopyranoside

Continued

N	Compound	N	Compound	N	Compound
106	Methyl formate	142	2H-Pyran, tetrahydro- 2-methyl-	177	Ethanol, 2-(2,3-butadienyloxy)-
107	Methyl propionate	143	2H-Pyran-2-one	179	n-Butyl ether
108	Montanol	144	Acetic acid, methyl ester	180	n-Capric acid isopropyl
109	2(3H)-Furanone, 5-ethyldihydro-	145	Acetone	181	n-Propyl acetate
110	2(3H)-Furanone, dihydro- 4-hydroxy-	146	Benzaldehyde, 2-hydroxy- 3-methoxy- (Vanillin)	182	Octane, 2,6,6 -trimethyl-
111	2(5H)-Furanone	147	Benzaldehyde, 4-hydroxy-	183	Octanoic Acid
112	2(5H)-Furanone, 5-methyl-	148	Benzene acetaldehyde, 2-methoxy-	184	Oxalic acid, ethyl propyl ester
113	2,2-Dimethyl pentyl cyclohexane carboxylate	149	Benzene acetic acid, 4-hydroxy- 3-methoxy-	185	Oxirane, (ethoxymethyl)-
114	2,3-Anhydro-d-galactosan	150	Benzeneacetic acid, 4-hydroxy-3-methoxy-, methyl ester	186	Oxirane, 2,3- dimethyl-
115	2,3-Anhydro-d-mannosan	151	Butanal	187	Oxirane, 3-hydroxypropyl-
116	2,3-Dihydrofuran	152	Butanal, 2-methyl-	188	Pentanal
117	2,3-O-Acetonemannosan	153	Butanal, 3-hydroxy-	189	Pentanoic acid
118	2,4-Diacetoxypentane	154	Butanal,2-ethyl-	190	Pentanoic acid, 2-methyl-4-oxo-, ethyl ester
119	2,5-Furandione, 3-methyl-	155	Butane, 1-methoxy-	191	Pentanoic acid,4-oxo-, butyl ester
120	2,5-Furandione, dihydro-3-methylene-	156	Butanedial	192	Phenol, 2,4-dimethyl-
121	2,5-Hexanedione	157	Butanedioic	193	Phenol, 2-methoxy- 4-methyl-
122	2-Acetylamino-3-hydroxy-propionic acid	158	Butanoic acid	194	Phenol, 2-methoxy- 6-(1-propenyl)-
123	2-Butanone, 4-hydroxy-	159	Butanoic acid, methylester	195	Phenol, 2-methoxy-1
124	2-Butenal, 2-methyl-	160	Butylated Hydroxy toluene	196	Phenol, 2-methoxy-4-methyl-
125	2-Butene-1, 4-diol	161	Butyrolactone	197	Phenol, 2-methoxy-4-propyl-
126	2-Butenoic acid, 2-methoxy-3-methyl-, methyl ester	162	Carbonicacid, isobutyl isohexyl ester	198	Phenol, 2-methyl-
127	2-Cyclopenten- 1-one	163	Crotonic acid	199	Phenol, 3-ethyl-
128	2-Cyclopenten- 1-one, 2-methyl-	164	Cyclobutane, methyl-	200	Phenol, 5-methoxy-2,3-dimethyl-
129	2-Cyclopenten- 1-one, 3-ethyl- 2-hydroxy-	165	Cyclobutanol	201	Propanal
130	2-Cyclopenten-1-one, 2-hydroxy-	166	Cyclobutanone, 2-methyl- 4-hydroxy-	202	Propanal, 2,3-dihydroxy-
131	2-Cyclopenten-1-one, 2-hydroxy-3,4 -dimethyl-	167	Cyclohexan- 1,4,5-triol -3-one -1-carboxylic acid	203	Propane, 1-methoxy-2-methyl-
132	2-Cyclopenten-1-one, 2-hydroxy-3-methyl-	168	Cyclohexane, ethyl-	204	Propane, 2-(ethenyloxy)-
133	2-Cyclopenten-1-one, 3-(acetyloxy)	169	Cyclohexanol,2-methyl-	205	Propanoic acid
134	2-Deoxy-D-glucose	170	Cyclohexanone, 4-hydroxy-	206	Propanoic acid, 2-methyl-, 1-methylethyl ester
135	2-Ethoxyethyl acetate	171	Cyclopentane, 1,1-dimethyl-	207	Propanoic acid, 3-hydroxy-, methyl ester
136	2-Furancarboxaldehyde, 5-(hydroxymethyl)-	172	Cyclopropyl carbinol	208	Styracitol
137	2-Furancarboxaldehyde, 5-methyl-	173	D-Erythro -Pentose, 2-deoxy-	209	Succinic anhydride
138	2-Furancarboxylic acid	174	D-Glucose, 6-O-a -D-galactopyranosyl-	210	trans-5 -Methyl- 2-isopropyl- 2-hexen
139	2-Furanmethanol, tetrahydro-	178	Ethanol, 2-(2-butoxyethoxy)-, acetate	211	Vanillin
140	2-Hexanone, 4-methyl-	175	d-Glycero -d-galacto -heptose		
141	2-Hexene, 2,5-dimethyl-	176	dl-Glyceraldehyde		

List of References

[1] M.R. Rover, P.H. Hall, P.A. Johnston, R.G. Smith, R.C. Brown., Stabilization of bio-oils using low temperature, low pressure hydrogenation, Fuel, (2015) 224–230.

[2] J. Remón, P. Arcelus-Arrillaga, L. García, J. Arauzo, Production of gaseous and liquid bio-fuels from the upgrading of lignocellulosic bio-oil in sub- and supercritical water: Effect of operating conditions on the process, Energy Conversion and Management, 119 (2016) 14-36.

[3] M.E. Rezac, Membrane reactor technology for the efficient conversion of biomass to industrial chemicals, in: Report No. 0224150.2016.

[4] M.D. Wales, W. Taraylor, M.E. Rezac, P.H. Pfromm, L. Schulte, J.P. Stanford, M. Young, M. Heidlage, Membrane reactors for multiphase hydrotreating of biomass: Overcoming gas-liquid mass transfer limitations, in: AIChE Spring Meeting & 10th Global Congress on Process Safety, Newberry (Hilton New Orleans Riverside), New Orleans, LA, USA, 2014.

[5] M. Chalid, A. Broekhuis, H. Heeres, J. Mol. Catal. A: Chem., 341 (2011) 14.

[6] N. Alonso-Fagúndez, M.L. Granados, R. Mariscal, M. Ojeda, ChemSusChem, 5 (2012) 1984.

[7] H.-J. Huang, S. Ramaswamy, Overview of Biomass Conversion Processes and Separation and Purification Technologies in Biorefineries, in: Shiri Ramaswamy, Hua-Jiang Huang, B.V. Ramaro (Eds.) Separation and Purification Technologies in Biorefineries, John Wiley & Sons, Ltd., Publication, 2013, pp. 3-35.

[8] K. Soyez, B. Kamm, M. Kamm, The Green Biorefinery, in: 1st International Green Biorefinery Conference, 1998, Neuruppin, Germany, 1997.

[9] Biorefinery, in: Biorefineries: For Biomass Upgrading Facilities, Springer London, London, 2010, pp. 75-92.

[10] S. Lima, A. Fernandes, M.M. Antunes, M. Pillinger, F. Ribeiro, A.A. Valente, Catal. Lett., 135 (2010) 41.

[11] Thermochemical Processes, in: Biorefineries: For Biomass Upgrading Facilities, Springer London, London, 2010, pp. 135-192.

[12] G. Centi, F. Trifiro, J.R. Ebner, V.M. Franchetti, Chem. Rev., 88 (1988) 55.

[13] F. Li, S.C. Srivatsa, S. Bhattacharya, A review on catalytic pyrolysis of microalgae to high-quality bio-oil with low oxygeneous and nitrogenous compounds, Renewable and Sustainable Energy Reviews, 108 (2019) 481-497.

[14] E. Furimsky, Catalytic hydrodeoxygenation, Applied Catalysis A: General, 199 (2000) 147-190.

[15] C.A. Fisk, T. Morgan, Y. Ji, M. Crocker, C. Crofcheck, S.A. Lewis, Bio-oil upgrading over platinum catalysts using in situ generated hydrogen, Applied Catalysis A: General, 358 (2009) 150-156.

[16] P. Li, X. Chen, X. Wang, J. Shao, G. Lin, H. Yang, Q. Yang, H. Chen, Catalytic Upgrading of Fast Pyrolysis Products with Fe-, Zr-, and Co-Modified Zeolites Based on Pyrolyzer–GC/MS Analysis, Energy & Fuels, 31 (2017) 3979-3986.

[17] T. Dong, J. Wang, C. Miao, Y. Zheng, S. Chen, Two-step in situ biodiesel production from microalgae with high free fatty acid content, Bioresource Technology, 136 (2013) 8-15.

[18] N.H. Zainan, S.C. Srivatsa, S. Bhattacharya, Catalytic pyrolysis of microalgae Tetraselmis suecica and characterization study using in situ Synchrotron-based Infrared Microscopy, Fuel, 161 (2015) 345-354.

[19] A. Demirbas, The influence of temperature on the yields of compounds existing in bio-oils obtained from biomass samples via pyrolysis, Fuel Processing Technology, 88 (2007) 591-597.

[20] R.H. Venderbosch, A.R. Ardiyanti, J. Wildschut, A. Oasmaa, H.J. Heeres, Stabilization of biomass-derived pyrolysis oils, Journal of Chemical Technology and Biotechnology, 85 (2010) 674-686.

[21] J. Wildschut, F.H. Mahfud, R.H. Venderbosch, H.J. Heeres, Hydrotreatment of Fast Pyrolysis Oil Using Heterogeneous Noble-Metal Catalysts, Industrial & Engineering Chemistry Research, 48 (2009) 10324-10334.

[22] A.V. Bridgwater, Renewable fuels and chemicals by thermal processing of biomass, Chemical Engineering Journal, 91 (2003) 87-102.

[23] A.R. Ardiyanti, S.A. Khromova, R.H. Venderbosch, V.A. Yakovlev, H.J. Heeres, Catalytic hydrotreatment of fast-pyrolysis oil using non-sulfided bimetallic Ni-Cu catalysts on a δ-Al2O3 support, Applied Catalysis B: Environmental, 117–118 (2012) 105-117.

[24] Q. Lu, X.-l. Yang, X.-f. Zhu, Analysis on chemical and physical properties of bio-oil pyrolyzed from rice husk, Journal of Analytical and Applied Pyrolysis, 82 (2008) 191-198.

[25] J. Wildschut, M. Iqbal, F.H. Mahfud, I.M. Cabrera, R.H. Venderbosch, H.J. Heeres, Insights in the hydrotreatment of fast pyrolysis oil using a ruthenium on carbon catalyst, Energy & Environmental Science, 3 (2010) 962-970.

[26] D.C. Elliott, T.R. Hart, G.G. Neuenschwander, L.J. Rotness, M.V. Olarte, A.H. Zacher, Y. Solantausta, Catalytic Hydroprocessing of Fast Pyrolysis Bio-oil from Pine Sawdust, Energy & Fuels, 26 (2012) 3891-3896.

[27] D.C. Elliott, G.G. Neuenschwander, Liquid Fuels by Low-Severity Hydrotreating of Biocrude, in: A.V. Bridgwater, D.G.B. Boocock (Eds.) Developments in Thermochemical Biomass Conversion: Volume 1 / Volume 2, Springer Netherlands, Dordrecht, 1997, pp. 611-621.

[28] J. Piskorz, D.S. Scott, The composition of oils obtained by the fast pyrolysis of different woods, 1987.

[29] M. Patel, A. Kumar, Production of renewable diesel through the hydroprocessing of lignocellulosic biomass-derived bio-oil: A review, Renewable and Sustainable Energy Reviews, 58 (2016) 1293-1307.

[30] S. Zhang, Y. Yan, T. Li, Z. Ren, Upgrading of liquid fuel from the pyrolysis of biomass, Bioresource Technology, 96 (2005) 545-550.

[31] R. López, C. Fernández, X. Gómez, O. Martínez, M.E. Sánchez, Thermogravimetric analysis of lignocellulosic and microalgae biomasses and their blends during combustion, Journal of Thermal Analysis and Calorimetry, 114 (2013) 295-305.

[32] H. Liu, Y. Chen, H. Yang, F.G. Gentili, U. Söderlind, X. Wang, W. Zhang, H. Chen, Hydrothermal carbonization of natural microalgae containing a high ash content, Fuel, 249 (2019) 441-448.

[33] A. Plis, J. Lasek, A. Skawińska, Kinetic analysis of the combustion process of Nannochloropsis gaditana microalgae based on thermogravimetric studies, Journal of Analytical and Applied Pyrolysis, 127 (2017) 109-119.

[34] X. Miao, Q. Wu, High yield bio-oil production from fast pyrolysis by metabolic controlling of Chlorella protothecoides, Journal of Biotechnology, 110 (2004) 85-93.

[35] Q. Guo, M. Wu, K. Wang, L. Zhang, X. Xu, Catalytic Hydrodeoxygenation of Algae Bio-oil over Bimetallic Ni–Cu/ZrO2 Catalysts, Industrial & Engineering Chemistry Research, 54 (2015) 890-899.

[36] U. Jena, K.C. Das, Comparative Evaluation of Thermochemical Liquefaction and Pyrolysis for Bio-Oil Production from Microalgae, Energy & Fuels, 25 (2011) 5472-5482.

[37] Z. Hu, Y. Zheng, F. Yan, B. Xiao, S. Liu, Bio-oil production through pyrolysis of blue-green algae blooms (BGAB): Product distribution and bio-oil characterization, Energy, 52 (2013) 119-125.

[38] R. Venderbosch, A. Ardiyanti, J. Wildschut, A. Oasmaa, H. Heeres, Stabilization of biomass-derived pyrolysisils Journal of Chemical Technology and Biotechnology, 5 (2010) 674-686.

[39] A. Oasmaa, Y. Solantausta, V. Arpiainen, E. Kuoppala, K. Sipilä., Fast pyrolysis bio-oils from wood and agricultural residues, Energy & Fuels, 2 (2010) 1380-1388.

[40] A. Gruia, Hydrotreating, in: D.S.J.S. JONES, P.R. PUJADO' (Eds.) Handbook of Petroleum Processing, Springer, P.O. Box 17, 3300 AA Dordrecht, The Netherlands., 2006, pp. 321-354.

[41] K. Jacobson, K.C. Maheria, A. Kumar Dalai, Bio-oil valorization: A review, Renewable and Sustainable Energy Reviews, 23 (2013) 91-106.

[42] C. Mauchausse, E. Kural, D.L. Trimm, N.W. Cant, Optimization of tungsten-based catalysts for the hydrotreatment of coal-derived liquids, Fuel, 71 (1992) 203-209.

[43] D.A. Bulushev, J.R.H. Ross, Catalysis for conversion of biomass to fuels via pyrolysis and gasification: A review, Catalysis Today, 171 (2011) 1-13.

[44] R.I. Masel, Principles of adsorption and reaction on solid surfaces, New York Chichester : Wiley, New York, Chichester, 1996.

[45] Y.G. Ptushinskiĭ, Low-temperature adsorption of gases on metal surfaces (Review), Low Temperature Physics, 30 (2004) 1-26.

[46] P. Ferrin, S. Kandoi, A.U. Nilekar, M. Mavrikakis, Hydrogen adsorption, absorption and diffusion on and in transition metal surfaces: A DFT study, Surface Science, 606 (2012) 679-689.

[47] D.C. Elliott, J. Hu, T.R. Hart, G.G. Neuenschwander, Palladium catalyzed hydrogenation of bio-oils and organic compounds, in, Google Patents, 2008.

[48] P.M. Mortensen, J.-D. Grunwaldt, P.A. Jensen, A.D. Jensen, Screening of Catalysts for Hydrodeoxygenation of Phenol as a Model Compound for Bio-oil, ACS Catalysis, 3 (2013) 1774-1785.

[49] A.R. Ardiyanti, S.A. Khromova, R.H. Venderbosch, V.A. Yakovlev, I.V. Melián-Cabrera, H.J. Heeres, Catalytic hydrotreatment of fast pyrolysis oil using bimetallic Ni–Cu catalysts on various supports, Applied Catalysis A: General, 449 (2012) 121-130.

[50] S. Wei, Y. Zhao, G. Fan, L. Yang, F. Li, Structure-dependent selective hydrogenation of cinnamaldehyde over high-surface-area CeO2-ZrO2 composites supported Pt nanoparticles, Chemical Engineering Journal, 322 (2017) 234-245.

[51] M. Zhou, P. Liu, K. Wang, J. Xu, J. Jiang, Catalytic hydrogenation and one step hydrogenation-esterification to remove acetic acid for bio-oil upgrading: model reaction study, Catalysis Science & Technology, 6 (2016) 7783-7792.

[52] H. Bergem, R. Xu, R.C. Brown, G.W. Huber, Low temperature aqueous phase hydrogenation of the light oxygenate fraction of bio-oil over supported ruthenium catalysts, Green Chemistry, 19 (2017) 3252-3262.

[53] Q. Yuan, D. Zhang, L.v. Haandel, F. Ye, T. Xue, E.J.M. Hensen, Y. Guan, Selective liquid phase hydrogenation of furfural to furfuryl alcohol by Ru/Zr-MOFs, Journal of Molecular Catalysis A: Chemical, 406 (2015) 58-64.

[54] Y. Liu, Y. Zheng, B. Du, R.R. Nasaruddin, T. Chen, J. Xie, Golden Carbon Nanotube Membrane for Continuous Flow Catalysis, Industrial & Engineering Chemistry Research, 56 (2017) 2999-3007.

[55] J.L. Fiorio, N. López, L.M. Rossi, Gold–Ligand-Catalyzed Selective Hydrogenation of Alkynes into cis-Alkenes via H2 Heterolytic Activation by Frustrated Lewis Pairs, ACS Catalysis, 7 (2017) 2973-2980.

[56] Y. Nakagawa, R. Tamura, M. Tamura, K. Tomishige, Combination of supported bimetallic rhodium–molybdenum catalyst and cerium oxide for hydrogenation of amide, Science and Technology of Advanced Materials, 16 (2015) 014901.

[57] N. Ota, M. Tamura, Y. Nakagawa, K. Okumura, K. Tomishige, Performance, Structure, and Mechanism of ReOx–Pd/CeO2 Catalyst for Simultaneous Removal of Vicinal OH Groups with H2, ACS Catalysis, 6 (2016) 3213-3226.

[58] Y. Takeda, M. Tamura, Y. Nakagawa, K. Okumura, K. Tomishige, Characterization of Re–Pd/SiO2 Catalysts for Hydrogenation of Stearic Acid, ACS Catalysis, 5 (2015) 7034-7047.

[59] K. Joseph Antony Raj, M.G. Prakash, R. Mahalakshmy, T. Elangovan, B. Viswanathan, Liquid phase hydrogenation of crotanaldehyde over nickel supported on titania, Journal of Molecular Catalysis A: Chemical, 366 (2013) 92-98.

[60] C. Wang, Z. Guo, Y. Yang, J. Chang, A. Borgna, Hydrogenation of Furfural as Model Reaction of Bio-Oil Stabilization under Mild Conditions Using Multiwalled Carbon Nanotube (MWNT)-Supported Pt Catalysts, Industrial & Engineering Chemistry Research, 53 (2014) 11284-11291.

[61] K. Fulajtárova, T. Soták, M. Hronec, I. Vávra, E. Dobročka, M. Omastová, Aqueous phase hydrogenation of furfural to furfuryl alcohol over Pd–Cu catalysts, Applied Catalysis A: General, 502 (2015) 78-85.

[62] A. Sanna, T.P. Vispute, G.W. Huber, Hydrodeoxygenation of the aqueous fraction of bio-oil with Ru/C and Pt/C catalysts, Applied Catalysis B: Environmental, 165 (2015) 446-456.

[63] T.P. Vispute, H. Zhang, A. Sanna, R. Xiao, G.W. Huber, Science, 330 (2010) 1222.

[64] X. Liao, Y. Zhang, J. Guo, L. Zhao, M. Hill, Z. Jiang, Y. Zhao, The Catalytic Hydrogenation of Maleic Anhydride on CeO2−δ-Supported Transition Metal Catalysts, Catalysts, 7 (2017) 272.

[65] D.C. Elliott, Historical developments in hydroprocessing bio-oils, Energy and Fuels, 21 (2007) 1792-1815.

[66] E. Laurent, B. Delmon, Study of the hydrodeoxygenation of carbonyl, car□ylic and guaiacyl groups over sulfided CoMo/γ-Al2O3 and NiMo/γ-Al2O3 catalysts: I. Catalytic reaction schemes, Applied Catalysis A: General, 109 (1994) 77-96.

[67] A. Bienholz, F. Schwab, P. Claus, Hydrogenolysis of glycerol over a highly active CuO/ZnO catalyst prepared by an oxalate gel method: influence of solvent and reaction temperature on catalyst deactivation, Green Chemistry, 12 (2010) 290-295.

[68] H. Liu, S. Liang, T. Jiang, B. Han, Y. Zhou, Hydrogenolysis of Glycerol to 1,2-Propanediol over Ru–Cu Bimetals Supported on Different Supports, CLEAN – Soil, Air, Water, 40 (2012) 318-324.

[69] F. de Miguel Mercader, M.J. Groeneveld, S.R.A. Kersten, C. Geantet, G. Toussaint, N.W.J. Way, C.J. Schaverien, K.J.A. Hogendoorn, Hydrodeoxygenation of pyrolysis oil fractions: process understanding and quality assessment through co-processing in refinery units, Energy & Environmental Science, 4 (2011) 985-997.

[70] T. Prasomsri, M. Shetty, K. Murugappan, Y. Román-Leshkov, Insights into the catalytic activity and surface modification of MoO3 during the hydrodeoxygenation of lignin-derived model compounds into aromatic hydrocarbons under low hydrogen pressures, Energy & Environmental Science, 7 (2014) 2660-2669.

[71] A. Oasmaa, E. Kuoppala, Y. Solantausta, Fast Pyrolysis of Forestry Residue. 2. Physicochemical Composition of Product Liquid, Energy & Fuels, 17 (2003) 433-443.

[72] A. Oasmaa, E. Kuoppala, S. Gust, Y. Solantausta, Fast Pyrolysis of Forestry Residue. 1. Effect of Extractives on Phase Separation of Pyrolysis Liquids, Energy & Fuels, 17 (2003) 1-12.

[73] J.D. Adjaye, N.N. Bakhshi, Production of hydrocarbons by catalytic upgrading of a fast pyrolysis bio-oil. Part II: Comparative catalyst performance and reaction pathways, Fuel Processing Technology, 45 (1995) 185-202.

[74] G. de la Puente, A. Gil, J.J. Pis, P. Grange, Effects of Support Surface Chemistry in Hydrodeoxygenation Reactions over CoMo/Activated Carbon Sulfided Catalysts, Langmuir, 15 (1999) 5800-5806.

[75] A. Gutierrez, R.K. Kaila, M.L. Honkela, R. Slioor, A.O.I. Krause, Hydrodeoxygenation of guaiacol on noble metal catalysts, Catalysis Today, 147 (2009) 239-246.

[76] V.N. Bui, D. Laurenti, P. Afanasiev, C. Geantet, Hydrodeoxygenation of guaiacol with CoMo catalysts. Part I: Promoting effect of cobalt on HDO selectivity and activity, Applied Catalysis B: Environmental, 101 (2011) 239-245.

[77] A. Centeno, E. Laurent, B. Delmon, Influence of the Support of CoMo Sulfide Catalysts and of the Addition of Potassium and Platinum on the Catalytic Performances for the Hydrodeoxygenation of Carbonyl, Carboxyl, and Guaiacol-Type Molecules, Journal of Catalysis, 154 (1995) 288-298.

[78] M. Ferrari, B. Delmon, P. Grange, Influence of the active phase loading in carbon supported molybdenum–cobalt catalysts for hydrodeoxygenation reactions, Microporous and Mesoporous Materials, 56 (2002) 279-290.

[79] A.B. Bindwal, A.H. Bari, P.D. Vaidya, Kinetics of low temperature aqueous-phase hydrogenation of model bio-oil compounds, Chemical Engineering Journal, 207–208 (2012) 725-733.

[80] A.B. Bindwal, P.D. Vaidya, Kinetics of Aqueous-Phase Hydrogenation of Levoglucosan over Ru/C Catalyst, Industrial & Engineering Chemistry Research, 52 (2013) 17781-17789.

[81] S. Zhang, Y. Yan, T. Li, Z. Ren, Lumping Kinetic Model for Hydrotreating of Bio-oil from the Fast Pyrolysis of Biomass, Energy Sources, Part A: Recovery, Utilization, and Environmental Effects, 31 (2009) 639-645.

[82] Z. Su-Ping, Study of Hydrodeoxygenation of Bio-Oil from the Fast Pyrolysis of Biomass, Energy Sources, 25 (2003) 57-65.

[83] Y.-H.E. Sheu, R.G. Anthony, E.J. Soltes, Kinetic studies of upgrading pine pyrolytic oil by hydrotreatment, Fuel Processing Technology, 19 (1988) 31-50.

[84] Hydrotreating (detailed), in https://oilrss.com/hydrotreating-detailed-overview , 2020.

[85] A. Iulianelli, T. Longo, A. Basile, Methanol steam reforming reaction in a Pd–Ag membrane reactor for CO-free hydrogen production, International Journal of Hydrogen Energy, 33 (2008) 5583-5588.

[86] A. Iulianelli, T. Longo, A. Basile, CO-free hydrogen production by steam reforming of acetic acid carried out in a Pd–Ag membrane reactor: The effect of co-current and counter-current mode, International Journal of Hydrogen Energy, 33 (2008) 4091-4096.

[87] J. Sunarso, S.S. Hashim, N. Zhu, W. Zhou, Perovskite oxides applications in high temperature oxygen separation, solid oxide fuel cell and membrane reactor: A review, Progress in Energy and Combustion Science, 61 (2017) 57-77.

[88] J. Caro, Basic Aspects of Membrane Reactors, in: Reference Module in Chemistry, Molecular Sciences and Chemical Engineering, Elsevier, 2017.

[89] R. Di Felice, Multiphase Membrane Reactors, in: Reference Module in Chemistry, Molecular Sciences and Chemical Engineering, Elsevier, 2017.

[90] S. Kanehashi, K. Nagai, Chapter 14 - Gas and Vapor Transport in Membranes, in: Membrane Characterization, Elsevier, 2017, pp. 309-336.

[91] G. Bagnato, A. Iulianelli, A. Sanna, A. Basile, Glycerol Production and Transformation: A Critical Review with Particular Emphasis on Glycerol Reforming Reaction for Producing Hydrogen in Conventional and Membrane Reactors, Membranes, 7 (2017) 17.

[92] M.D. Dolan, N.C. Dave, A.Y. Ilyushechkin, L.D. Morpeth, K.G. McLennan, Composition and operation of hydrogen-selective amorphous alloy membranes, Journal of Membrane Science, 285 (2006) 30-55.

[93] E.E. McLeary, J.C. Jansen, F. Kapteijn, Zeolite based films, membranes and membrane reactors: Progress and prospects, Microporous and Mesoporous Materials, 90 (2006) 198-220.

[94] M. Liu, X. Zhu, R. Chen, Q. Liao, H. Feng, L. Li, Catalytic membrane microreactor with Pd/γ-Al2O3 coated PDMS film modified by dopamine for hydrogenation of nitrobenzene, Chemical Engineering Journal, 301 (2016) 35-41.

[95] Y.X. Chunqing Liu, Shijan Liao, Daorong Yu, Mono- and bimetallic catalytic hollow- fiber reactors for the selective hydrogenation of butadiene in 1-butene, Applied Catalysis A: General, (1998) 23-29.

[96] J.P. Stanford, M.C. Soto, P.H. Pfromm, M.E. Rezac, Aqueous phase hydrogenation of levulinic acid using a porous catalytic membrane reactor, Catalysis Today, 268 (2016) 19-28.

[97] P.B. Francesca Liguori, Cristiana Giordano, Haruo Saw, Partial hydrogenation reactions over Pd-containing hybrid inorganic/polymeric catalytic membranes, Applied Catalysis A: General (2013) 81– 88.

[98] H.K. H.C. Aran, J.M. Jani, M. Wessling, L. Lefferts, R.G.H. Lammertink, Influence of geometrical and operational parameters on the performance of porous catalytic membrane reactors, Chemical Engineering Journal, (2012) 814–821.

[99] G.C. Aldo Bottino, Antonio Comite, Adriana Del Borghi, Renzo Di Felice, Catalytic ceramic membrane in a three-phase reactor for the competitive hydrogenation–isomerisation of methylenecyclohexane, Separation and Purification Technology (2004) 239–245.

[100] G.C. A. Bottino, A. Comite, R. Di Felice, Polymeric and ceramic membranes in three-phase catalytic membrane reactors for the hydrogenation of methylenecyclohexane, Desalination (2002) 41 I-416.

[101] D.F. Gisela Bengtson, Catalytic membrane reactor for the selective hydrogenation of edible oil: platinum versus palladium catalyst, Desalination, (2006) 666–667.

[102] P.B. Francesca Liguori, Haruo Sawa, Continuous flow hydrogenation reactions by Pd catalysts onto hybrid ZrO2/PVA materials, Applied Catalysis A: General (2014) 58–65.

[103] B. Dou, H. Zhang, Y. Song, L. Zhao, B. Jiang, M. He, C. Ruan, H. Chen, Y. Xu, Hydrogen production from the thermochemical conversion of biomass: issues and challenges, Sustainable Energy & Fuels, 3 (2019) 314-342.

[104] A. Iulianelli, V. Palma, G. Bagnato, C. Ruocco, Y. Huang, N.T. Veziroğlu, A. Basile, From bioethanol exploitation to high grade hydrogen generation: Steam reforming promoted by a Co-Pt catalyst in a Pd-based membrane reactor, Renewable Energy, 119 (2018) 834-843.

[105] J.R. Bartels, M.B. Pate, N.K. Olson, An economic survey of hydrogen production from conventional and alternative energy sources, International Journal of Hydrogen Energy, 35 (2010) 8371-8384.

[106] A.V. Bridgwater, D. Meier, D. Radlein, An overview of fast pyrolysis of biomass, Organic Geochemistry, 30 (1999) 1479-1493.

[107] P. Unrean, B.C. Lai Fui, E. Rianawati, M. Acda, Comparative techno-economic assessment and environmental impacts of rice husk-to-fuel conversion technologies, Energy, 151 (2018) 581-593.

[108] M. Magdeldin, T. Kohl, M. Järvinen, Techno-economic assessment of the by-products contribution from non-catalytic hydrothermal liquefaction of lignocellulose residues, Energy, 137 (2017) 679-695.

[109] S.B. Glisic, J.M. Pajnik, A.M. Orlović, Process and techno-economic analysis of green diesel production from waste vegetable oil and the comparison with ester type biodiesel production, Applied Energy, 170 (2016) 176-185.

[110] J.L. Carrasco, S. Gunukula, A.A. Boateng, C.A. Mullen, W.J. DeSisto, M.C. Wheeler, Pyrolysis of forest residues: An approach to techno-economics for bio-fuel production, Fuel, 193 (2017) 477-484.

[111] B. BioLiquids, in https://www.btg-btl.com/en/applications/oilproperties, 2018.

[112] F. Menegazzo, C. Pizzolitto, D. Zanardo, M. Signoretto, C. Buysschaert, G. Bény, A. Di Michele, Hydrogen Production by Ethanol Steam Reforming on Ni-Based Catalysts: Effect of the Support and of CaO and Au Doping, ChemistrySelect, 2 (2017) 9523-9531.

[113] R. Haul, S. J. Gregg, K. S. W. Sing: Adsorption, Surface Area and Porosity. 2. Auflage, Academic Press, London 1982. 303 Seiten, Preis: $ 49.50, Berichte der Bunsengesellschaft für physikalische Chemie, 86 (1982) 957-957.

[114] A. Kloekhorst, J. Wildschut, H.J. Heeres, Catalytic hydrotreatment of pyrolytic lignins to give alkylphenolics and aromatics using a supported Ru catalyst, Catalysis Science & Technology, 4 (2014) 2367-2377.

[115] A. Figoli, C. Ursino, F. Galiano, E. Di Nicolò, P. Campanelli, M.C. Carnevale, A. Criscuoli, Innovative hydrophobic coating of perfluoropolyether (PFPE) on commercial hydrophilic membranes for DCMD application, Journal of Membrane Science, 522 (2017) 192-201.

[116] S.-i. Sawada, C. Ursino, F. Galiano, S. Simone, E. Drioli, A. Figoli, Effect of citrate-based non-toxic solvents on poly(vinylidene fluoride) membrane preparation via thermally induced phase separation, Journal of Membrane Science, 493 (2015) 232-242.

[117] M. Pasandideh-Fard, P. Chen, J. Mostaghimi, A.W. Neumann, The generalized Laplace equation of capillarity I. Thermodynamic and hydrostatic considerations of the fundamental equation for interfaces, Advances in Colloid and Interface Science, 63 (1996) 151-177.

[118] R.S. Hebbar, A.M. Isloor, A.F. Ismail, Chapter 12 - Contact Angle Measurements, in: Membrane Characterization, Elsevier, 2017, pp. 219-255.

[119] K. Wang, A.A. Abdala, N. Hilal, M.K. Khraisheh, Chapter 13 - Mechanical Characterization of Membranes, in: Membrane Characterization, Elsevier, 2017, pp. 259-306.

[120] J.M. Douglas, Conceptual Design of Chemical Processes, McGraw-Hill Higher Education, 1988.

[121] R. Thilakaratne, M.M. Wright, R.C. Brown, A techno-economic analysis of microalgae remnant catalytic pyrolysis and upgrading to fuels, Fuel, 128 (2014) 104-112.

[122] T.R. Brown, R. Thilakaratne, R.C. Brown, G. Hu, Techno-economic analysis of biomass to transportation fuels and electricity via fast pyrolysis and hydroprocessing, Fuel, 106 (2013) 463-469.

[123] M. M. Wright, J. A. Satrio, R.C. Brown, Techno-Economic Analysis of Biomass Fast Pyrolysis to Transportation Fuels, in, National renewable energy laboratory (NREL), 2010.

[124] M. Auersvald, B. Shumeiko, M. Staš, D. Kubička, J. Chudoba, P. Šimáček, Quantitative Study of Straw Bio-oil Hydrodeoxygenation over a Sulfided NiMo Catalyst, ACS Sustainable Chemistry & Engineering, 7 (2019) 7080-7093.

[125] C.Y. Yang, Z.M. Zhao, Z.Z. Wu, X.H. Yang, Study on Separation of Furfural from Bio-Oil, Applied Mechanics and Materials, 295-298 (2013) 273-278.

[126] E.D. Gomes, A.E. Rodrigues, Lignin biorefinery: Separation of vanillin, vanillic acid and acetovanillone by adsorption, Separation and Purification Technology, 216 (2019) 92-101.

[127] F. Menegazzo, E. Ghedini, M. Signoretto, 5-Hydroxymethylfurfural (HMF) Production from Real Biomasses, Molecules, 23 (2018) 2201.

[128] X. Liu, B. Zhang, B. Fei, X. Chen, J. Zhang, X. Mu, Tunable and selective hydrogenation of furfural to furfuryl alcohol and cyclopentanone over Pt supported on biomass-derived porous heteroatom doped carbon, Faraday Discussions, 202 (2017) 79-98.

[129] G. Bagnato, A. Figoli, C. Ursino, F. Galiano, A. Sanna, A novel Ru–polyethersulfone (PES) catalytic membrane for highly efficient and selective hydrogenation of furfural to furfuryl alcohol, Journal of Materials Chemistry A, 6 (2018) 4955-4965.

[130] X. Li, P. Jia, T. Wang, Furfural: A Promising Platform Compound for Sustainable Production of C4 and C5 Chemicals, ACS Catalysis, 6 (2016) 7621-7640.

[131] M. Fache, B. Boutevin, S. Caillol, Vanillin Production from Lignin and Its Use as a Renewable Chemical, ACS Sustainable Chemistry & Engineering, 4 (2016) 35-46.

[132] Ö. Metin, A. Mendoza-Garcia, D. Dalmızrak, M.S. Gültekin, S. Sun, FePd alloy nanoparticles assembled on reduced graphene oxide as a catalyst for selective transfer hydrogenation of nitroarenes to anilines using ammonia borane as a hydrogen source, Catalysis Science & Technology, 6 (2016) 6137-6143.

[133] J.-P. Lange, E. van der Heide, J. van Buijtenen, R. Price, Furfural—A Promising Platform for Lignocellulosic Biofuels, ChemSusChem, 5 (2012) 150-166.

[134] J. Du, J. Zhang, Y. Sun, W. Jia, Z. Si, H. Gao, X. Tang, X. Zeng, T. Lei, S. Liu, L. Lin, Catalytic transfer hydrogenation of biomass-derived furfural to furfuryl alcohol over in-situ prepared nano Cu-Pd/C catalyst using formic acid as hydrogen source, Journal of Catalysis, 368 (2018) 69-78.

[135] L. Liu, H. Lou, M. Chen, Selective hydrogenation of furfural to tetrahydrofurfuryl alcohol over Ni/CNTs and bimetallic CuNi/CNTs catalysts, International Journal of Hydrogen Energy, 41 (2016) 14721-14731.

[136] B. Chen, F. Li, Z. Huang, G. Yuan, Tuning catalytic selectivity of liquid-phase hydrogenation of furfural via synergistic effects of supported bimetallic catalysts, Applied Catalysis A: General, 500 (2015) 23-29.

[137] S. Sitthisa, T. Pham, T. Prasomsri, T. Sooknoi, R.G. Mallinson, D.E. Resasco, Conversion of furfural and 2-methylpentanal on Pd/SiO2 and Pd–Cu/SiO2 catalysts, Journal of Catalysis, 280 (2011) 17-27.

[138] D. Shi, Q. Yang, C. Peterson, A.-F. Lamic-Humblot, J.-S. Girardon, A. Griboval-Constant, L. Stievano, M.T. Sougrati, V. Briois, P.A.J. Bagot, R. Wojcieszak, S. Paul, E. Marceau, Bimetallic Fe-Ni/SiO2 catalysts for furfural hydrogenation: Identification of the interplay between Fe and Ni during deposition-precipitation and thermal treatments, Catalysis Today, 334 (2019) 162-172.

[139] S.C. Shit, R. Singuru, S. Pollastri, B. Joseph, B.S. Rao, N. Lingaiah, J. Mondal, Cu–Pd bimetallic nanoalloy anchored on a N-rich porous organic polymer for high-performance hydrodeoxygenation of biomass-derived vanillin, Catalysis Science & Technology, 8 (2018) 2195-2210.

[140] S. Tian, Z. Wang, W. Gong, W. Chen, Q. Feng, Q. Xu, C. Chen, C. Chen, Q. Peng, L. Gu, H. Zhao, P. Hu, D. Wang, Y. Li, Temperature-Controlled Selectivity of Hydrogenation and Hydrodeoxygenation in the Conversion of Biomass Molecule by the Ru1/mpg-C3N4 Catalyst, Journal of the American Chemical Society, 140 (2018) 11161-11164.

[141] H. Li, Z. Liu, Hydrodeoxygenation of vanillin as model compound for pyrolysis oil over carboxylic carbon nanotubes-supported Ni catalysts, Bioresource Technology Reports, 5 (2019) 86-90.

[142] F. Zhang, S. Zheng, Q. Xiao, Y. Zhong, W. Zhu, A. Lin, M. Samy El-Shall, Synergetic catalysis of palladium nanoparticles encaged within amine-functionalized UiO-66 in the hydrodeoxygenation of vanillin in water, Green Chemistry, 18 (2016) 2900-2908.

[143] H. Jiang, X. Yu, X. Peng, H. Zhang, R. Nie, X. Lu, D. Zhou, Q. Xia, Efficient aqueous hydrodeoxygenation of vanillin over a mesoporous carbon nitride-modified Pd nanocatalyst, RSC Advances, 6 (2016) 69045-69051.

[144] J.L. Santos, M. Alda-Onggar, V. Fedorov, M. Peurla, K. Eränen, P. Mäki-Arvela, M.Á. Centeno, D.Y. Murzin, Hydrodeoxygenation of vanillin over carbon supported metal catalysts, Applied Catalysis A: General, 561 (2018) 137-149.

[145] P.A. Lazaridis, S. Karakoulia, A. Delimitis, S.M. Coman, V.I. Parvulescu, K.S. Triantafyllidis, d-Glucose hydrogenation/hydrogenolysis reactions on noble metal (Ru, Pt)/activated carbon supported catalysts, Catalysis Today, 257 (2015) 281-290.

[146] J. Liu, L.L. Zhang, J. Zhang, T. Liu, X.S. Zhao, Bimetallic ruthenium–copper nanoparticles embedded in mesoporous carbon as an effective hydrogenation catalyst, Nanoscale, 5 (2013) 11044-11050.

[147] J. Zhang, L. Lin, J. Zhang, J. Shi, Efficient conversion of d-glucose into d-sorbitol over MCM-41 supported Ru catalyst prepared by a formaldehyde reduction process, Carbohydrate Research, 346 (2011) 1327-1332.

[148] P.M. de Souza, L. Silvester, A.G.M. da Silva, C.G. Fernandes, T.S. Rodrigues, S. Paul, P.H.C. Camargo, R. Wojcieszak, Exploiting the Synergetic Behavior of PtPd Bimetallic Catalysts in the Selective Hydrogenation of Glucose and Furfural, Catalysts, 9 (2019) 132.

[149] I. Ro, I.B. Aragao, Z.J. Brentzel, Y. Liu, K.R. Rivera-Dones, M.R. Ball, D. Zanchet, G.W. Huber, J.A. Dumesic, Intrinsic activity of interfacial sites for Pt-Fe and Pt-Mo catalysts in the hydrogenation of carbonyl groups, Applied Catalysis B: Environmental, 231 (2018) 182-190.

[150] J. Ftouni, A. Muñoz-Murillo, A. Goryachev, J.P. Hofmann, E.J.M. Hensen, L. Lu, C.J. Kiely, P.C.A. Bruijnincx, B.M. Weckhuysen, ZrO2 Is Preferred over TiO2 as Support for the Ru-Catalyzed Hydrogenation of Levulinic Acid to γ-Valerolactone, ACS Catalysis, 6 (2016) 5462-5472.

[151] W. Gong, C. Chen, Y. Zhang, H. Zhou, H. Wang, H. Zhang, Y. Zhang, G. Wang, H. Zhao, Efficient Synthesis of Furfuryl Alcohol from H2-Hydrogenation/Transfer Hydrogenation of Furfural Using Sulfonate Group Modified Cu Catalyst, ACS Sustainable Chemistry & Engineering, 5 (2017) 2172-2180.

[152] Crystallography Open Database, http://www.crystallography.net/cod/, in, 2018.

[153] G. Agostini, E. Groppo, A. Piovano, R. Pellegrini, G. Leofanti, C. Lamberti, Preparation of Supported Pd Catalysts: From the Pd Precursor Solution to the Deposited Pd2+ Phase, Langmuir, 26 (2010) 11204-11211.

[154] A.A. Vedyagin, A.M. Volodin, R.M. Kenzhin, V.V. Chesnokov, I.V. Mishakov, CO Oxidation over Pd/ZrO2 Catalysts: Role of Support′s Donor Sites, Molecules, 21 (2016) 1289.

[155] B. Qi, L. Di, W. Xu, X. Zhang, Dry plasma reduction to prepare a high performance Pd/C catalyst at atmospheric pressure for CO oxidation, Journal of Materials Chemistry A, 2 (2014) 11885-11890.

[156] J. Jin, C. Li, C.-W. Tsang, B. Xu, C. Liang, Catalytic combustion of methane over Pd/Ce–Zr oxides washcoated monolithic catalysts under oxygen lean conditions, RSC Advances, 5 (2015) 102147-102156.

[157] Y.H. Wang, W.G. Gao, H. Wang, Y.E. Zheng, W. Na, K.Z. Li, Structure–activity relationships of Cu–ZrO2 catalysts for CO2 hydrogenation to methanol: interaction effects and reaction mechanism, RSC Advances, 7 (2017) 8709-8717.

[158] G. Wang, L. Chen, Y. Sun, J. Wu, M. Fu, D. Ye, Carbon dioxide hydrogenation to methanol over Cu/ZrO2/CNTs: effect of carbon surface chemistry, RSC Advances, 5 (2015) 45320-45330.

[159] K. Li, H. Wang, Y. Wei, D. Yan, Direct conversion of methane to synthesis gas using lattice oxygen of CeO2–Fe2O3 complex oxides, Chemical Engineering Journal, 156 (2010) 512-518.

[160] H. Singh, A. Rai, R. Yadav, A.K. Sinha, Glucose hydrogenation to sorbitol over unsupported mesoporous Ni/NiO catalyst, Molecular Catalysis, 451 (2018) 186-191.

[161] A. Romero, A. Nieto-Márquez, E. Alonso, Bimetallic Ru:Ni/MCM-48 catalysts for the effective hydrogenation of d-glucose into sorbitol, Applied Catalysis A: General, 529 (2017) 49-59.

[162] N. Li, G.W. Huber, Aqueous-phase hydrodeoxygenation of sorbitol with Pt/SiO2–Al2O3: Identification of reaction intermediates, Journal of Catalysis, 270 (2010) 48-59.

[163] X. Zhang, L.J. Durndell, M.A. Isaacs, C.M.A. Parlett, A.F. Lee, K. Wilson, Platinum-Catalyzed Aqueous-Phase Hydrogenation of d-Glucose to d-Sorbitol, ACS Catalysis, 6 (2016) 7409-7417.

[164] Á. Ibarra, A. Veloso, J. Bilbao, J.M. Arandes, P. Castaño, Dual coke deactivation pathways during the catalytic cracking of raw bio-oil and vacuum gasoil in FCC conditions, Applied Catalysis B: Environmental, 182 (2016) 336-346.

[165] M.M. Rahman, R. Liu, J. Cai, Catalytic fast pyrolysis of biomass over zeolites for high quality bio-oil – A review, Fuel Processing Technology, 180 (2018) 32-46.

[166] W.B. Widayatno, G. Guan, J. Rizkiana, J. Yang, X. Hao, A. Tsutsumi, A. Abudula, Upgrading of bio-oil from biomass pyrolysis over Cu-modified β-zeolite catalyst with high selectivity and stability, Applied Catalysis B: Environmental, 186 (2016) 166-172.

[167] B. Puértolas, T.C. Keller, S. Mitchell, J. Pérez-Ramírez, Deoxygenation of bio-oil over solid base catalysts: From model to realistic feeds, Applied Catalysis B: Environmental, 184 (2016) 77-86.

[168] W. Yin, A. Kloekhorst, R.H. Venderbosch, M.V. Bykova, S.A. Khromova, V.A. Yakovlev, H.J. Heeres, Catalytic hydrotreatment of fast pyrolysis liquids in batch and continuous set-ups using a bimetallic Ni–Cu catalyst with a high metal content, Catalysis Science & Technology, 6 (2016) 5899-5915.

[169] B.J. O'Neill, E.I. Gürbüz, J.A. Dumesic, Reaction kinetics studies of the conversions of formic acid and butyl formate over carbon-supported palladium in the liquid phase, Journal of Catalysis, 290 (2012) 193-201.

[170] K.A. Resende, C.A. Teles, G. Jacobs, B.H. Davis, D.C. Cronauer, A. Jeremy Kropf, C.L. Marshall, C.E. Hori, F.B. Noronha, Hydrodeoxygenation of phenol over zirconia supported Pd bimetallic catalysts. The effect of second metal on catalyst performance, Applied Catalysis B: Environmental, 232 (2018) 213-231.

[171] A. Bjelić, M. Grilc, M. Huš, B. Likozar, Hydrogenation and hydrodeoxygenation of aromatic lignin monomers over Cu/C, Ni/C, Pd/C, Pt/C, Rh/C and Ru/C catalysts: Mechanisms, reaction micro-kinetic modelling and quantitative structure-activity relationships, Chemical Engineering Journal, 359 (2019) 305-320.

[172] P. Sirous-Rezaei, Y.-K. Park, Catalytic hydropyrolysis of lignin: Suppression of coke formation in mild hydrodeoxygenation of lignin-derived phenolics, Chemical Engineering Journal, (2019).

[173] Q. Han, M.U. Rehman, J. Wang, A. Rykov, O.Y. Gutiérrez, Y. Zhao, S. Wang, X. Ma, J.A. Lercher, The synergistic effect between Ni sites and Ni-Fe alloy sites on hydrodeoxygenation of lignin-derived phenols, Applied Catalysis B: Environmental, 253 (2019) 348-358.

[174] I. Hita, T. Cordero-Lanzac, F.J. García-Mateos, M.J. Azkoiti, J. Rodríguez-Mirasol, T. Cordero, J. Bilbao, Enhanced production of phenolics and aromatics from raw bio-oil using HZSM-5 zeolite additives for PtPd/C and NiW/C catalysts, Applied Catalysis B: Environmental, 259 (2019) 118112.

[175] H. Duan, J. Dong, X. Gu, Y.-K. Peng, W. Chen, T. Issariyakul, W.K. Myers, M.-J. Li, N. Yi, A.F.R. Kilpatrick, Y. Wang, X. Zheng, S. Ji, Q. Wang, J. Feng, D. Chen, Y. Li, J.-C. Buffet, H. Liu, S.C.E. Tsang, D. O'Hare, Hydrodeoxygenation of water-insoluble bio-oil to alkanes using a highly dispersed Pd–Mo catalyst, Nature Communications, 8 (2017) 591.

[176] Q. Xia, Z. Chen, Y. Shao, X. Gong, H. Wang, X. Liu, S.F. Parker, X. Han, S. Yang, Y. Wang, Direct hydrodeoxygenation of raw woody biomass into liquid alkanes, Nature Communications, 7 (2016) 11162.

[177] A. Gutierrez, R.K. Kaila, M.L. Honkela, R. Slioor, A.O.I. Krause, Hydrodeoxygenation of guaiacol on noble metal catalysts, Catalysis Today, 147 (2009) 239-246.

[178] L. Nie, P.M. de Souza, F.B. Noronha, W. An, T. Sooknoi, D.E. Resasco, Selective conversion of m-cresol to toluene over bimetallic Ni–Fe catalysts, Journal of Molecular Catalysis A: Chemical, 388-389 (2014) 47-55.

[179] D.-d. Li, J.-w. Zhang, J.-z. Jiang, C. Cai, Amphiphilic cellulose supported PdNi alloy nanoparticles towards biofuel upgrade under mild conditions, Catalysis Communications, 122 (2019) 43-46.

[180] G. Bagnato, M. Signoretto, C. Pizzolitto, F. Menegazzo, X. Xi, G. ten Brink, B. Kooi, H. Heeres, A. Sanna, Hydrogenation of biobased aldehydes to mono-alcohols using bimetallic catalysts, ACS Sustainable Chemistry & Engineering under reviwer (2020).

[181] J. Sun, A.M. Karim, H. Zhang, L. Kovarik, X.S. Li, A.J. Hensley, J.-S. McEwen, Y. Wang, Carbon-supported bimetallic Pd–Fe catalysts for vapor-phase hydrodeoxygenation of guaiacol, Journal of Catalysis, 306 (2013) 47-57.

[182] P.D.L. Mercera, J.G. van Ommen, E.B.M. Doesburg, A.J. Burggraaf, J.R.H. Roes, Stabilized tetragonal zirconium oxide as a support for catalysts Evolution of the texture and structure on calcination in static air, Applied Catalysis, 78 (1991) 79-96.

[183] A.R. Ardiyanti, A. Gutierrez, M.L. Honkela, A.O.I. Krause, H.J. Heeres, Hydrotreatment of wood-based pyrolysis oil using zirconia-supported mono- and bimetallic (Pt, Pd, Rh) catalysts, Applied Catalysis A: General, 407 (2011) 56-66.

[184] X. Li, G. Chen, C. Liu, W. Ma, B. Yan, J. Zhang, Hydrodeoxygenation of lignin-derived bio-oil using molecular sieves supported metal catalysts: A critical review, Renewable and Sustainable Energy Reviews, 71 (2017) 296-308.

[185] Y. Li, C. Zhang, Y. Liu, S. Tang, G. Chen, R. Zhang, X. Tang, Coke formation on the surface of Ni/HZSM-5 and Ni-Cu/HZSM-5 catalysts during bio-oil hydrodeoxygenation, Fuel, 189 (2017) 23-31.

[186] S. Tamura, T. Mashimo, K. Yamamoto, Z. Kelgenbaeva, W. Ma, X. Kang, M. Koinuma, H. Isobe, A. Yoshiasa, Synthesis of Pd-Fe System Alloy Nanoparticles by Pulsed Plasma in Liquid, Nanomaterials, 8 (2018) 1068.

[187] Y. Xiong, W. Ye, W. Chen, Y. Wu, Q. Xu, Y. Yan, H. Zhang, J. Wu, D. Yang, PdCu alloy nanodendrites with tunable composition as highly active electrocatalysts for methanol oxidation, RSC Advances, 7 (2017) 5800-5806.

[188] M.A. Nahil, X. Wang, C. Wu, H. Yang, H. Chen, P.T. Williams, Novel bi-functional Ni–Mg–Al–CaO catalyst for catalytic gasification of biomass for hydrogen production with in situ CO2 adsorption, RSC Advances, 3 (2013) 5583.

[189] M.M. Yung, A.K. Starace, M.B. Griffin, J.D. Wells, R.E. Patalano, K.R. Smith, J.A. Schaidle, Restoring ZSM-5 performance for catalytic fast pyrolysis of biomass: Effect of regeneration temperature, Catalysis Today, 323 (2019) 76-85.

[190] M.R. Rover, P.H. Hall, P.A. Johnston, R.G. Smith, R.C. Brown, Stabilization of bio-oils using low temperature, low pressure hydrogenation, Fuel, 153 (2015) 224-230.

[191] W.L. Queen, M.R. Hudson, E.D. Bloch, J.A. Mason, M.I. Gonzalez, J.S. Lee, D. Gygi, J.D. Howe, K. Lee, T.A. Darwish, M. James, V.K. Peterson, S.J. Teat, B. Smit, J.B. Neaton, J.R. Long, C.M. Brown, Comprehensive study of carbon dioxide adsorption in the metal–organic frameworks M2(dobdc) (M = Mg, Mn, Fe, Co, Ni, Cu, Zn), Chemical Science, 5 (2014) 4569-4581.

[192] A.B. Jain, P.D. Vaidya, Kinetics of Aqueous-Phase Hydrogenation of Model Bio-oil Compounds over a Ru/C Catalyst, Energy & Fuels, 29 (2015) 361-368.

[193] R. Hilten, J. Weber, J.R. Kastner, Continuous Catalytic Esterification and Hydrogenation of a Levoglucosan/Acetic Acid Mixture for Production of Ethyl Levulinate/Acetate and Valeric Biofuels, Energy & Fuels, 30 (2016) 9480-9489.

[194] X. Hu, R.J.M. Westerhof, L. Wu, D. Dong, C.-Z. Li, Upgrading biomass-derived furans via acid-catalysis/hydrogenation: the remarkable difference between water and methanol as the solvent, Green Chemistry, 17 (2015) 219-224.

[195] T.P. Vispute, H. Zhang, A. Sanna, R. Xiao, G.W. Huber, Renewable Chemical Commodity Feedstocks from Integrated Catalytic Processing of Pyrolysis Oils, Science, 330 (2010) 1222-1227.

[196] J. Shi, M. Zhao, Y. Wang, J. Fu, X. Lu, Z. Hou, Upgrading of aromatic compounds in bio-oil over ultrathin graphene encapsulated Ru nanoparticles, Journal of Materials Chemistry A, 4 (2016) 5842-5848.

[197] G. Chieffi, C. Giordano, M. Antonietti, D. Esposito, FeNi nanoparticles with carbon armor as sustainable hydrogenation catalysts: towards biorefineries, Journal of Materials Chemistry A, 2 (2014) 11591-11596.

[198] B. Sarkar, C. Pendem, L.N.S. Konathala, T. Sasaki, R. Bal, Pt nanoparticle supported on nanocrystalline CeO2: highly selective catalyst for upgradation of phenolic derivatives present in bio-oil, Journal of Materials Chemistry A, 2 (2014) 18398-18404.

[199] A. Corma, S. Iborra, A. Velty, Chemical Routes for the Transformation of Biomass into Chemicals, Chemical Reviews, 107 (2007) 2411-2502.

[200] H. Li, X. Chen, J. Ren, H. Deng, F. Peng, R. Sun, Functional relationship of furfural yields and the hemicellulose-derived sugars in the hydrolysates from corncob by microwave-assisted hydrothermal pretreatment, Biotechnology for Biofuels, 8 (2015) 127.

[201] D. Santos, U.F. Silva, F.A. Duarte, C.A. Bizzi, E.M.M. Flores, P.A. Mello, Ultrasound-assisted acid hydrolysis of cellulose to chemical building blocks: Application to furfural synthesis, Ultrasonics Sonochemistry, (2017).

[202] K. Kuroda, K. Miyamura, H. Satria, K. Takada, K. Ninomiya, K. Takahashi, Hydrolysis of Cellulose Using an Acidic and Hydrophobic Ionic Liquid and Subsequent Separation of Glucose Aqueous Solution from the Ionic Liquid and 5-(Hydroxymethyl)furfural, ACS Sustainable Chemistry & Engineering, 4 (2016) 3352-3356.

[203] H. Deka, M. Misra, A. Mohanty, Renewable resource based “all green composites” from kenaf biofiber and poly(furfuryl alcohol) bioresin, Industrial Crops and Products, 41 (2013) 94-101.

[204] V.V. Pushkarev, N. Musselwhite, K. An, S. Alayoglu, G.A. Somorjai, High Structure Sensitivity of Vapor-Phase Furfural Decarbonylation/Hydrogenation Reaction Network as a Function of Size and Shape of Pt Nanoparticles, Nano Letters, 12 (2012) 5196-5201.

[205] C.P. Jiménez-Gómez, J.A. Cecilia, I. Márquez-Rodríguez, R. Moreno-Tost, J. Santamaría-González, J. Mérida-Robles, P. Maireles-Torres, Gas-phase hydrogenation of furfural over Cu/CeO2 catalysts, Catalysis Today, 279 (2017) 327-338.

[206] X. Chen, L. Zhang, B. Zhang, X. Guo, X. Mu, Highly selective hydrogenation of furfural to furfuryl alcohol over Pt nanoparticles supported on g-C3N4 nanosheets catalysts in water, 6 (2016) 28558.

[207] M.W. Nolte, A. Saraeian, B.H. Shanks, Hydrodeoxygenation of cellulose pyrolysis model compounds using molybdenum oxide and low pressure hydrogen, Green Chemistry, (2017).

[208] Y. Nakagawa, K. Takada, M. Tamura, K. Tomishige, Total Hydrogenation of Furfural and 5-Hydroxymethylfurfural over Supported Pd–Ir Alloy Catalyst, ACS Catalysis, 4 (2014) 2718-2726.

[209] S. Liu, Y. Amada, M. Tamura, Y. Nakagawa, K. Tomishige, Performance and characterization of rhenium-modified Rh-Ir alloy catalyst for one-pot conversion of furfural into 1,5-pentanediol, Catalysis Science & Technology, 4 (2014) 2535-2549.

[210] R. Fang, H. Liu, R. Luque, Y. Li, Efficient and selective hydrogenation of biomass-derived furfural to cyclopentanone using Ru catalysts, Green Chemistry, 17 (2015) 4183-4188.

[211] J. Yang, J. Ma, Q. Yuan, P. Zhang, Y. Guan, Selective hydrogenation of furfural on Ru/Al-MIL-53: a comparative study on the effect of aromatic and aliphatic organic linkers, RSC Advances, 6 (2016) 92299-92304.

[212] Á. O'Driscoll, T. Curtin, W.Y. Hernández, P. Van Der Voort, J.J. Leahy, Hydrogenation of Furfural with a Pt–Sn Catalyst: The Suitability to Sustainable Industrial Application, Organic Process Research & Development, 20 (2016) 1917-1929.

[213] J. Llop Castelbou, K.C. Szeto, W. Barakat, N. Merle, C. Godard, M. Taoufik, C. Claver, A new approach for the preparation of well-defined Rh and Pt nanoparticles stabilized by phosphine-functionalized silica for selective hydrogenation reactions, Chemical Communications, 53 (2017) 3261-3264.

[214] I. Romanenko, M. Lechner, F. Wendler, C. Horenz, C. Streb, F.H. Schacher, POMbranes: polyoxometalate-functionalized block copolymer membranes for oxidation catalysis, Journal of Materials Chemistry A, 5 (2017) 15789-15796.

[215] L. Meng, M. Kanezashi, X. Yu, T. Tsuru, Enhanced decomposition of sulfur trioxide in the water-splitting iodine-sulfur process via a catalytic membrane reactor, Journal of Materials Chemistry A, 4 (2016) 15316-15319.

[216] H. Li, A. Caravella, H.Y. Xu, Recent progress in Pd-based composite membranes, Journal of Materials Chemistry A, 4 (2016) 14069-14094.

[217] W.J. Koros, Y.H. Ma, T. Shimidzu, Terminology for membranes and membrane processes (IUPAC Recommendations 1996), in: Pure and Applied Chemistry, 1996, pp. 1479.

[218] G. Bagnato, A. Iulianelli, A. Vita, C. Italiano, M. Laganà, C. Fabiano, C. Rossi, A. Basile, Pure Hydrogen Production from Steam Reforming of Bio-Sources, Int. J. Memb. Science Tech., 2 (2015) 48-56.

[219] E.C. Mengistie, J.-F. Lahitte, #xe7, ois, Development of Flow-Through Polymeric Membrane Reactor for Liquid Phase Reactions: Experimental Investigation and Mathematical Modeling, International Journal of Chemical Engineering, 2017 (2017) 8.

[220] W.-S. Lee, J.-C. Lee, H.-T. Oh, S.-W. Baek, M. Oh, C.-H. Lee, Performance, economic and exergy analyses of carbon capture processes for a 300 MW class integrated gasification combined cycle power plant, Energy, 134 (2017) 731-742.

[221] R. Bernstein, E. Antón, M. Ulbricht, UV-Photo Graft Functionalization of Polyethersulfone Membrane with Strong Polyelectrolyte Hydrogel and Its Application for Nanofiltration, ACS Applied Materials & Interfaces, 4 (2012) 3438-3446.

[222] D.X. Ye, T.M. Lu, T. Karabacak, Influence of Nanotips on the Hydrophilicity of Metallic Nanorod Surfaces, Physical Review Letters, 100 (2008) 256102.

[223] L.Y. Ng, A. Ahmad, A.W. Mohammad, Alteration of polyethersulphone membranes through UV-induced modification using various materials: A brief review, Arabian Journal of Chemistry, 10 (2017) S1821-S1834.

[224] H. Wang, S.-J. Lee, M.V. Olarte, A.H. Zacher, Bio-oil Stabilization by Hydrogenation over Reduced Metal Catalysts at Low Temperatures, ACS Sustainable Chemistry & Engineering, 4 (2016) 5533-5545.

[225] J. Tan, J. Cui, X. Cui, T. Deng, X. Li, Y. Zhu, Y. Li, Graphene-Modified Ru Nanocatalyst for Low-Temperature Hydrogenation of Carbonyl Groups, ACS Catalysis, 5 (2015) 7379-7384.

[226] M.D. Wales, L.B. Joos, W.A. Traylor, P. Pfromm, M. Rezac, Composite catalytic tubular membranes for selective hydrogenation in three-phase systems, Catalysis Today, 268 (2016) 12-18.

[227] H.A. Kramers, K.R. Westerterp, Elements of chemical reactor design and operation, (1963).

[228] J.C. Crittenden, R.R. Trussell, D.W. Hand, K.J. Howe, G. Tchobanoglous, Water Treatment: Principles and Design, 2012.

[229] I. Graça, J.M. Lopes, H.S. Cerqueira, M.F. Ribeiro, Bio-oils Upgrading for Second Generation Biofuels, Industrial & Engineering Chemistry Research, 52 (2013) 275-287.

[230] Y.M. Isa, E.T. Ganda, Bio-oil as a potential source of petroleum range fuels, Renewable and Sustainable Energy Reviews, 81 (2017) 69-75.

[231] A.V. Bridgwater, Review of fast pyrolysis of biomass and product upgrading, Biomass and Bioenergy, 38 (2012) 68-94.

[232] G. Lyu, Estimation and Comparison of Bio-Oil Components from Different Pyrolysis Conditions, Frontiers in Energy Research, 3 (2015).

[233] S. Czernik, A.V. Bridgwater, Overview of Applications of Biomass Fast Pyrolysis Oil, Energy & Fuels, 18 (2004) 590-598.

[234] J. Meng, A. Moore, D.C. Tilotta, S.S. Kelley, S. Adhikari, S. Park, Thermal and Storage Stability of Bio-Oil from Pyrolysis of Torrefied Wood, Energy & Fuels, 29 (2015) 5117-5126.

[235] P.M. Mortensena, J.-D. Grunwaldt, P.A. Jensena, K.G. Knudsenc, A.D. Jensena, A review of catalytic upgrading of bio-oil to engine fuels, Applied Catalysis A: General, 407 (2011) 1-19.

[236] H. Wang, J. Male, Y. Wang, Recent Advances in Hydrotreating of Pyrolysis Bio-Oil and Its Oxygen-Containing Model Compounds, ACS Catalysis, 3 (2013) 1047-1070.

[237] K. Alibegovic, D.G. Morgan, Y. Losovyj, M. Pink, B.D. Stein, N.V. Kuchkina, E.S. Serkova, K.E. Salnikova, Z.B. Shifrina, V.G. Matveeva, E.M. Sulman, L.M. Bronstein, Efficient Furfuryl Alcohol Synthesis from Furfural over Magnetically Recoverable Catalysts: Does the Catalyst Stabilizing Medium Matter?, ChemistrySelect, 2 (2017) 5485-5491.

[238] K.E. Salnikova, V.G. Matveeva, Y.V. Larichev, A.V. Bykov, G.N. Demidenko, I.P. Shkileva, M.G. Sulman, The liquid phase catalytic hydrogenation of furfural to furfuryl alcohol, Catalysis Today, 329 (2019) 142-148.

[239] W. Yu, Y. Tang, L. Mo, P. Chen, H. Lou, X. Zheng, One-step hydrogenation–esterification of furfural and acetic acid over bifunctional Pd catalysts for bio-oil upgrading, Bioresource Technology, 102 (2011) 8241-8246.

[240] S. Pati, J. Ashok, N. Dewangan, T. Chen, S. Kawi, Ultra-thin (~1 μm) Pd–Cu membrane reactor for coupling CO2 hydrogenation and propane dehydrogenation applications, Journal of Membrane Science, 595 (2020) 117496.

[241] I. Venditti, L. Fontana, F. Scaramuzzo, M. Russo, C. Battocchio, L. Carlini, L. Gonon, V. Mareau, I. Fratoddi, Nanocomposite Based on Functionalized Gold Nanoparticles and Sulfonated Poly(ether ether ketone) Membranes: Synthesis and Characterization, Materials, 10 (2017) 258.

[242] R. Dittmeyer, Svajda, K. & Reif, M, A Review of Catalytic Membrane Layers for Gas/Liquid Reactions | SpringerLink, Topics In Catalysis, 29 (2004) 3-27.

[243] X. Zhu, H. Feng, R. Chen, Q. Liao, D. Ye, B. Zhang, J. Liu, M. Liu, G. Chen, Experimental study on the durability of the polydopamine functionalized gas–liquid–solid microreactor for nitrobenzene hydrogenation, RSC Advances, 8 (2018) 5661-5669.

[244] W. Qing, X. Li, S. Shao, X. Shi, J. Wang, Y. Feng, W. Zhang, W. Zhang, Polymeric catalytically active membranes for reaction-separation coupling: A review, Journal of Membrane Science, 583 (2019) 118-138.

[245] D. Unlu, N.D. Hilmioglu, Pervaporation catalytic membrane reactor application over functional chitosan membrane, Journal of Membrane Science, 559 (2018) 138-147.

[246] M.K. Haque, K. Kawai, T. Suzuki, Glass transition and enthalpy relaxation of amorphous lactose glass, Carbohydrate Research, 341 (2006) 1884-1889.

[247] T. Huang, J. Song, S. He, T. Li, X.-M. Li, T. He, Enabling sustainable green close-loop membrane lithium extraction by acid and solvent resistant poly (ether ether ketone) membrane, Journal of Membrane Science, 589 (2019) 117273.

[248] J.C. Jansen, E. Drioli, Poly(ether ether ketone) derivative membranes—a review of their preparation, properties and potential, Polymer Science, Series A, (2009).

[249] F. Galiano, K. Briceño, T. Marino, A. Molino, K.V. Christensen, A. Figoli, Advances in biopolymer-based membrane preparation and applications, Journal of Membrane Science, 564 (2018) 562-586.

[250] J. Jansen, E. Drioli, Poly(ether ether ketone) derivative membranes—a review of their preparation, properties and potential, 2009.

[251] W. Wang, C.J. Luo, J. Huang, M. Edirisinghe, PEEK surface modification by fast ambient-temperature sulfonation for bone implant applications, Journal of The Royal Society Interface, 16 (2019) 20180955.

[252] T. Marino, F. Russo, A. Criscuoli, A. Figoli, TamiSolve® NxG as novel solvent for polymeric membrane preparation, Journal of Membrane Science, 542 (2017) 418-429.

[253] A. Iulianelli, G. Clarizia, A. Gugliuzza, D. Ebrasu, A. Bevilacqua, F. Trotta, A. Basile, Sulfonation of PEEK-WC polymer via chloro-sulfonic acid for potential PEM fuel cell applications, International Journal of Hydrogen Energy, 35 (2010) 12688-12695.

[254] A. Regina, E. Fontananova, E. Drioli, M. Casciola, M. Sganappa, F. Trotta, Preparation and characterization of sulfonated PEEK-WC membranes for fuel cell applications: A comparison between polymeric and composite membranes, Journal of Power Sources, 160 (2006) 139-147.

[255] O. Benhabiles, F. Galiano, T. Marino, H. Mahmoudi, H. Lounici, A. Figoli, Preparation and Characterization of TiO2-PVDF/PMMA Blend Membranes Using an

Alternative Non-Toxic Solvent for UF/MF and Photocatalytic Application, Molecules, 24 (2019).

[256] A. Gugliuzza, G. Clarizia, G. Golemme, E. Drioli, New breathable and waterproof coatings for textiles: effect of an aliphatic polyurethane on the formation of PEEK-WC porous membranes, European Polymer Journal, 38 (2002) 235-242.

[257] P.K. Rakshit, R.K. Voolapalli, S. Upadhyayula, Acetic acid hydrogenation to ethanol over supported Pt-Sn catalyst: Effect of Bronsted acidity on product selectivity, Molecular Catalysis, 448 (2018) 78-90.

[258] K. Srirangan, L. Akawi, M. Moo-Young, C.P. Chou, Towards sustainable production of clean energy carriers from biomass resources, Applied Energy, 100 (2012) 172-186.

[259] C.A. García-Velásquez, C.A. Cardona, Comparison of the biochemical and thermochemical routes for bioenergy production: A techno-economic (TEA), energetic and environmental assessment, Energy, 172 (2019) 232-242.

[260] M.C.C. Maguyon, S.C. Capareda, Evaluating the effects of temperature on pressurized pyrolysis of Nannochloropsis oculata based on products yields and characteristics, Energy Conversion and Management, 76 (2013) 764-773.

[261] T. J. Lundquist, I. C. Woertz, N. W. T. Quinn, J.R. Benemann, A Realistic Technology and Engineering Assessment of Algae Biofuel Production, in, Energy Biosciences Institute, Berkeley, California, 2010, pp. 1-178.

[262] P. Nautiyal, K.A. Subramanian, M.G. Dastidar, Production and characterization of biodiesel from algae, Fuel Processing Technology, 120 (2014) 79-88.

[263] D. Humbird, R. Davis, L. Tao, C. Kinchin, D. Hsu, A. Aden, P. Schoen, J. Lukas, B. Olthof, M. Worley, D. Sexton, D. Dudgeon, Process Design and Economics for Biochemical Conversion of Lignocellulosic Biomass to Ethanol: Dilute-Acid Pretreatment and Enzymatic Hydrolysis of Corn Stover, in, ; National Renewable Energy Laboratory (NREL), Golden, CO., 2011, pp. Medium: ED; Size: 147 pp.

[264] J. Singh, S. Gu, Commercialization potential of microalgae for biofuels production, Renewable and Sustainable Energy Reviews, 14 (2010) 2596-2610.

[265] M.-J. Paik, H. Kim, J. Lee, J. Brand, K.-R. Kim, Separation of triacylglycerols and free fatty acids in microalgal lipids by solid-phase extraction for separate fatty acid profiling analysis by gas chromatography, Journal of Chromatography A, 1216 (2009) 5917-5923.

[266] J.-G. Na, J.K. Han, Y.-K. Oh, J.-H. Park, T.S. Jung, S.S. Han, H.C. Yoon, S.H. Chung, J.-N. Kim, C.H. Ko, Decarboxylation of microalgal oil without hydrogen into hydrocarbon for the production of transportation fuel, Catalysis Today, 185 (2012) 313-317.

[267] M. Fatih Demirbas, Biorefineries for biofuel upgrading: A critical review, Applied Energy, 86 (2009) S151-S161.

[268] A.O. Alabi, M. Tampier, E. Bibeau, S. Seed, B.C.I. Council, Microalgae technologies & processes for biofuels-bioenergy production in British Columbia : current technology, suitability & barriers to implementation : final report, (2009).

[269] X. Li, S. Duniam, H. Gurgenci, Z. Guan, A. Veeraragavan, Full scale experimental study of a small natural draft dry cooling tower for concentrating solar thermal power plant, Applied Energy, 193 (2017) 15-27.

[270] C. Xin, M.M. Addy, J. Zhao, Y. Cheng, S. Cheng, D. Mu, Y. Liu, R. Ding, P. Chen, R. Ruan, Comprehensive techno-economic analysis of wastewater-based algal biofuel production: A case study, Bioresource Technology, 211 (2016) 584-593.

[271] T. Aysu, N.A. Abd Rahman, A. Sanna, Catalytic pyrolysis of Tetraselmis and Isochrysis microalgae by nickel ceria based catalysts for hydrocarbon production, Energy, 103 (2016) 205-214.

[272] T. Aysu, A. Sanna, Nannochloropsis algae pyrolysis with ceria-based catalysts for production of high-quality bio-oils, Bioresource Technology, 194 (2015) 108-116.

[273] N.A.A. Rahman, J. Fermoso, A. Sanna, Effect of Li-LSX-zeolite on the in-situ catalytic deoxygenation and denitrogenation of Isochrysis sp. microalgae pyrolysis vapours, Fuel Processing Technology, 173 (2018) 253-261.

[274] M.M. Wright, D.E. Daugaard, J.A. Satrio, R.C. Brown, Techno-economic analysis of biomass fast pyrolysis to transportation fuels, Fuel, 89 (2010) S2-S10.

[275] Y. Qiu, Y.-L. He, P. Li, B.-C. Du, A comprehensive model for analysis of real-time optical performance of a solar power tower with a multi-tube cavity receiver, Applied Energy, 185 (2017) 589-603.

[276] L.J. Snowden-Swan, K.A. Spies, G.J. Lee, Y. Zhu, Life cycle greenhouse gas emissions analysis of catalysts for hydrotreating of fast pyrolysis bio-oil, Biomass and Bioenergy, 86 (2016) 136-145.

[277] EIA, Natural Gas Industrial Price, in https://www.eia.gov/naturalgas/data.php , 2017.

[278] R. Turton, Analysis, synthesis, and design of chemical processes, Prentice Hall, Upper Saddle River, N.J., 2009.

[279] J.R. Couper, W.R. Penney, J.R. Fair, S.M. Walas, 21 - Costs of Individual Equipment, in: Chemical Process Equipment (Third Edition), Butterworth-Heinemann, Boston, 2012, pp. 731-741.

[280] J.H. Gary, G.E. Handwerk, M.J. Kaiser, Petroleum Refining: Technology and Economics, Fifth Edition, 2007.

[281] Solar Two Demonstrates Clean Power for the Future, in, DOE, 2000.

[282] M. Mehos, C. Turchi, J. Vidal, M. Wagner, Z. Ma, C. Ho, W. Kolb, C. Andraka, A. Kruizenga, Concentrating Solar Power Gen3 Demonstration Roadmap, in, National Renewable Energy Laboratory (NREL), 2017.

[283] J. Kanter, Europe Considers New Taxes to Promote 'Clean' Energy, The New York times, (2010).

[284] E. technologies, Cost estimation for pyrolyser, in https://www.researchgate.net/publication/280719547_Feedstock_Supply_System_Design_and_Economics_for_Conversion_of_Lignocellulosic_Biomass_to_Hydrocarbon_Fuels_Conversion_Pathway_Fast_Pyrolysis_and_Hydrotreating_Bio-oil_Pathway_The_2017_Design_Case, 2013.

[285] R. Davis, A. Aden, P.T. Pienkos, Techno-economic analysis of autotrophic microalgae for fuel production, Applied Energy, 88 (2011) 3524-3531.

[286] J.C. Quinn, R. Davis, The potentials and challenges of algae based biofuels: A review of the techno-economic, life cycle, and resource assessment modeling, Bioresource Technology, 184 (2015) 444-452.

[287] BP, Statistical Review of World Energy, in https://www.bp.com/content/dam/bp/business-sites/en/global/corporate/pdfs/energy-economics/statistical-review/bp-stats-review-2019-full-report.pdf, 2019.

[288] P. Pfleiderer, C.-F. Schleussner, K. Kornhuber, D. Coumou, Summer weather becomes more persistent in a 2 °C world, Nature Climate Change, 9 (2019) 666-671.

[289] G. Blöschl, J. Hall, A. Viglione, R.A.P. Perdigão, J. Parajka, B. Merz, D. Lun, B. Arheimer, G.T. Aronica, A. Bilibashi, M. Boháč, O. Bonacci, M. Borga, I. Čanjevac, A. Castellarin, G.B. Chirico, P. Claps, N. Frolova, D. Ganora, L. Gorbachova, A. Gül, J. Hannaford, S. Harrigan, M. Kireeva, A. Kiss, T.R. Kjeldsen, S. Kohnová, J.J. Koskela, O. Ledvinka, N. Macdonald, M. Mavrova-Guirguinova, L. Mediero, R. Merz, P. Molnar, A. Montanari, C. Murphy, M. Osuch, V. Ovcharuk, I. Radevski, J.L. Salinas, E. Sauquet, M. Šraj, J. Szolgay, E. Volpi, D. Wilson, K. Zaimi, N. Živković, Changing climate both increases and decreases European river floods, Nature, 573 (2019) 108-111.

[290] V. Strezov, H.M. Anawar, Renewable Energy Systems from Biomass: Efficiency, Innovation and Sustainability, CRC Press, 2018.

[291] C. Lindfors, A. Oasmaa, A. Välimäki, T. Ohra-aho, H. Punkkinen, C. Bajamundi, K. Onarheim, Standard liquid fuel for industrial boilers from used wood, Biomass and Bioenergy, 127 (2019) 105265.

[292] A. Krutof, K.A. Hawboldt, Upgrading of biomass sourced pyrolysis oil review: focus on co-pyrolysis and vapour upgrading during pyrolysis, Biomass Conversion and Biorefinery, 8 (2018) 775-787.

[293] G. Marroquín-Sánchez, J. Ancheyta-Juárez, Catalytic hydrotreating of middle distillates blends in a fixed-bed pilot reactor, Applied Catalysis A: General, 207 (2001) 407-420.

[294] H. Pucher, N. Schwaiger, R. Feiner, P. Pucher, L. Ellmaier, M. Siebenhofer, Catalytic hydrodeoxygenation of dehydrated liquid phase pyrolysis oil, International Journal of Energy Research, 38 (2014) 1964-1974.

[295] F.D.M. Mercader, P.J.J. Koehorst, H.J. Heeres, S.R.A. Kersten, J.A. Hogendoorn, Competition between hydrotreating and polymerization reactions during pyrolysis oil hydrodeoxygenation, AIChE Journal, 57 (2011) 3160-3170.

[296] R.G. Mortaza Gholizadeh, Xun Hu, Sri Kadarwati, Roel Westerhof, Weerawut Chaiwat, Md Mahmudul Hasan, Chun-Zhu Li, Importance of hydrogen and bio-oil inlet temperature during the hydrotreatment of bio-oil, Fuel Processing Technology (2016) 132-140.

[297] D.R. Parapati, V.K. Guda, V.K. Penmetsa, P.H. Steele, S.K. Tanneru, Single stage hydroprocessing of pyrolysis oil in a continuous packed-bed reactor, Environmental Progress & Sustainable Energy, 33 (2014) 726-731.

[298] D.R. Parapati, V.K. Guda, V.K. Penmetsa, S.K. Tanneru, B. Mitchell, P.H. Steele, Comparison of reduced and sulfided CoMo/γ-Al2O3 catalyst on hydroprocessing of pretreated bio-oil in a continuous packed-bed reactor, Environmental Progress & Sustainable Energy, 34 (2015) 1174-1179.

[299] G. Bagnato, A. Sanna, Process and Techno-Economic Analysis for Fuel and Chemical Production by Hydrodeoxygenation of Bio-Oil, Catalysts, 9 (2019) 1021.

[300] G. Bagnato, F. Boulet, A. Sanna, Effect of Li-LSX zeolite, NiCe/Al2O3 and NiCe/ZrO2 on the production of drop-in bio-fuels by pyrolysis and hydrotreating of Nannochloropsis and isochrysis microalgae, Energy, 179 (2019) 199-213.

[301] M.M. Wright, Y. Román-Leshkov, W.H. Green, Investigating the techno-economic trade-offs of hydrogen source using a response surface model of drop-in biofuel production via bio-oil upgrading, Biofuels, Bioproducts and Biorefining, 6 (2012) 503-520.

[302] Y. Zhu, M.J. Biddy, S.B. Jones, D.C. Elliott, A.J. Schmidt, Techno-economic analysis of liquid fuel production from woody biomass via hydrothermal liquefaction (HTL) and upgrading, Applied Energy, 129 (2014) 384-394.

[303] J.M. Douglas, Conceptual design of chemical process, Singapore, 1988.

[304] H. Song, S.Y. Lee, Enzyme Microb. Technol., 39 (2006) 352.

[305] X. Li, B. Ho, Y. Zhang, Green Chem., 18 (2016) 2976.

[306] M.S. Peters, K.D. Timmerhaus, Plant design and economics for chemical engineers, McGraw-Hill, 1991.

[307] S. Jones, P. Meyer, L. Snowden-Swan, A. Padmaperuma, E. Tan, A. Dutta, J. Jacboson, K. Cafferty, Process Design and Economics for the Conversion of Lignocellulosic Biomass to Hydrocarbon Fuels, in, U.S. Department of Energy, 2013.

[308] L. Negahdar, J.U. Oltmanns, S. Palkovits, R. Palkovits, Kinetic investigation of the catalytic conversion of cellobiose to sorbitol, Applied Catalysis B: Environmental, 147 (2014) 677-683.

[309] O.A. Abdelrahman, A. Heyden, J.Q. Bond, Analysis of Kinetics and Reaction Pathways in the Aqueous-Phase Hydrogenation of Levulinic Acid To Form γ-Valerolactone over Ru/C, ACS Catalysis, 4 (2014) 1171-1181.

[310] D. Richard, M.d.L. Delgado-Nuñez, Kinetics of the degradation by catalytic hydrogenation of tyrosol, a model molecule present in olive oil waste waters, Journal of Chemical Technology & Biotechnology, 78 (2003) 927-934.

[311] H. Olcay, L. Xu, Y. Xu, G.W. Huber, Aqueous-Phase Hydrogenation of Acetic Acid over Transition Metal Catalysts, ChemCatChem, 2 (2010) 1420-1424.

[312] S. Thangalazhy-Gopakumar, S. Adhikari, H. Ravindran, R.B. Gupta, O. Fasina, M. Tu, S.D. Fernando, Physiochemical properties of bio-oil produced at various temperatures from pine wood using an auger reactor, Bioresource Technology, 101 (2010) 8389-8395.

[313] C. Branca, GC/MS characterization of liquids generated from low-temperature pyrolysis of wood Indus rial Engineering Chemistry Research, 14 (2003) 3190-3202.

[314] M. Garcia-Perez, S. Wang, J.S. M., M. Rhodes, W-J. Lee, C.-Z. Li., Effects of temperature on the formation of lignin-derived oligomers during the fast pyrolysis of mallee woody biomass, Energy & Fuels, 3 (2008) 2022-2032.

[315] M. Djokic, T Dijkmans, G. Yildiz, W. Prins, K.V. Geem, Quantitative analysis of crude and stabilized bio-oils by comprehensive two-dimensional gas-chromatography, Journal of Chromatography ACS Catalysis, (2012) 131-140.

[316] Y. Liu, Q. Shi, Y. Zhang, Y. He, K. Chung, S. Zhao, C. Zu, Characterization of red pine pyrolysis bio-oil by gas chromatography-mass spectrometry and negative-ion electrospray ionization fourier transform ion cyclotron resonance mass spectrometry., Energy & Fuels, , 7 (2012) 4532-4539.

[317] W. Desisto, N. Hill, S. Beis, S. Mukkamala, J. Joseph, C. Baker, T. Ong, E. Stemmler, M. Wheeler, B. Frederick, A. van Heiningen. . “” Fast pyrolysis of pine sawdust in a fluidized-bed reactor., Energy & Fuels, 4 (2010) 2642-2651.

[318] K. Kim, I. Eom, S. Lee, D. Choi, H. Yeo, I-G. Choi, J Choi Investigation of physicochemical properties of biooils produced from yellow poplar wood (Liriodendron tulipifera) at various temperatures and residence times, Journal of Analytical and Applied Pyrolysis, 1 (2011) 2-9.

[319] A. Bridgwater, S. Czernik, J. Diebold, D. Meier, A. Oasmaa, C. Peacocke, J. Piskorz, R.D. Fast, Pyrolysis of Biomass: A Handbook, Volume 1, UK: CPL Press, ed., 1999.

[320] S. Chu, The pyrolysis chemistry of a β-O-4 type oligomeric lignin model compound, Green Chemistry, 125-136 (2013).

[321] R. Bayerbach, Characterization of the water-insoluble fraction from fast pyrolysis liquids (pyrolytic lignin): Part III. Molar mass characteristics by SEC, MALDI-TOF-MS, LDI-TOF-MS, and PyFIMS, Journal of Analytical and Applied Pyrolysis, 2 (2006) 95-101.

[322] https://www.valero.com/en-us, 2019.

[323] J.M. Smith, H.C.V. Ness, M.M. Abbott, Introduction to chemical engineering thermodynamics, McGraw-Hill, Boston, 2005.

[324] P. Nag, Basic & applied thermodynamics, McGraw Hill, Boston, 2017.

[325] D.C. Elliott, T.R. Hart, G.G. Neuenschwander, L.J. Rotness, A.H. Zacher, Catalytic hydroprocessing of biomass fast pyrolysis bio-oil to produce hydrocarbon products, Environmental Progress & Sustainable Energy, 28 (2009) 441-449.

[326] A. Aho, S. Roggan, K. Eranen, T. Salmi, D.Y. Murzin, Continuous hydrogenation of glucose with ruthenium on carbon nanotube catalysts, Catalysis Science & Technology, 5 (2015) 953-959.

[327] J. Li, H.S.M.P. Soares, J.A. Moulijn, M. Makkee, Simultaneous hydrolysis and hydrogenation of cellobiose to sorbitol in molten salt hydrate media, Catalysis Science & Technology, 3 (2013) 1565-1572.

[328] https://www.linde-engineering.com/internet.global.lindeengineering.global/en/images/ H2_1_1_e_12_150dpi_NB19_4258.pdf?v=11.0, 2019.

[329] J.H. Gary, G.E. Handwerk, Petroleum Refining, Taylor & Francis, 2001.

[330] A. Kremser, Theoretical analysis of absorption process, Natl. Petroleum News, 22 (1930) 42.

[331] V.M.T.M. Silva, P.S. Gomes, A.E. Rodrigues, Use of Ion Exchange Resins in Continuous Chromatography for Sugar Processing, in: D. Inamuddin, M. Luqman (Eds.) Ion Exchange Technology II: Applications, Springer Netherlands, Dordrecht, 2012, pp. 109-135.

[332] B. Pynnonen, Simulated moving bed processing: escape from the high-cost box, Journal of Chromatography A, 827 (1998) 143-160.

[333] D. Sengupta, R.W. Pike, Chemicals from Biomass, in: W.-Y. Chen, T. Suzuki, M. Lackner (Eds.) Handbook of Climate Change Mitigation and Adaptation, Springer New York, New York, NY, 2014, pp. 1-38.

[334] Trading economics, in https://tradingeconomics.com/euro-area/interest-rate , 2019.